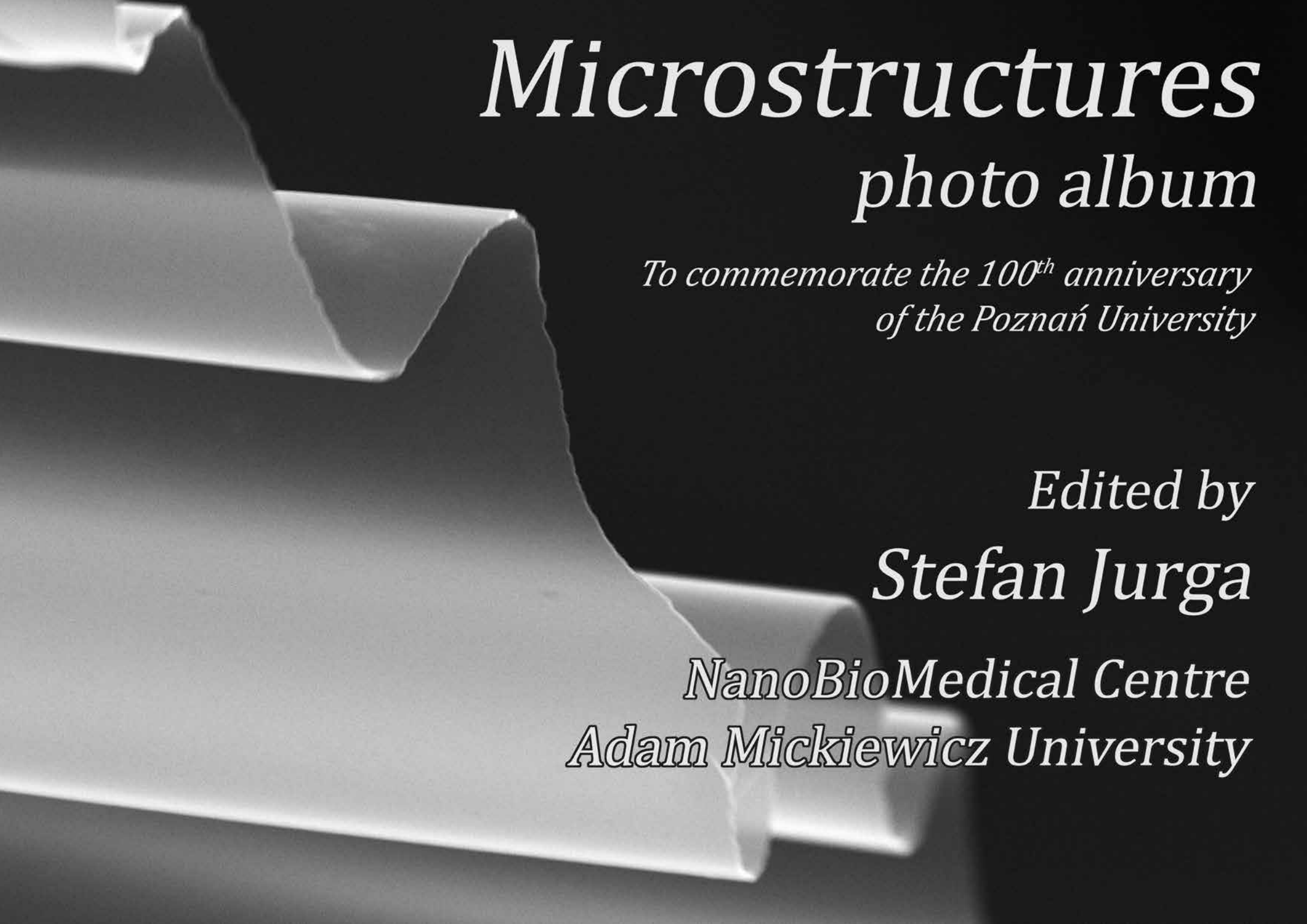

Microstructures
photo album

To commemorate the 100th anniversary of the Poznań University

Edited by

Stefan Jurga

NanoBioMedical Centre
Adam Mickiewicz University

Title: „Microstructures - photo album”
Editor in Chief: Prof. dr hab. Stefan Jurga, Director of NanoBioMedical Centre, AMU
Editor: Krzysztof Tadyszak
Publisher: Krzysztof Tadyszak
Imprint: Krzysztof Tadyszak
Place of Publishing: NanoBioMedical Centre at the Adam Mickiewicz University, ul Umultowska 85, Poznań, Poland
Date of online publishing: 22.10.2018
ISBN: 978-83-950131-0-2

List of co-authors and projects which funded their studies:
Krzysztof Tadyszak (KT) - „Analysis of the magnetic interactions in the two- and three-dimensional graphene oxide structures”, (NCN, Grant no. UMO-2016/21/D/ST3/00975), and „Quantification of cancer tissue oxygenation measured with BOLD-MRI - calibration with oximetry EPRI”, (NCN, Grant no. UMO-2014/15/B/ST4/04946).
Olena Ivashchenko (OI) - „Self-organizing magnetite/silver nanoparticles: biomedical potential and microstructure analysis”, (NCN, Grant no. UMO-2016/23/B/ST8/00640).
Barbara Peplińska (BP) - „Self-organizing magnetite/silver nanoparticles: biomedical potential and microstructure analysis”, (NCN, Grant no. UMO-2016/23/B/ST8/00640).
Jagoda Litowczenko (JL) - „Design and fabrication of matrices based on polymers and carbon nanostructures with specified topography for neural stem cells growth and differentiation”, (NCN, Grant no. UMO-2016/23/N/ST5/00955).
Igor Iatsunskyi (II) - „Novel 1D photonic metal oxide nanostructures for early stage cancer detection”, (Horizon 2020 - no. CanBioSE 778157), and „Investigation of biophotonical and electrical properties for novel nanocomposites based on porous silicon - zinc oxide”, (NCN, Grant no. UMO-2016/21D/ST3/00962).
Karol Załęski (KZ) - „Transport properties of graphene-based lateral spin valves with Heusler alloys”, (NCN, Grant no. UMO-2016/23/D/ST3/02121).
Alicja Warowicka (AW) - „Natural products derived from Chelidonjum majus plant as potential photosensitizers for the photodynamic therapy (PDT) of cervical cancer”, (NCN, Grant no. UMO--2012/05/N/NZ9/01337).
Błażej Scheibe (BS) - „Fabrication and characterization of structural properties of MAX phases and MXenes based on titanium carbides obtained at carbon nanomaterials”, (NCN, Grant no. UMO-2014/13/D/ST5/02824).
Dorota Flak (DF) - „Functionalization of graphene quantum dots with ligands specifically recognizing cancer cells”, (NCN, Grant no. UMO-2017/01/X/ST5/00134).
Beata Wereszczyńska (BW) - „The influence of therapeutic components on contrasting efficiency of liposomal paramagnetic system in MRI” (NCN, Grant no. UMO-2016/23/N/ST3/01878).
Jacek Wychowaniec (JW) - „Spatial organization of nanoparticles via polymeric self-assembling systems” (NCN, Grant no. UMO-2013/11/B/ST3/04190).
Maciej Kasprzak (MK) - „Phononic Crystals for Heat and Sound Nanodevices” (FNP, Grant no. Homing/2016-1/2).
Klaudia Golba (KG) - „Środowiskowe interdyscyplinarne studia doktoranckie w zakresie nanotechnologii” No. POWR.03.02.00-00-I032/16 under the European Social Fund – Operational Programme Knowledge Education Development, Axis III Higher Education for Economy and Development, Action 3.2 PhD Programme.
Radosław Mrówczyński (RM) - „Synthesis and properties of new multimodal, hybrid dendrimers-magnetic nanoparticles materials and their evaluation in combined anticancer therapy” (NCBR, Grant no. LIDER/11/0055/L-7/15/NCBiR/2016), and „New, multifunctional nanoparticles for combined photothermal and gene silencing cancer therapy” (NCN, Grant no. 2016/21/B/ST8/00477).
Patryk Florczak (PF) - „Electrochemical control of chemical content and structure of GOF and RGO-metal composites to improve their capability to hydrogen sorption” (NCN, Grant no. 2017/25/B/ST8/01634).
Ahmed Subrati (AS) - „Electrochemical control of chemical content and structure of GOF and RGO-metal composites to improve their capability to hydrogen sorption” (NCN, Grant no. 2017/25/B/ST8/01634).
Piotr Graczyk (PG) - „Pulsed Laser Deposition of gadolinium molybdate (GMO) thin films - study of its mutiferroic properties”, (NCN, Grant no. 2015/17/N/ST5/01988).
Ahmet Kertmen (AK) - „Impact of the engineered mono-dispersed Fe3O4@SiO2 nanoparticles on a fungal enzyme inhibition in vitro”, (NCN, Grant no. 2015/17/N/NZ7/0108).
Mikhael Bechelany (MB) - „Novel 1D photonic metal oxide nanostructures for early stage cancer detection”, (Horizon 2020 - no. CanBioSE 778157).
Emerson Coy (EC) - „Pulsed Laser Deposition of gadolinium molybdate (GMO) thin films - study of its mutiferroic properties”, (NCN, Grant no. 2015/17/N/ST5/01988).
Edgar Gonzalez (EG)
Nataliya Babayevska (NB)
Katarzyna Szcześniak (KSz)
Mateusz Kempiński (MKi)
Bartosz Kawczyński (BK)
Marek Nowak (MN)

This book was prepared by the employees of the NanoBioMedical Center at the Adam Mickiewicz University to commemorate the 100th anniversary of the Poznań University foundation. In this book, we present photographs of advanced nano and micro-materials prepared at our Centre, captured thanks to the cutting-edge and innovative microscopic techniques: scanning and transmission electron microscopy, scanning ion microscopy, atomic force microscopy. By combining science and art in a creative way, we endeavor to capture the attention of young audience and ultimately encourage them to pursue scientific subjects in their future careers.

UNIWERSYTET POZNAŃSKI 1919·2019
UAM UMP UPP AWF

NanoBioMedical Centre
Adam Mickiewicz University in Poznań

NanoBioMedical Centre research group (BK, MN, 4.10.2018)

Contents

Highly oriented pyrolitic graphite

Highly pure and ordered form of synthetic graphite, characterised by a low mosaic spread angle (less than 1°); individual graphite crystallites are well aligned to each other. Although it is not a monocrystal, it possesses some anisotropic properties of a graphite monocrystal. Images were taken by a focused ion beam microscope.

8 *Highly oriented pyrolitic graphite (KZ, 200x)*

Highly oriented pyrolitic graphite (KZ, 450x)

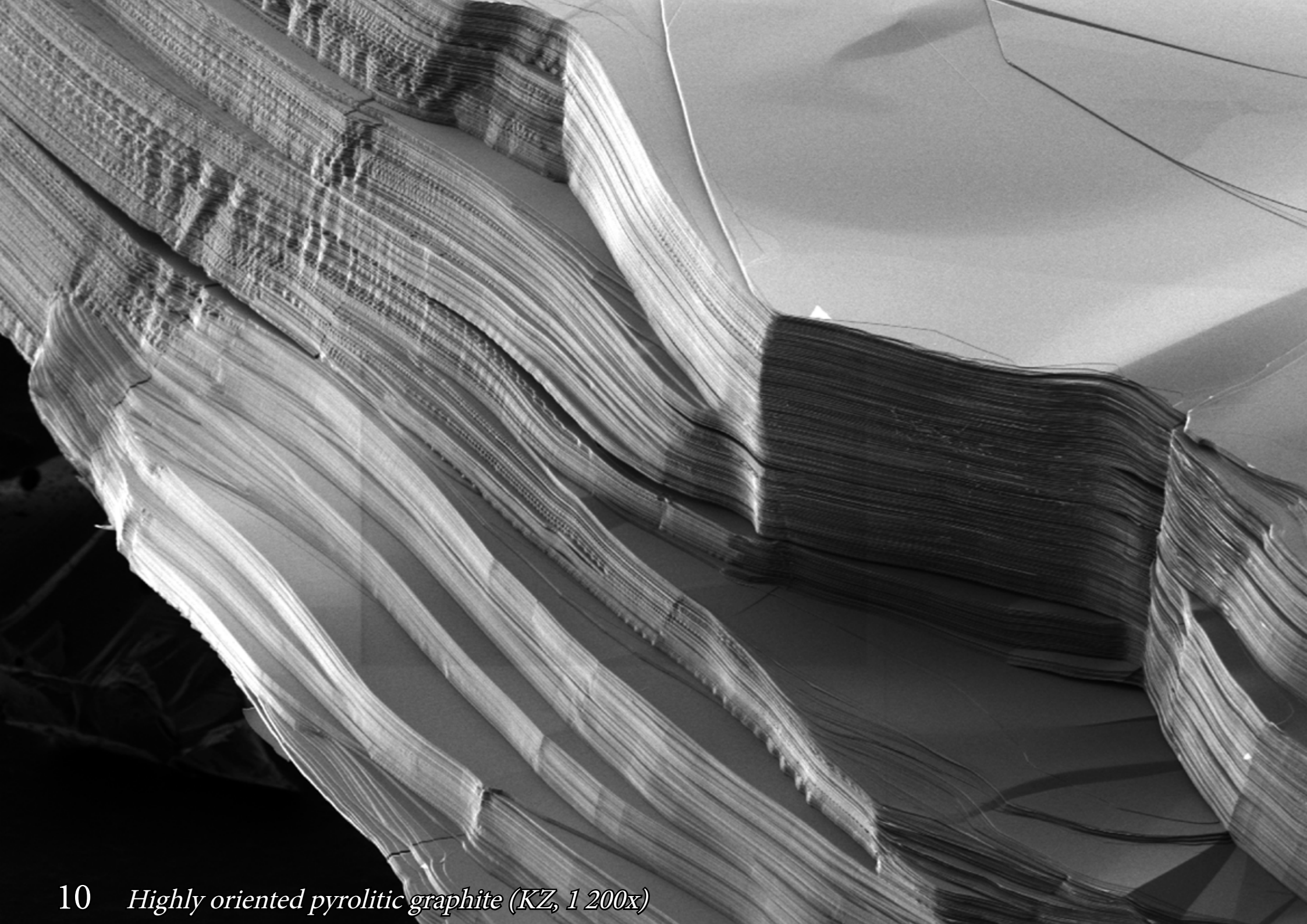

10 *Highly oriented pyrolitic graphite (KZ, 1 200x)*

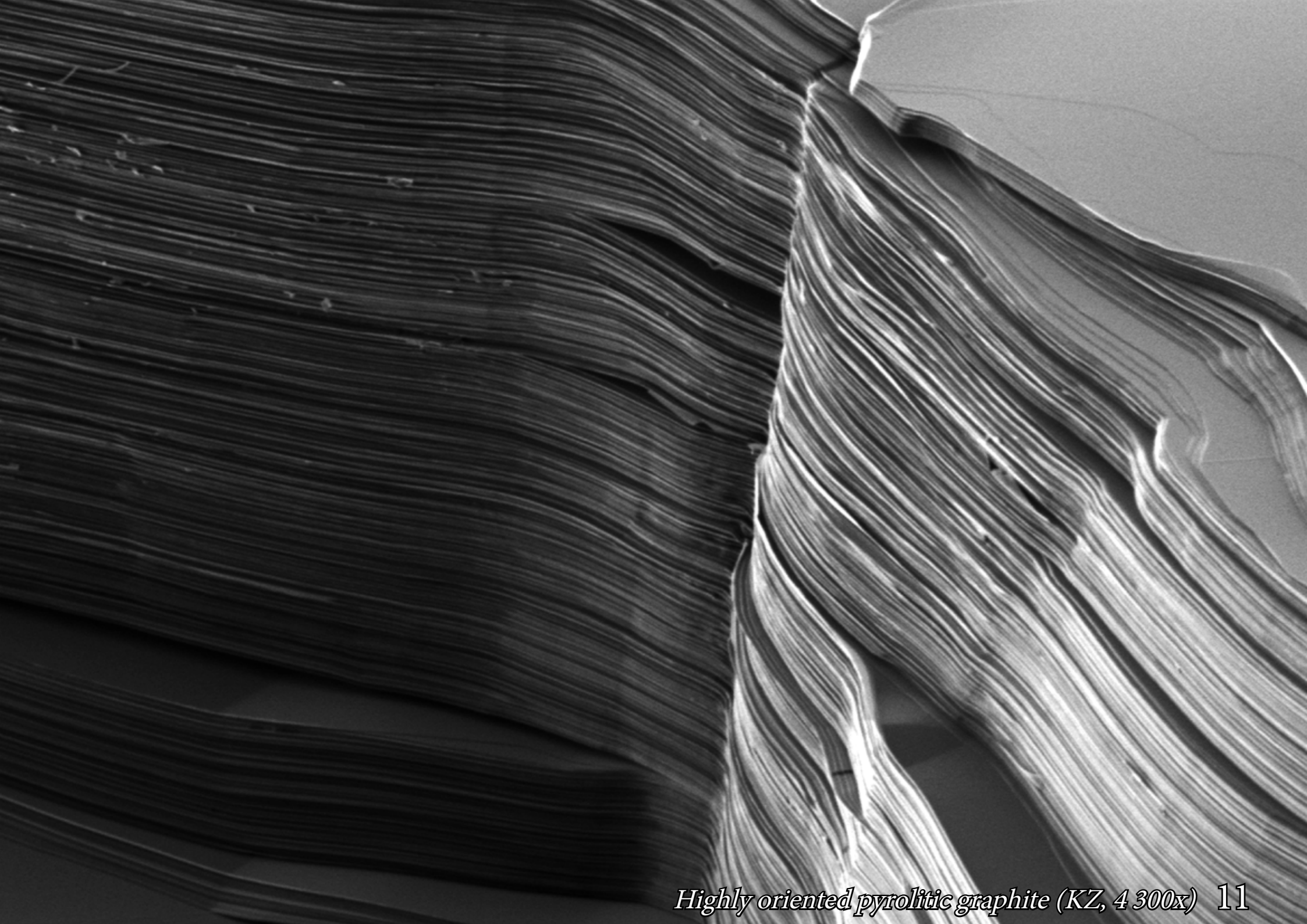

Highly oriented pyrolitic graphite (KZ, 4 300x) 11

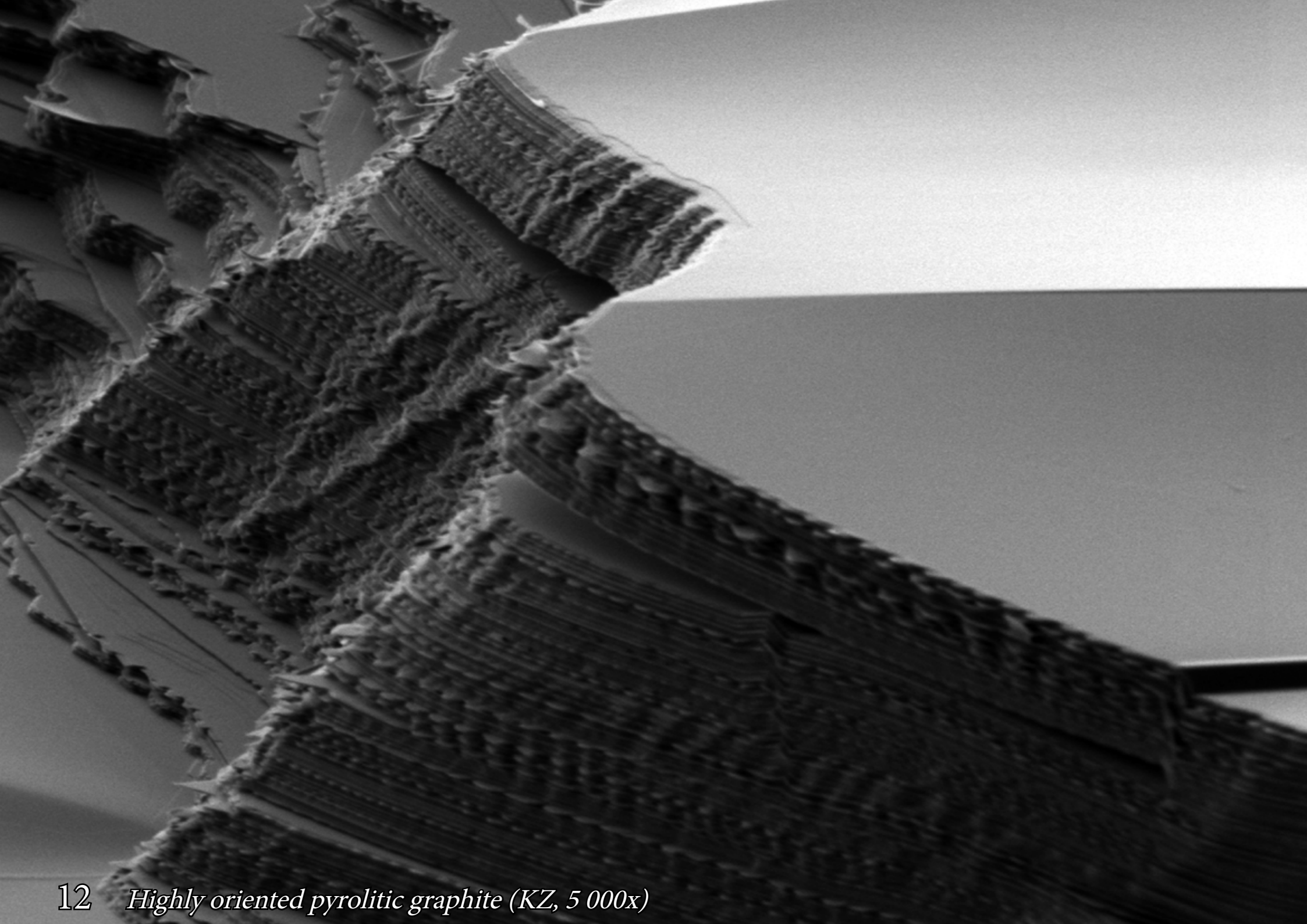

12 *Highly oriented pyrolitic graphite (KZ, 5 000x)*

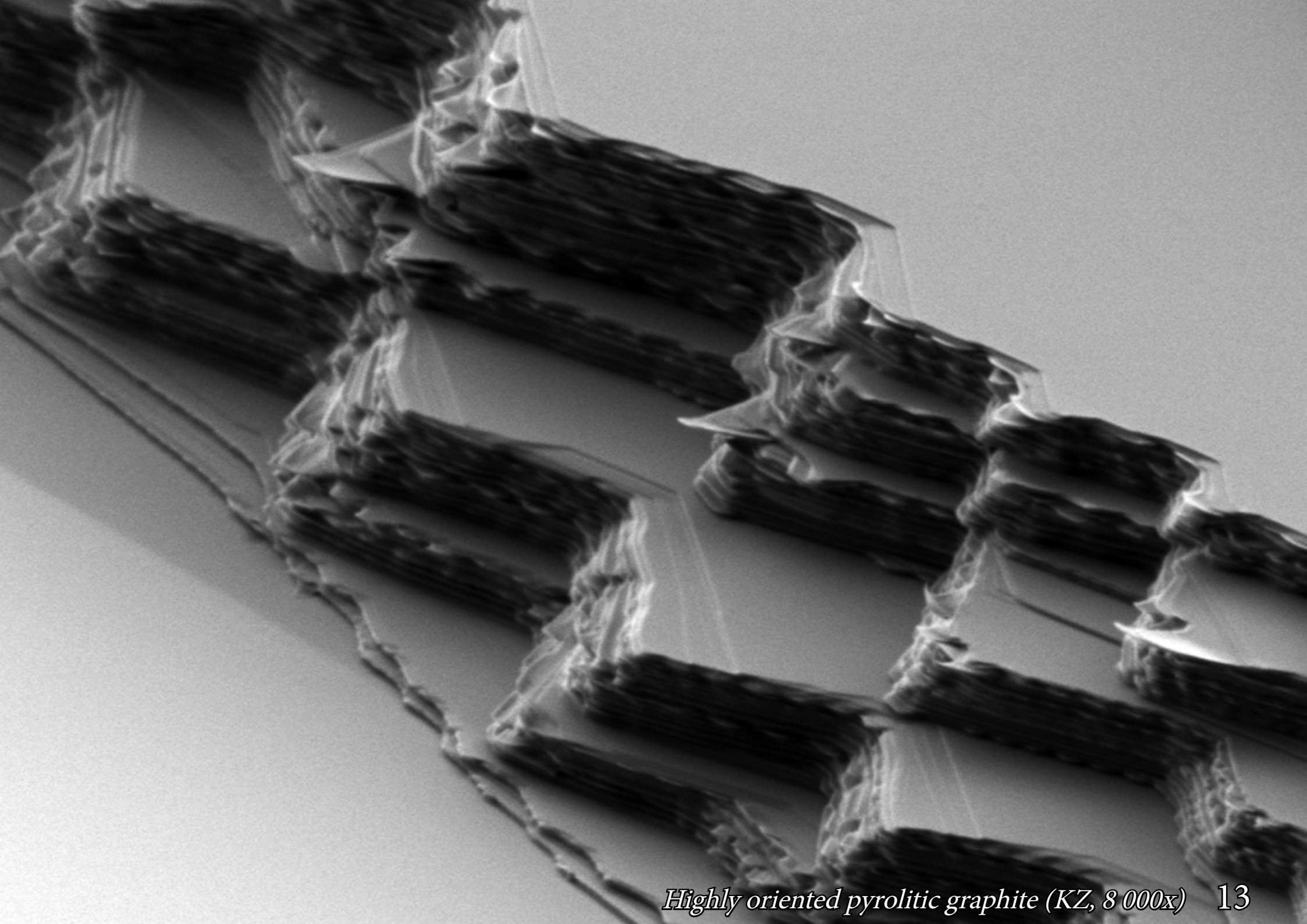

Highly oriented pyrolitic graphite (KZ, 8 000x)

2D phononic structures

Two dimensional (2D) periodic structures are obtained on silicon membranes via focused ion beam. This periodic hole structure restricts the range of possible mechanical waves (phonons) propagating through the material.

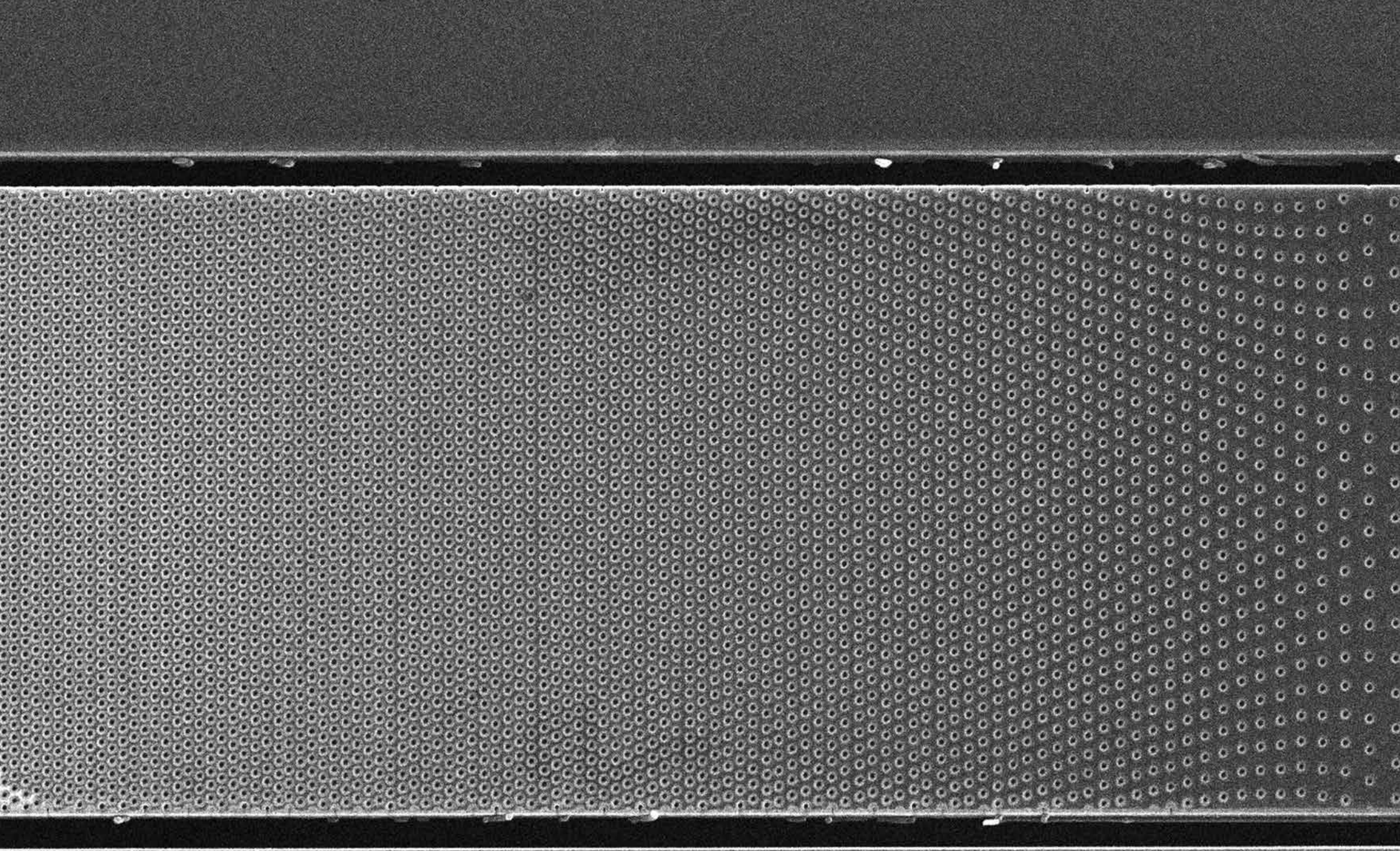

2D phononic crystal with variable period in one dimension (MK, 3 300x)

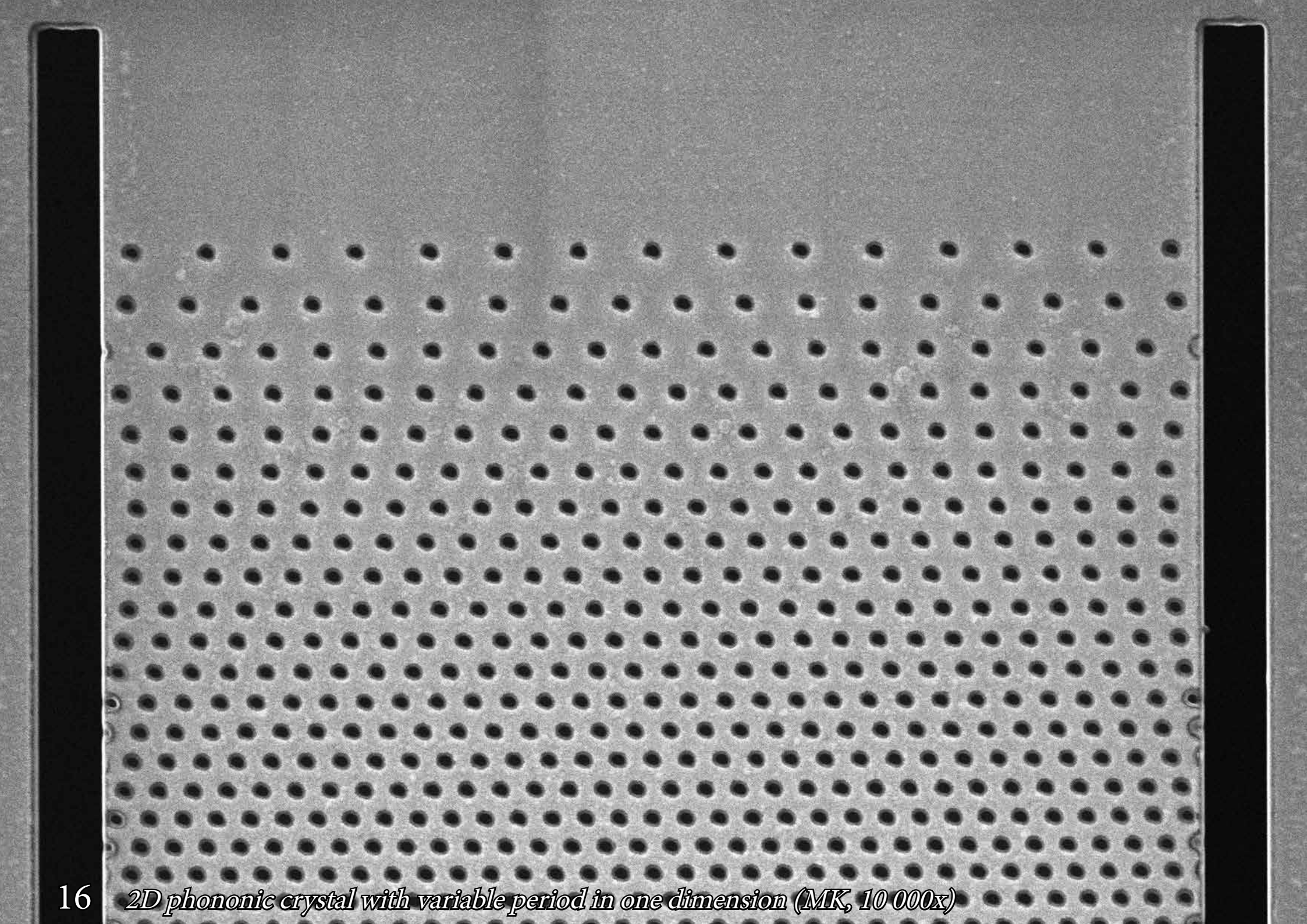

16 *2D phononic crystal with variable period in one dimension (MK, 10 000x)*

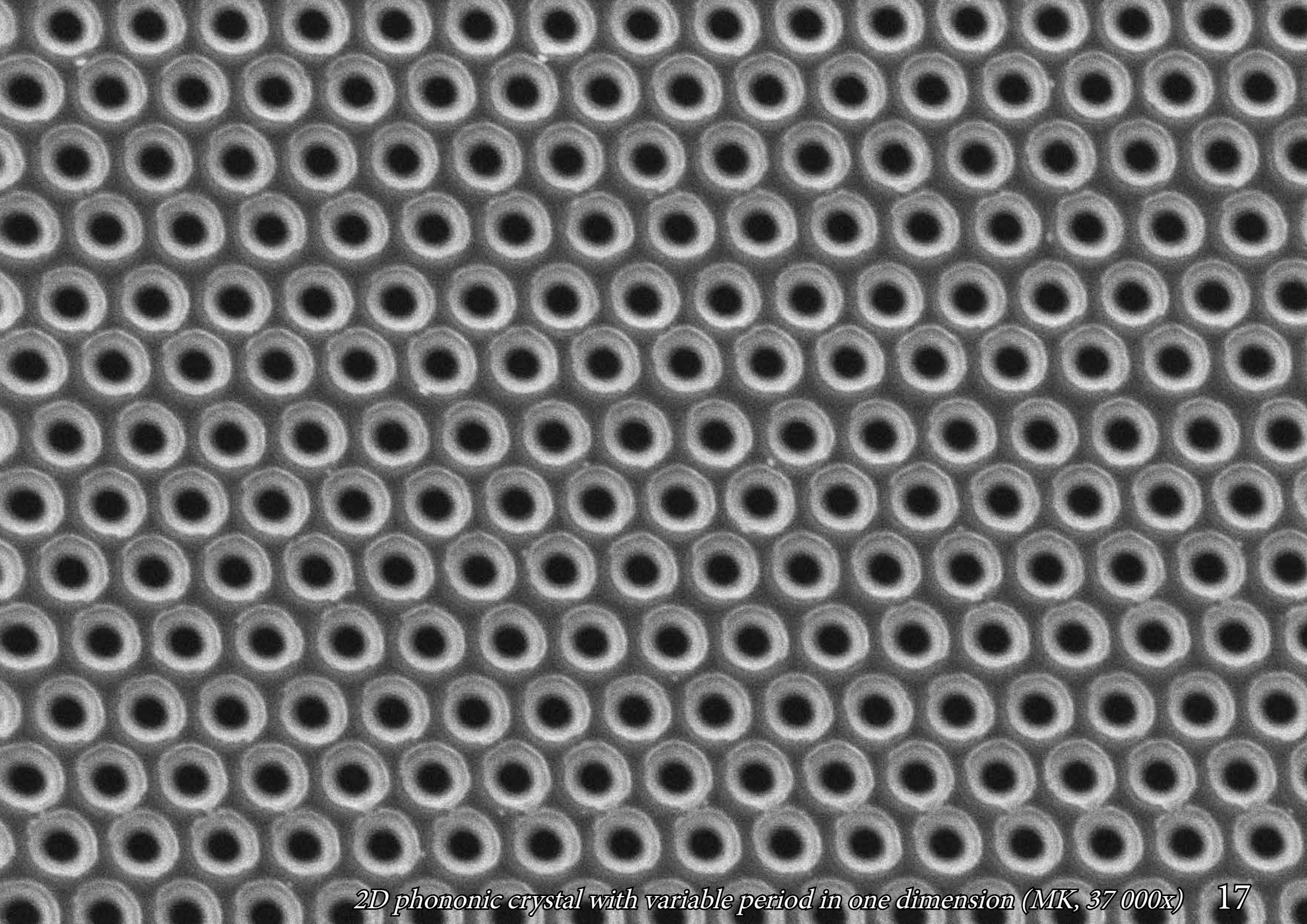

2D phononic crystal with variable period in one dimension (MK, 37 000x) 17

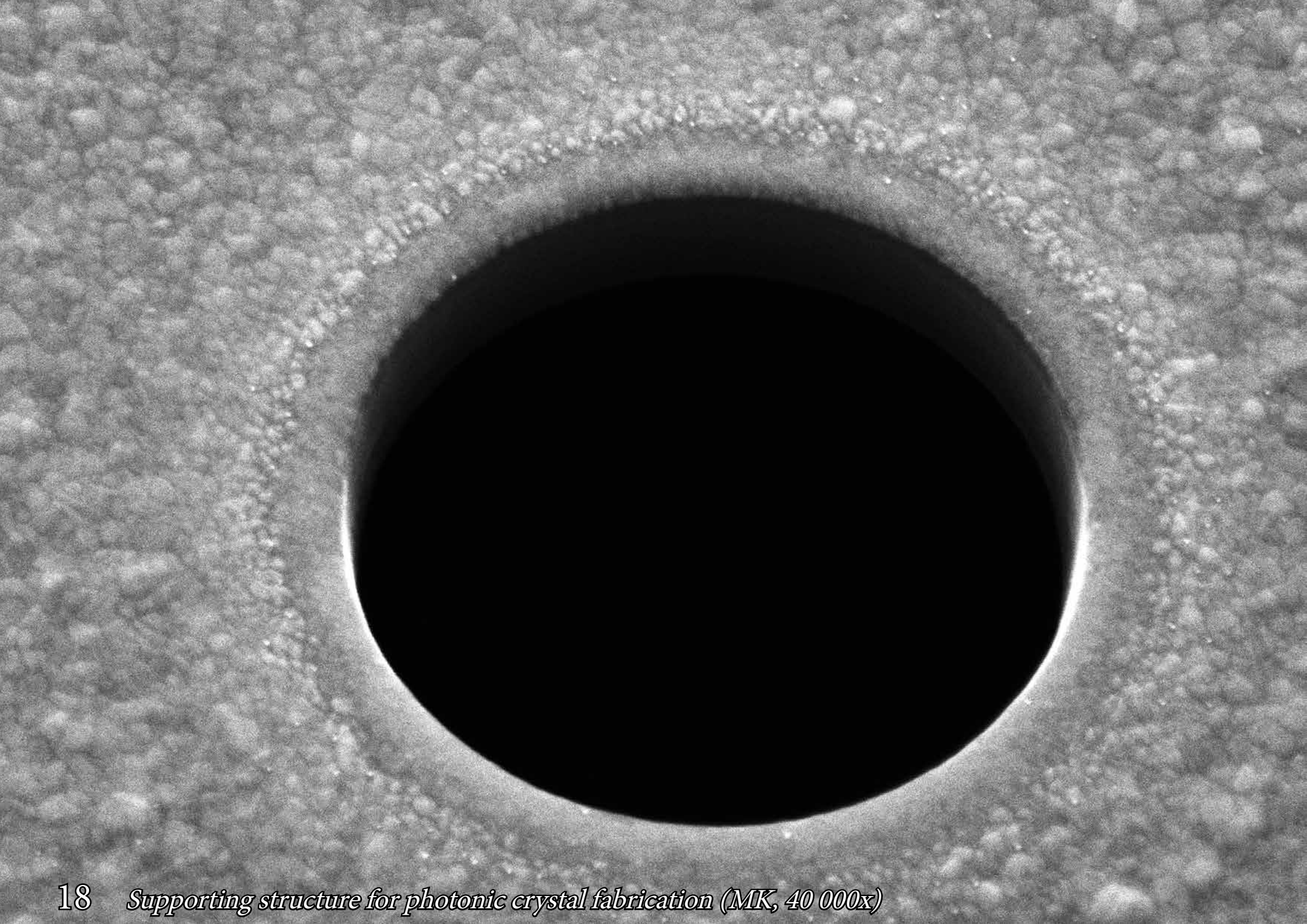

18 *Supporting structure for photonic crystal fabrication (MK, 40 000x)*

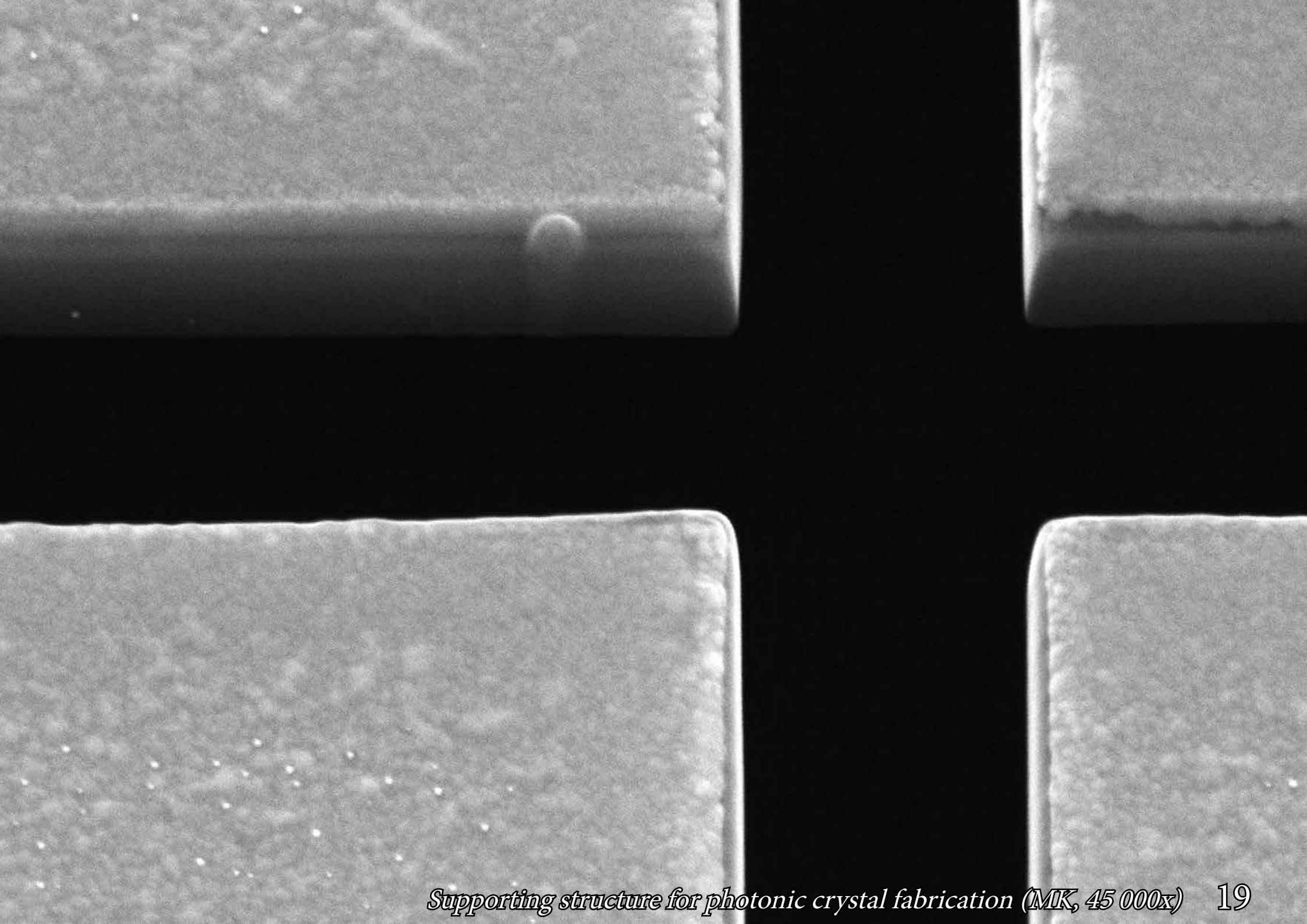

Supporting structure for photonic crystal fabrication (MK, 45 000x)

Graphene oxide flakes

Single graphene oxide flakes (average size is around 2 μm) dispersed on gold and silicon dioxide surface. Can be used for flexible electronics applications e.g. field effect transistors (FET), memristors, sensors.

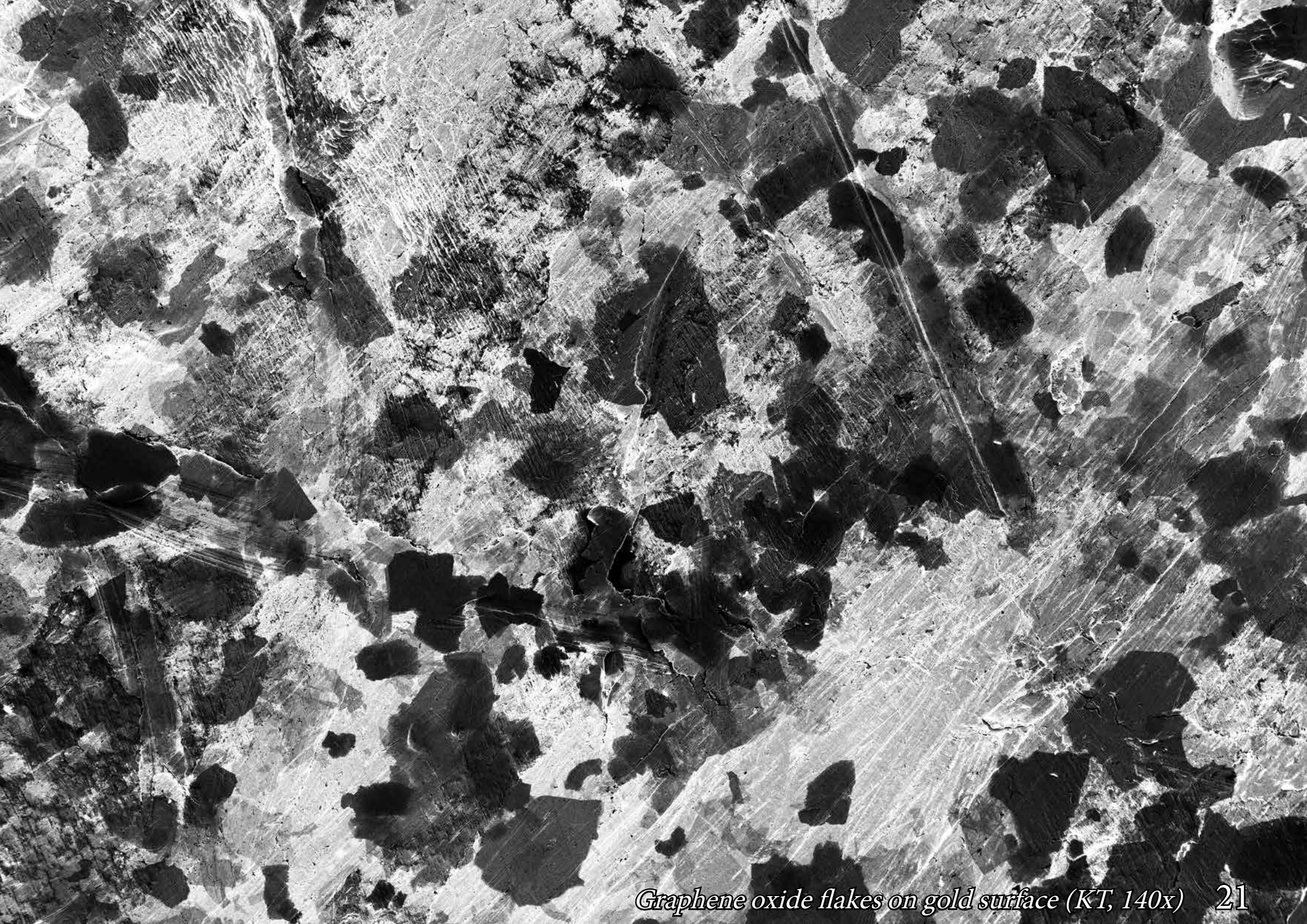

Graphene oxide flakes on gold surface (KT, 140x)

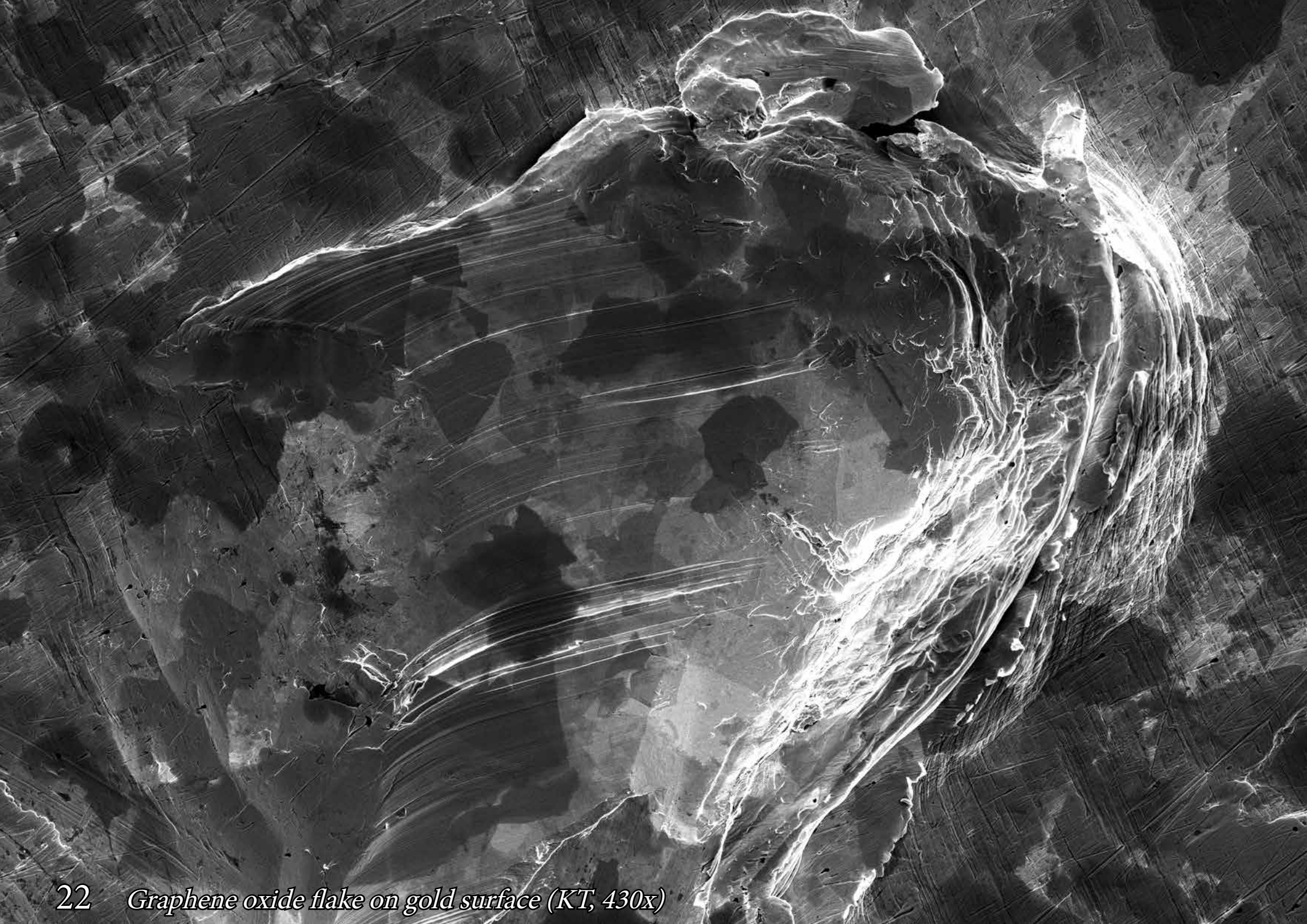

22 *Graphene oxide flake on gold surface (KT, 430x)*

Graphene oxide flakes on gold surface (KT, 430x)

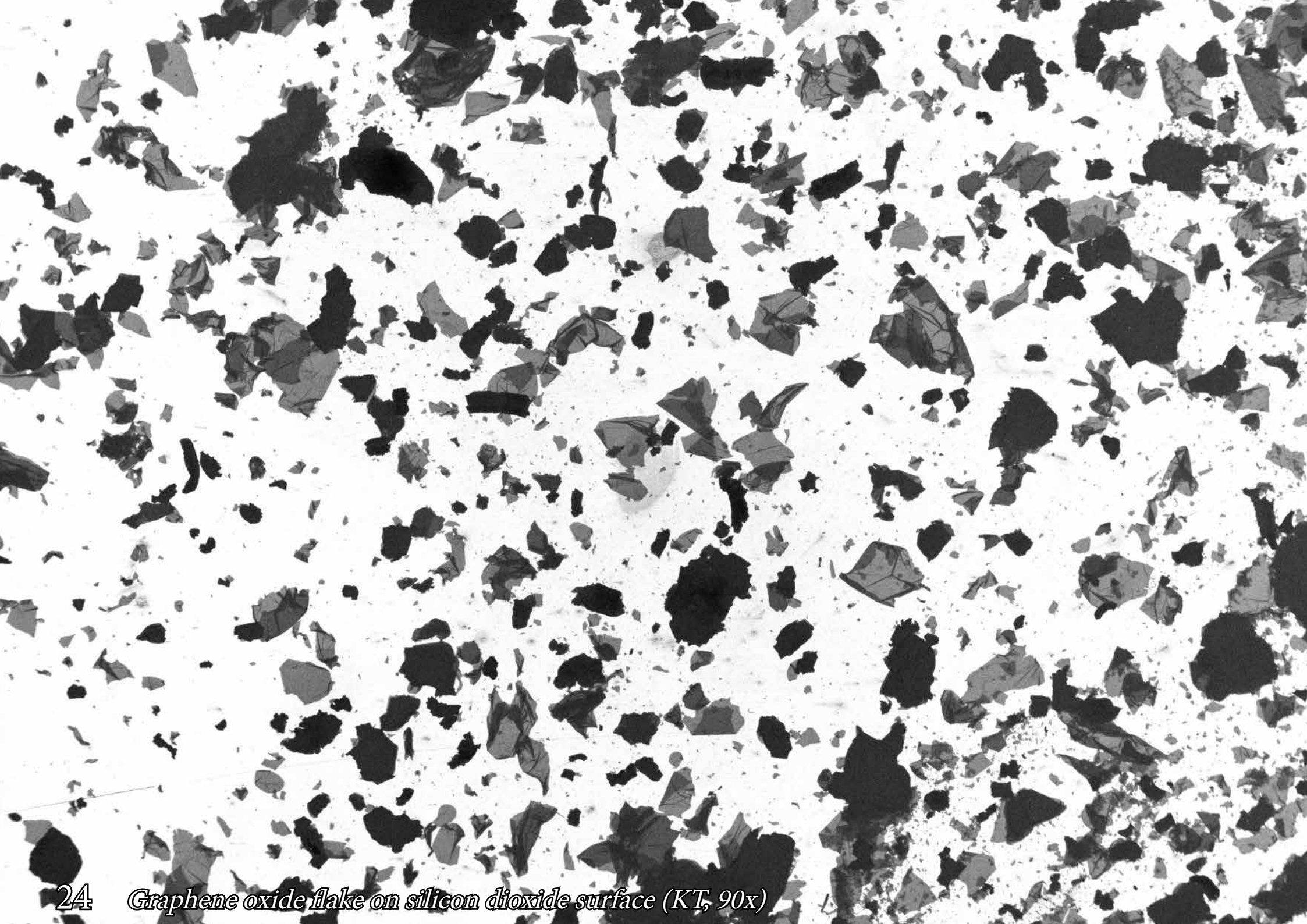

24 *Graphene oxide flake on silicon dioxide surface (KT, 90x)*

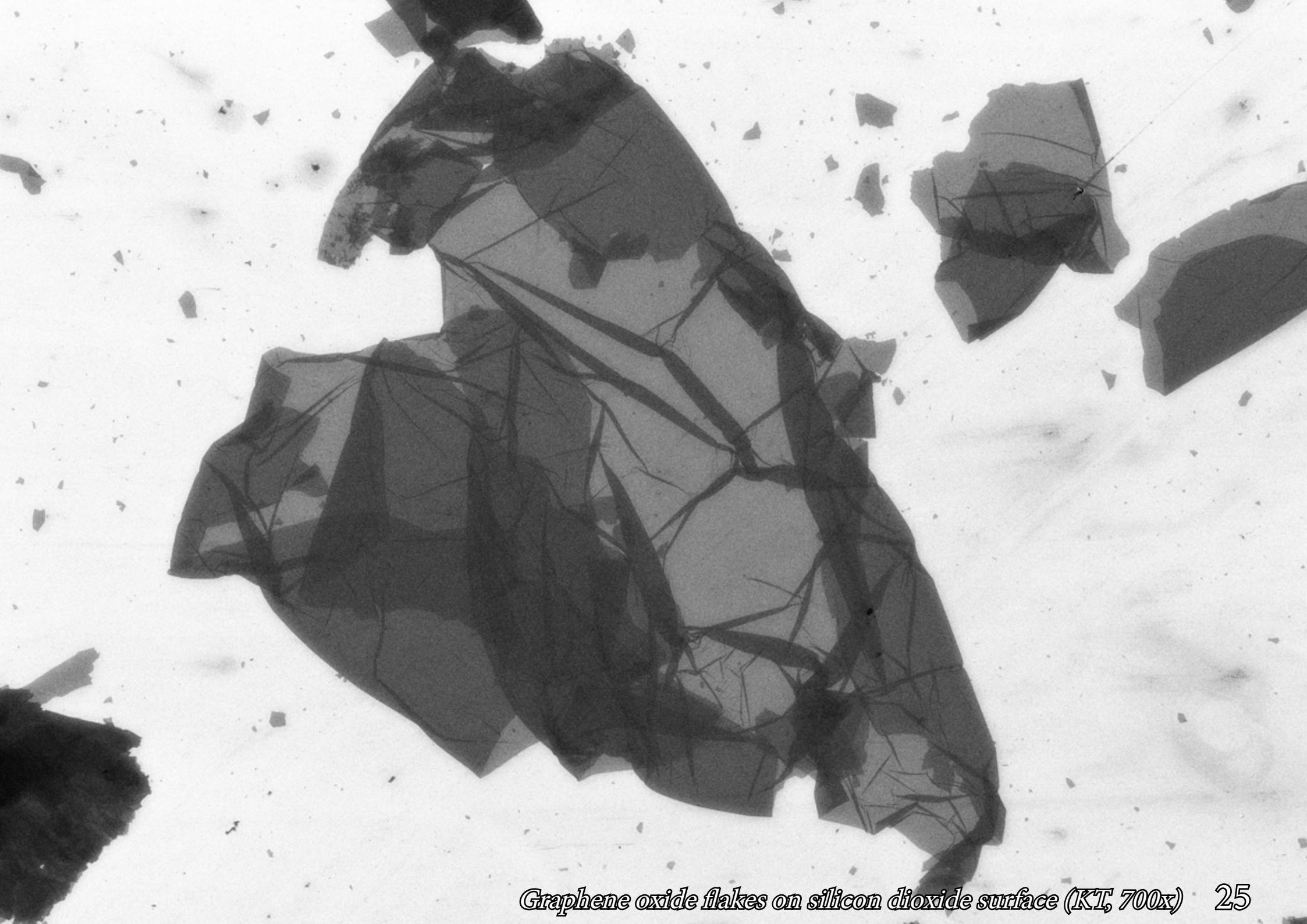

Graphene oxide flakes on silicon dioxide surface (KT, 700x)

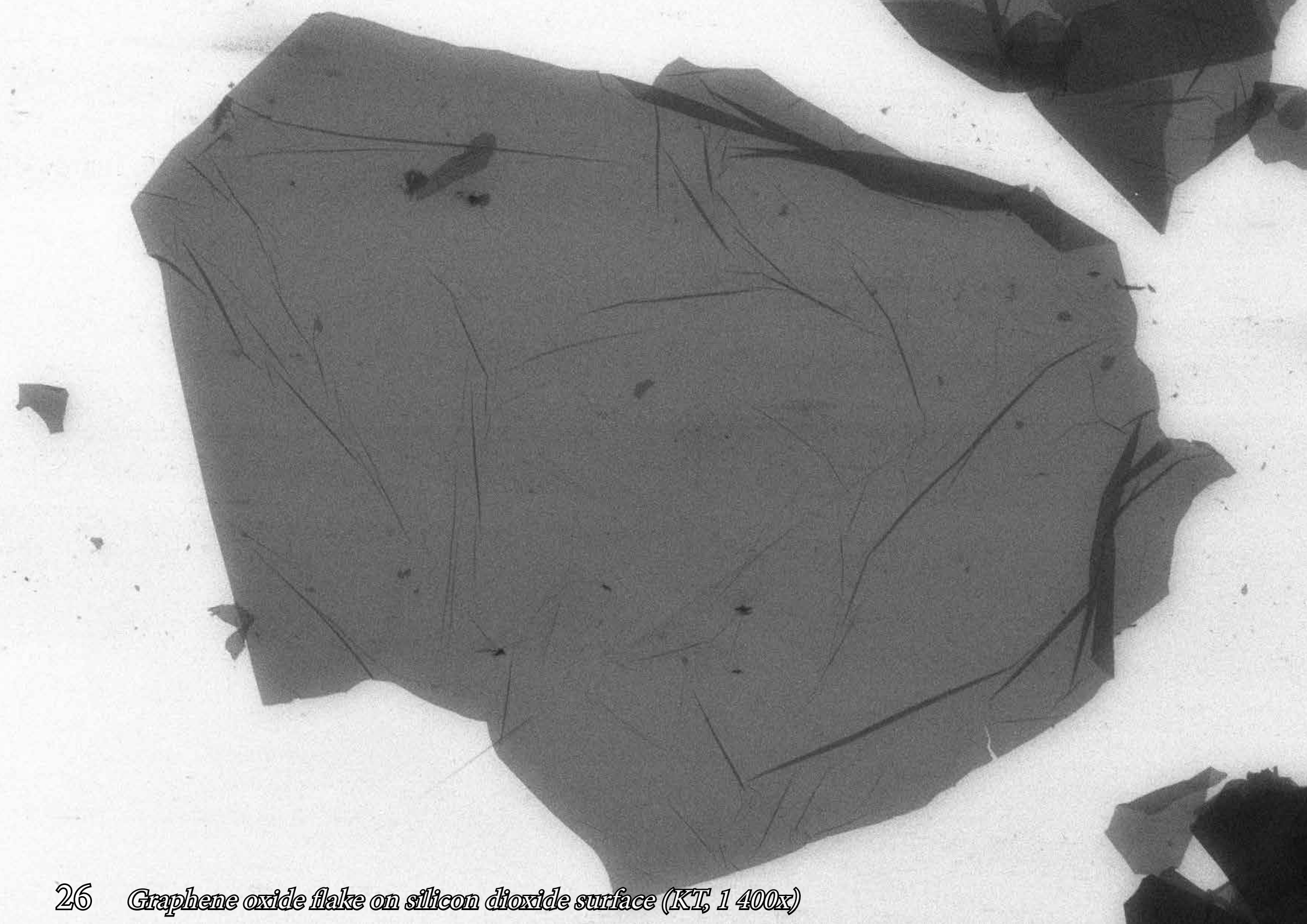

26 *Graphene oxide flake on silicon dioxide surface (KT, 1 400x)*

Graphene oxide paper

Vacuum dried graphene oxide paper is self-standing stack of graphene oxide flakes with size in the range of 0.9 - 46 μm. For scanning electron microscopy images, all samples were coated with a thin layer of gold (~10 nm).

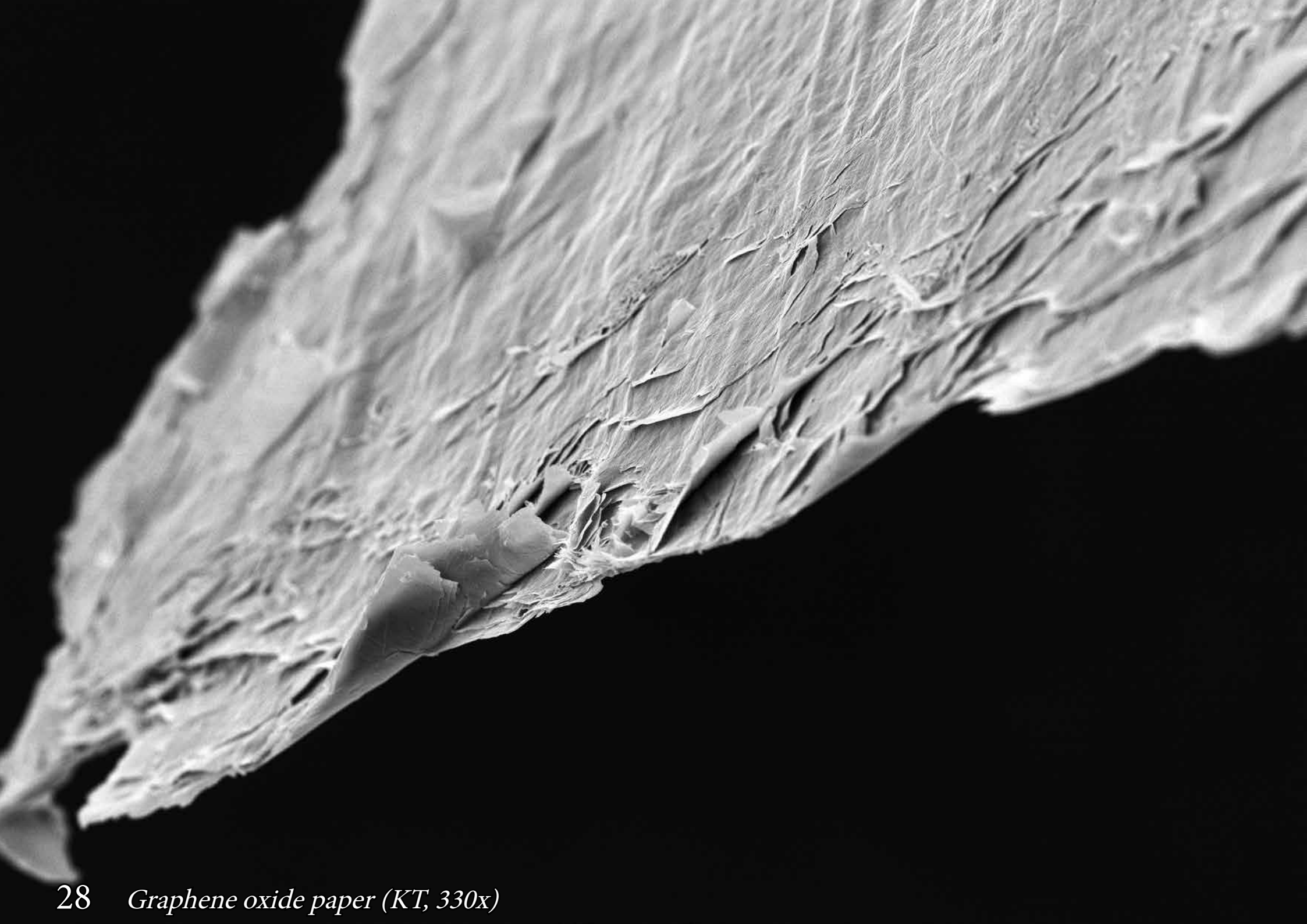

28 *Graphene oxide paper (KT, 330x)*

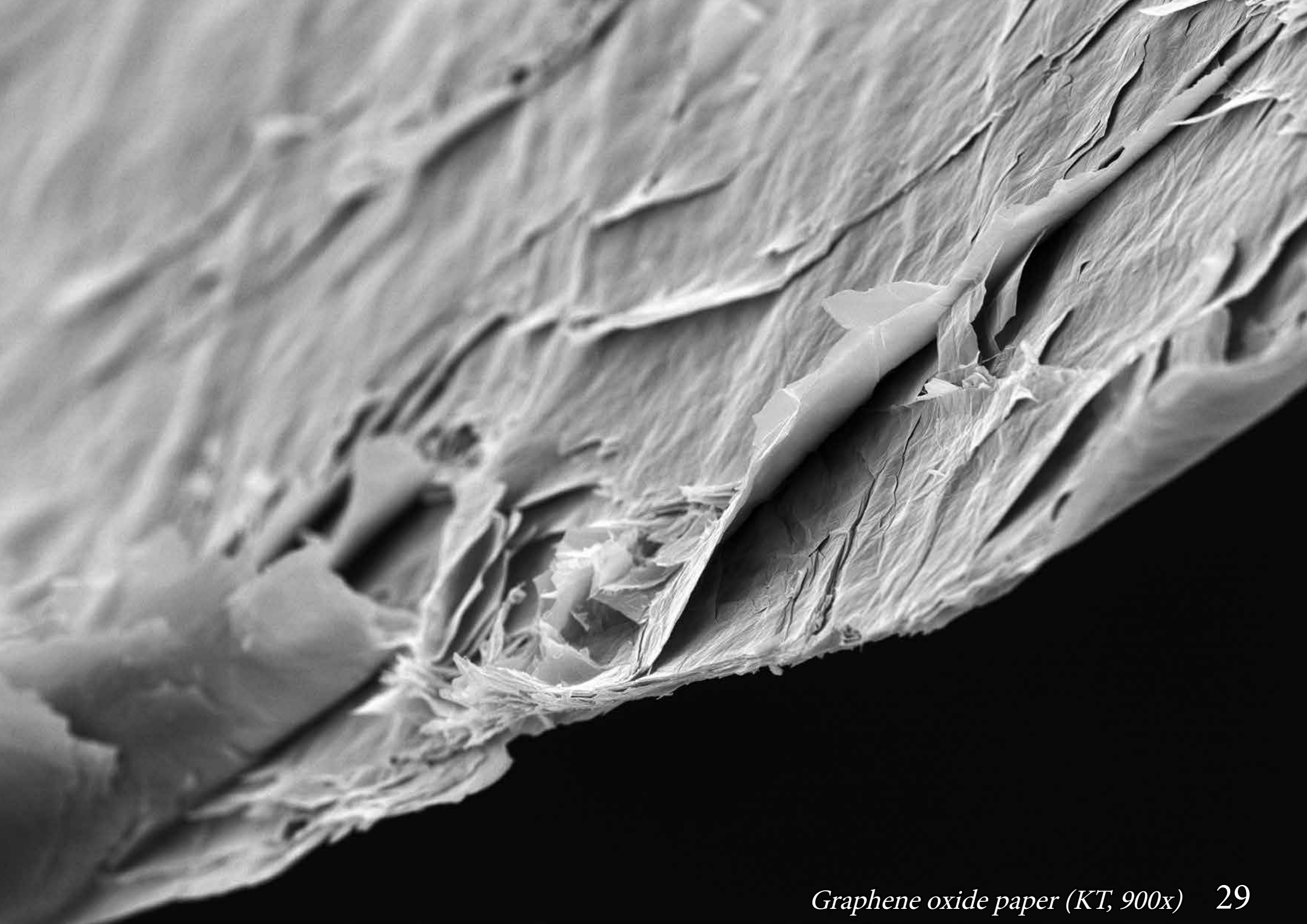

Graphene oxide paper (KT, 900x)

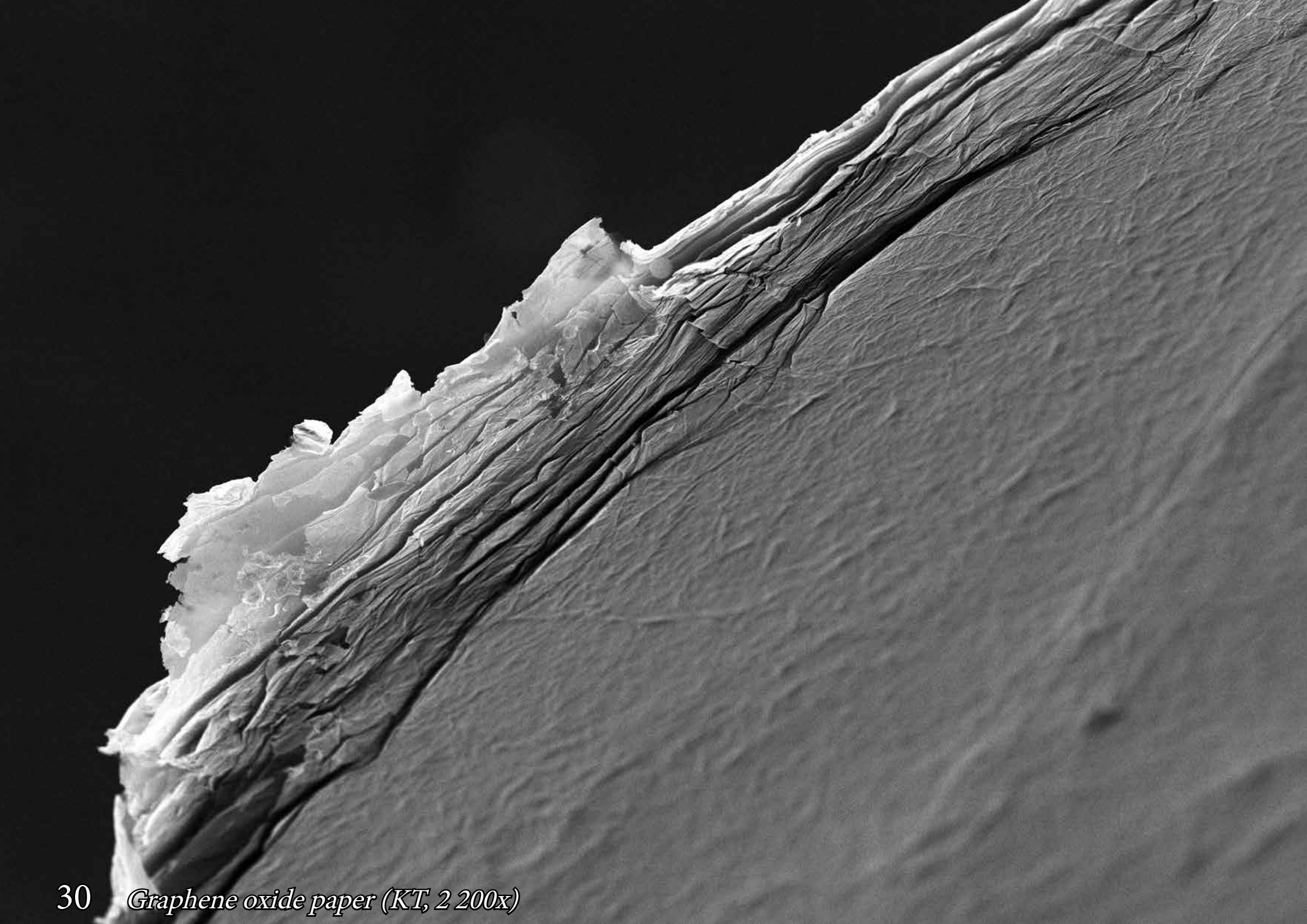

 Graphene oxide paper (KT, 2 200x)

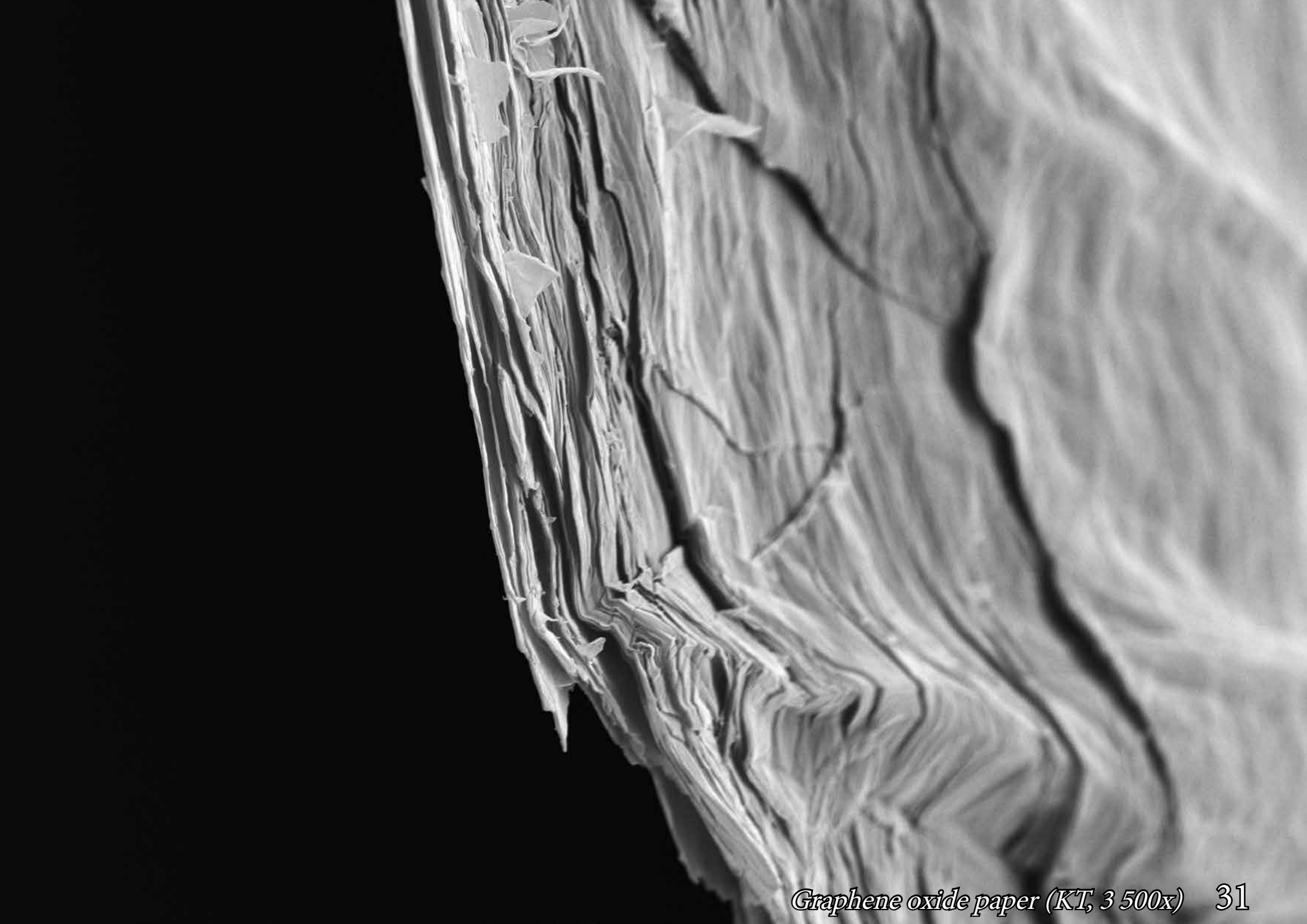

Graphene oxide paper (KT, 3 500x)

Graphite oxide framework

Graphite oxide layers (GO) are linked together by specific organic compounds, forming graphite oxide framework (GOF) material. Such materials have rigid, ordered structure, developed surface area, regular and well defined pore size, depending on the linkers chosen. It is a promising material for hydrogen storage application. The average size of flakes is 500 μm.

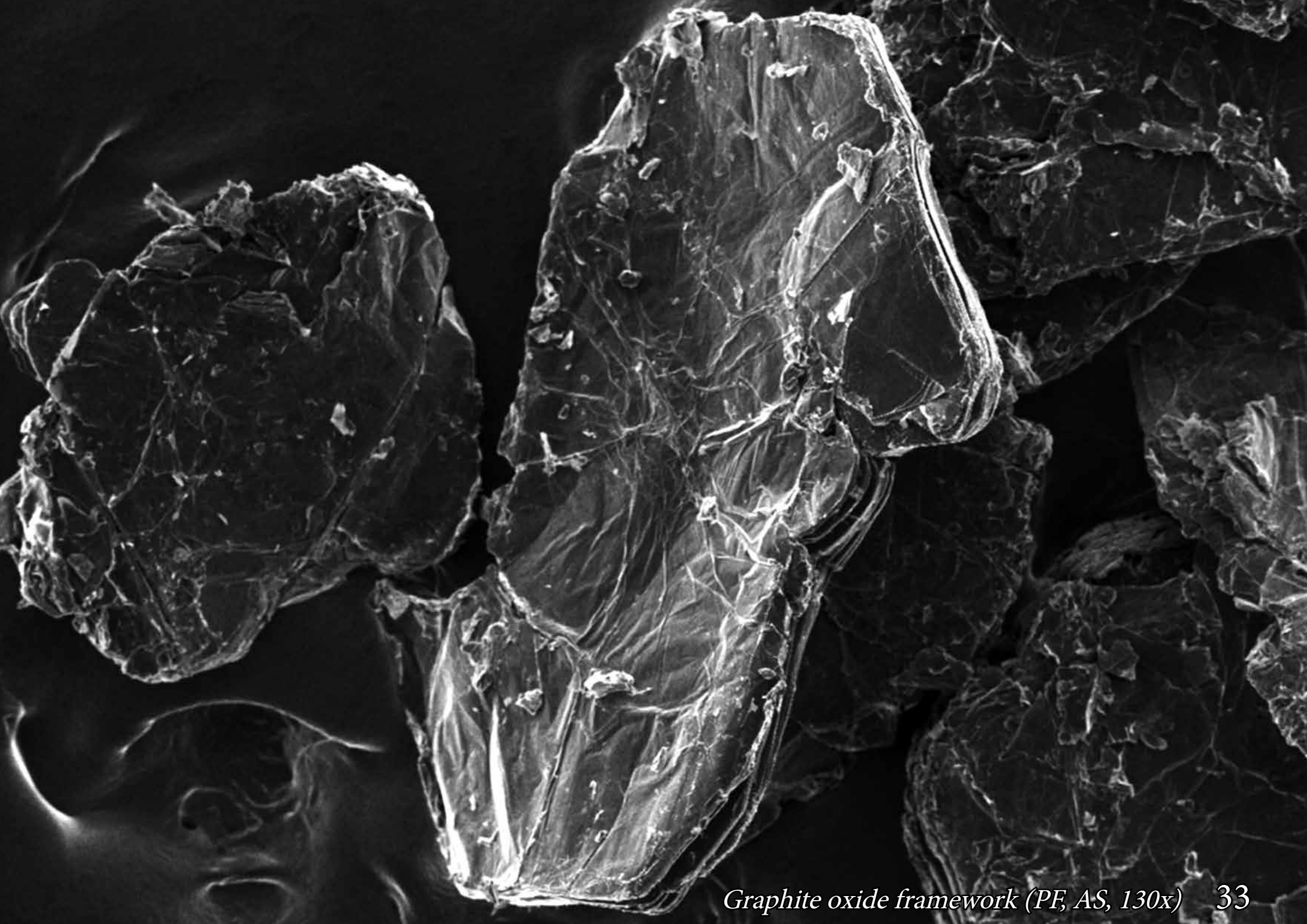

Graphite oxide framework (PF, AS, 130x)

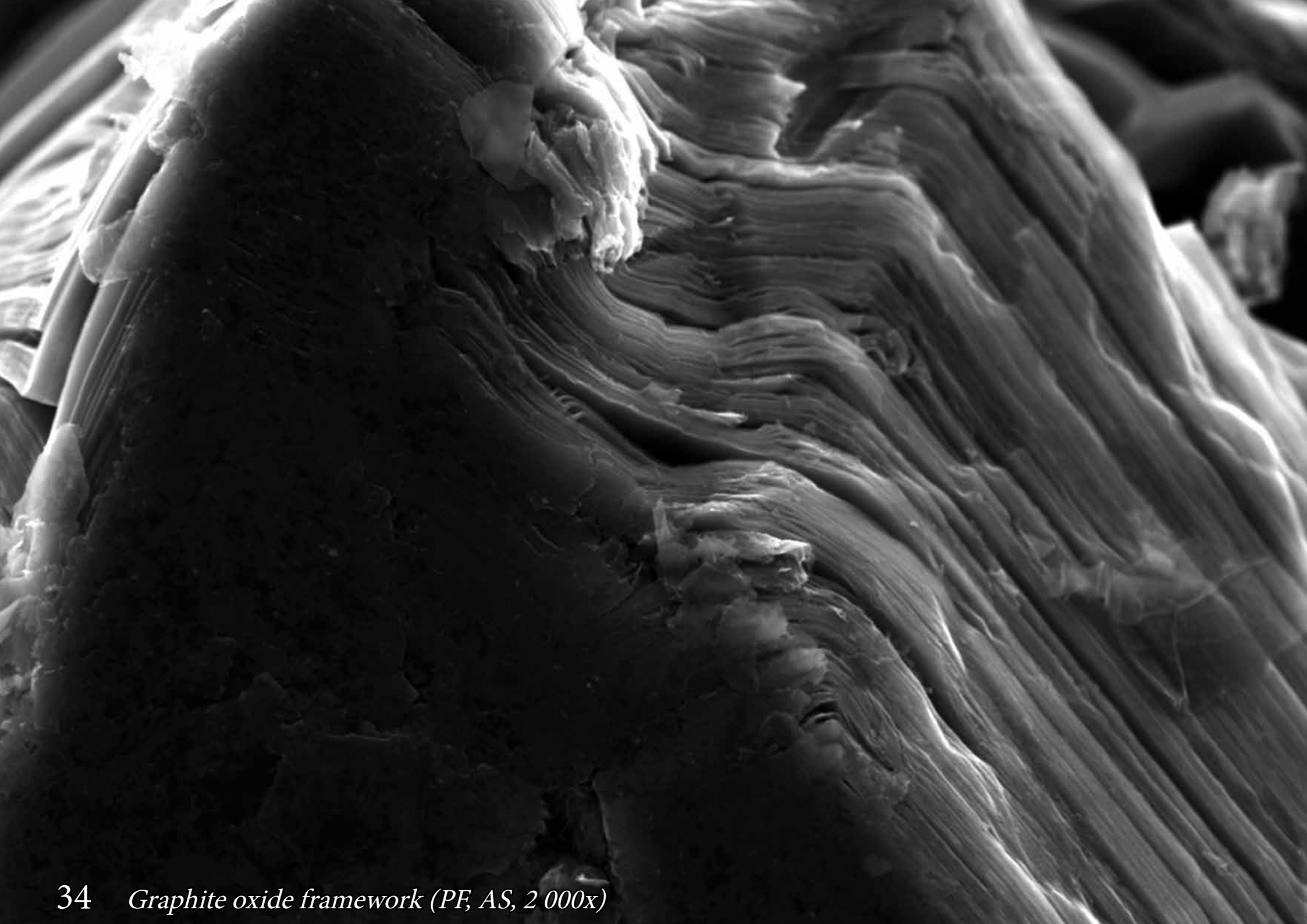

34 *Graphite oxide framework (PF, AS, 2 000x)*

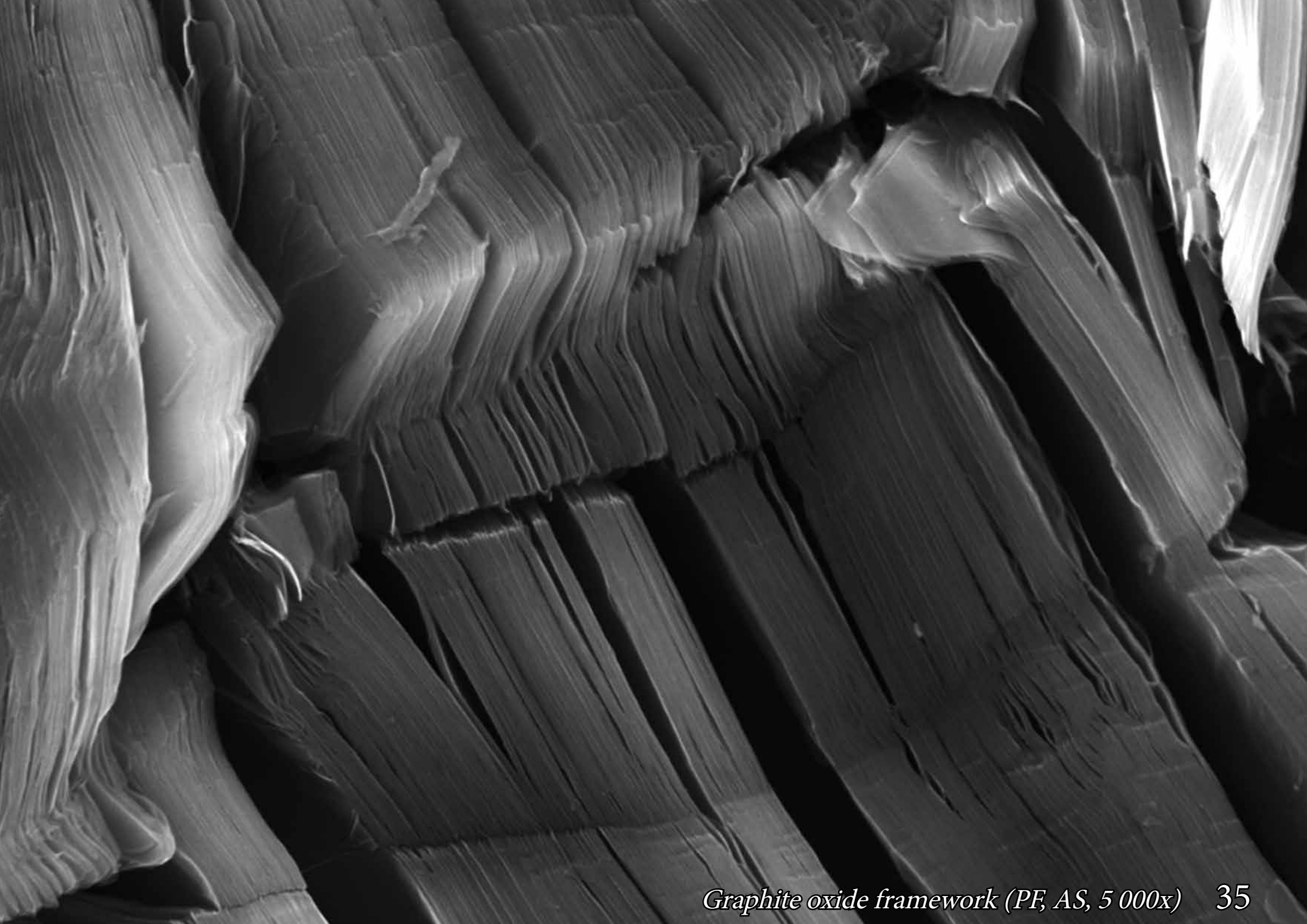

Graphite oxide framework (PF, AS, 5 000x)

MAX phases and MXenes

Scanning electron microscopy images of Ti_3AlC_2 sintered MAX phases in form of nanoparticles and pallets, and $Ti_3C_2T_x$ MXene prepared via hydrofluoric acid etching of Al compound from parental MAX phases.

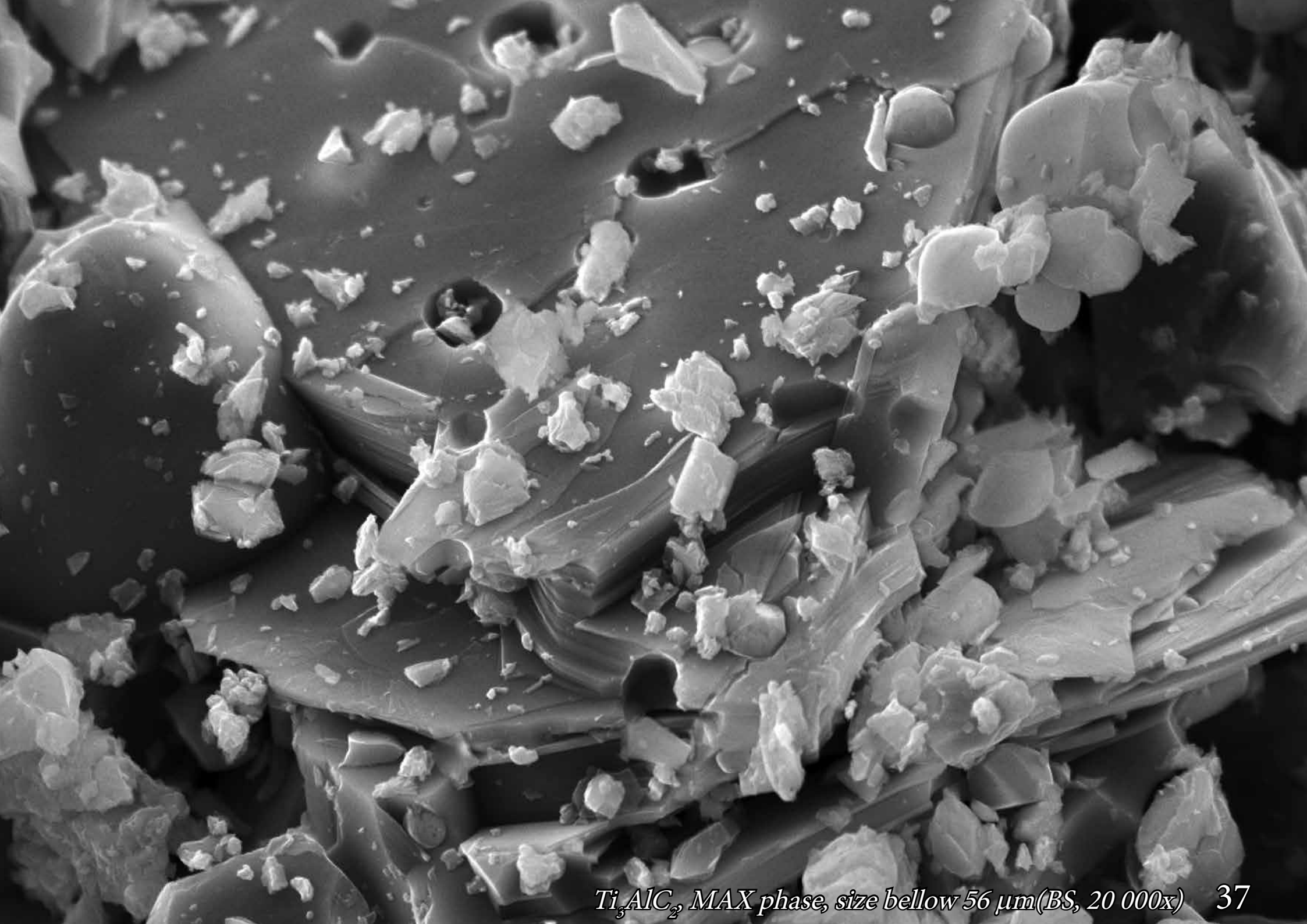

Ti_3AlC_2, MAX phase, size bellow 56 µm(BS, 20 000x)

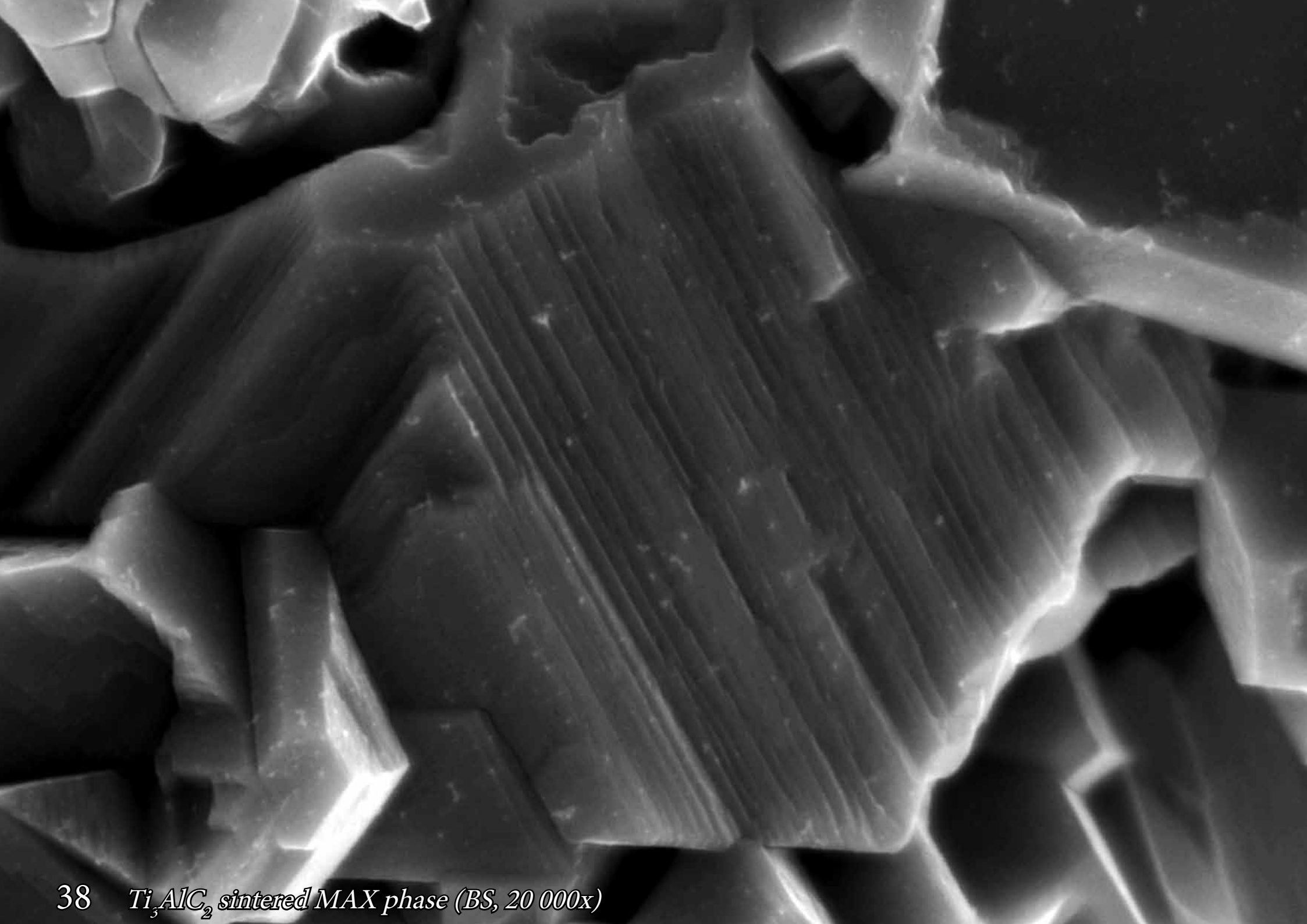

38 *Ti_3AlC_2 sintered MAX phase (BS, 20 000x)*

$Ti_3C_2T_x$ MXene (BS, 20 000x) 39

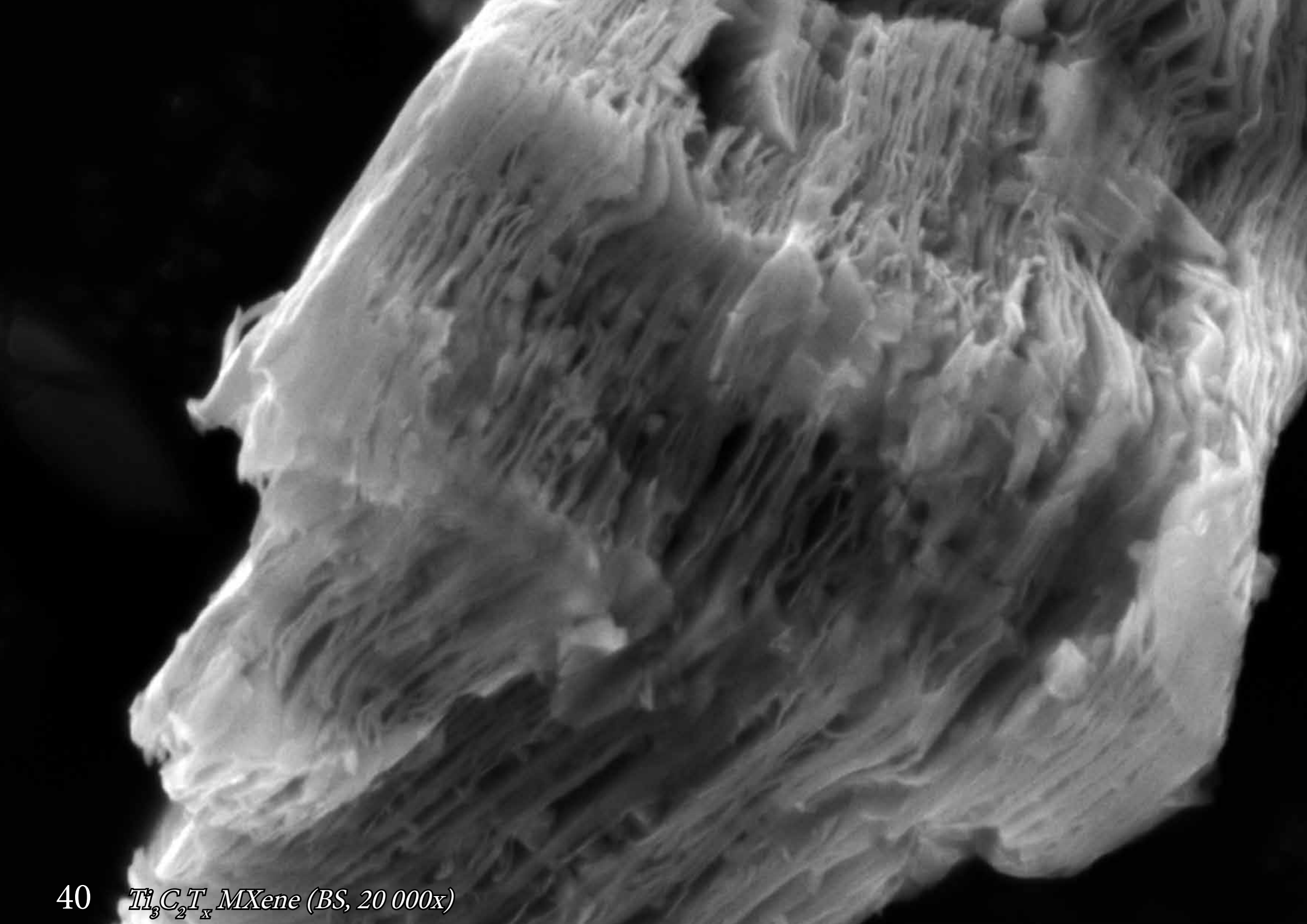

40 $Ti_3C_2T_x$ MXene (BS, 20 000x)

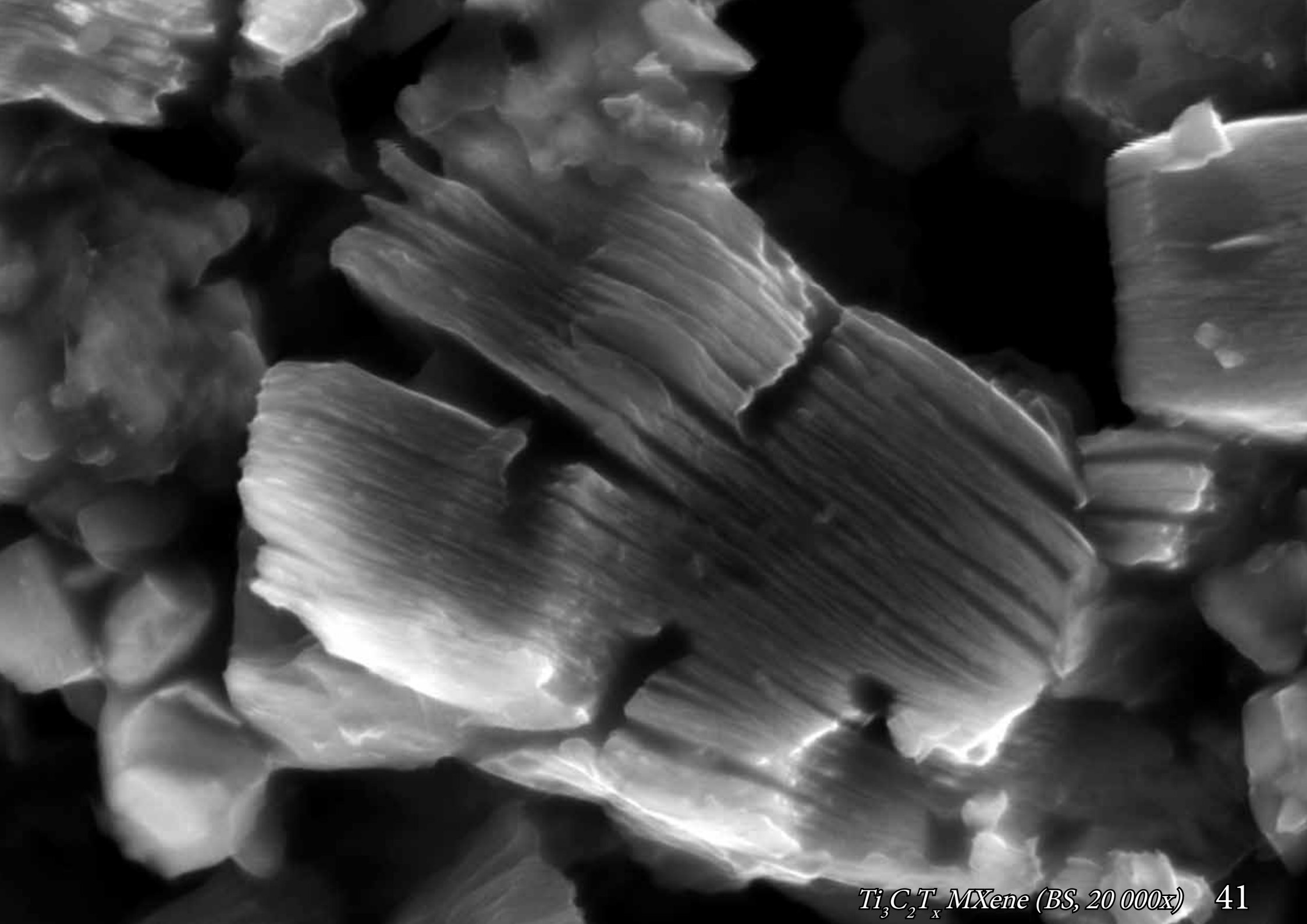

$Ti_3C_2T_x$ MXene (BS, 20 000x) 41

MXene phases composite

Multi-layered MXene structures were deposited by dip coating layer-by-layer technique (LBL) on pre-made electrospun polymeric fibres. Scanning electron microscopy images exhibit the distribution of $Ti_3C_2T_x$ particles within the pre-formed scaffold, typically used for tissue engineering applications.

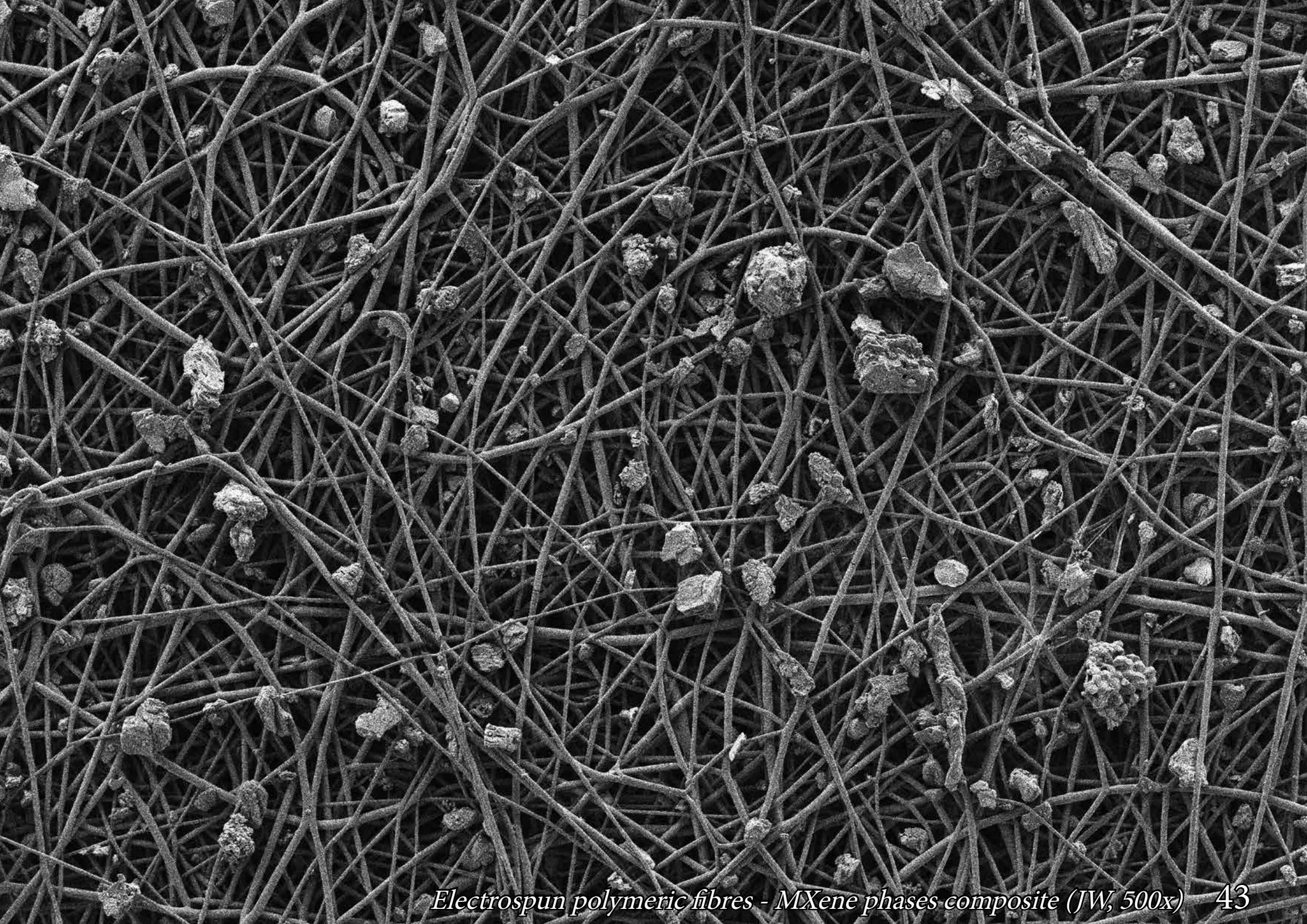

Electrospun polymeric fibres - MXene phases composite (JW, 500x)

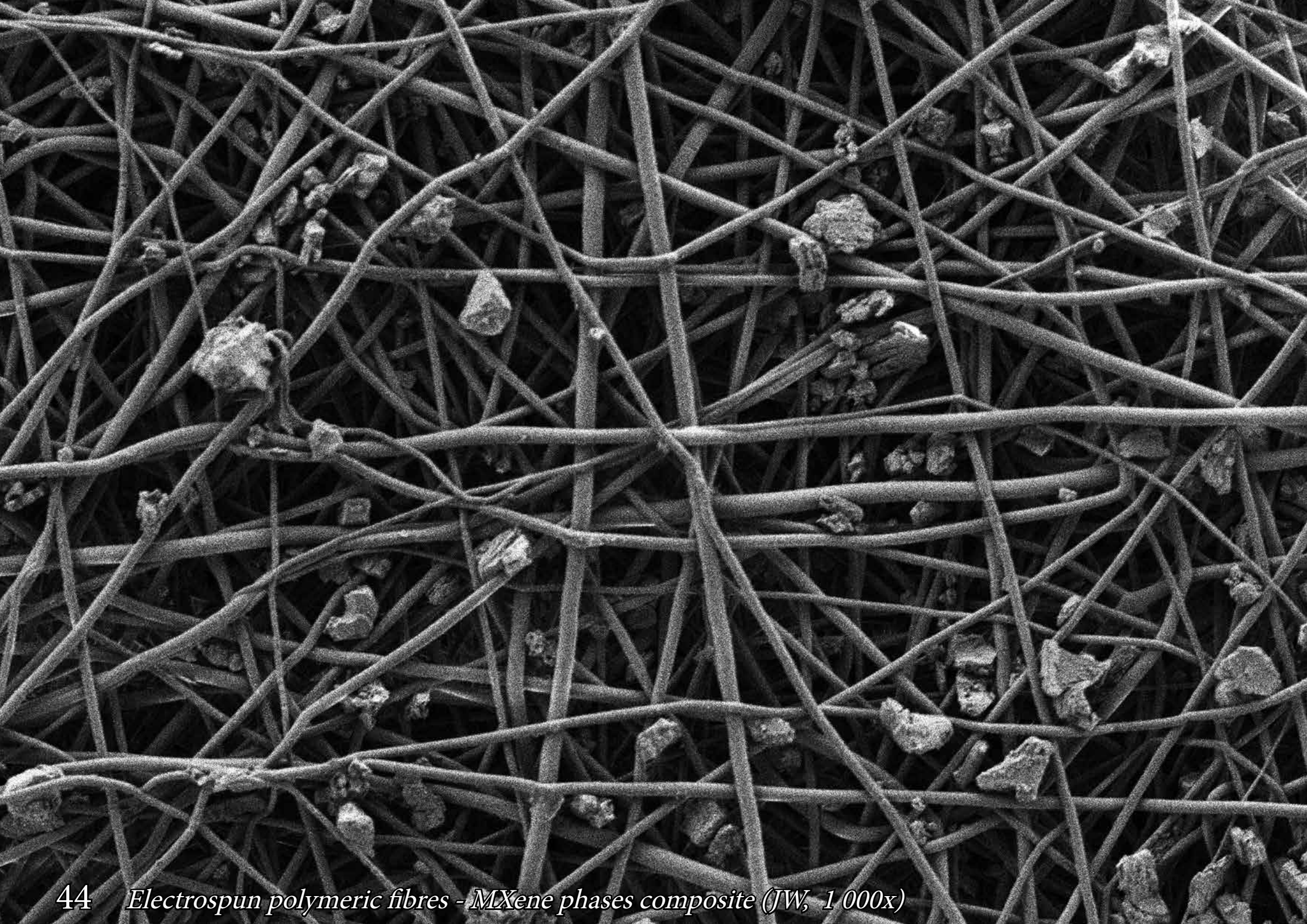

44 *Electrospun polymeric fibres - MXene phases composite (JW, 1 000x)*

Electrospun polymeric fibres - MXene phases composite (JW, 500x)

Human cells on graphene oxide paper

Non-malignant human embryonic kidney (HEK-293) and human malignant neuroblastoma (SH-SY5Y) cell lines were chosen for evaluation of their attachment on graphene oxide paper. HEK cells colonized the surface of graphene oxide paper more efficiently than neuroblastoma.

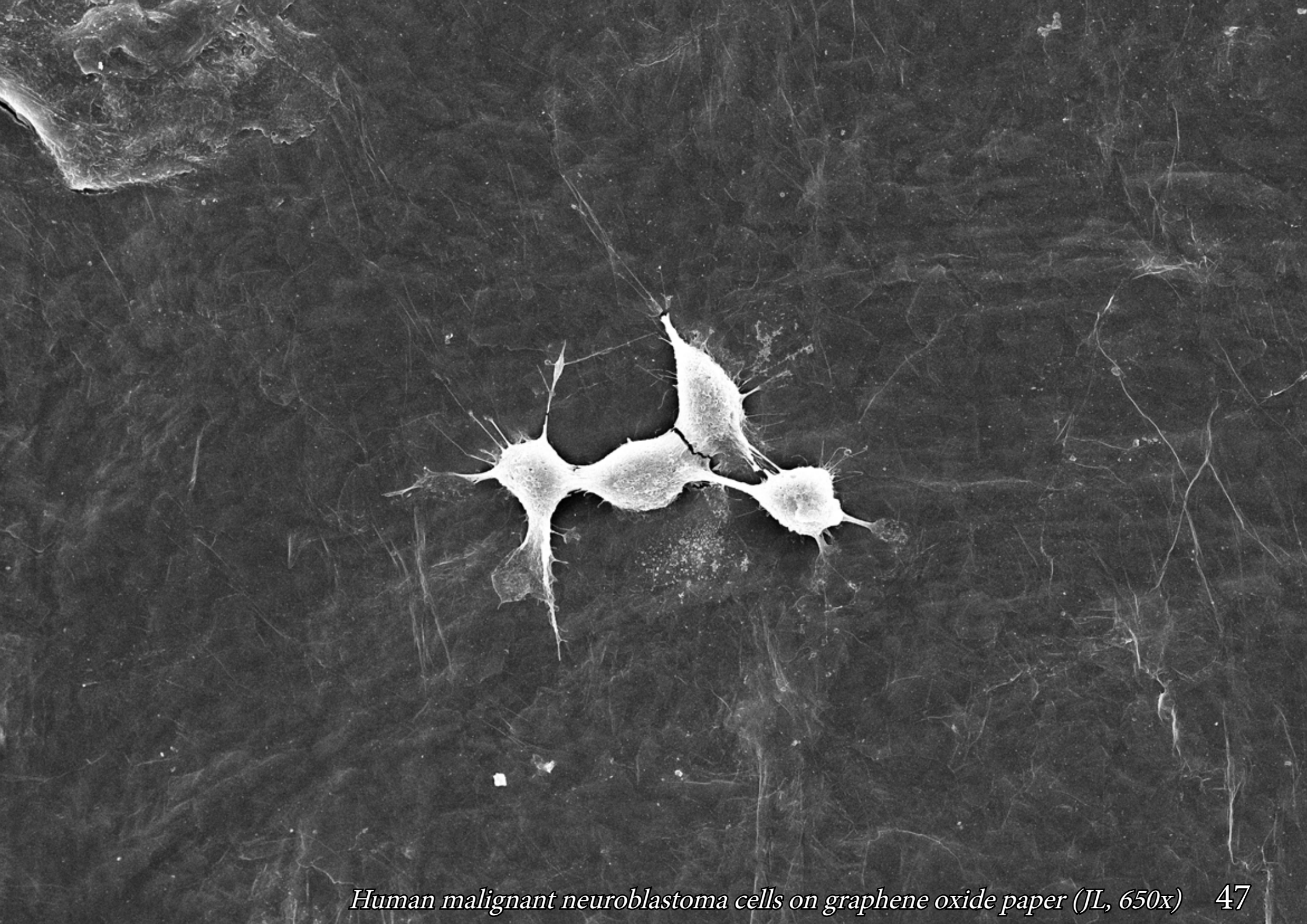

Human malignant neuroblastoma cells on graphene oxide paper (JL, 650x)

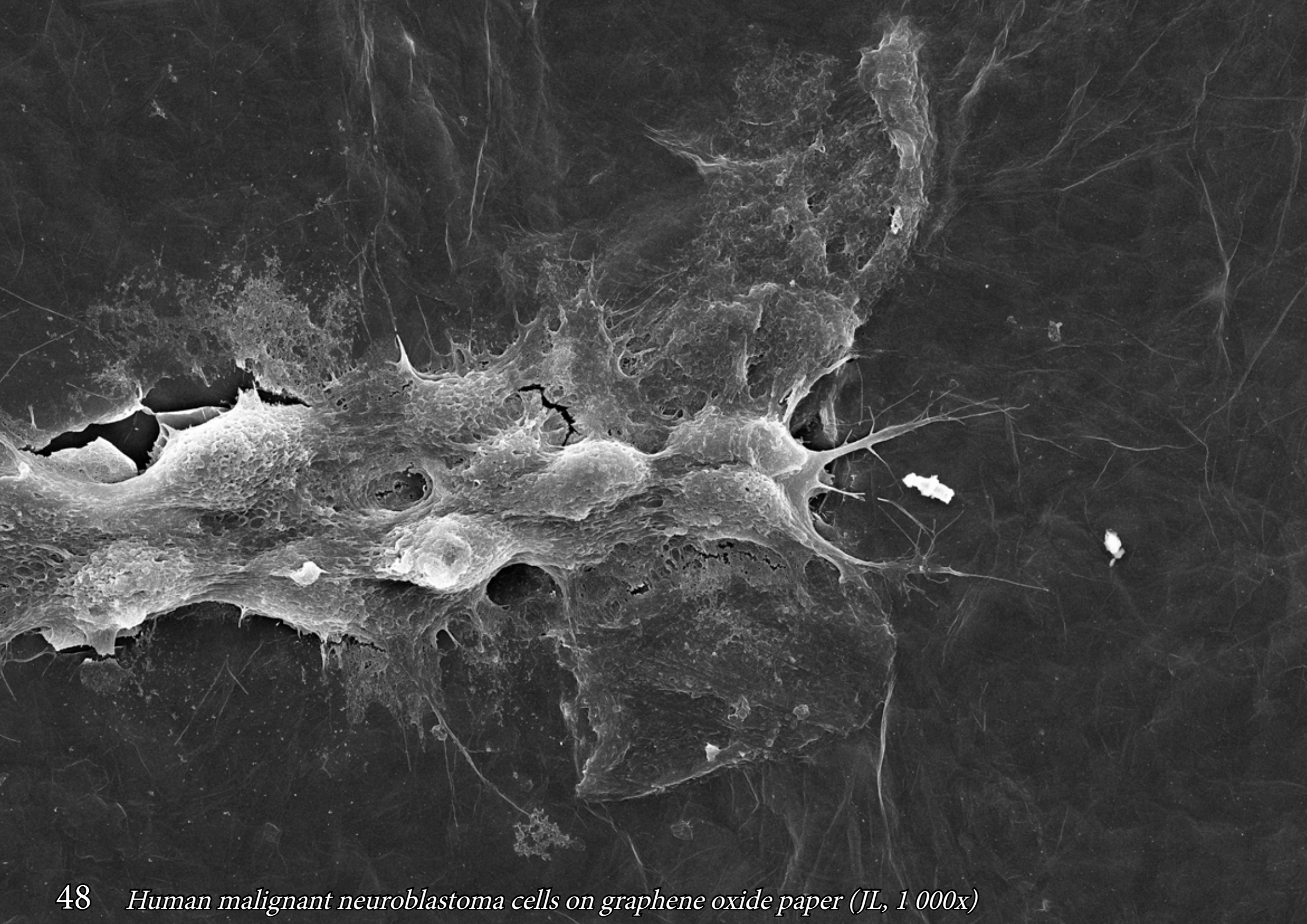

48 *Human malignant neuroblastoma cells on graphene oxide paper (JL, 1 000x)*

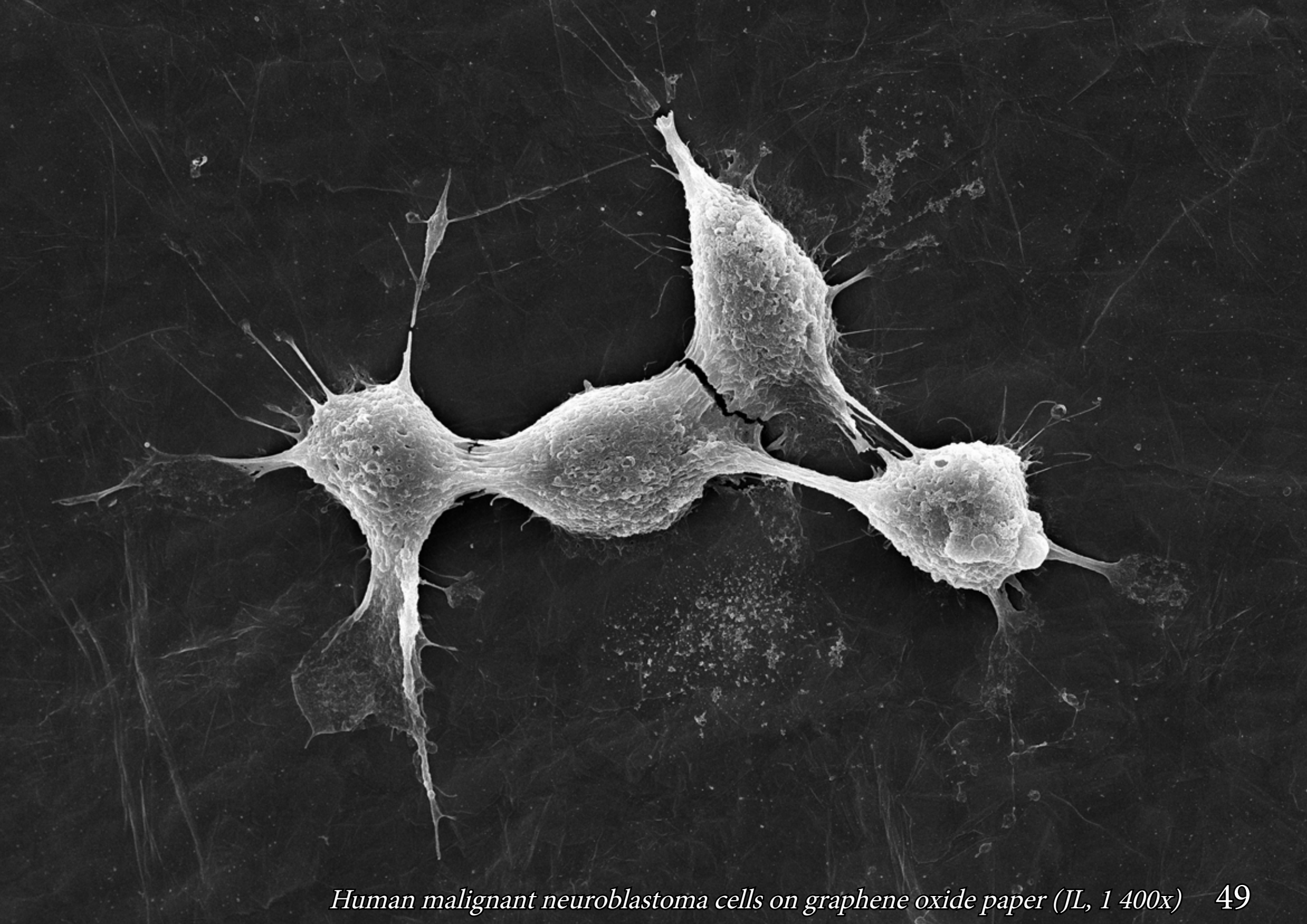

Human malignant neuroblastoma cells on graphene oxide paper (JL, 1 400x)

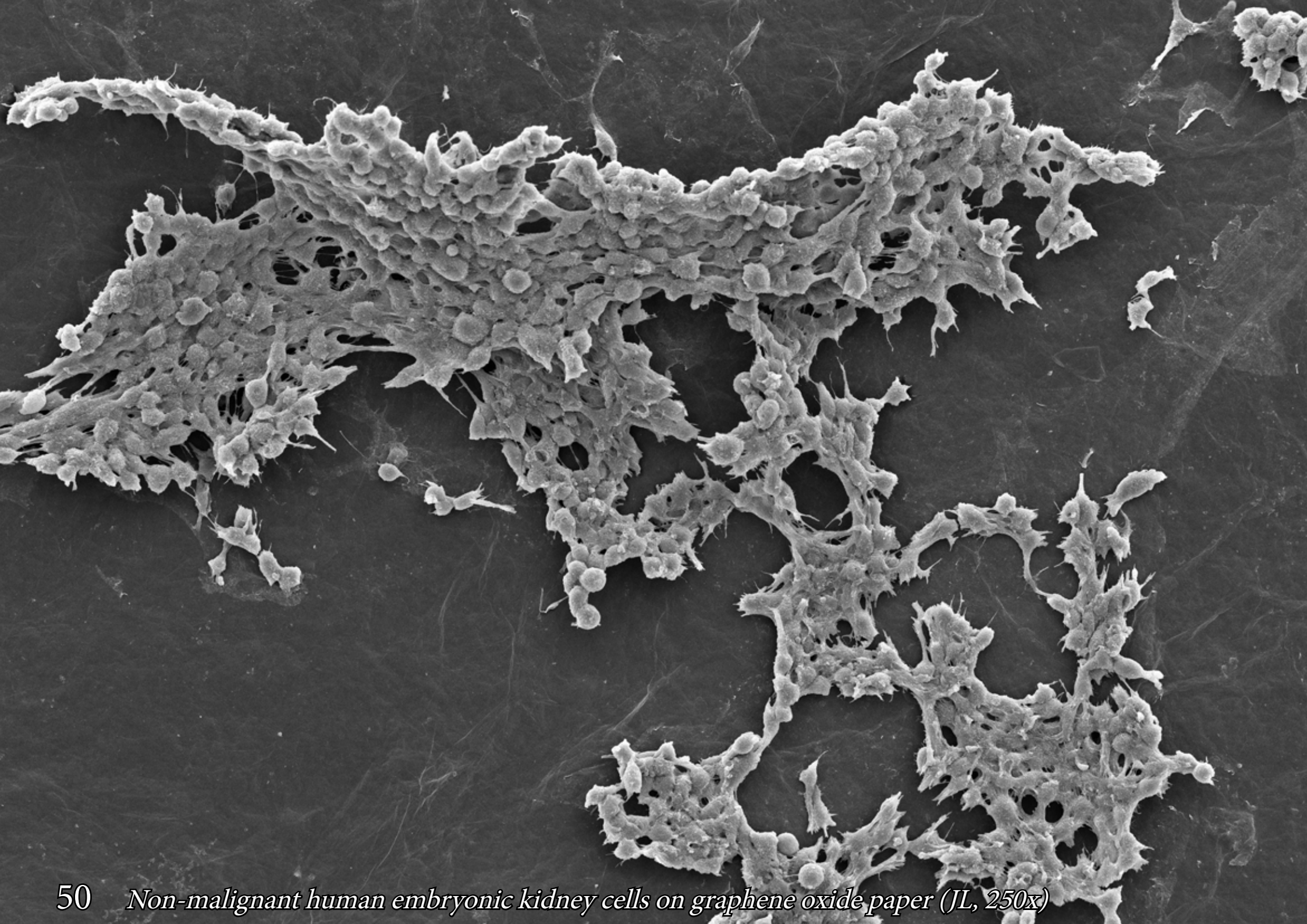

50 *Non-malignant human embryonic kidney cells on graphene oxide paper (JL, 250x)*

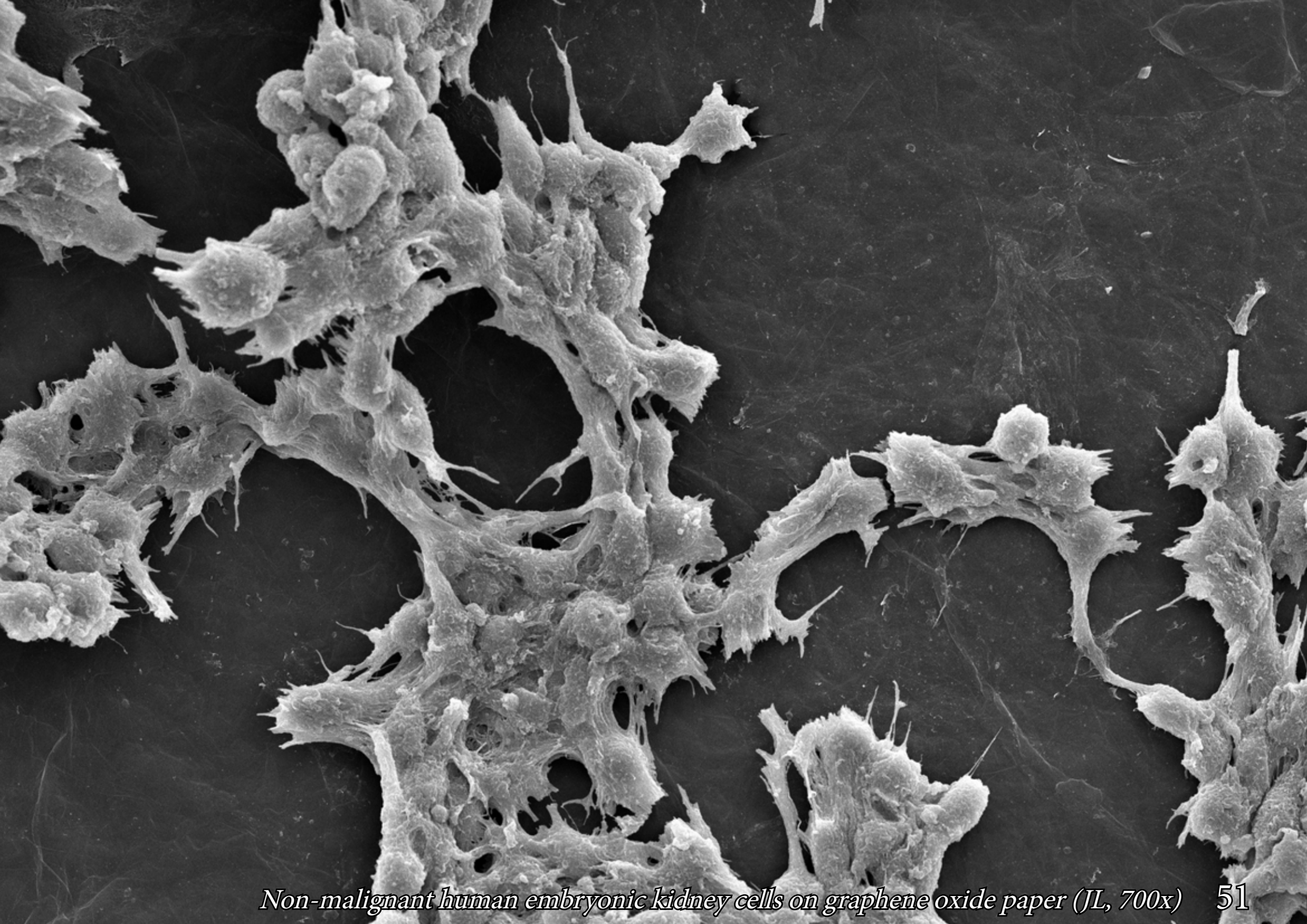

Non-malignant human embryonic kidney cells on graphene oxide paper (JL, 700x)

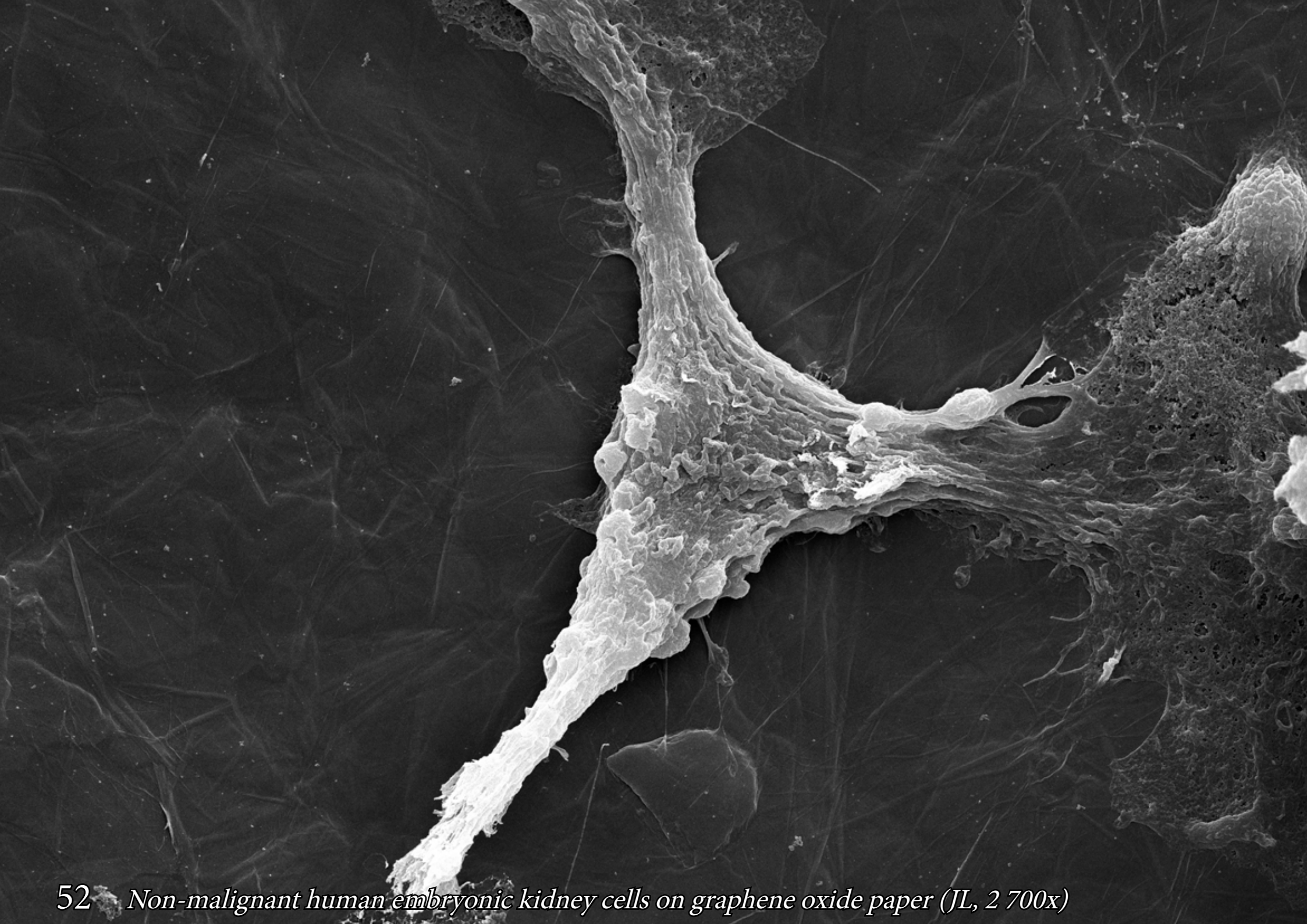

 Non-malignant human embryonic kidney cells on graphene oxide paper (JL, 2 700x)

Graphene oxide aerogels

Gels are porous solid state structures filled with liquid or gas. If the liquid is removed and the volume of the dried solid state structure is maintained then this structure is called an aerogel. Next few slides show aerogels made of connected graphene oxide flakes. This interconnection is mediated through oxygen functionalities such as: carboxyl (-COOH) or hydroxyl (-OH) groups.

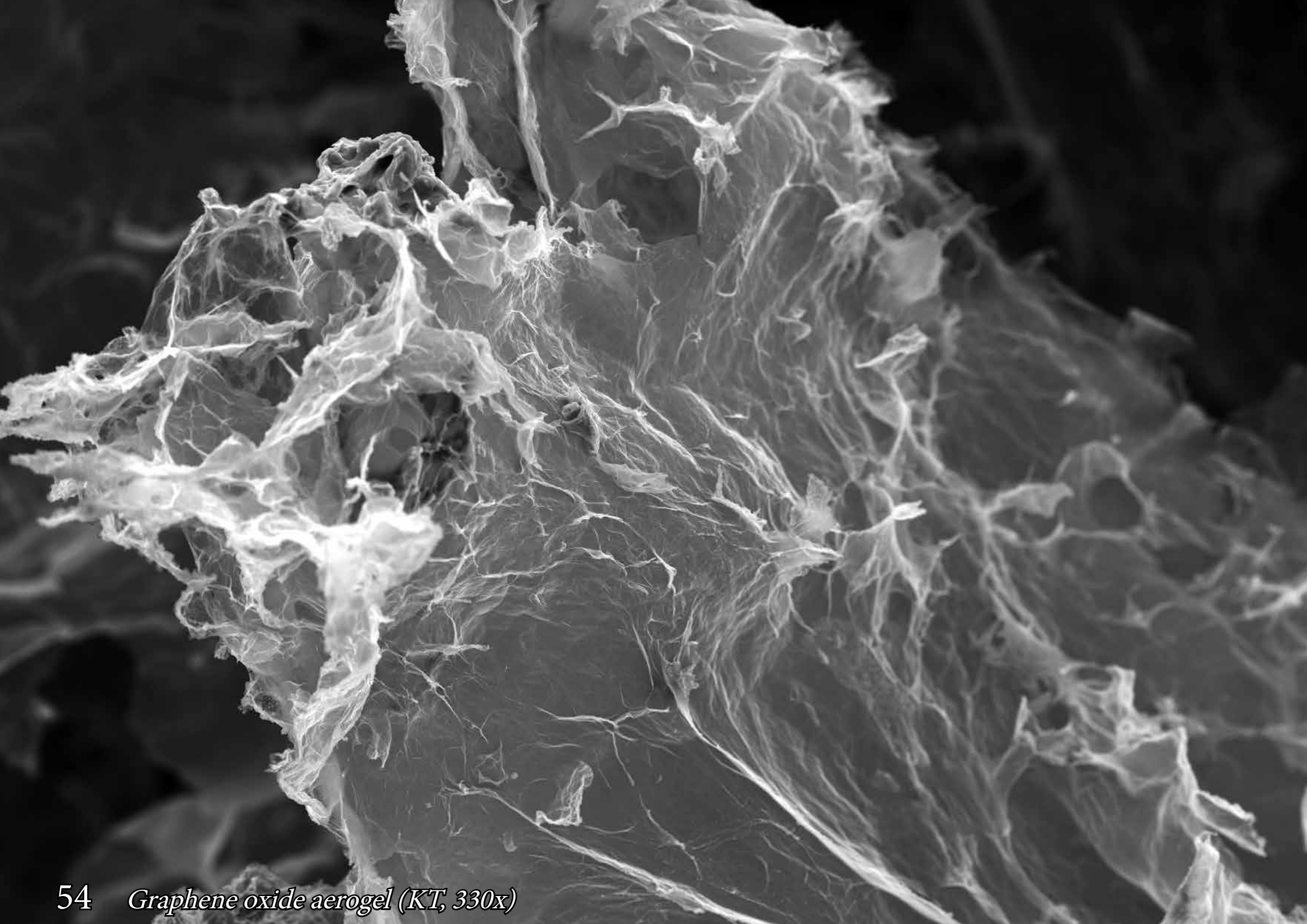

54 *Graphene oxide aerogel (KT, 330x)*

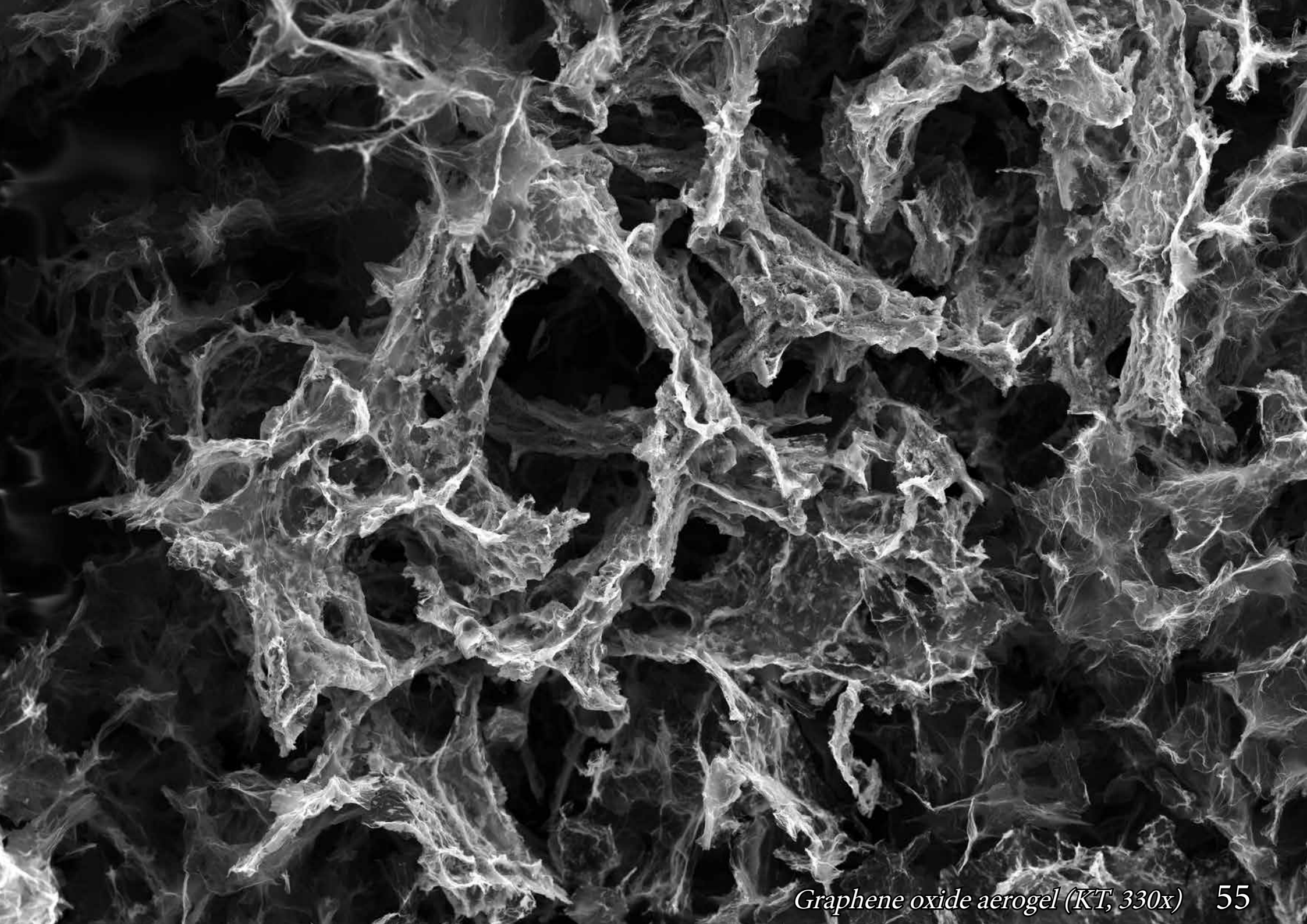

Graphene oxide aerogel (KT, 330x)

56 *Graphene oxide aerogel (KT, 600x)*

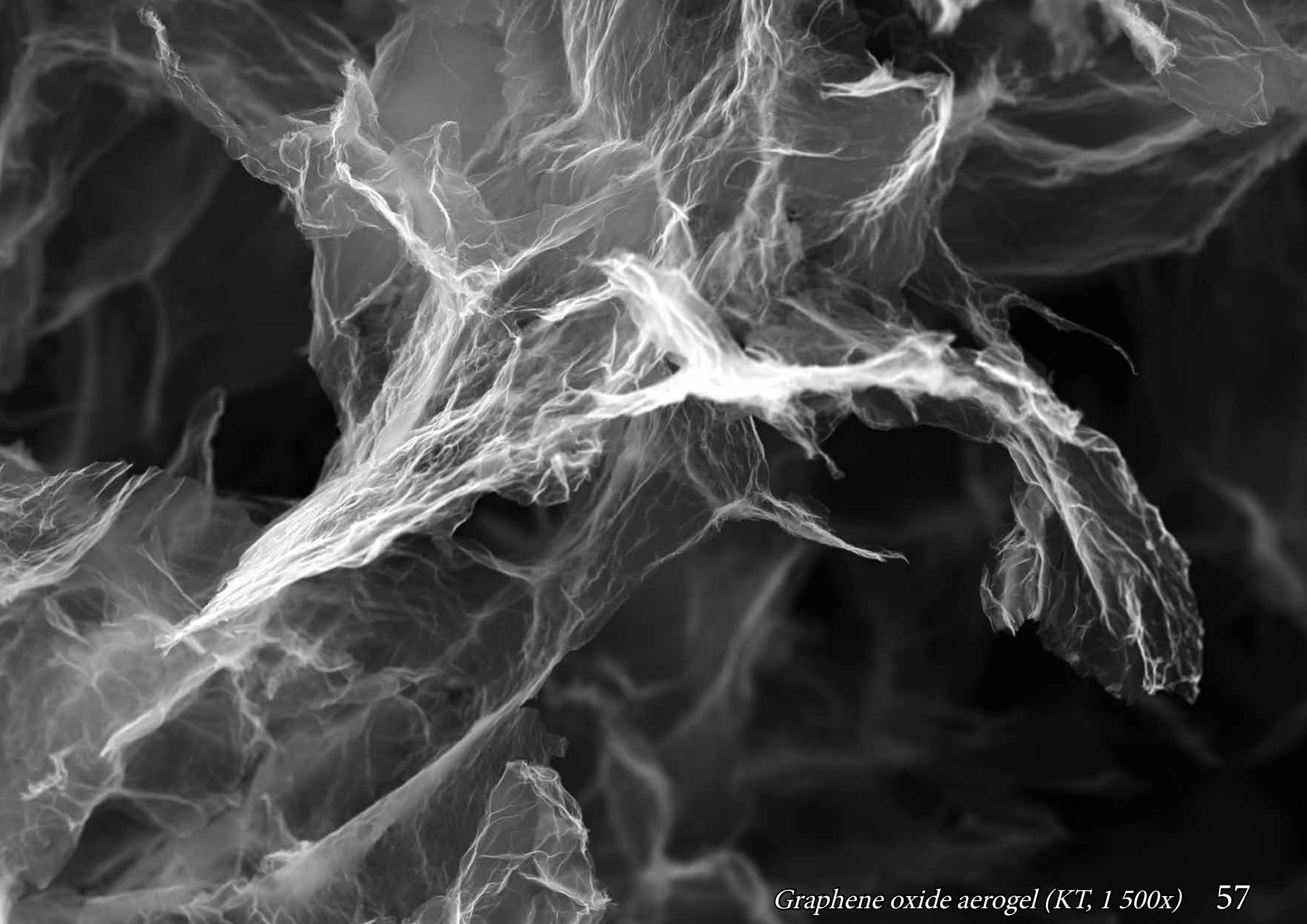

Graphene oxide aerogel (KT, 1 500x)

Graphene oxide fibers

As earlier mentioned, aerogles are dry solid state structures left intact during drying procedure (almost unchanged volume), however one can ask what happens when the structure collapses? Collapsed aerogels are called xerogels, which can be formed into many shapes including fibers, shown in the subsequent images.

Graphene oxide fiber (KT, 250x)

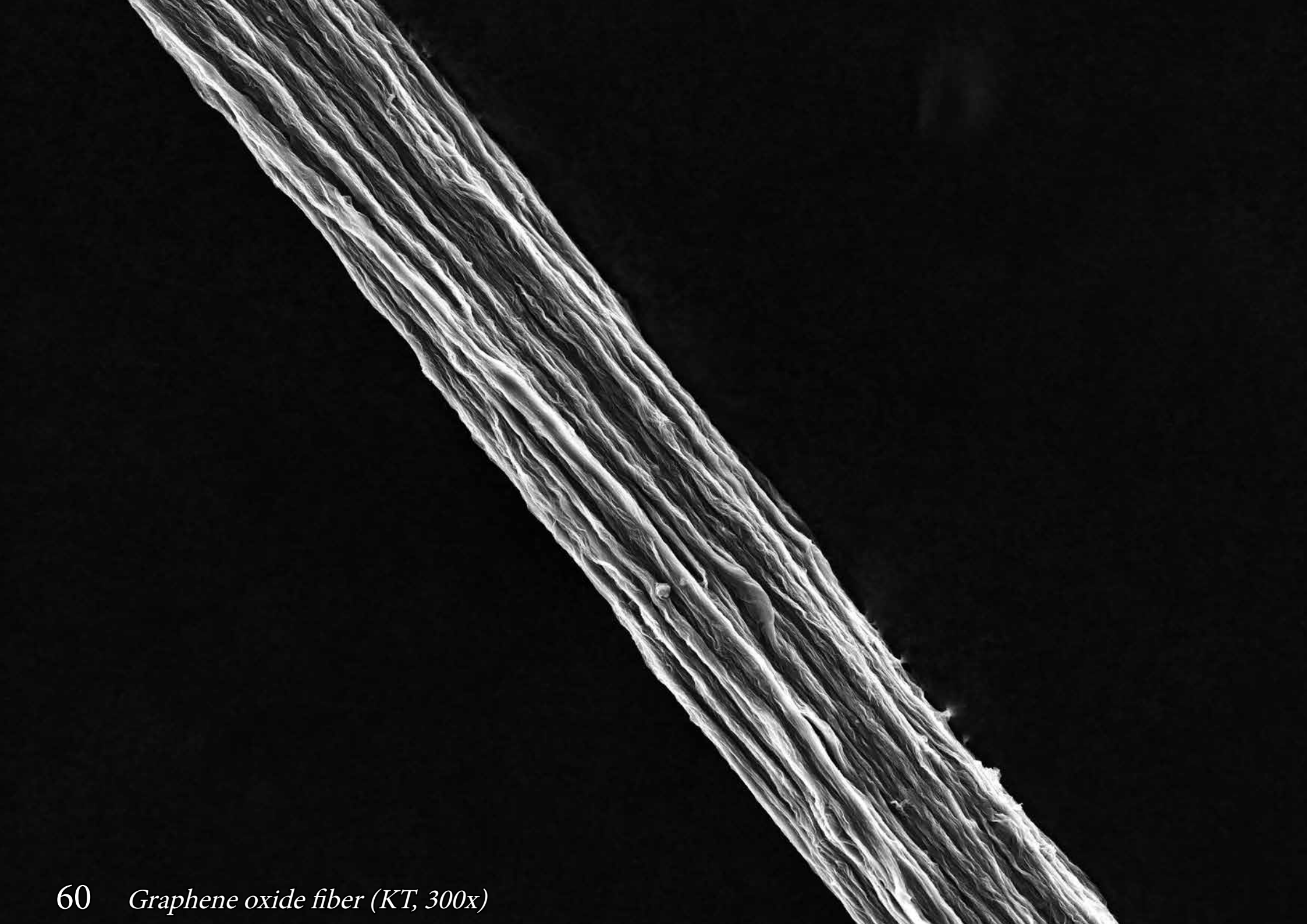

60 *Graphene oxide fiber (KT, 300x)*

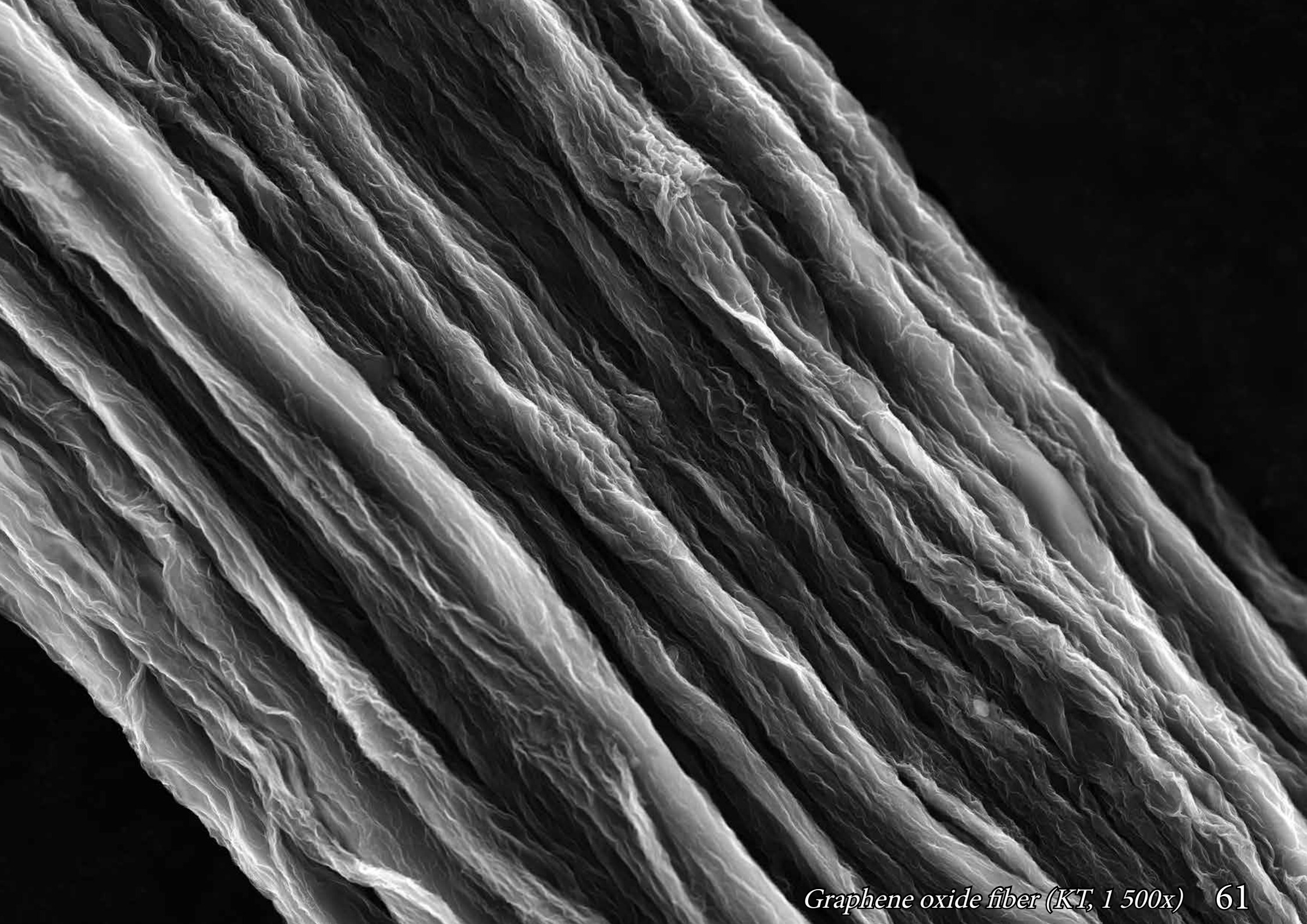

Graphene oxide fiber (KT, 1 500x)

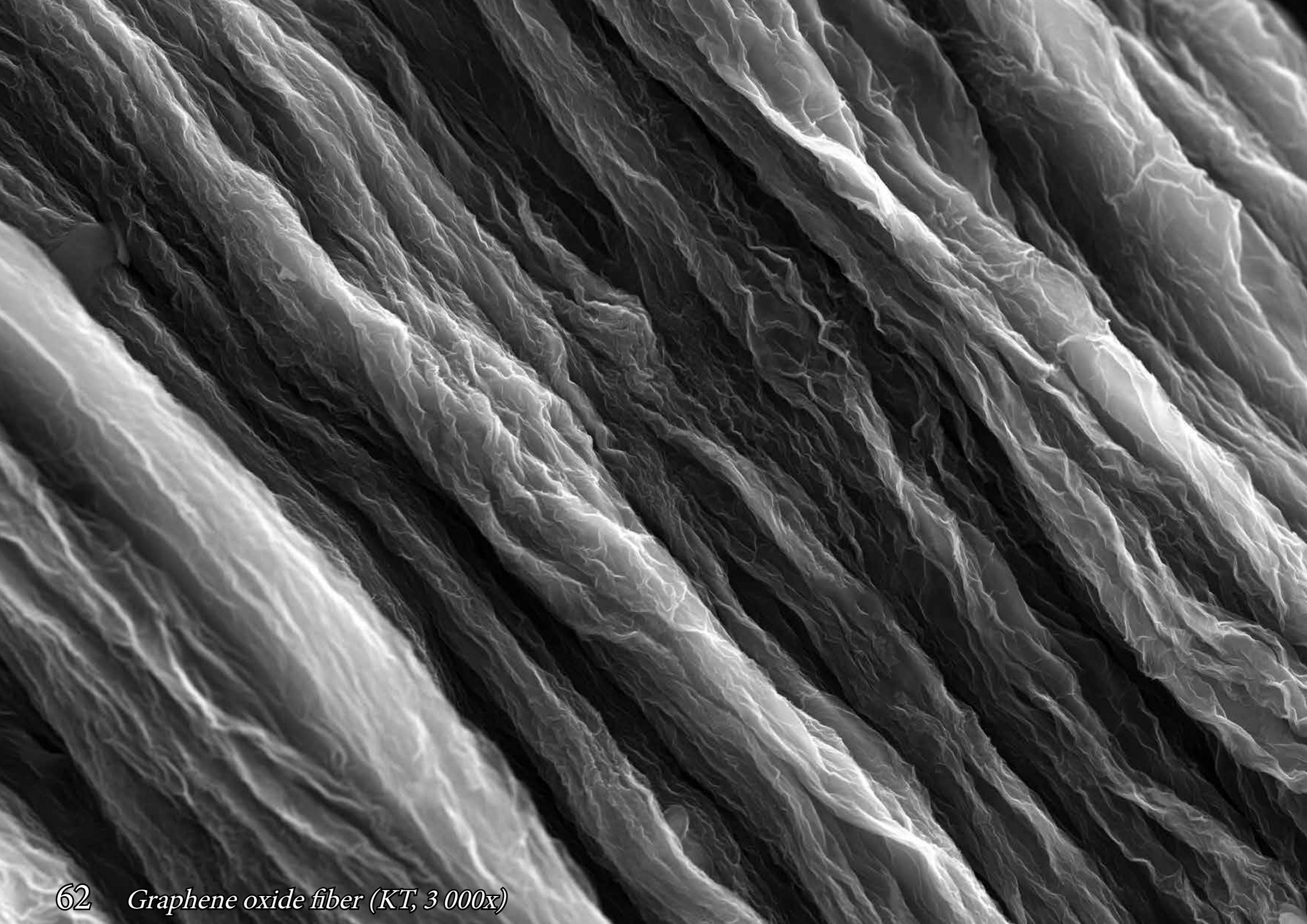

62 *Graphene oxide fiber (KT, 3 000x)*

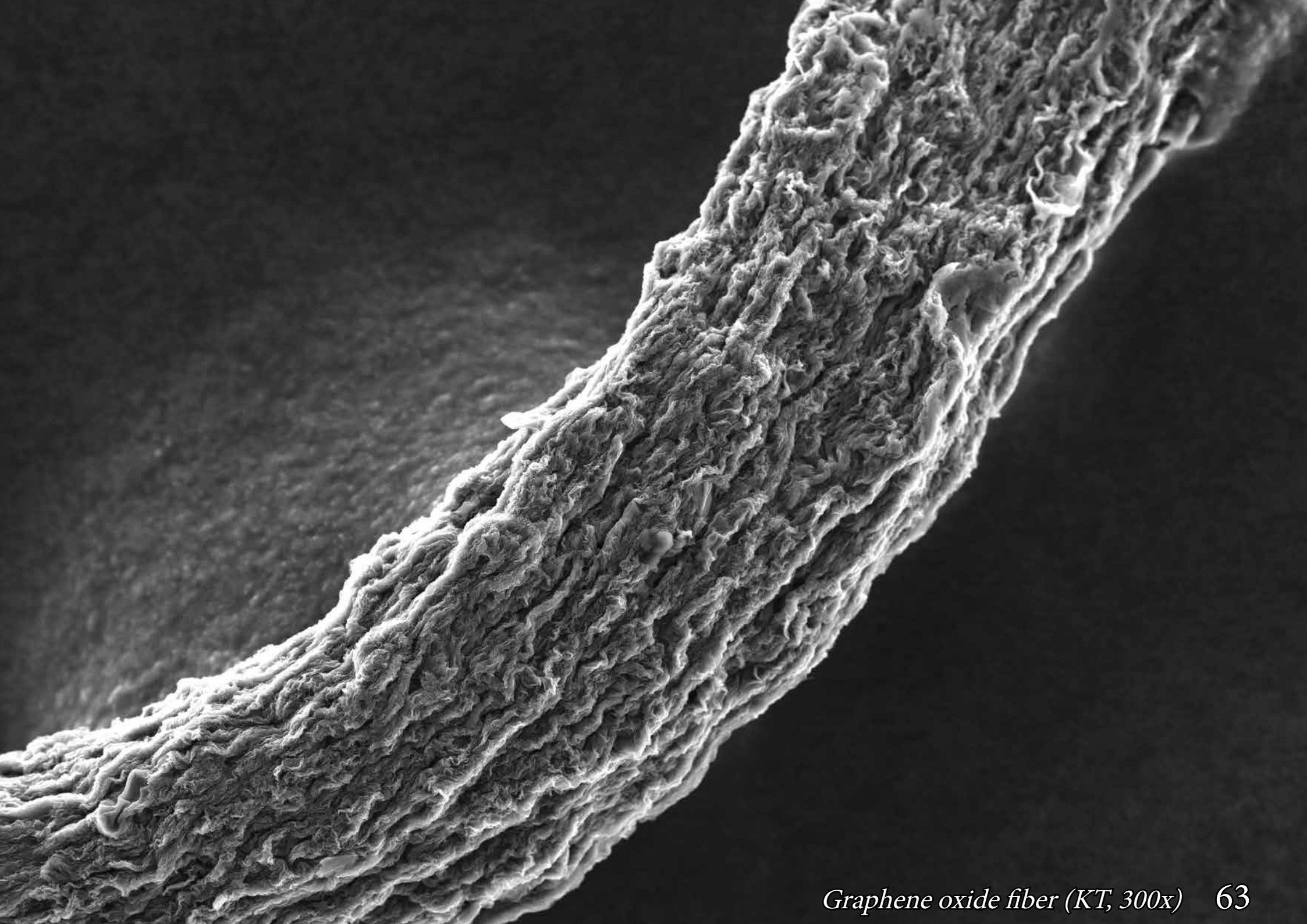

Graphene oxide fiber (KT, 300x)

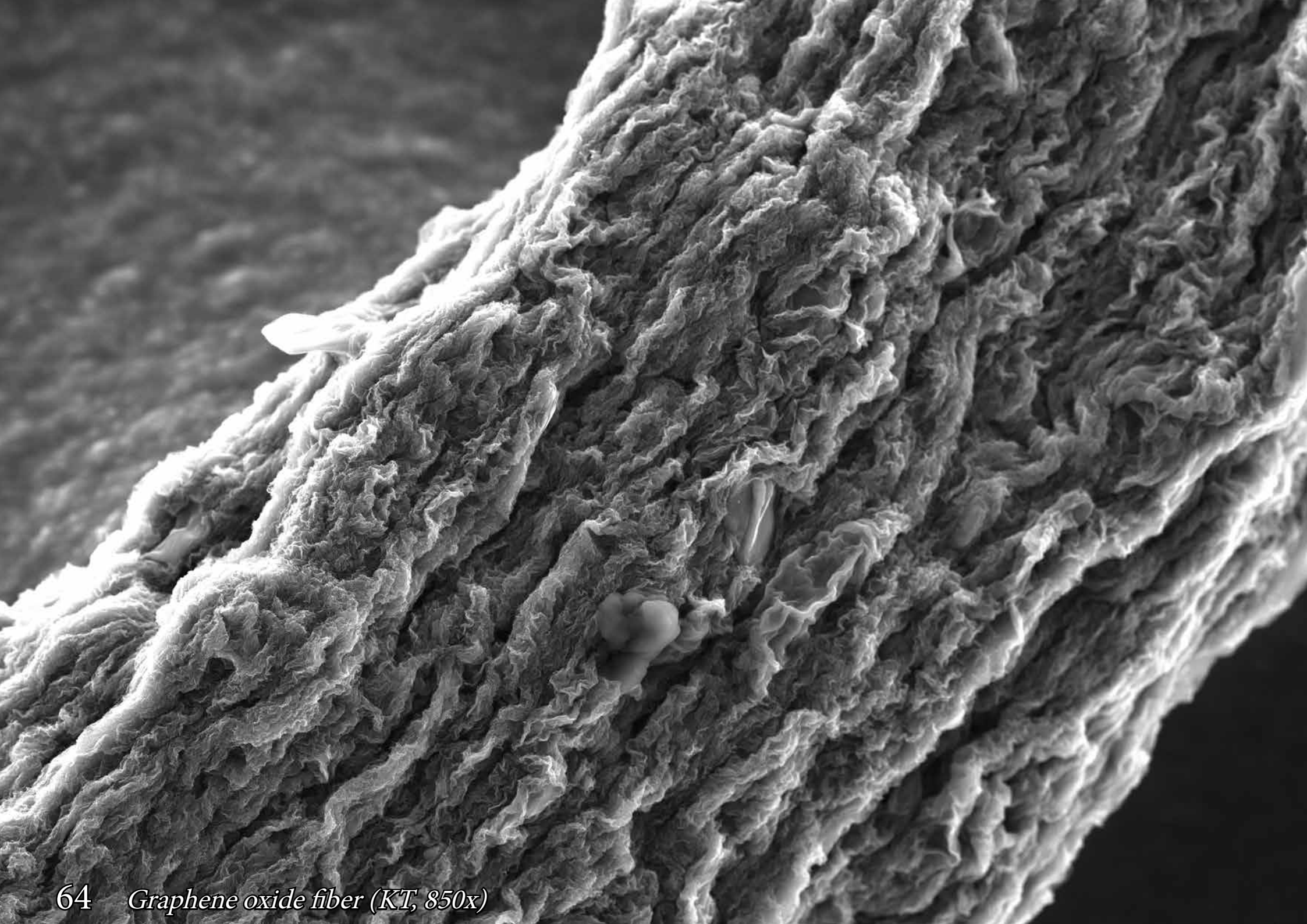

64 *Graphene oxide fiber (KT, 850x)*

Graphene oxide fiber after Ga^+ ions milling, FIB image (KZ, 2 500x)

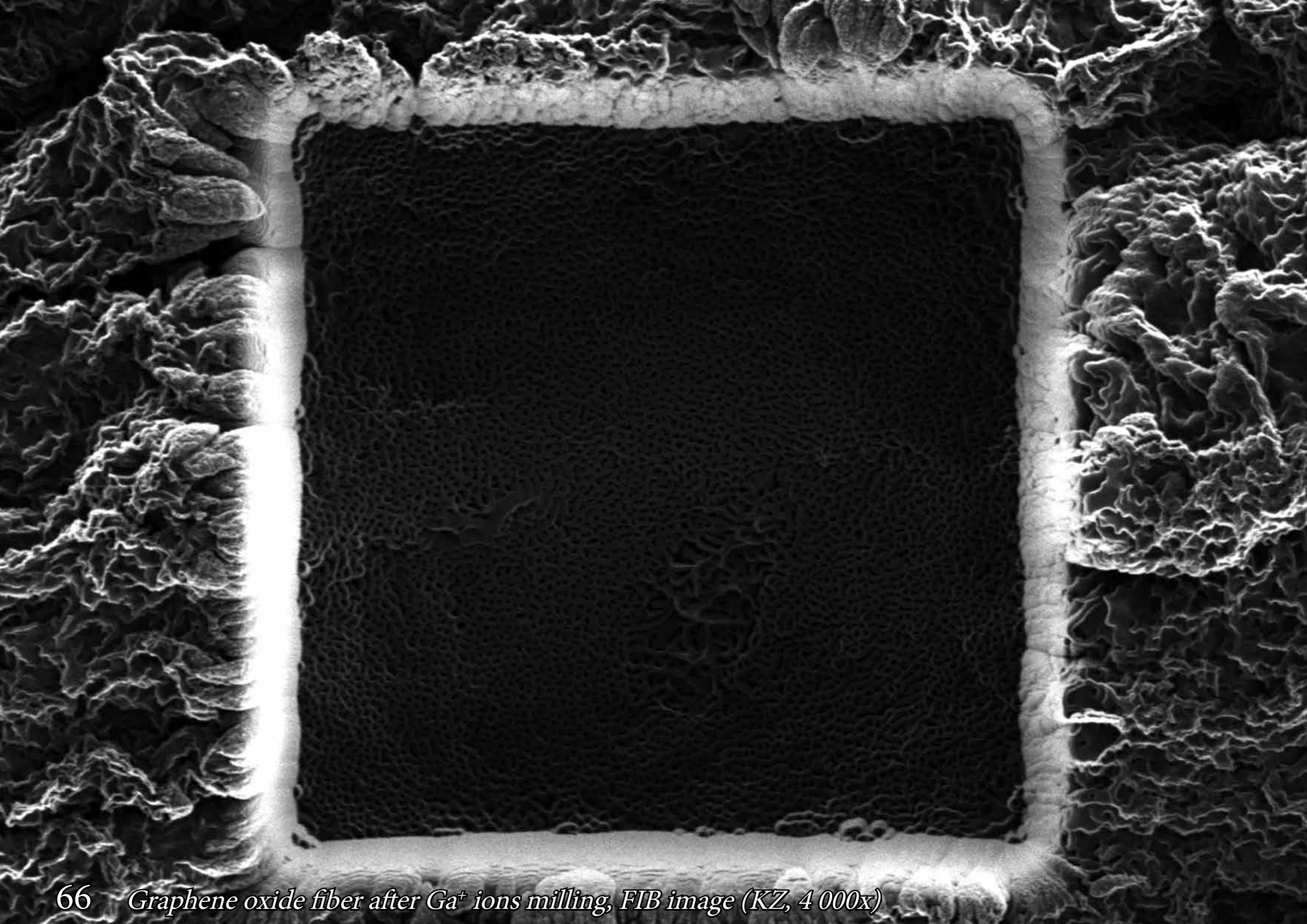

66 *Graphene oxide fiber after Ga^+ ions milling, FIB image (KZ, 4 000x)*

Graphene oxide fiber after Ga^+ ions milling, FIB image (KZ, 5 000x)

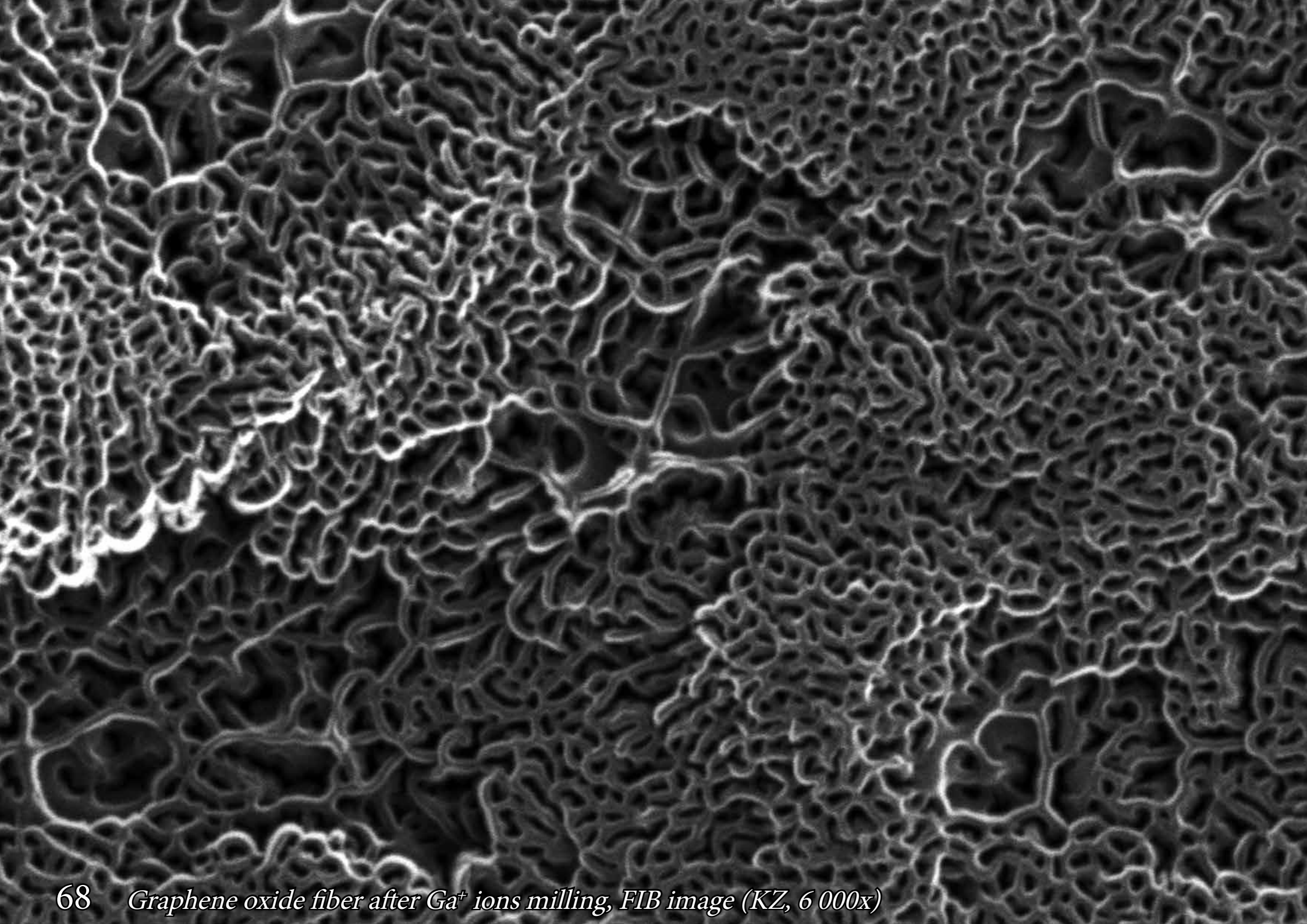

68 *Graphene oxide fiber after Ga^+ ions milling, FIB image (KZ, 6 000x)*

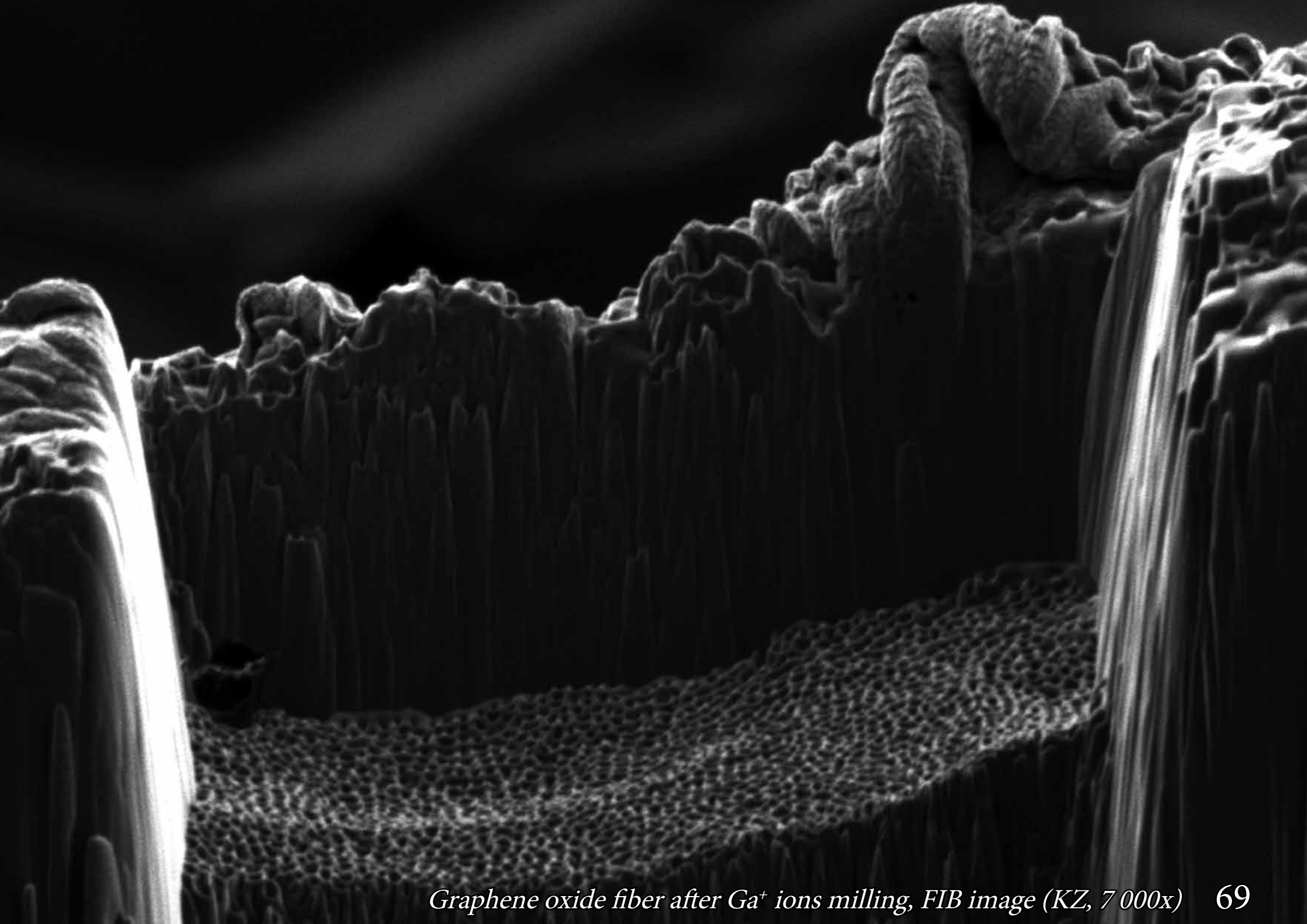

Graphene oxide fiber after Ga^+ ions milling, FIB image (KZ, 7 000x)

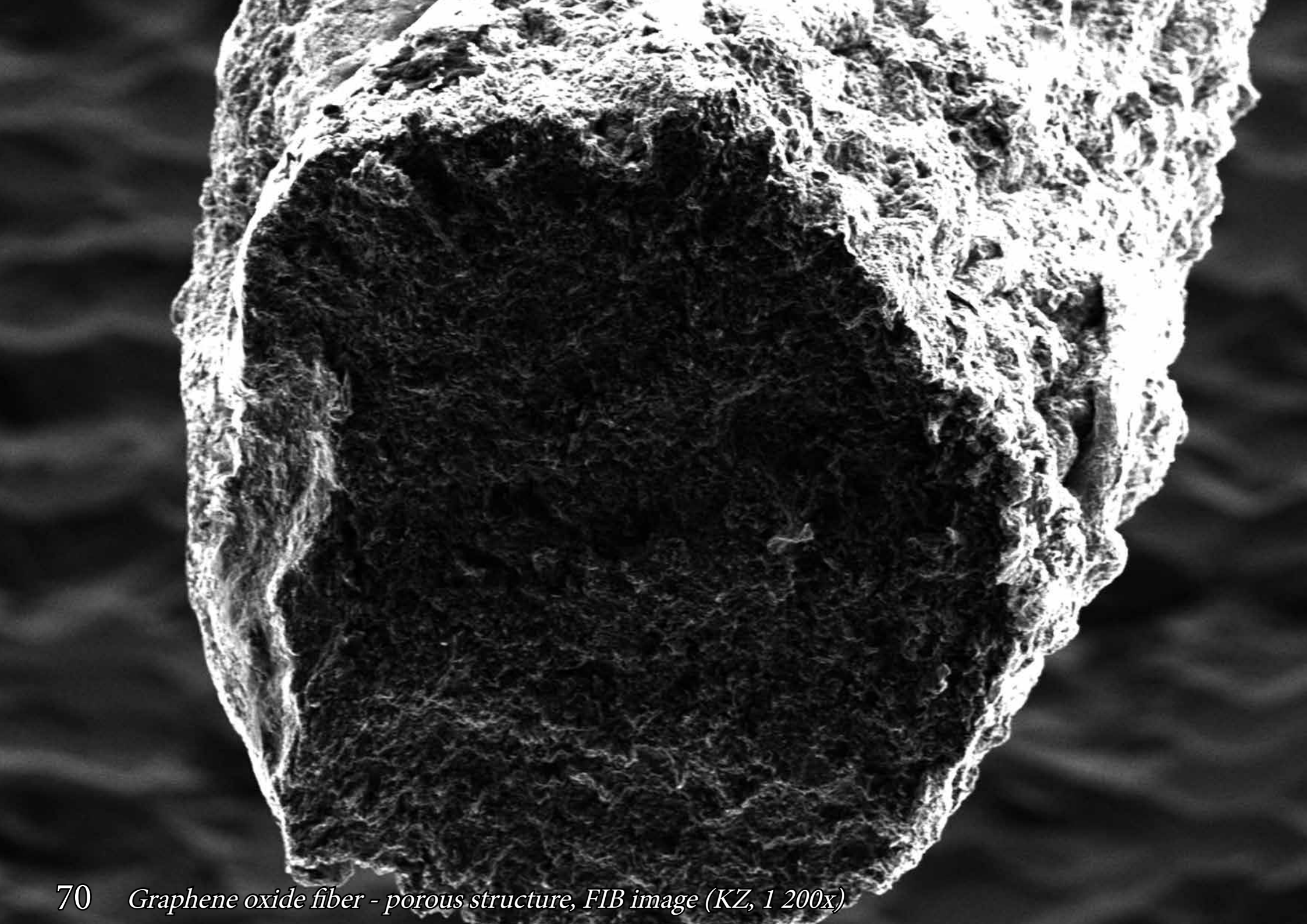

70 *Graphene oxide fiber - porous structure, FIB image (KZ, 1 200x)*

Human cells on partially reduced graphene oxide fibers

Xerogels of partially reduced graphene oxide (prGO) can be used as conductive scaffolds for cell growth. Here we show non-malignant human kidney embryonic (HEK-293) cells attached to 60 μm thick prGO fibers.

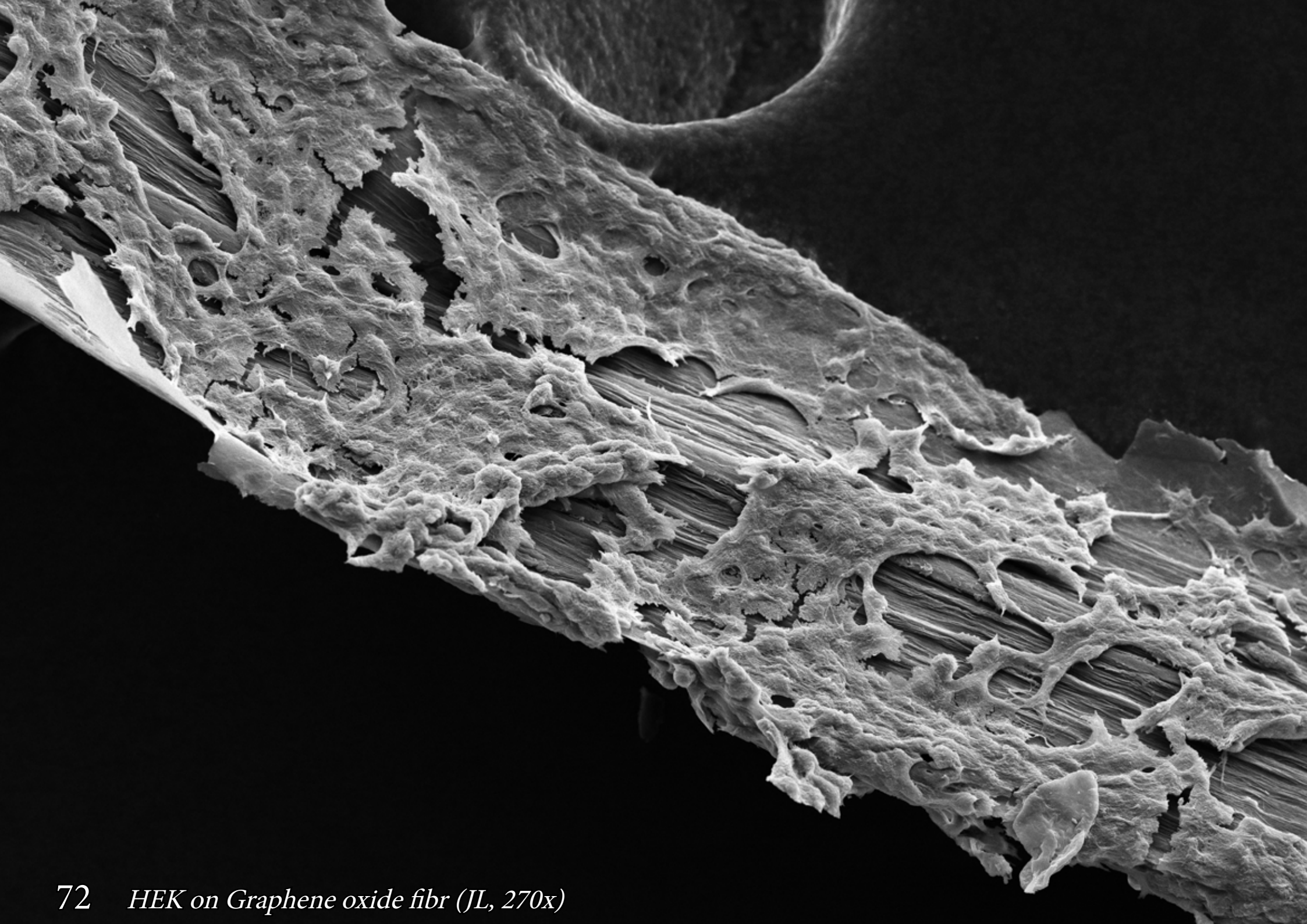

72 *HEK on Graphene oxide fibr (JL, 270x)*

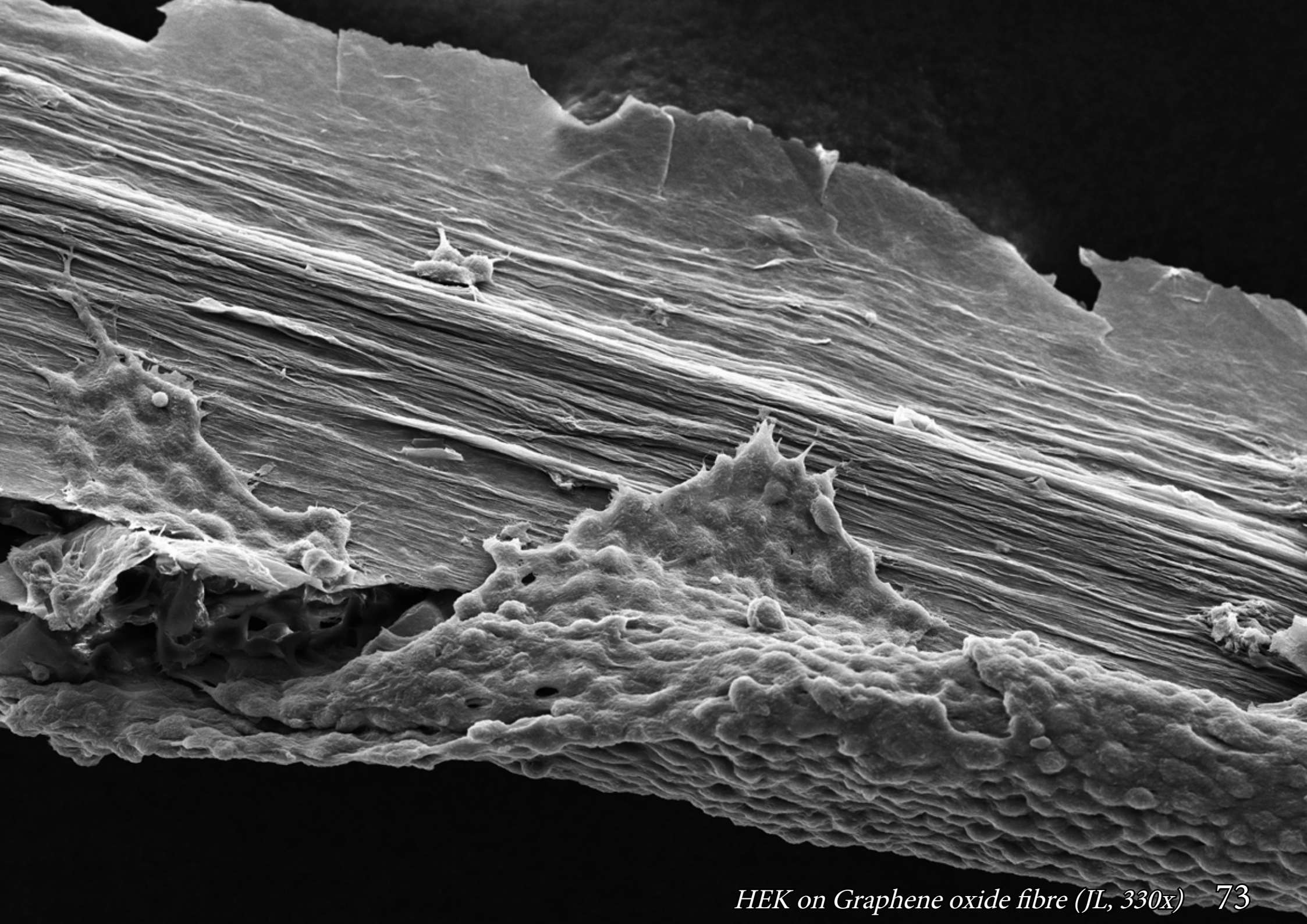

HEK on Graphene oxide fibre (JL, 330x)

74 *HEK on Graphene oxide fibre (JL, 600x)*

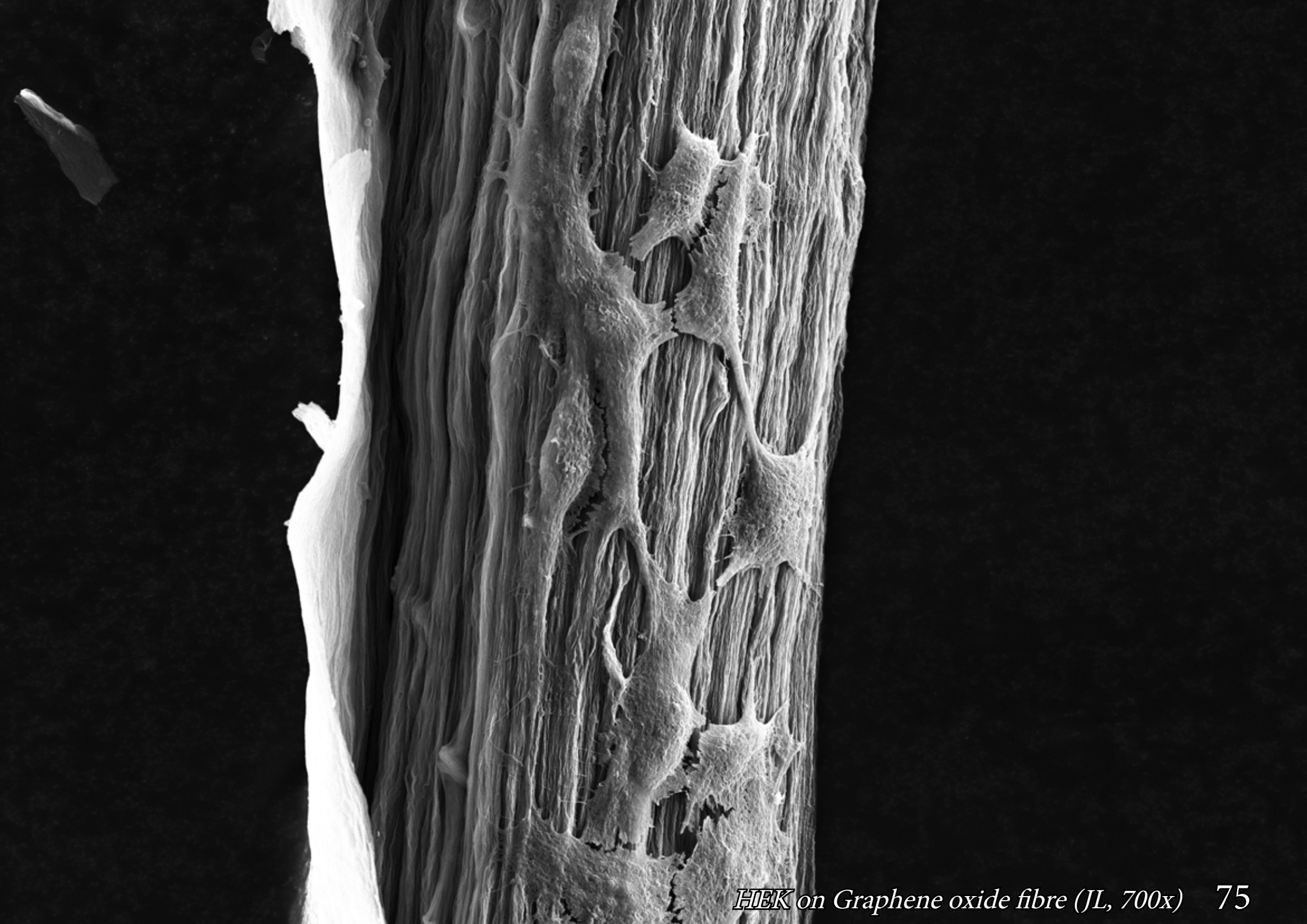

HEK on Graphene oxide fibre (JL, 700x)

76 *HEK on Graphene oxide fibre (JL, 700x)*

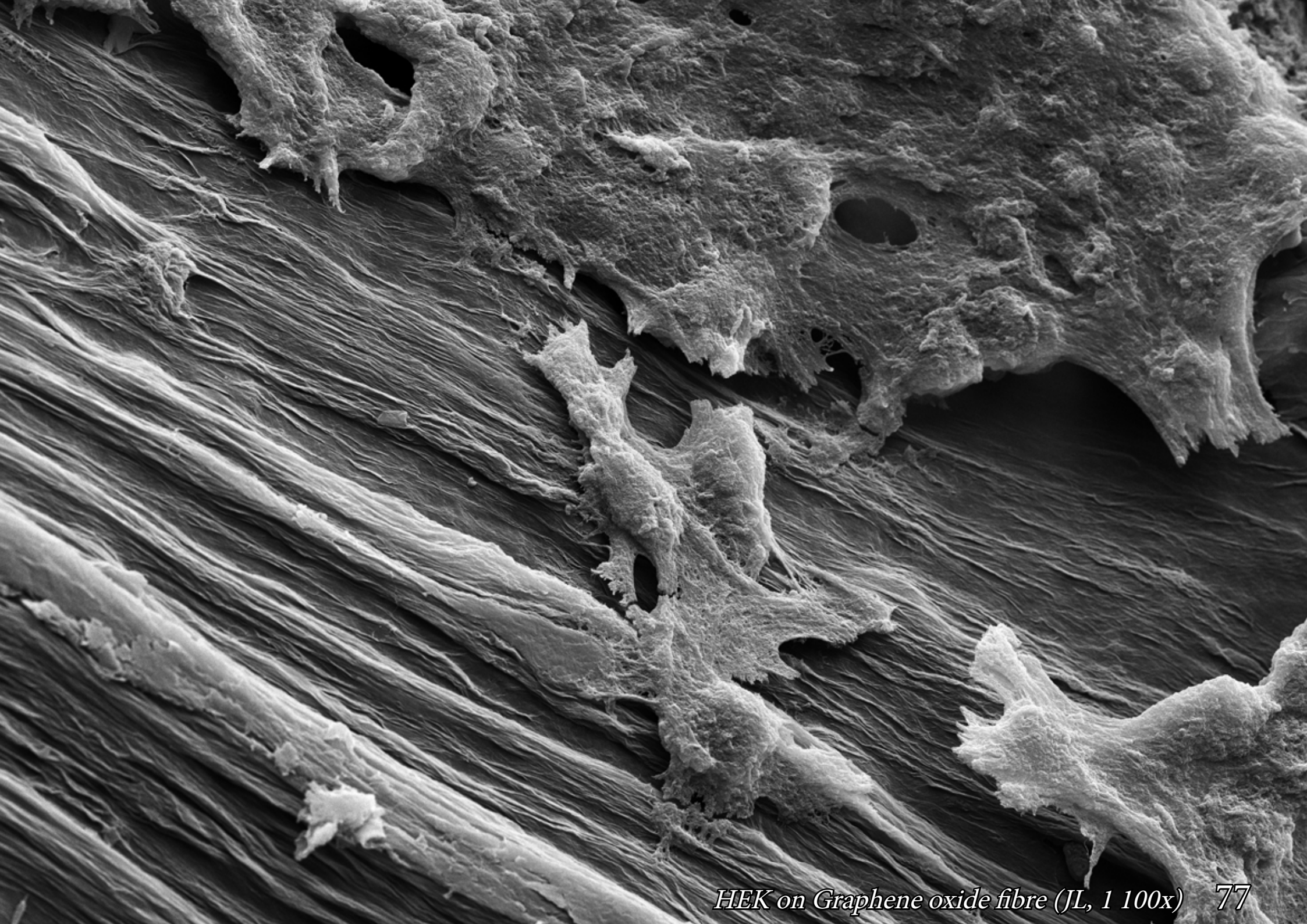

HEK on Graphene oxide fibre (JL, 1 100x) 77

78 *HEK on Graphene oxide fibre (JL, 1 200x)*

HEK on Graphene oxide fibre (JL, 1 400x)

80 *HEK on Graphene oxide fibre (JL, 1 900x)*

Activated carbon fibers

Phenol, resin based microporous activated carbon fibers with nanometer pores are obtained after carbonisation of the precursor. Surface grooves are the result of activation process, which removes amorphous carbon and increases the specific surface area above 1000 m^2/g.

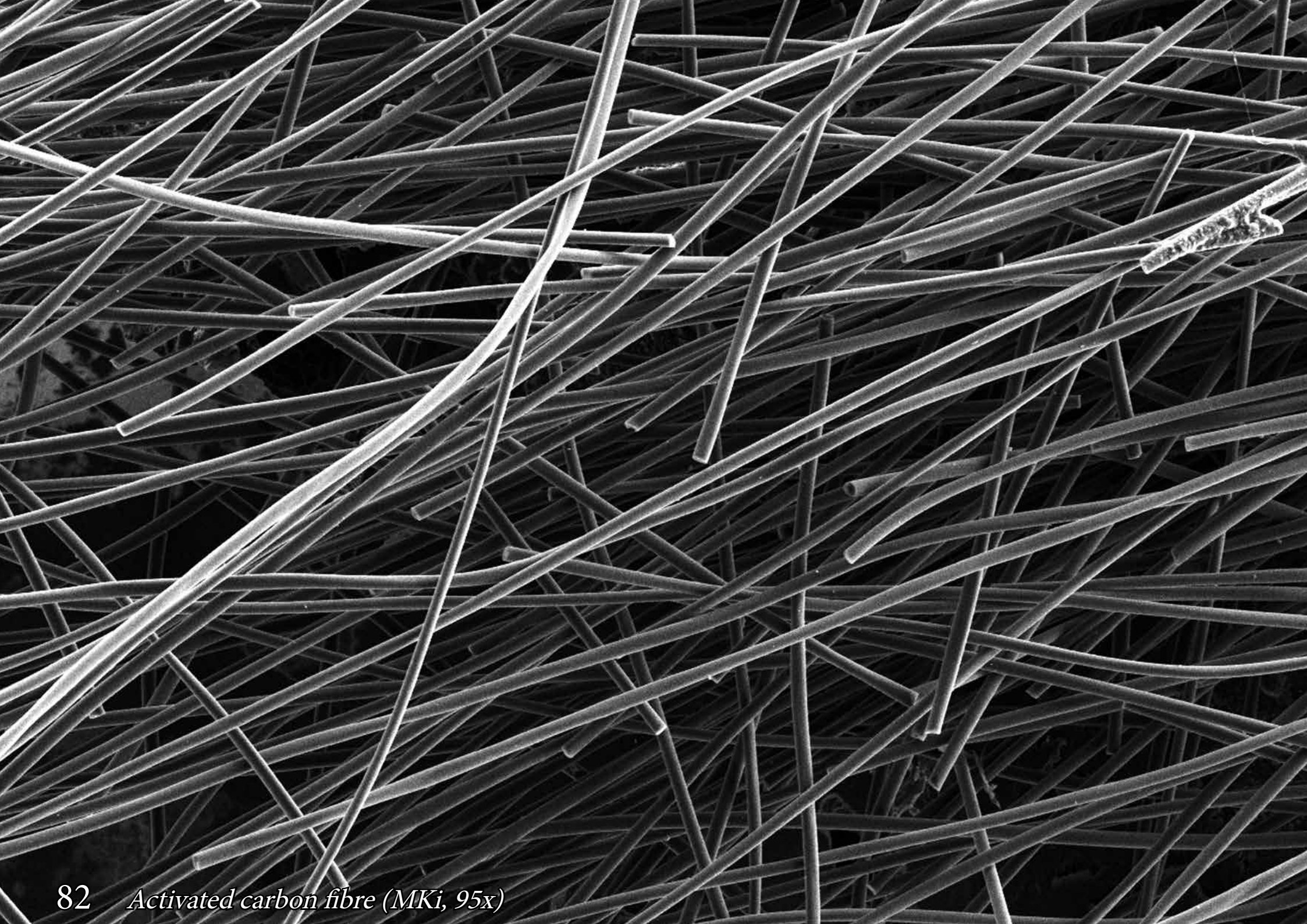

82 *Activated carbon fibre (MKi, 95x)*

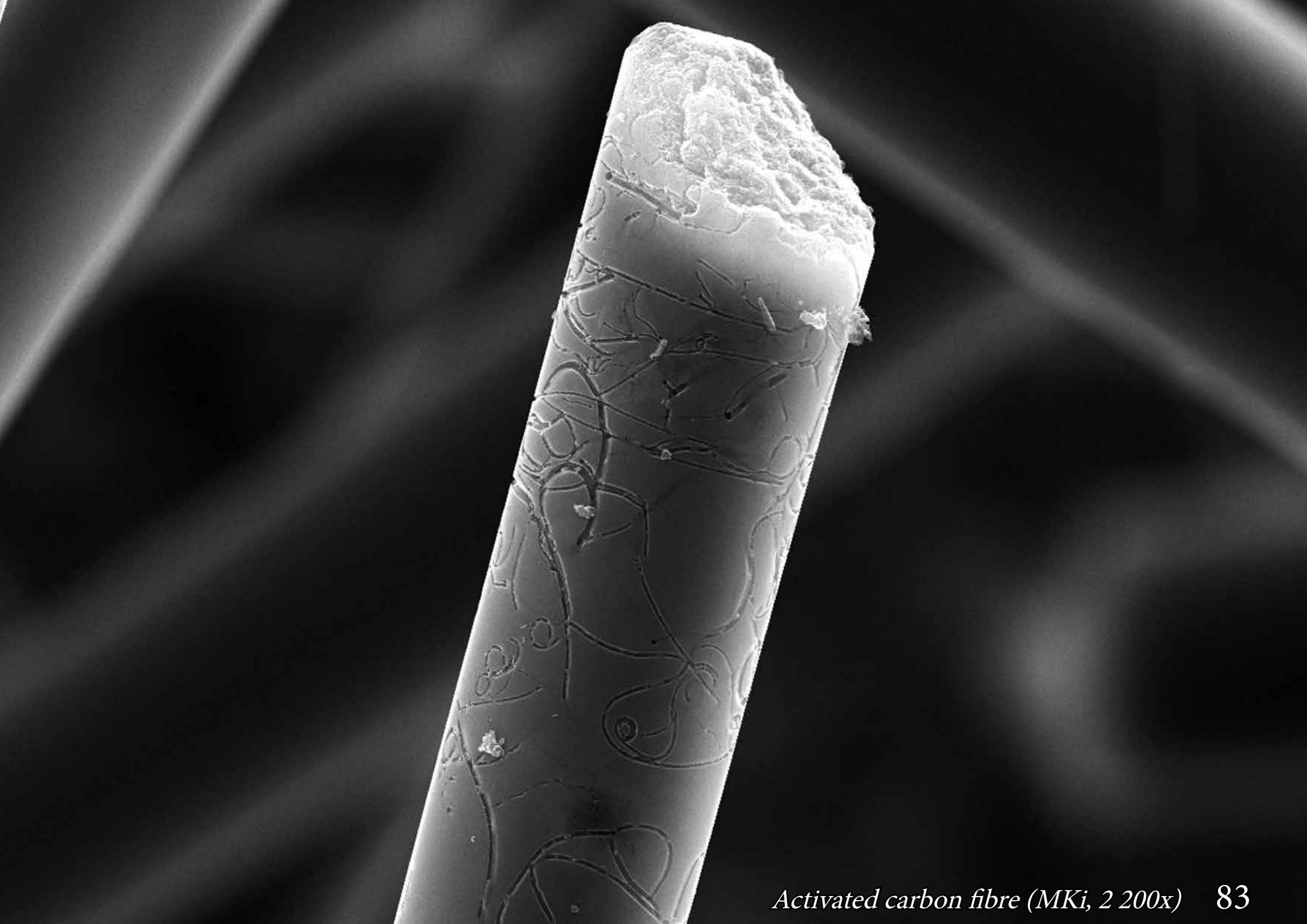

Activated carbon fibre (MKi, 2 200x)

84 *Activated carbon fibre (MKi, 5 500x)*

Silica nanoparticles

Silicon oxide (SiO_2) nanoparticles are non-agglomerated, uniform spherical shape with diameter of 700 nm and are one of the most basic blocks of nanotechnology.

Spherically shaped mesoporous silica (SiO_2) nanoparticles with average diameter of around 50 nm, measured by the transmission electron microscopy (TEM).

„Bean-like" shaped mesoporous silica nanoparticles (SiO_2) measured by the transmission electron microscopy (TEM).

86 *Silica nanoparticles (KT, 4 000x)*

Silica naniparticles (KT, 8 000x)

88 *Silica nanoparticles (KT, 1 300x)*

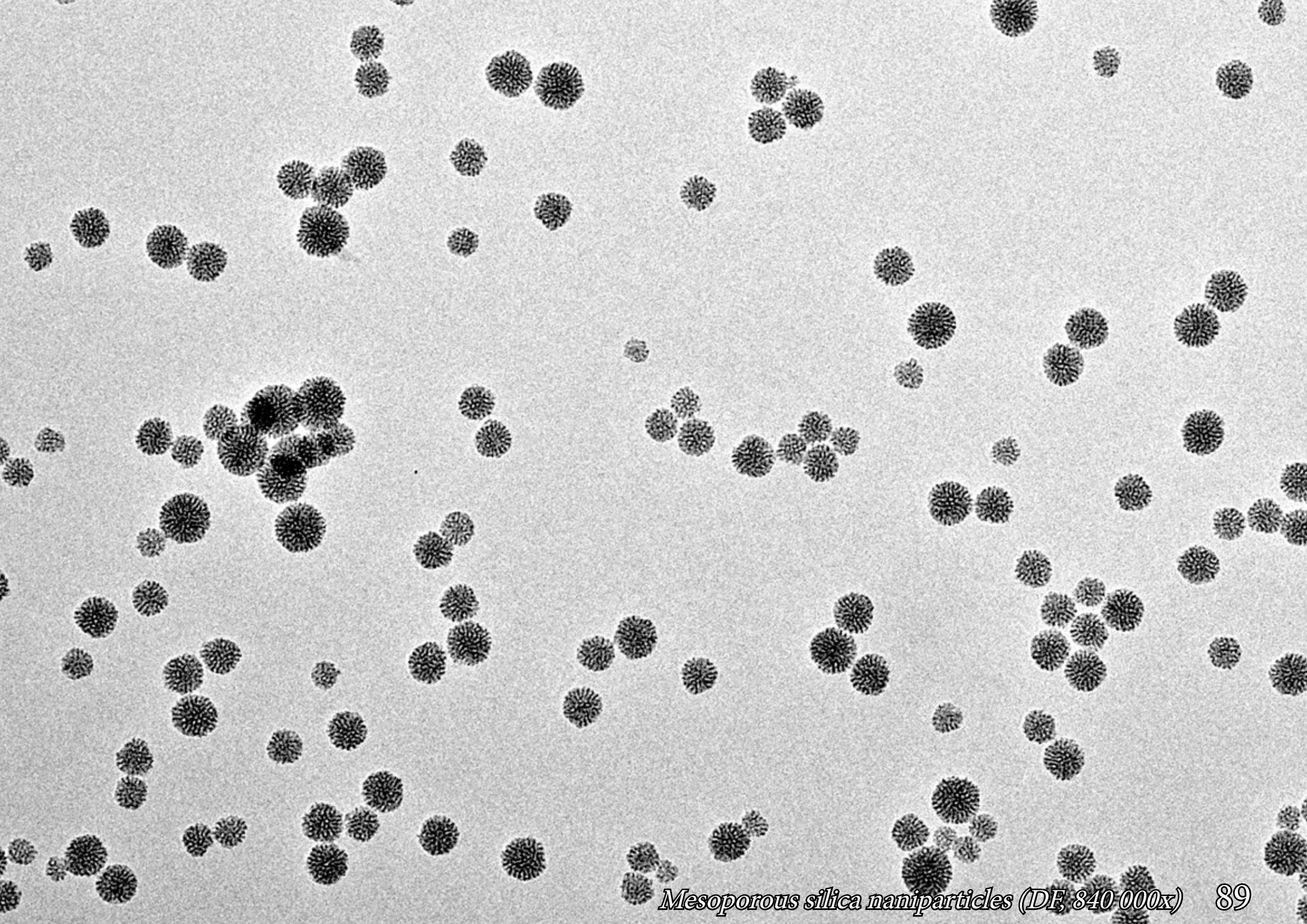

Mesoporous silica naniparticles (DF, 840 000x)

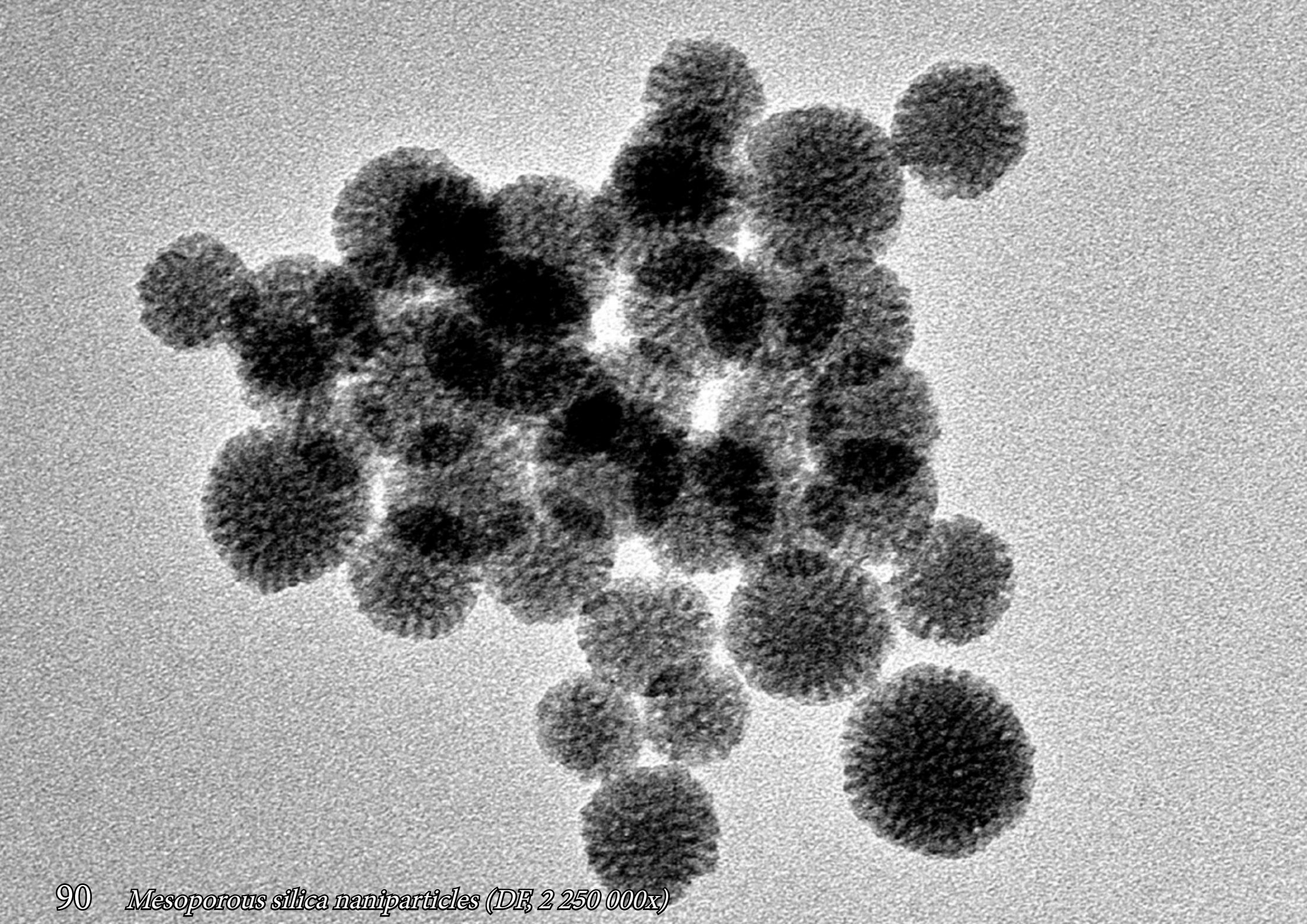

90 *Mesoporous silica naniparticles (DF, 2 250 000x)*

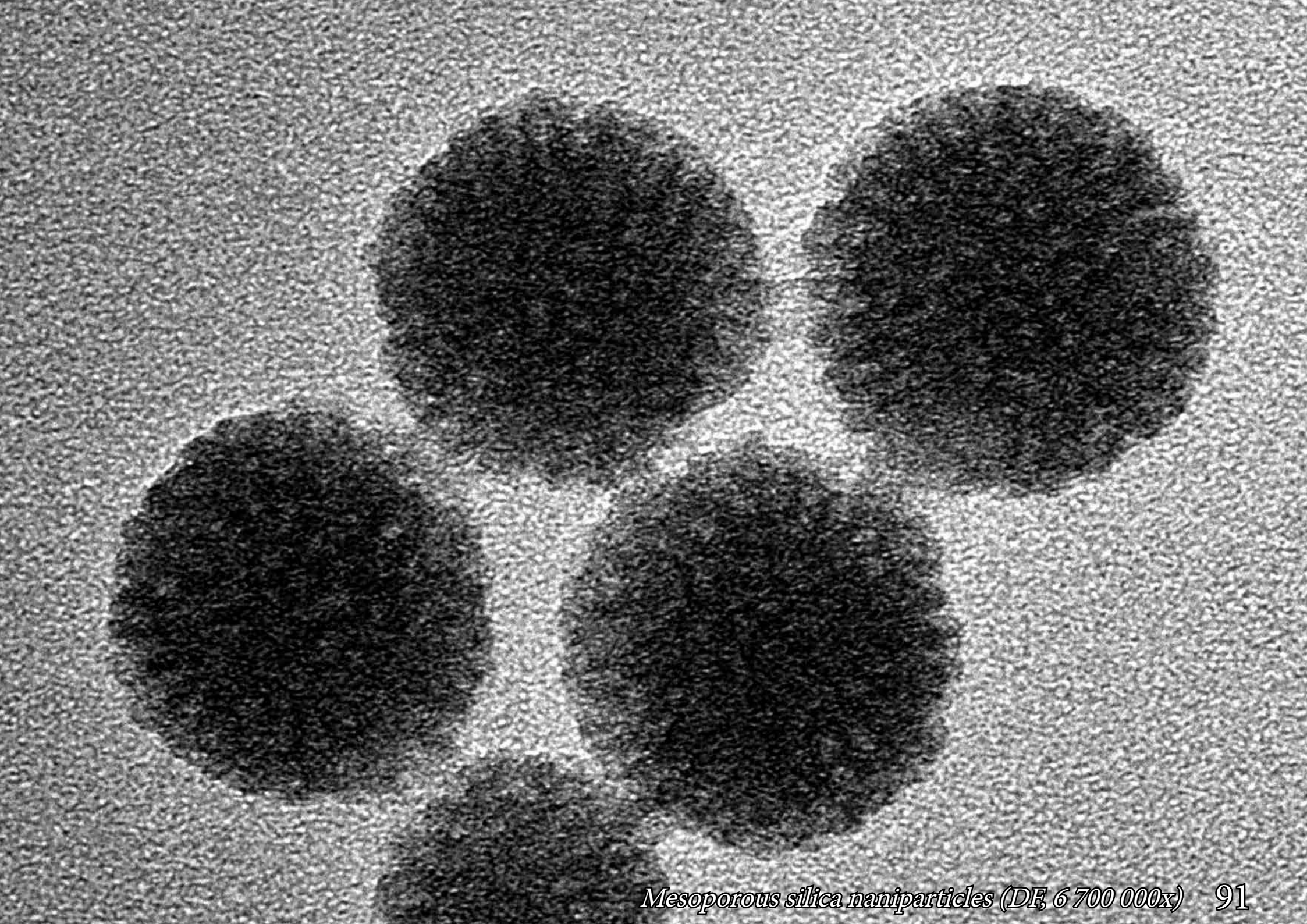

Mesoporous silica naniparticles (DF, 6 700 000x)

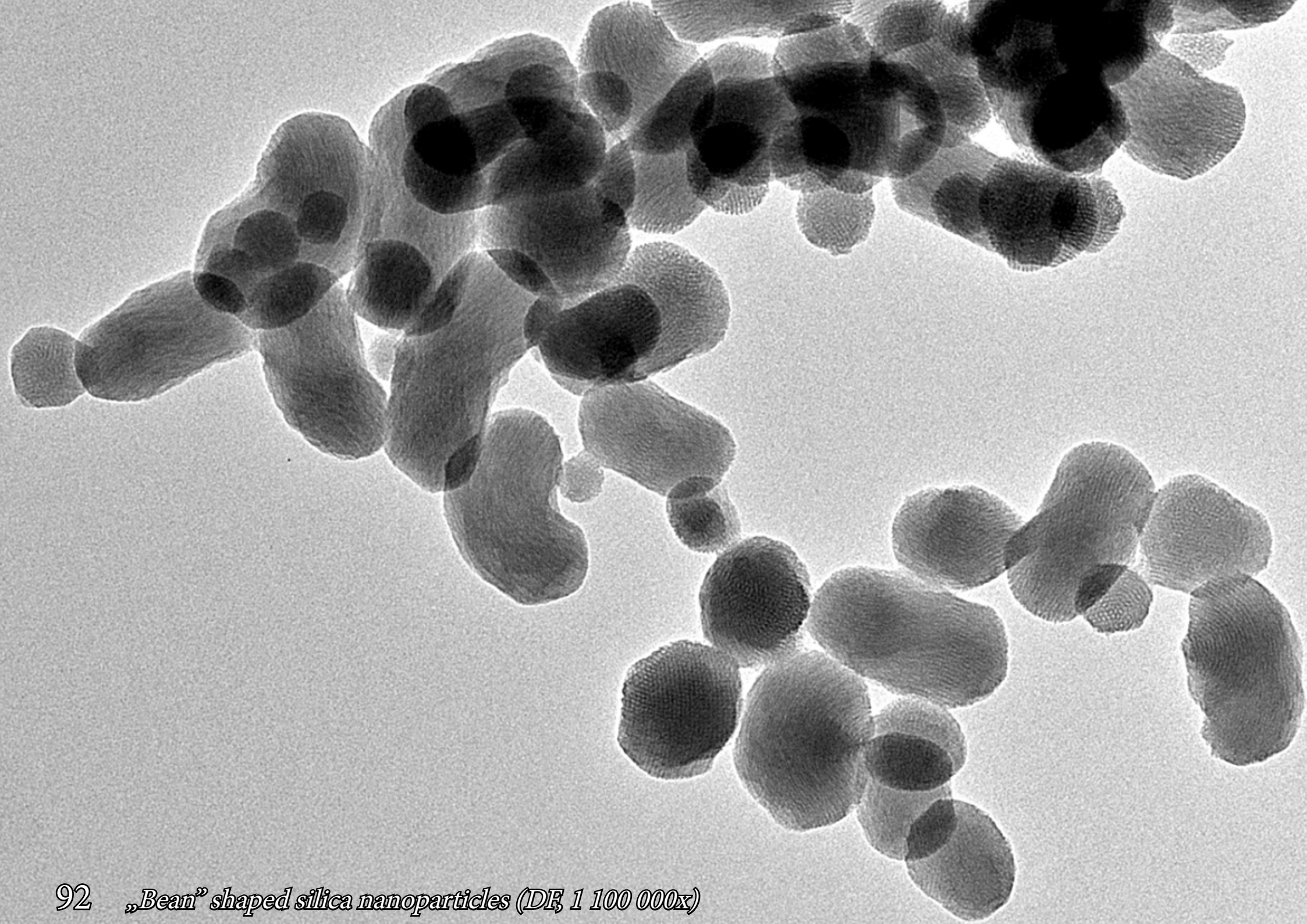

92 „Bean" shaped silica nanoparticles (DF, 1 100 000x)

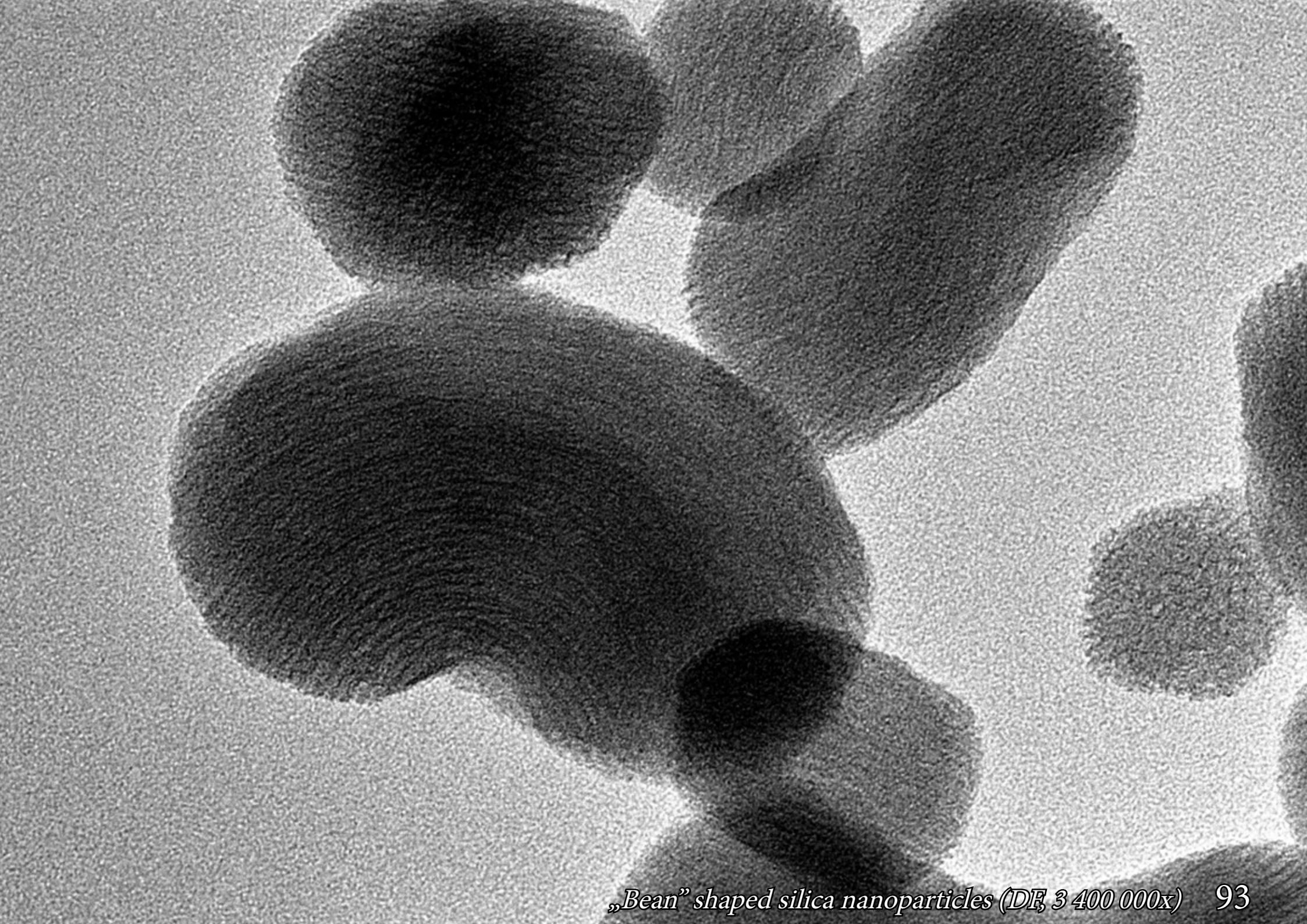

„Bean” shaped silica nanoparticles (DF, 3 400 000x)

Fe_3O_4/SiO_2 nanoparticles

A novel silica-condensation mechanism based on the existence of a dynamic oleate bilayer, which constitutes the most experimentally supported hypothesis on the formation of Iron Oxide nanoparticles coated with Silica in an oil-in-water system. It is expected to be one of the highest yielding methods known to date for the production of these particles.

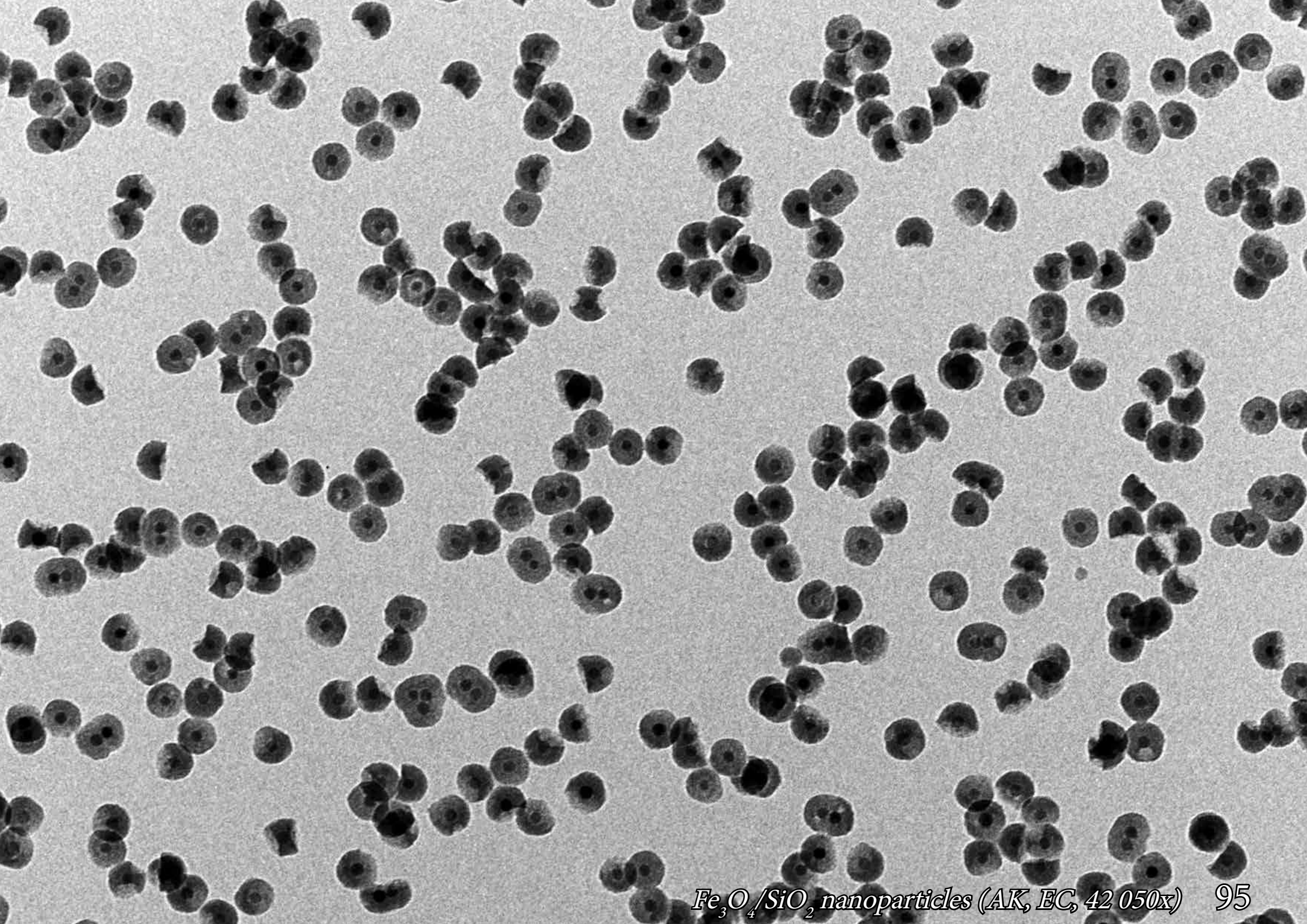

Fe_3O_4/SiO_2 nanoparticles (AK, EC, 42 050x)

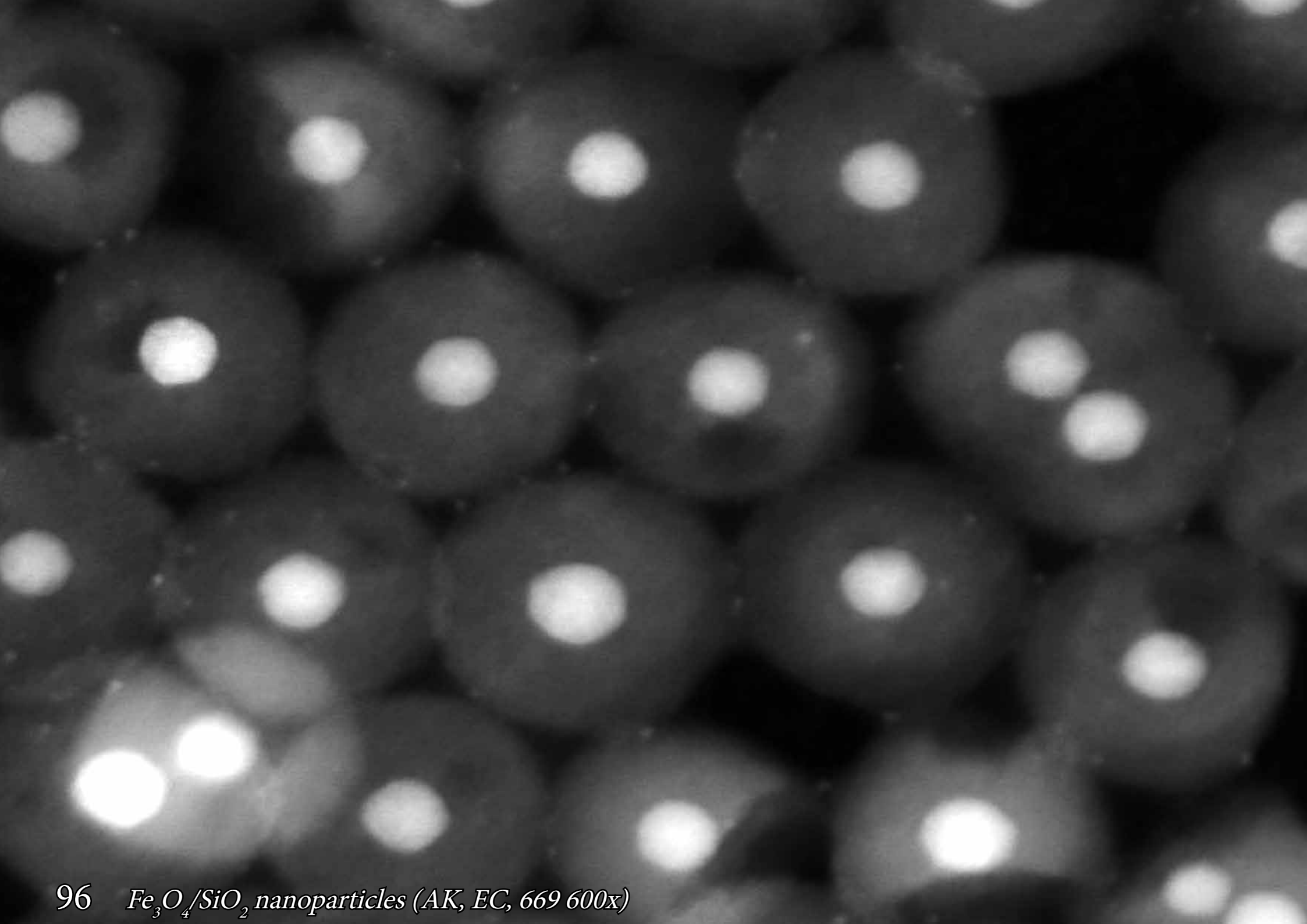

96 *Fe_3O_4/SiO_2 nanoparticles (AK, EC, 669 600x)*

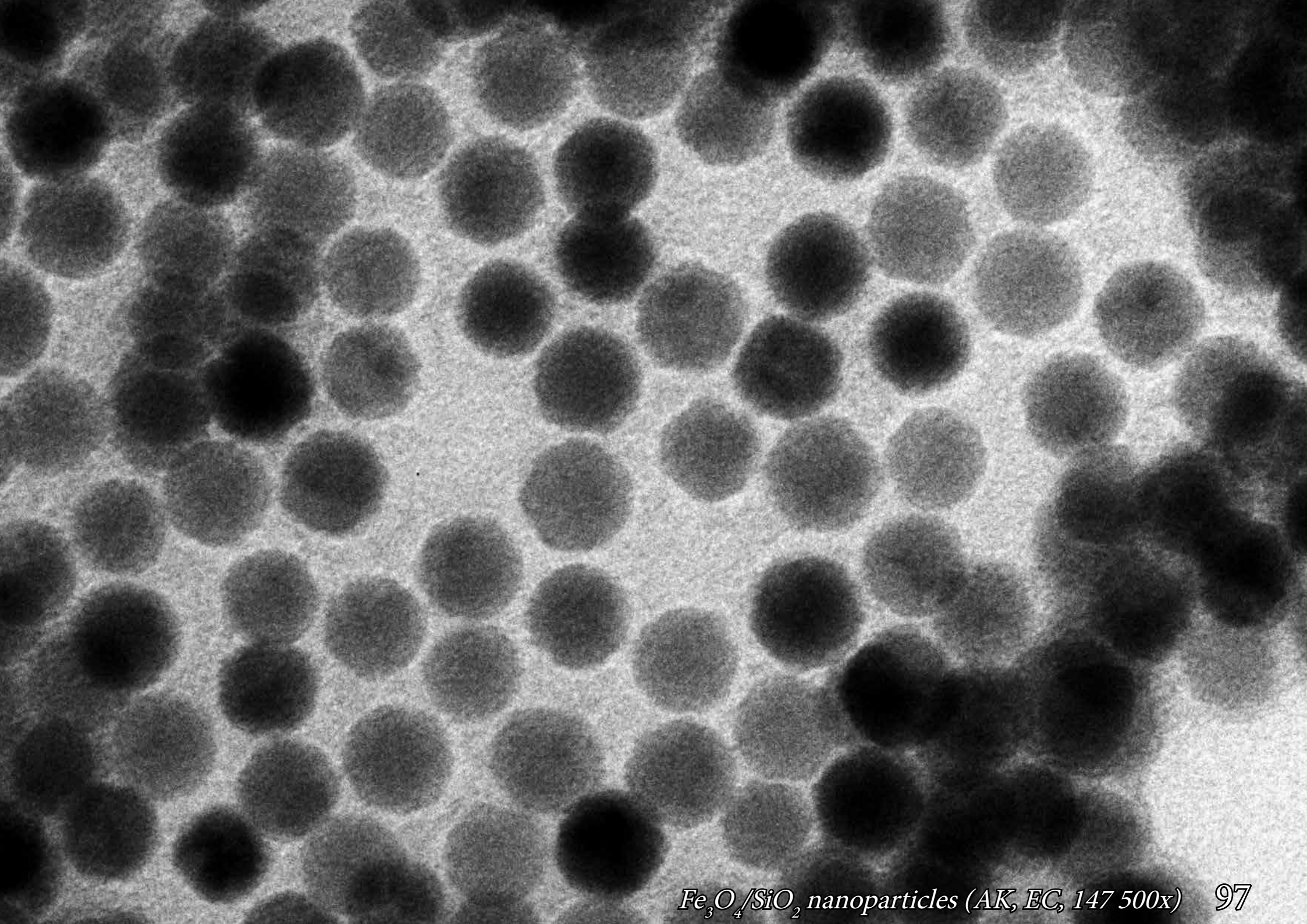

Fe_3O_4/SiO_2 nanoparticles (AK, EC, 147 500x) 97

Metallic Pd/Ag/Au nanoparticles

Polymetallic hollow nanoparticles with very different morphology and composition, obtained by the simultaneous or sequential action of galvanic replacement and the Kirkendall effect. The research allows controlling shape, diffusion and yield, with minor modifications in the chemical environment, all of them taking place at room temperature.

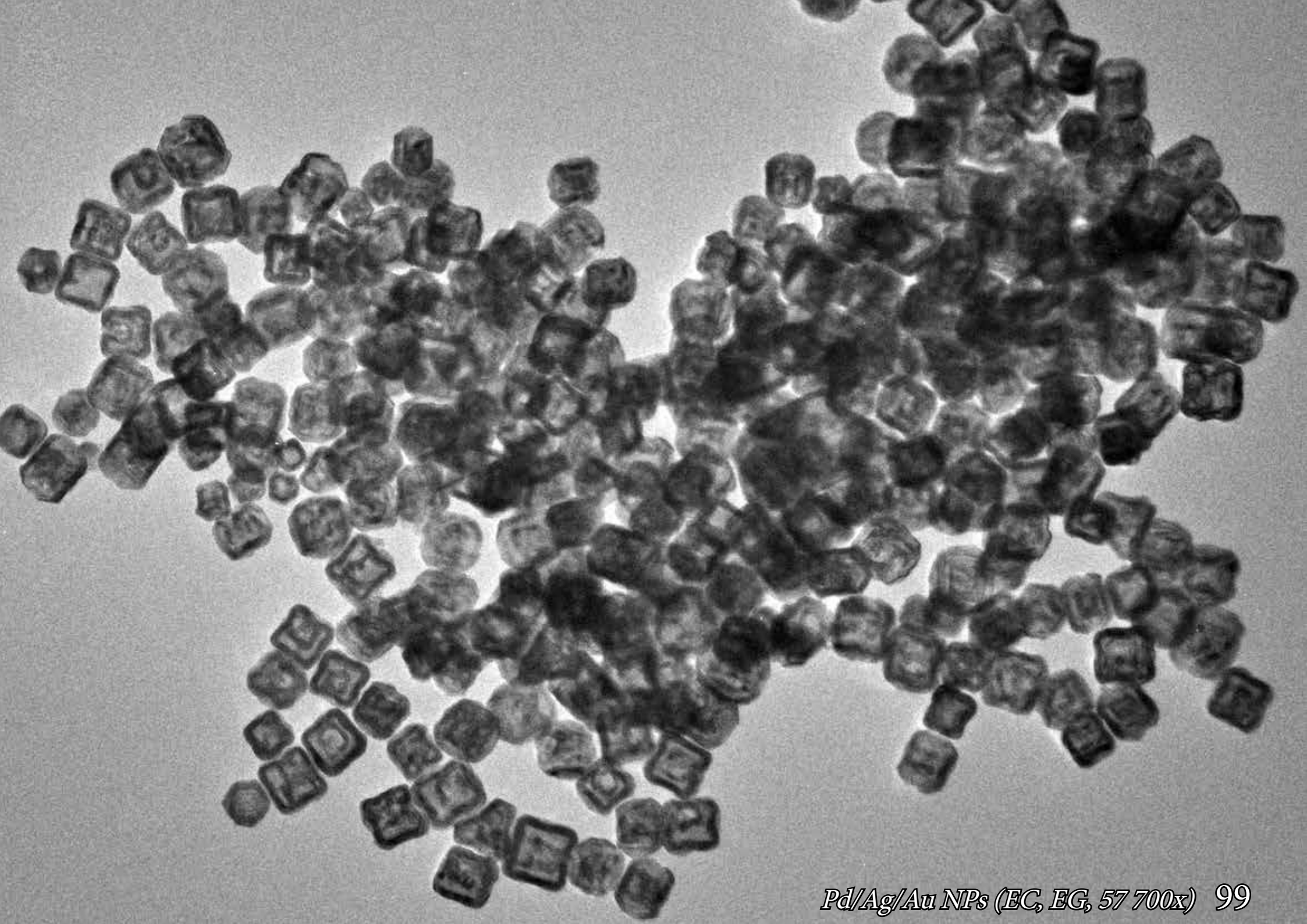

Pd/Ag/Au NPs (EC, EG, 57 700x) 99

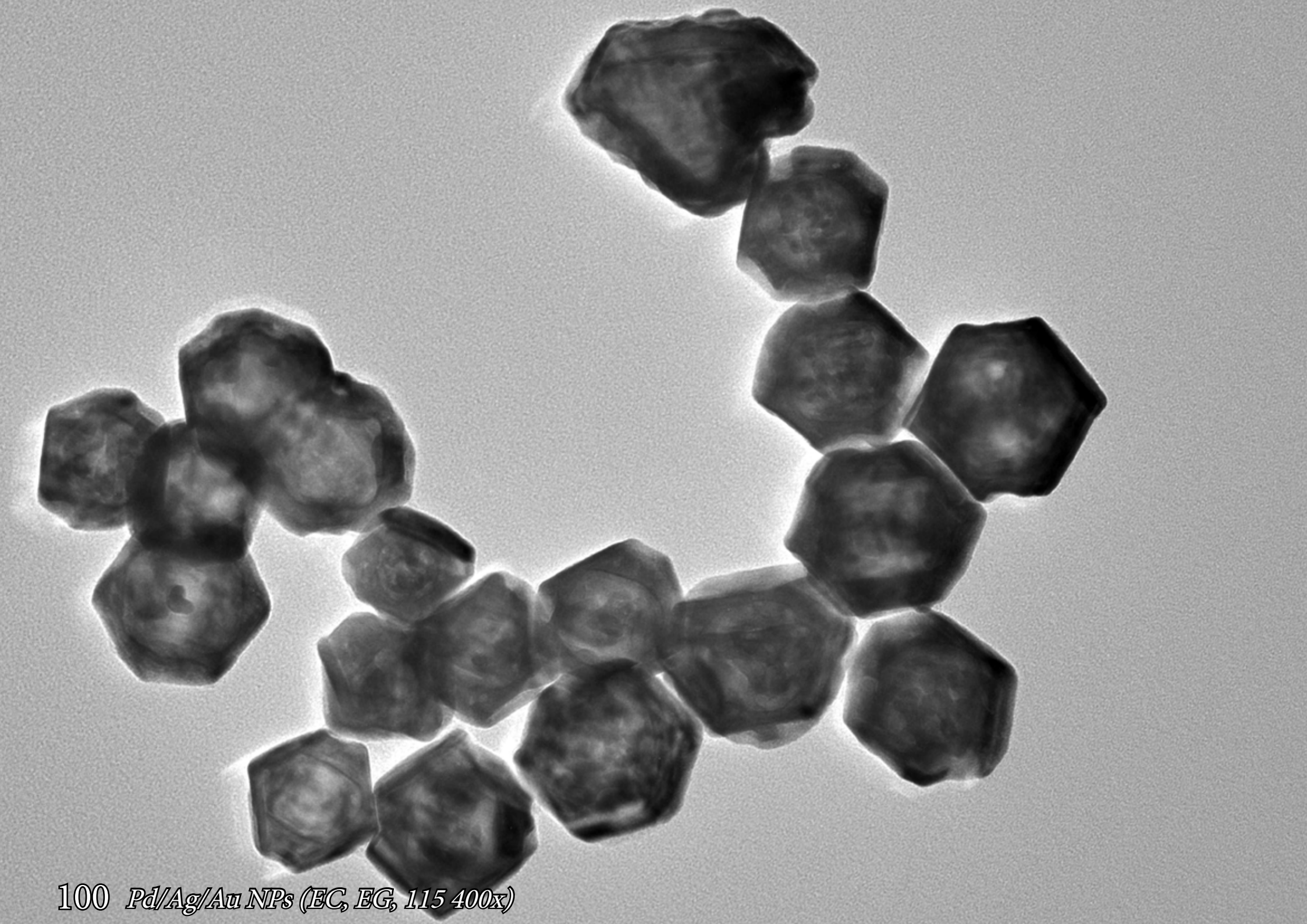

100 *Pd/Ag/Au NPs (EC, EG, 115 400x)*

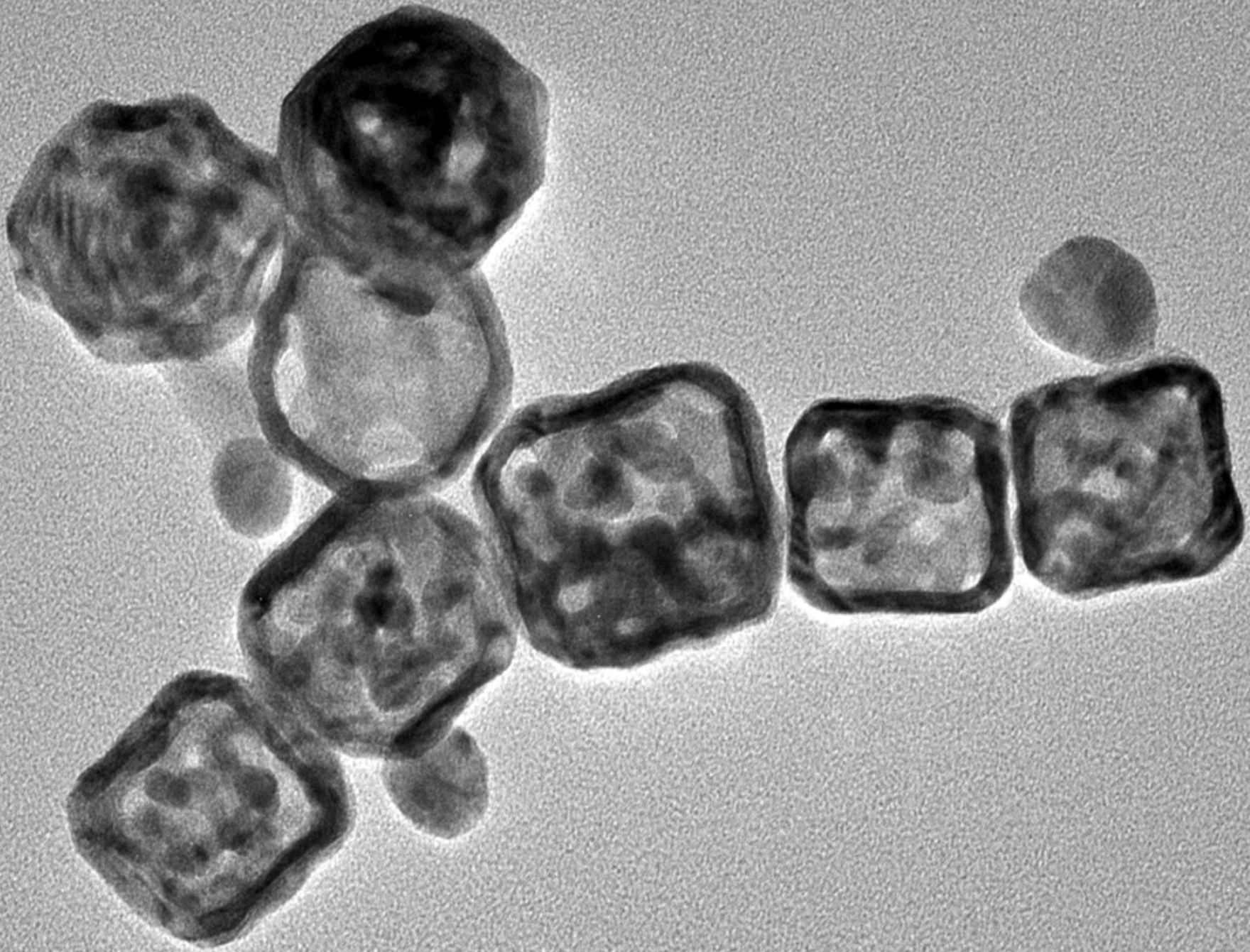

Pd/Ag/Au NPs (EC, EG, 230 800x) 101

Polydopamine nanoparticles

Polydopamine nanoparticles with sizes of 40 nm, 100 nm and 200 nm were obtained. These materials belong to rising stars of nanomedicine since they are frequently used as platforms for preparation multimodal nanostructures for advanced anticancer therapies merging chemo- and photothermal therapies as well as gene therapy. Consequently, the therapeutic outcome of such modalities is higher than those routinely used in cancer therapy since they result in higher cancer eradication which has been proved by extensive *in-vitro* and *in-vivo* studies.

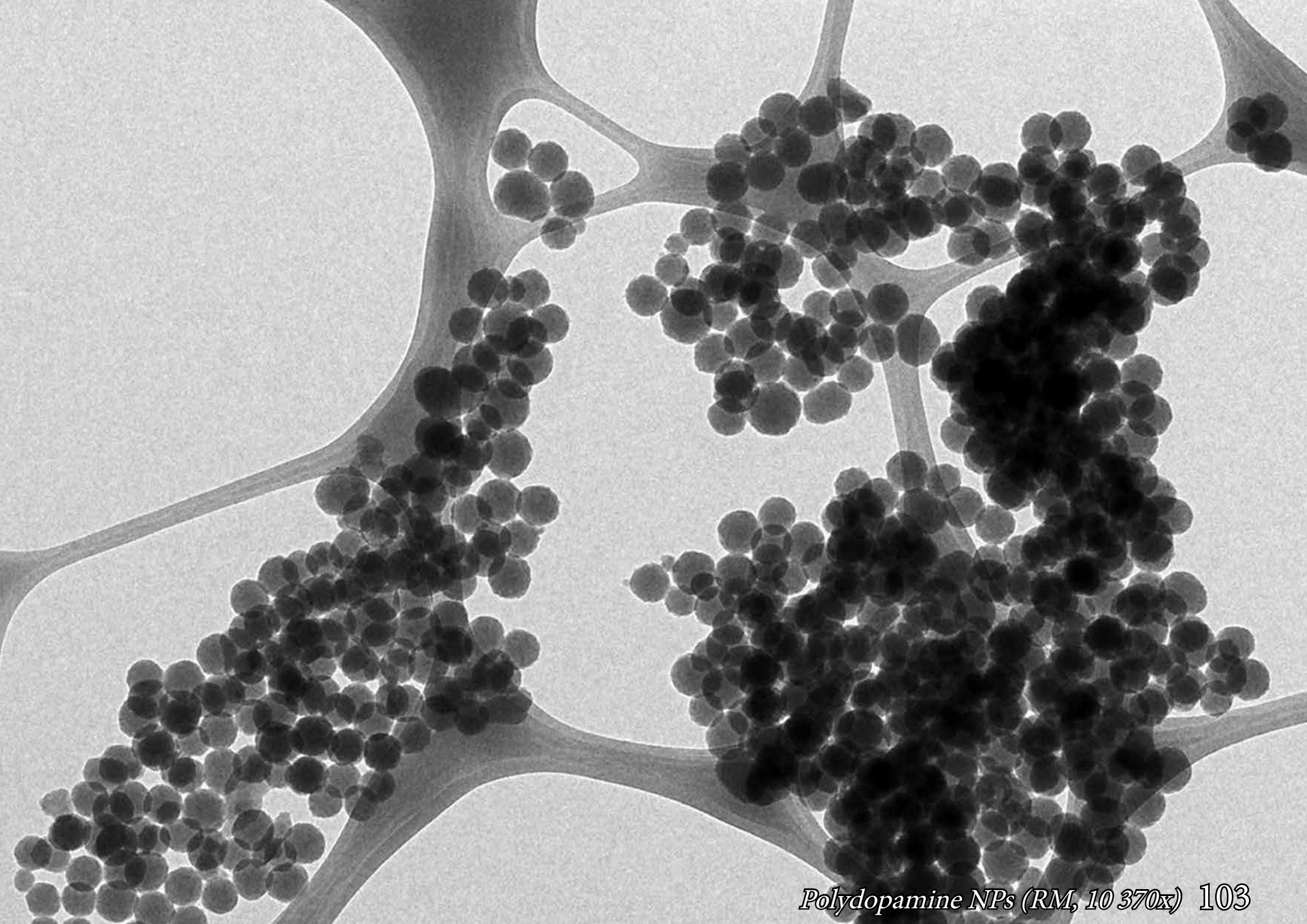

Polydopamine NPs (RM, 10 370x) 103

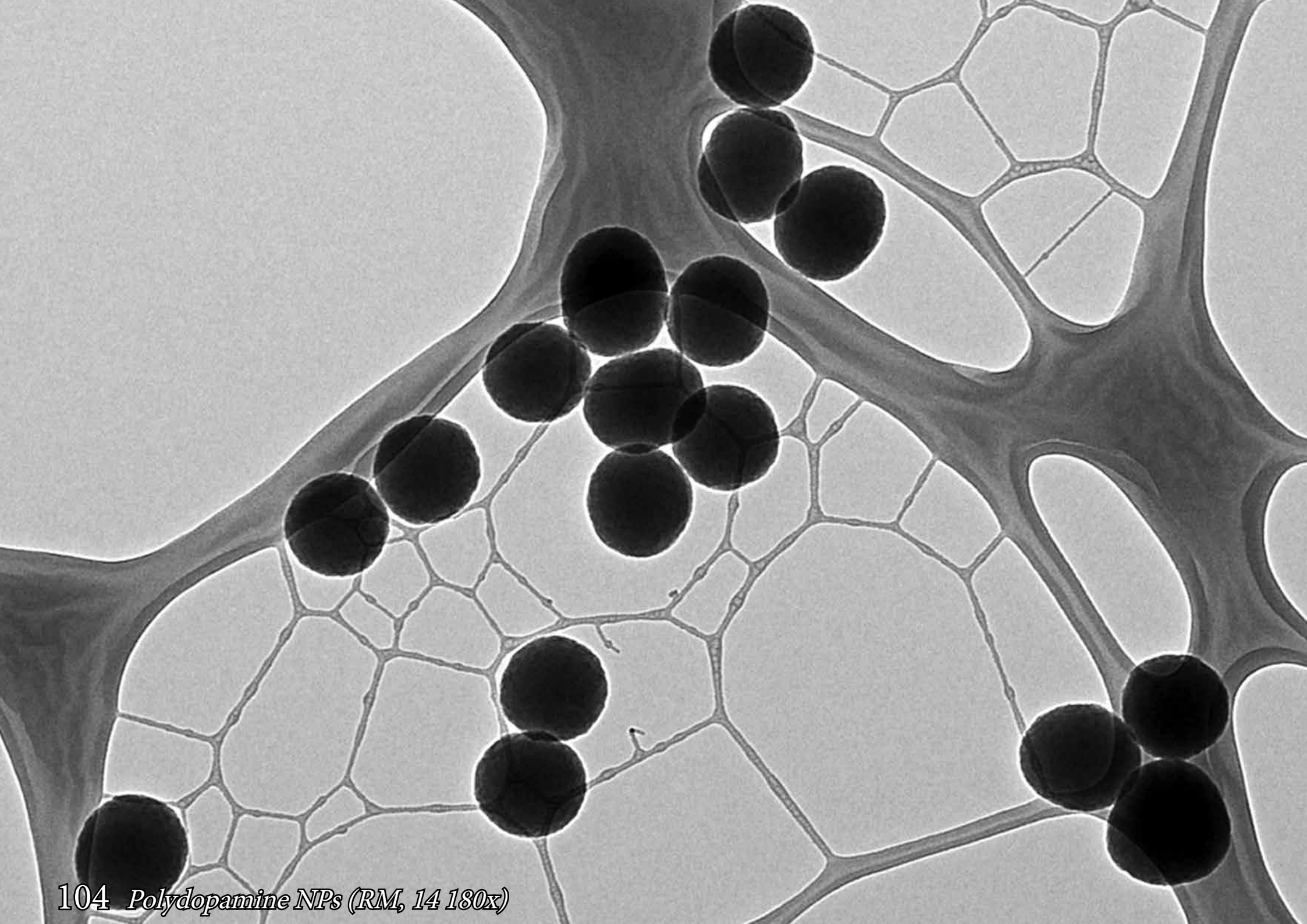

104 *Polydopamine NPs (RM, 14 180x)*

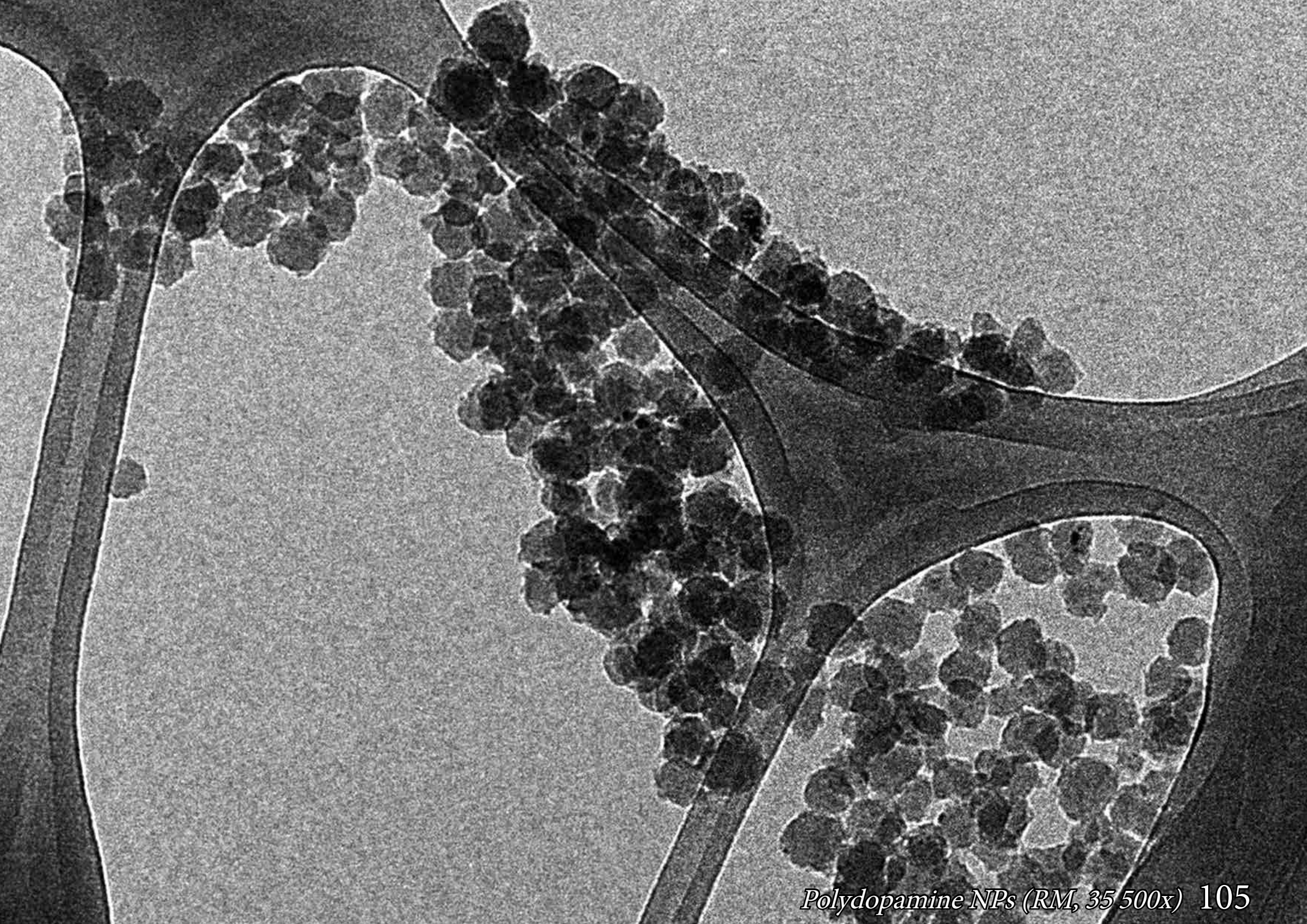

Polydopamine NPs (RM, 35 500x) 105

Rod and star-shaped gold nanoparticles

Nanoparticles were synthesized using seed-mediated growth methods. Later these different shapes of nanoparticles were used to prepare polymer composites, based on the use of transdermal drug delivery systems. The main goal of this research was to investigate the anti-bacterial properties on the surface and in the polymer matrices.

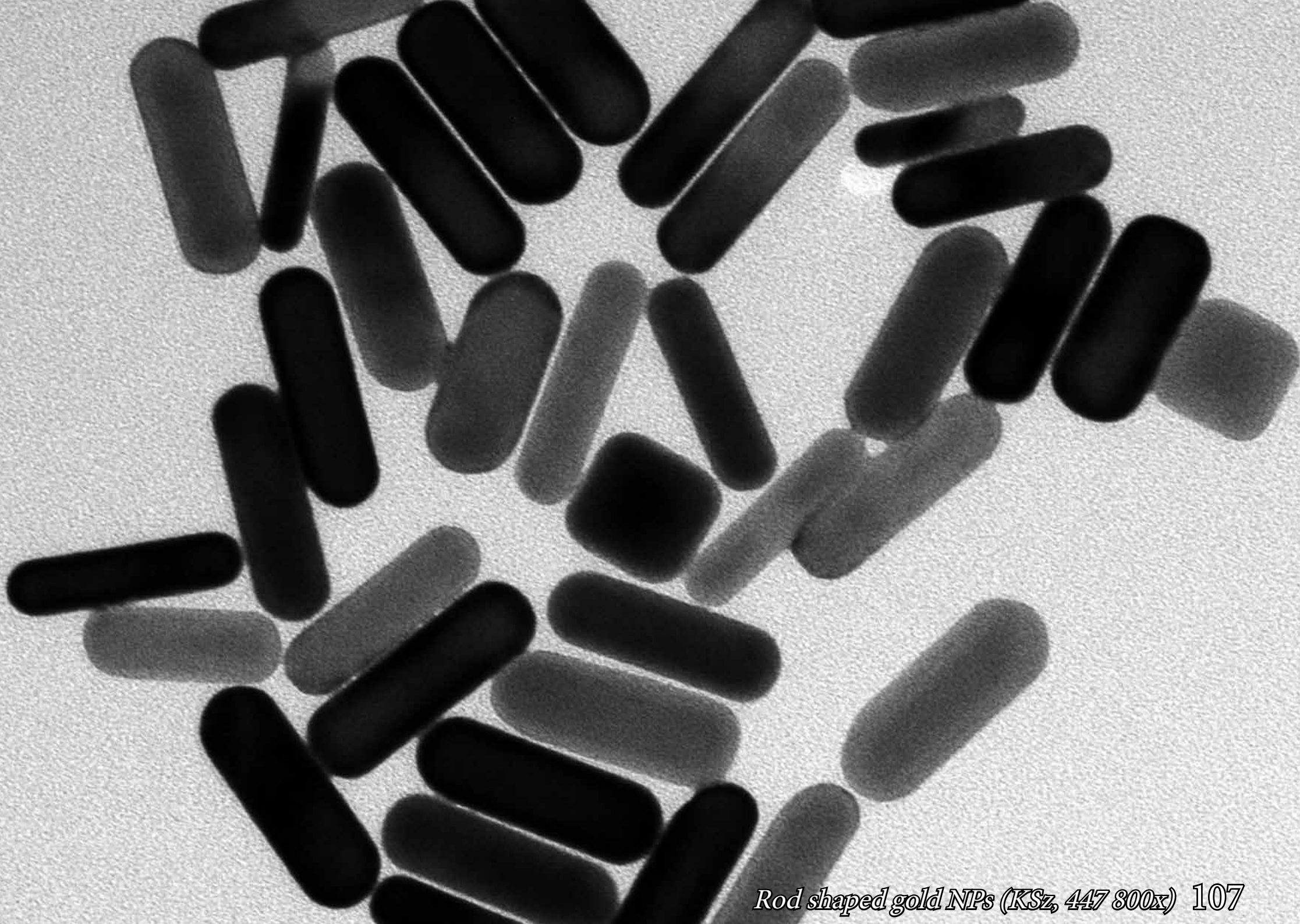

Rod shaped gold NPs (KSz, 447 800x) 107

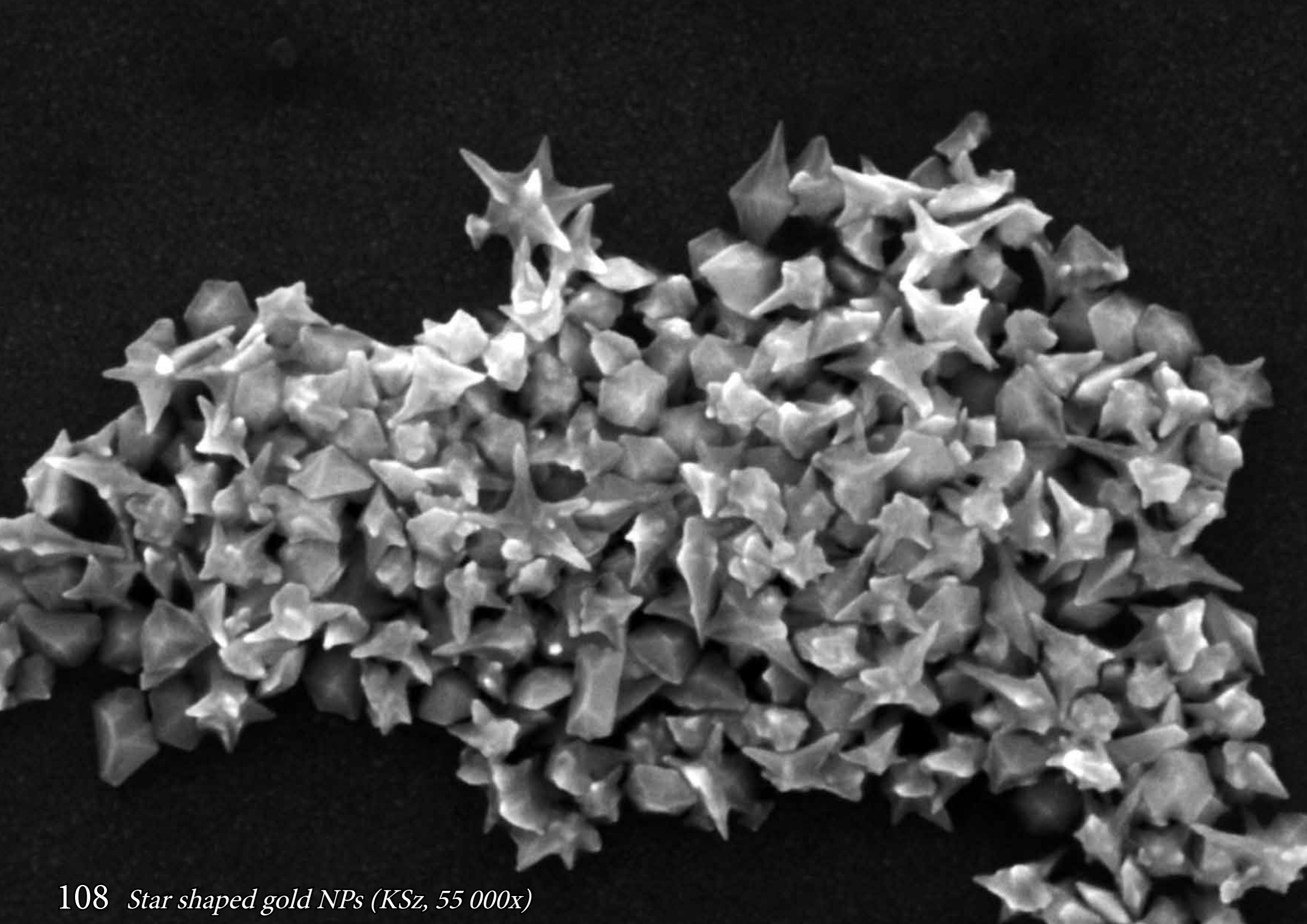

108 *Star shaped gold NPs (KSz, 55 000x)*

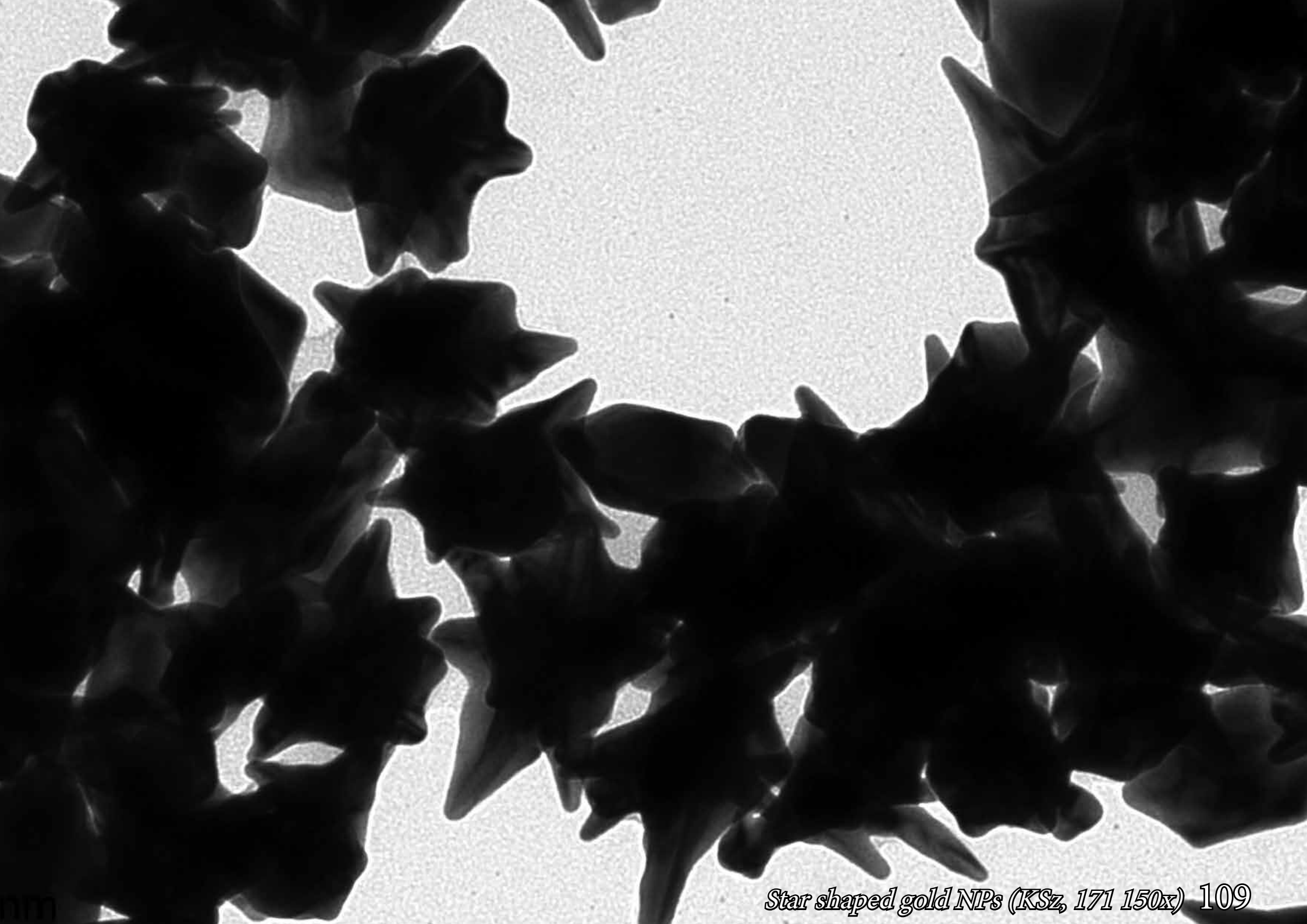

Star shaped gold NPs (KSz, 171 150x) 109

Thin films of gadolinium molybdate

AFM micrographs of the topographic reconstruction observed in the ferroelectric GMO phase, from a fully amorphous to a granular ferroelectric one. The reconstruction takes a sort of leaf-like (dendritic) behaviour, in which midribs and veins are observed, and assumed to work as nucleation fronts, as well as allow the oxygen diffusion and inclusion on the reconstructed surfaces.

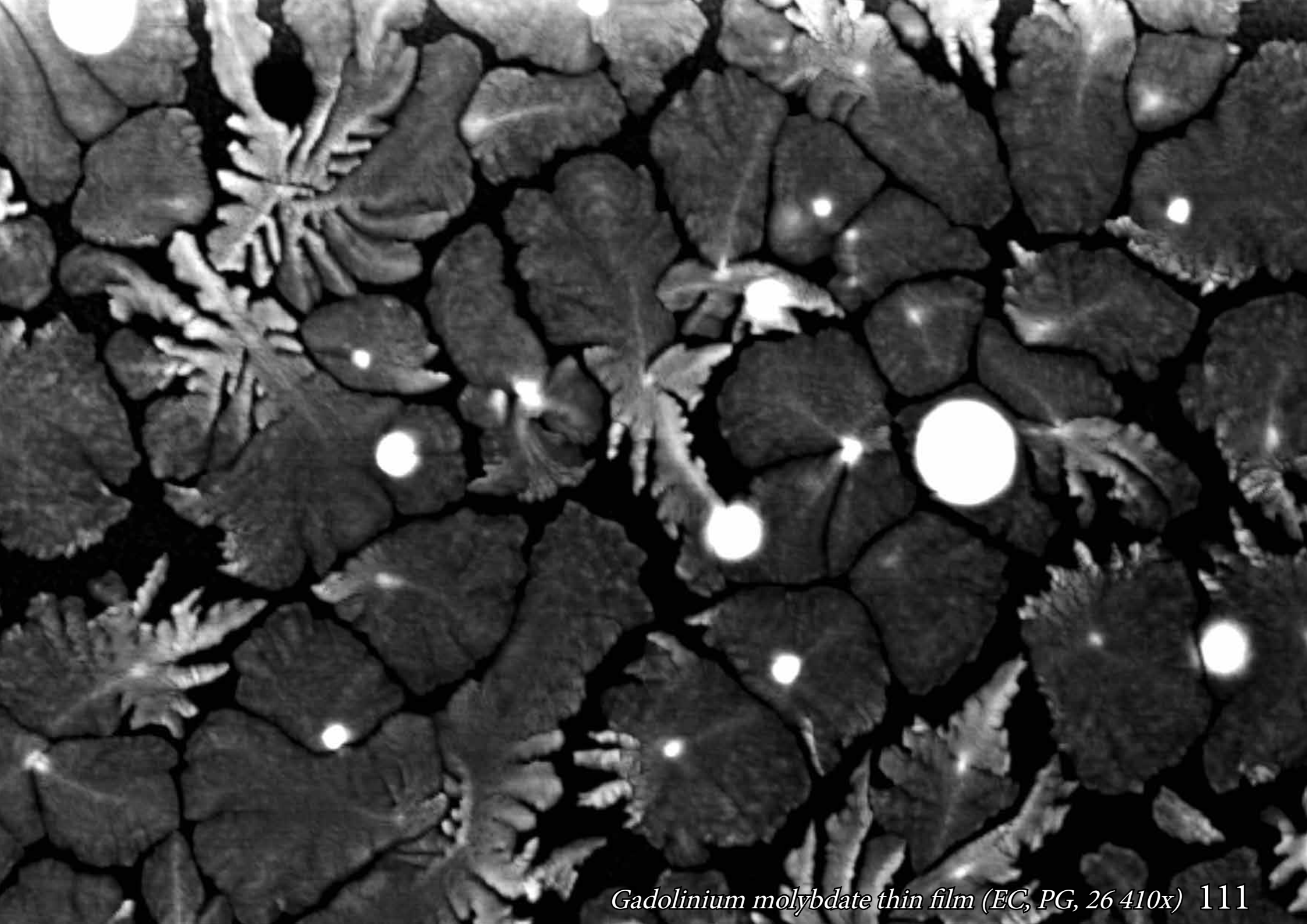

Gadolinium molybdate thin film (EC, PG, 26 410x) 111

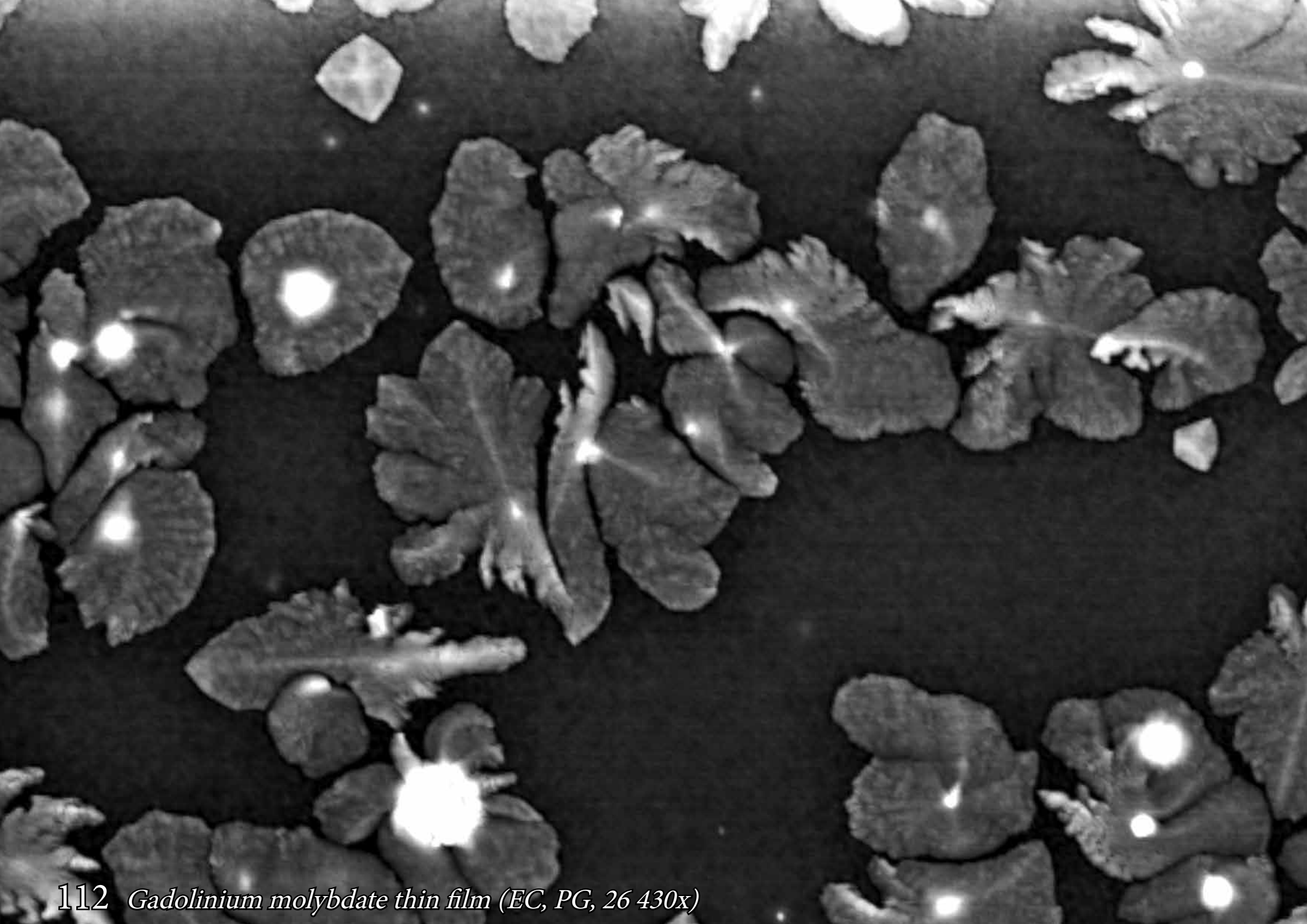

112 *Gadolinium molybdate thin film (EC, PG, 26 430x)*

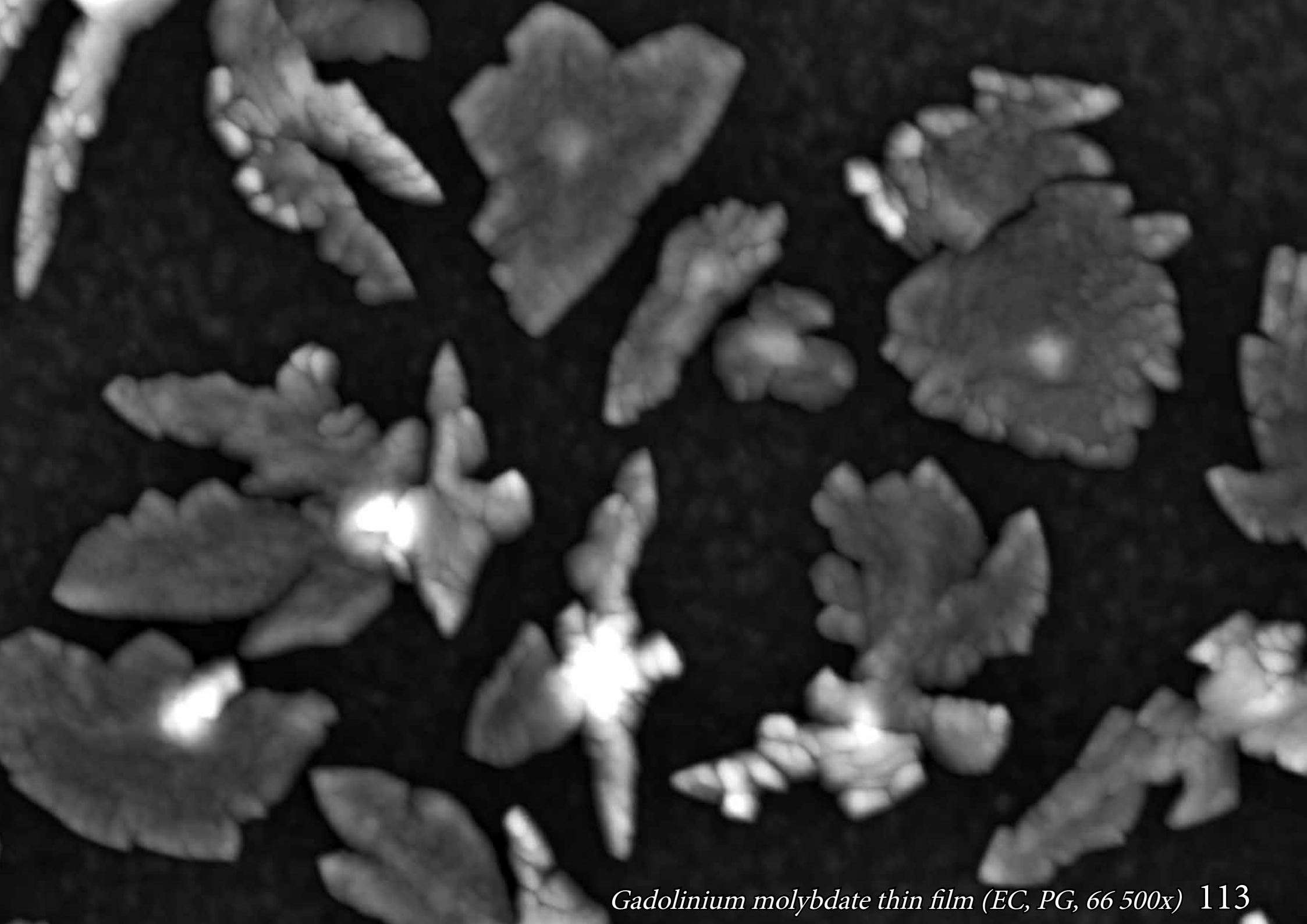

Gadolinium molybdate thin film (EC, PG, 66 500x) 113

Polymeric PVP fibers

Fibers were fabricated by electrospinning method from aqueous polyvinylpyrrolidone (PVP) solution. In this method, fibers are spun under the driving electric force that draws charged threads of polymer solution to form fibrillar mats, which could be potentially used as scaffolds in biomedical applications.

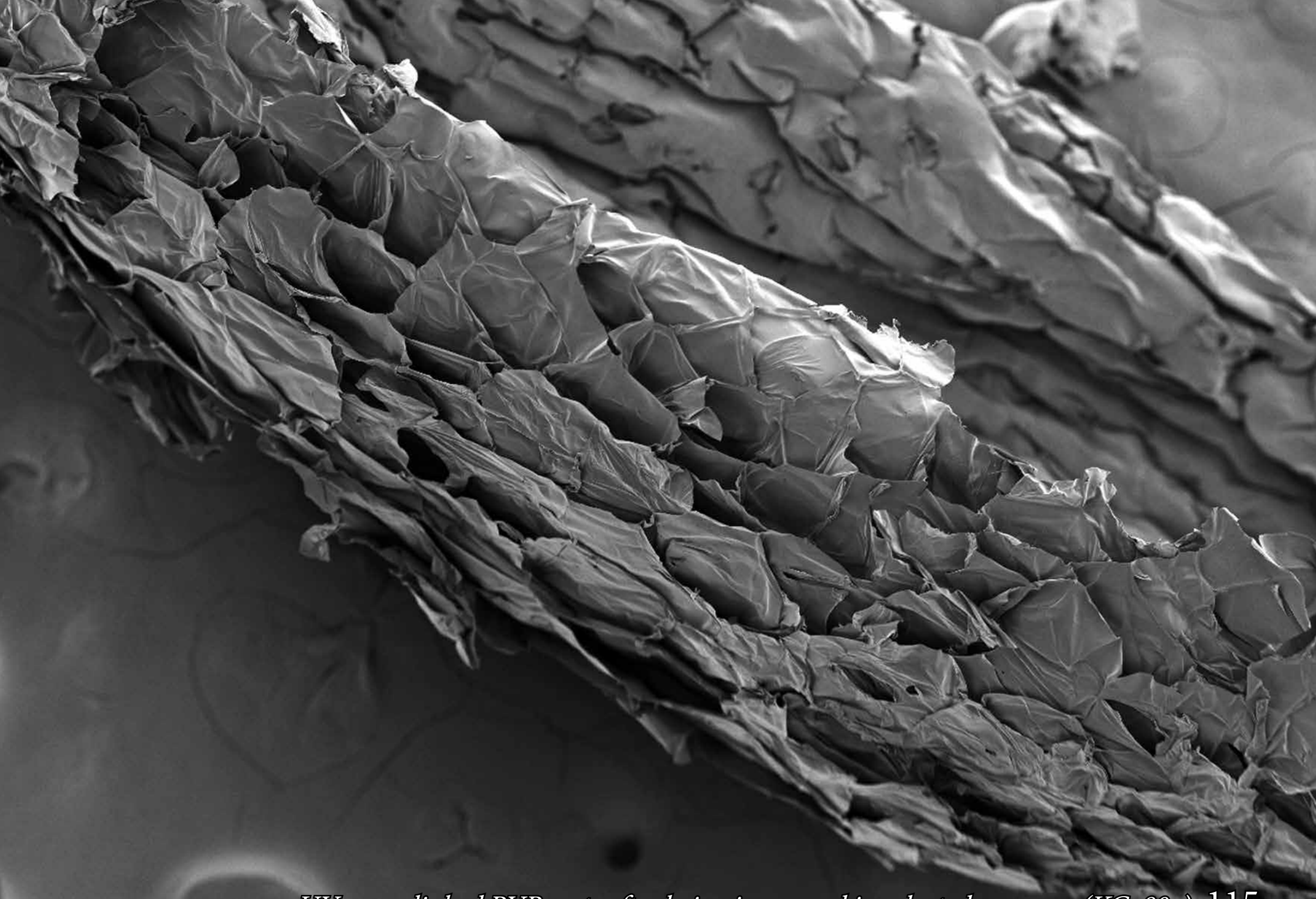

UV cross-linked PVP mats after being immersed in selected enzymes (KG, 80x)

116 *UV cross-linked PVP mats after being immersed in water (KG, 1 800x)*

PVP fibers (KG, 2 000x) 117

Boron nitride nanotubes

Boron nitride nanotubes with tunable dimensions were made by combining atomic layer deposition (ALD) of boron nitride on carbon nanofibers as template supports. The nanotubes present good mechanical properties and their absorption is up to 110 times their own weight in oils while repelling water.

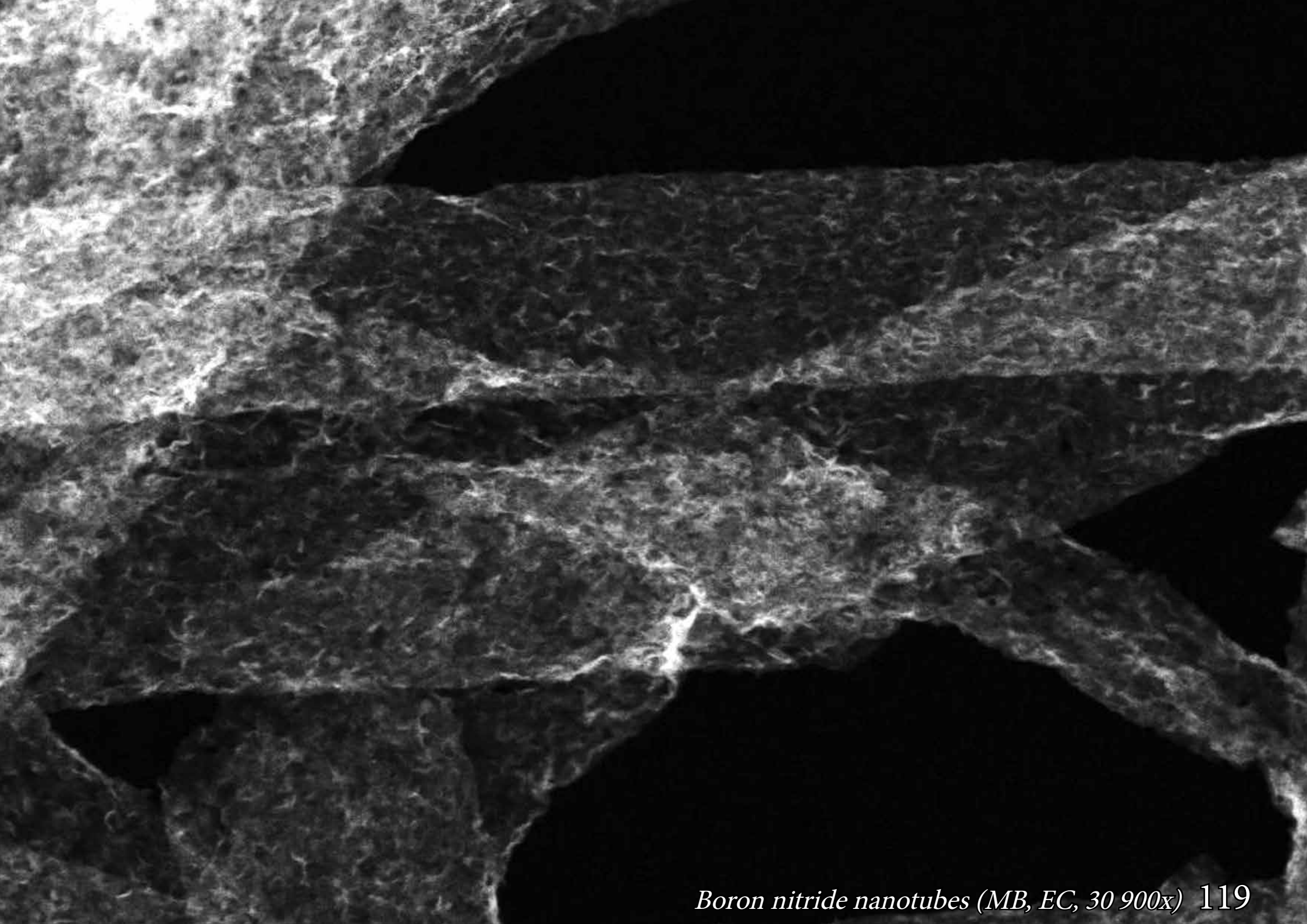

Boron nitride nanotubes (MB, EC, 30 900x) 119

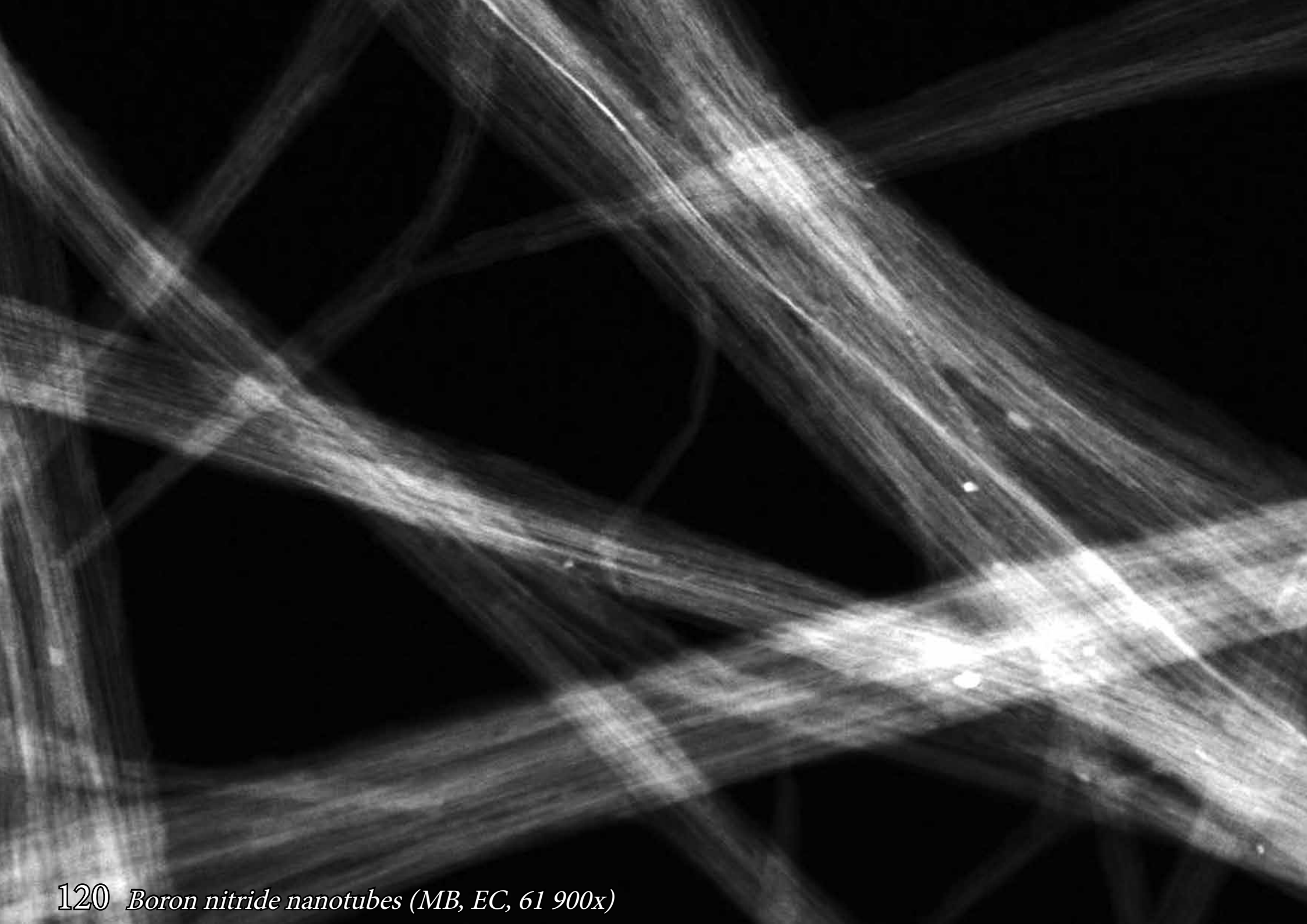

120 *Boron nitride nanotubes (MB, EC, 61 900x)*

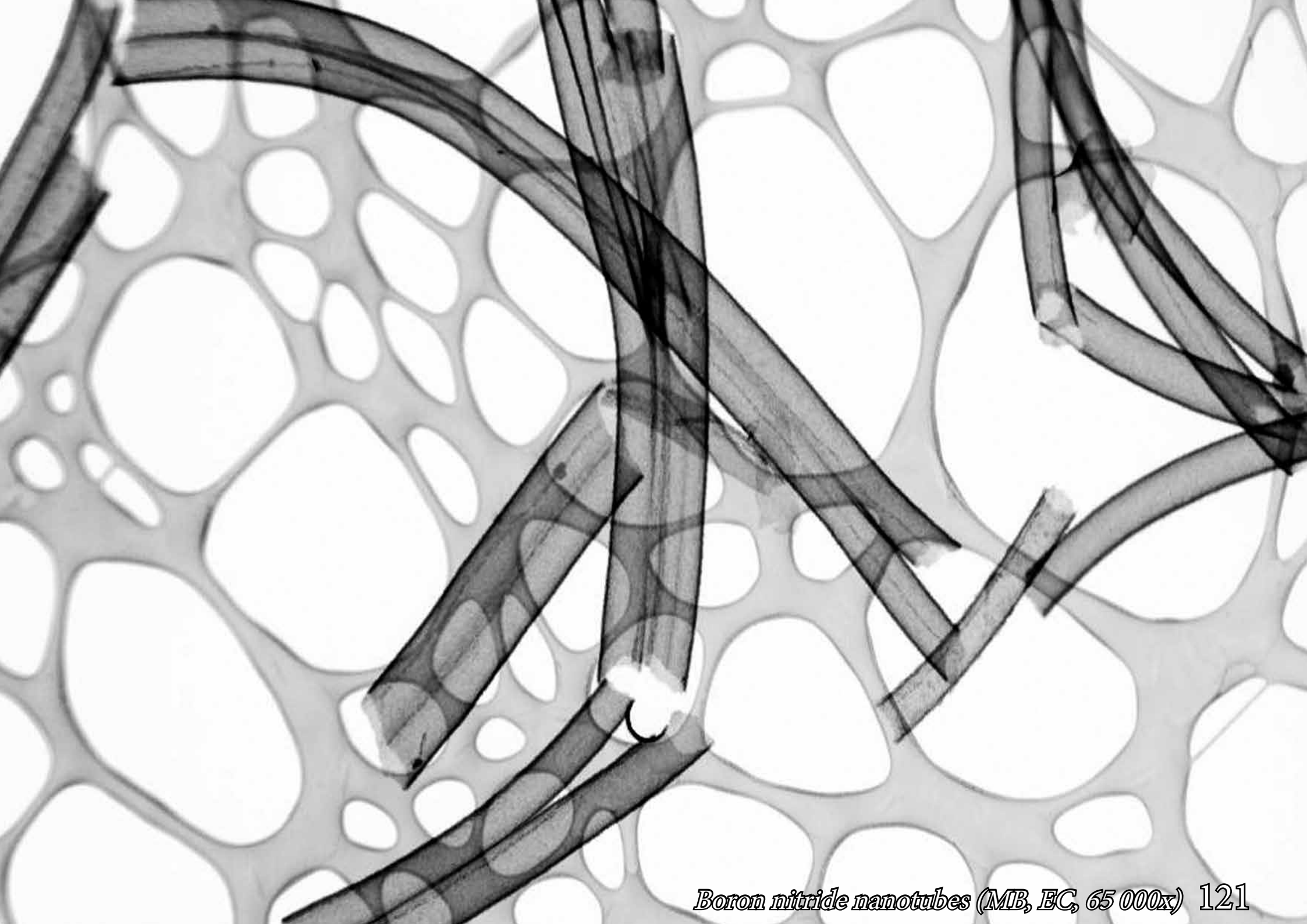

Boron nitride nanotubes (MB, EC, 65 000x) 121

Zinc phthalocyanine crystals

Phthalocyanine micro crystals doped with zinc can serve as therapeutic agent in cancer treatment. In combination with liposomes, zinc phthalocyanine molecules can be delivered to the cancerous tissue as photosensitizer for photodynamic therapy.

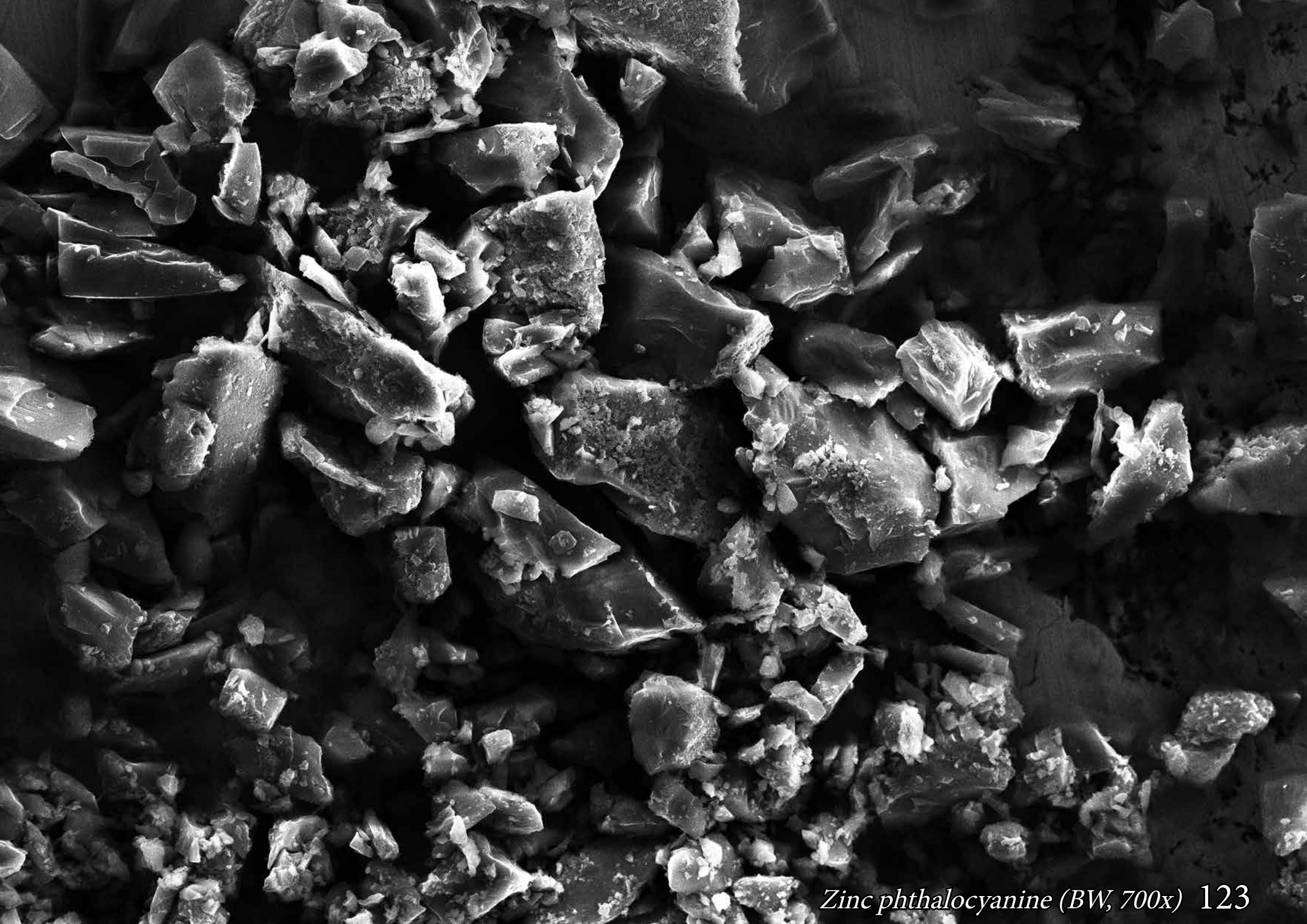

Zinc phthalocyanine (BW, 700x)

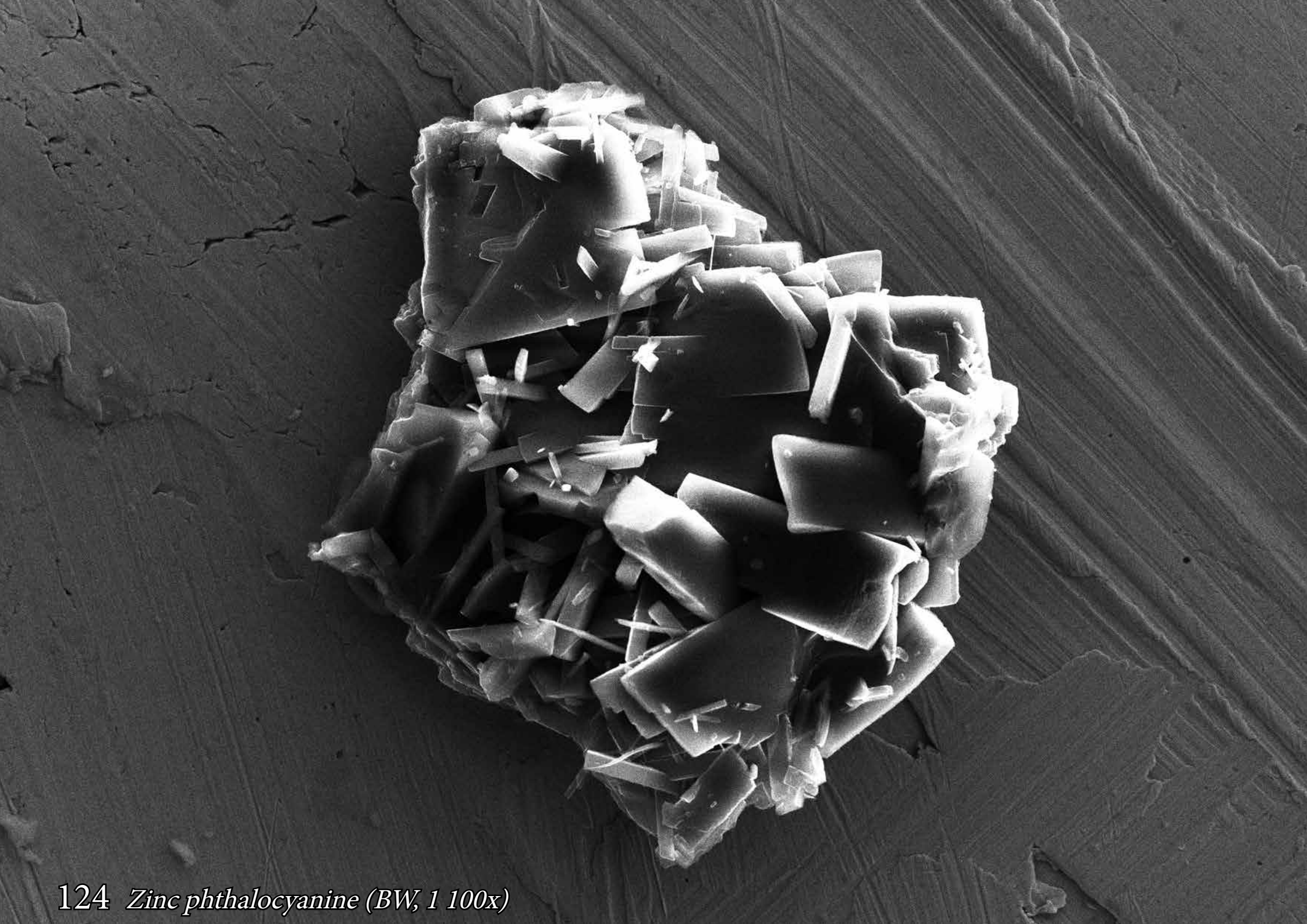

124 *Zinc phthalocyanine (BW, 1 100x)*

Zinc phthalocyanine (BW, 3500x) 125

Silica/GO aerogel composite

Composites of silicon nanoparticles ~900 nm with partially reduced graphene oxide aerogels. The presented structures can be used as electrode material for high-performance supercapacitors.

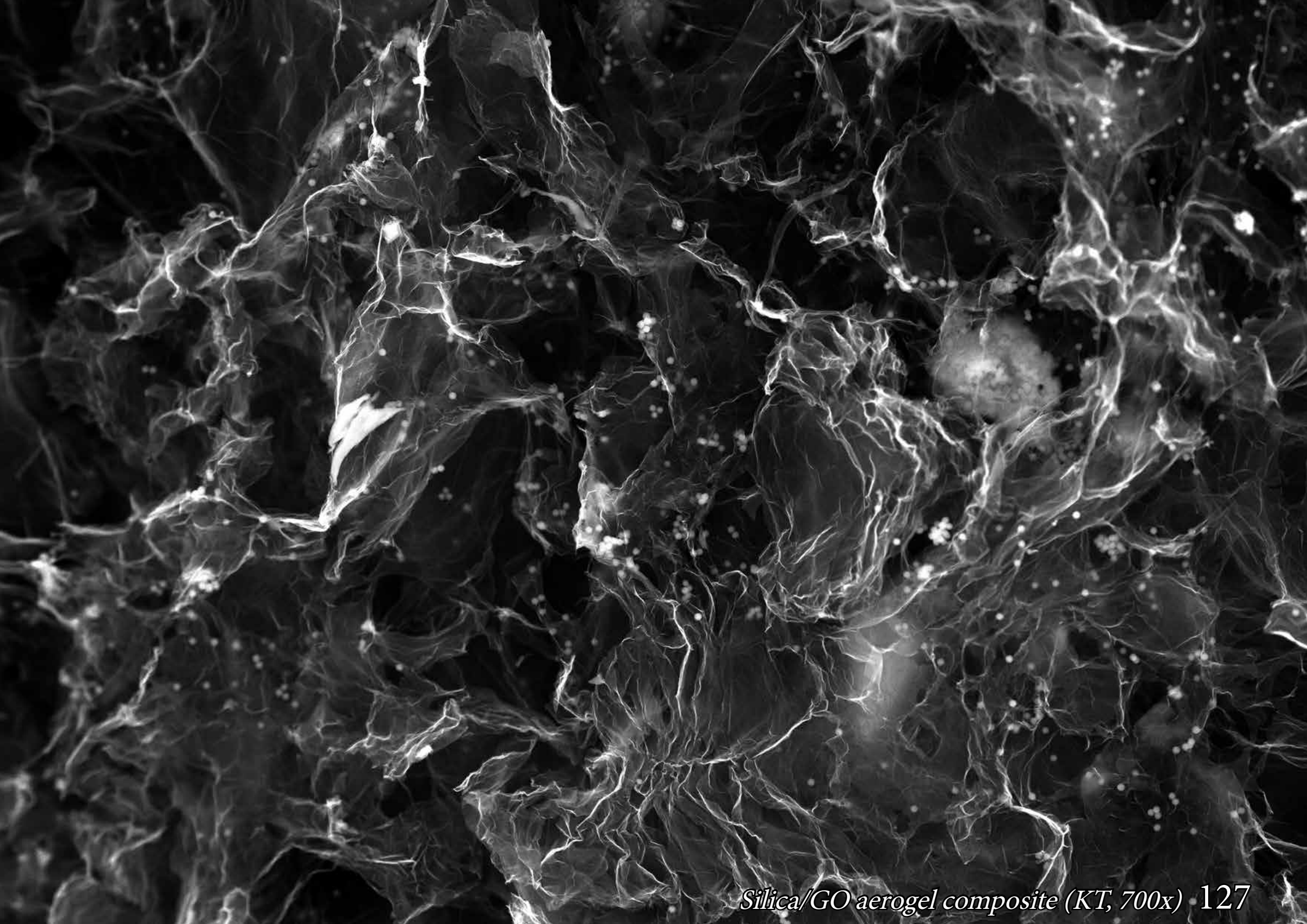

Silica/GO aerogel composite (KT, 700x) 127

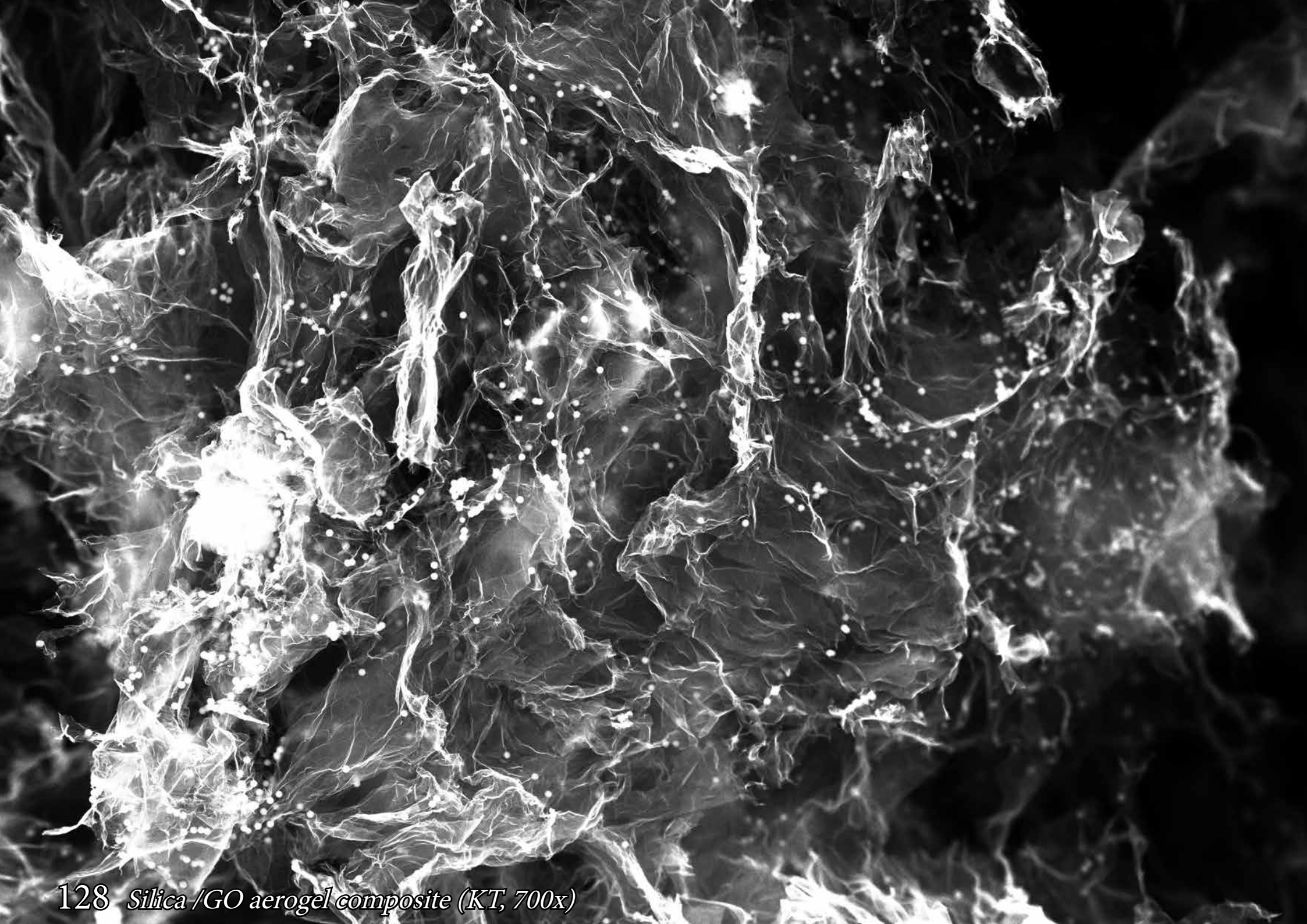

128 *Silica /GO aerogel composite (KT, 700x)*

Silica/GO aerogel composite (KT, 2 000x) 129

Vitreous carbon foams

Highly viscous organic resin of plant or synthetic origin in anaerobic conditions and at high temperature (1000 °C) carbonizes and forms porous non-crystalline carbon structure presented on the subsequent micrographs. To control and form pores in the structure, a blowing agent is added during carbonization process. It resembles bread baking process.

Vitreous carbon foam (KT, 120x) 131

132 *Vitreous carbon foam (KT, 190x)*

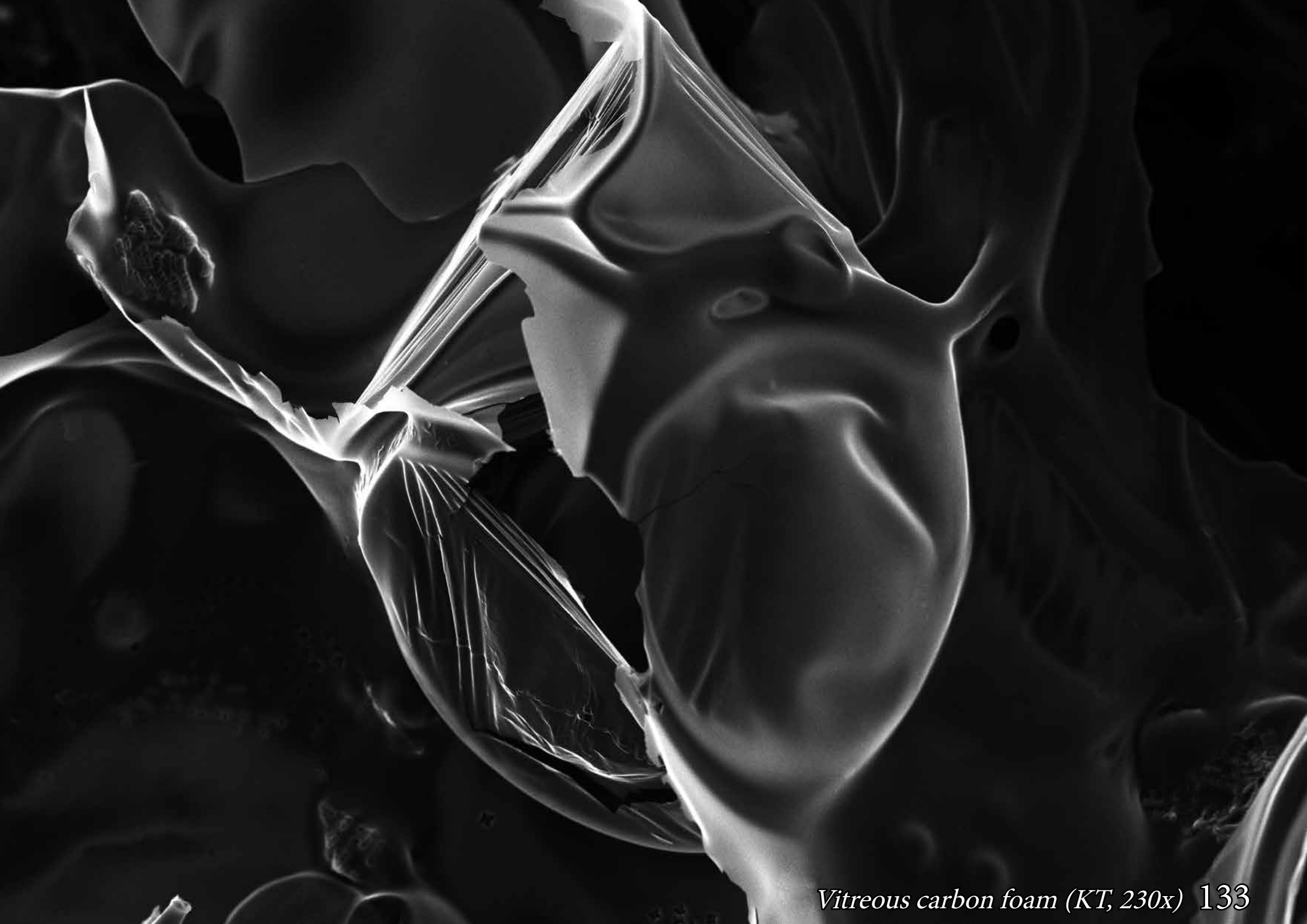

Vitreous carbon foam (KT, 230x)

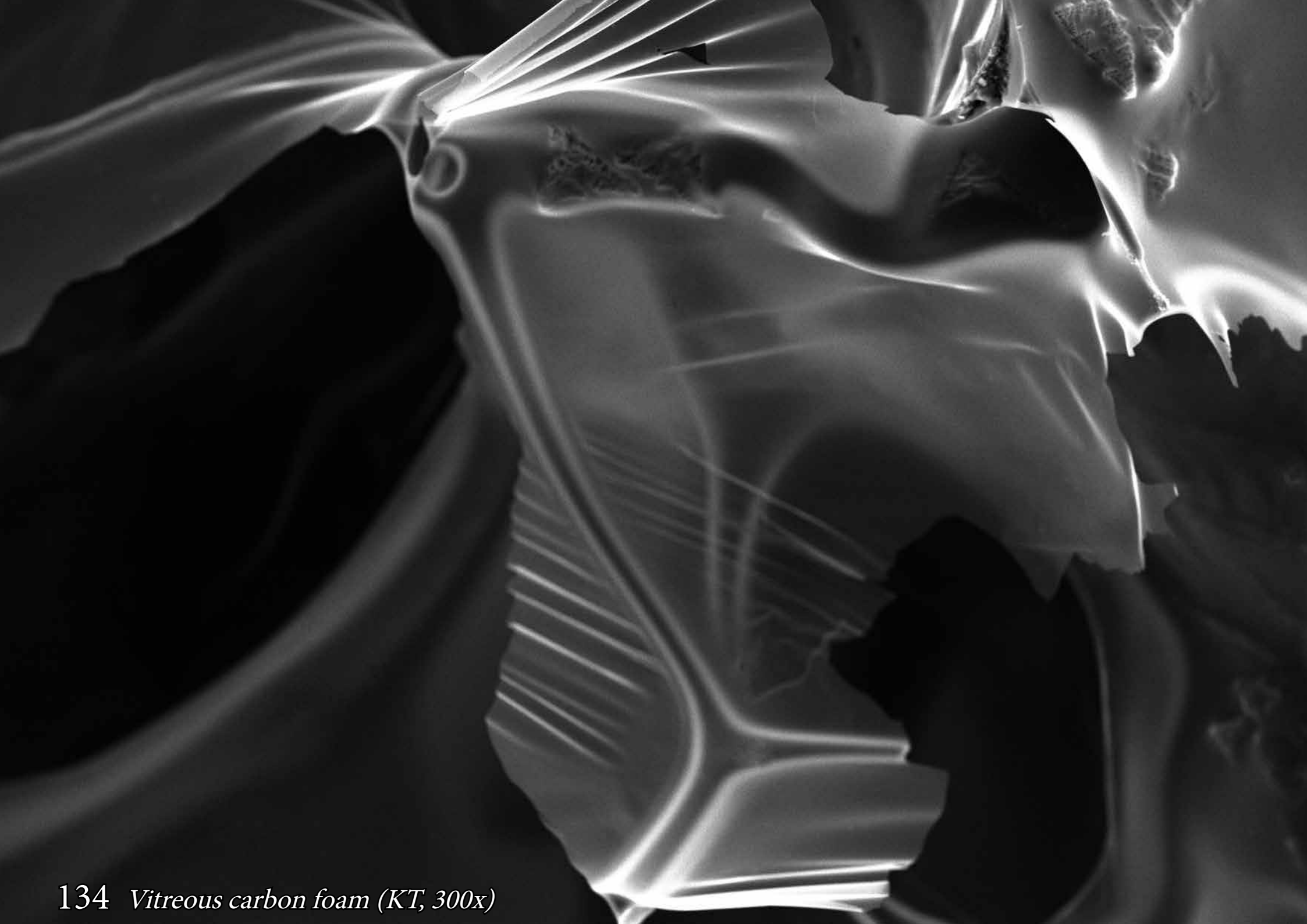

134 *Vitreous carbon foam (KT, 300x)*

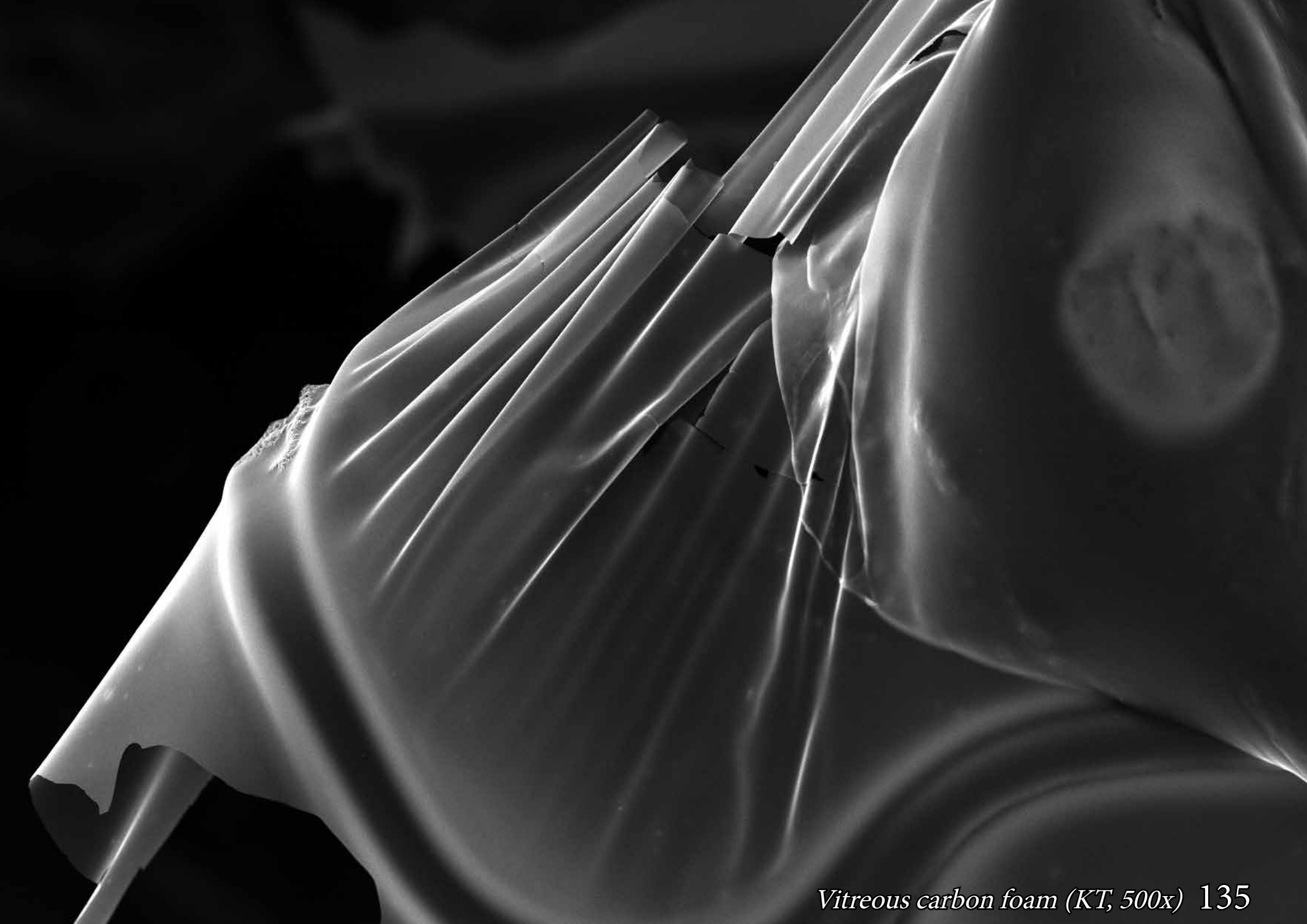

Vitreous carbon foam (KT, 500x) 135

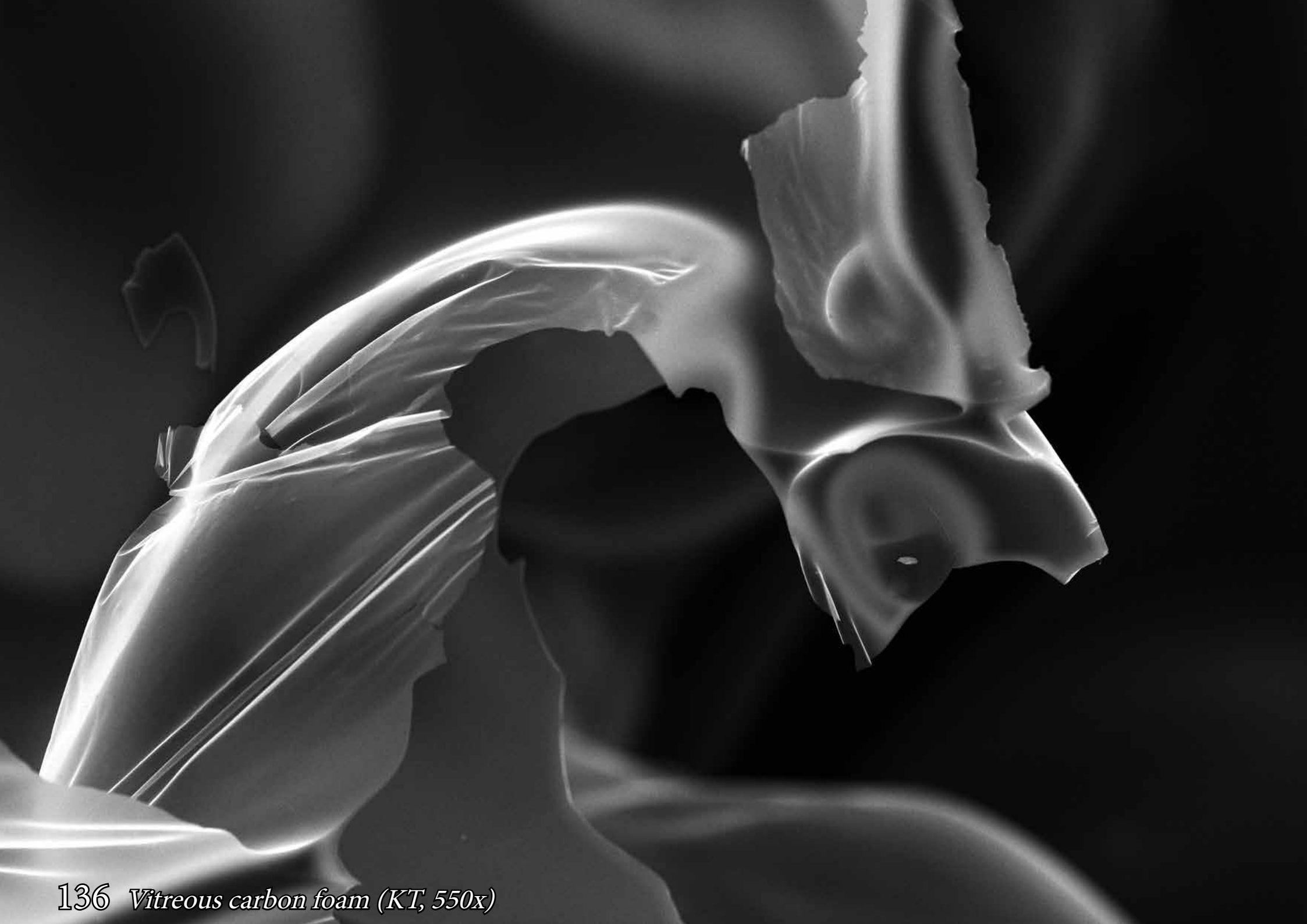

136 *Vitreous carbon foam (KT, 550x)*

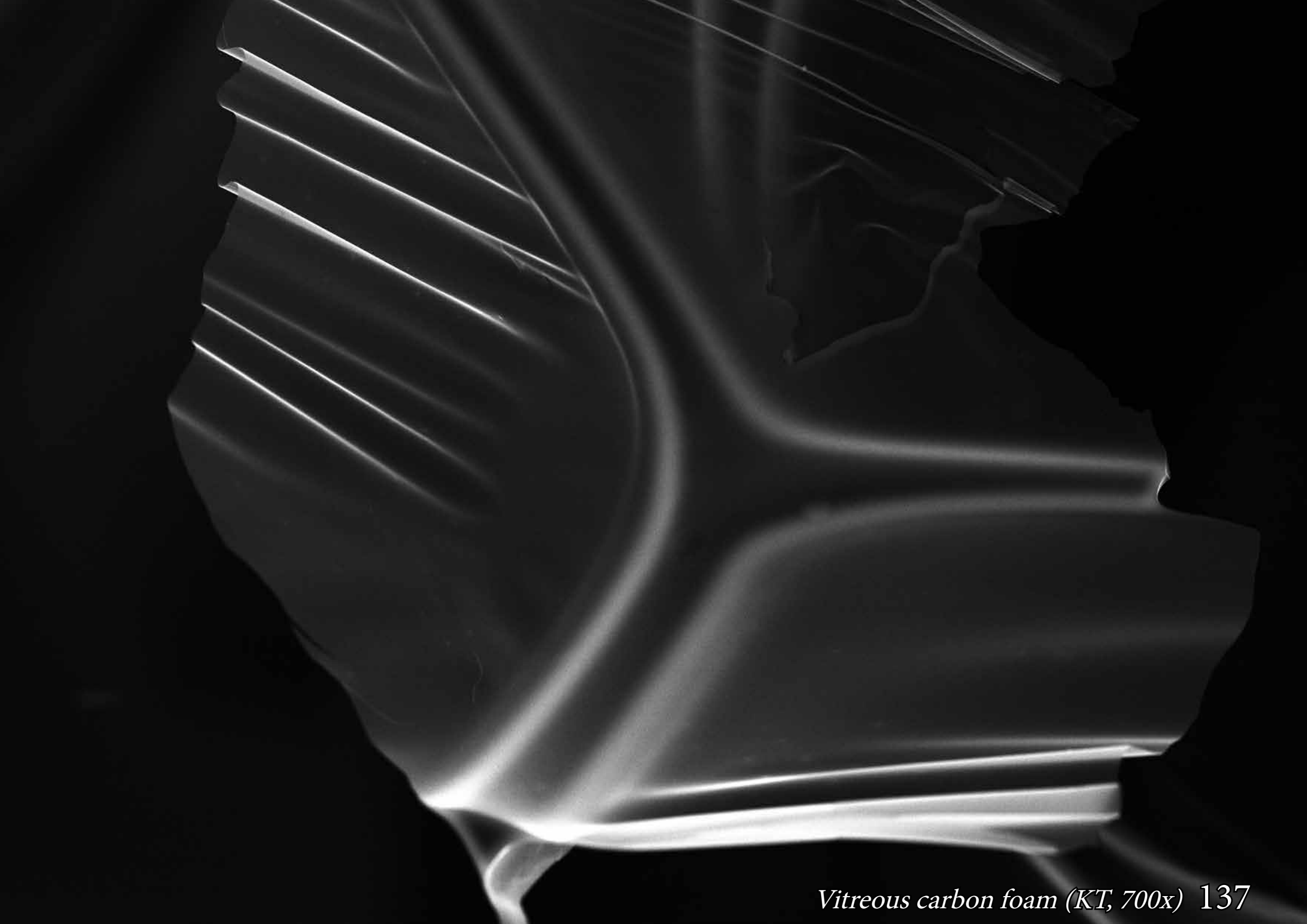

Vitreous carbon foam (KT, 700x) 137

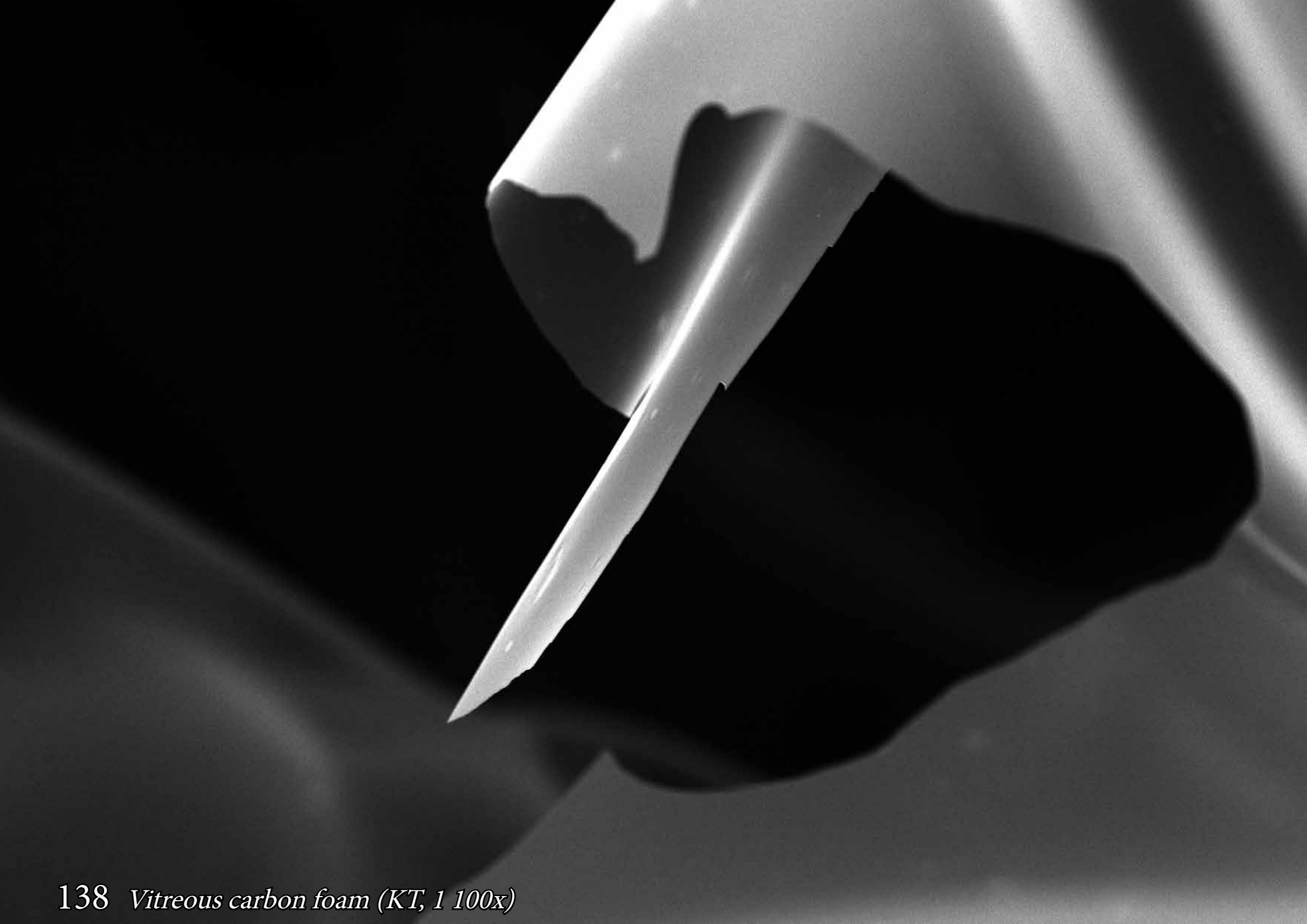

138 *Vitreous carbon foam (KT, 1 100x)*

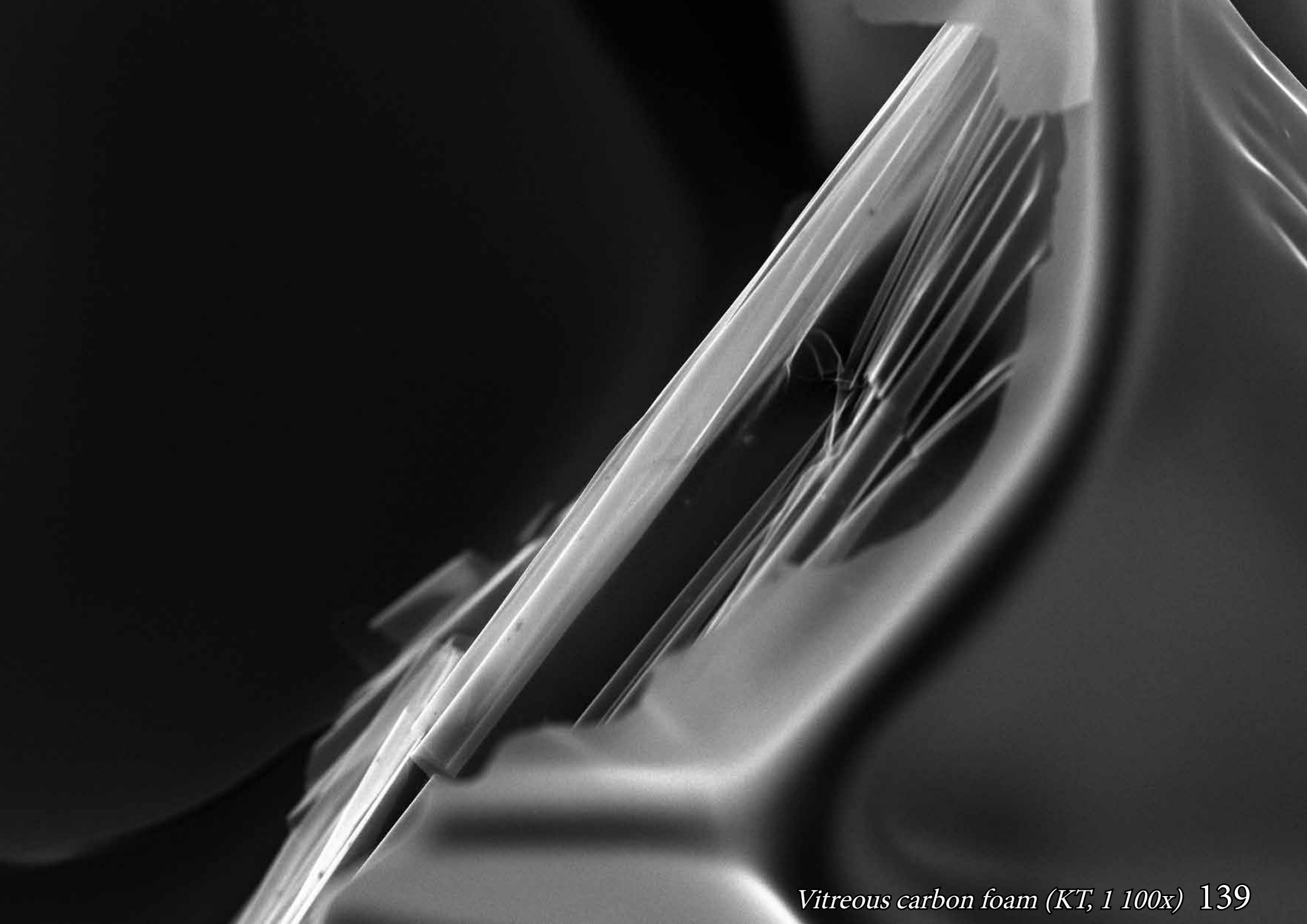

Vitreous carbon foam (KT, 1 100x) 139

140 *Vitreous carbon foam (KT, 1 600x)*

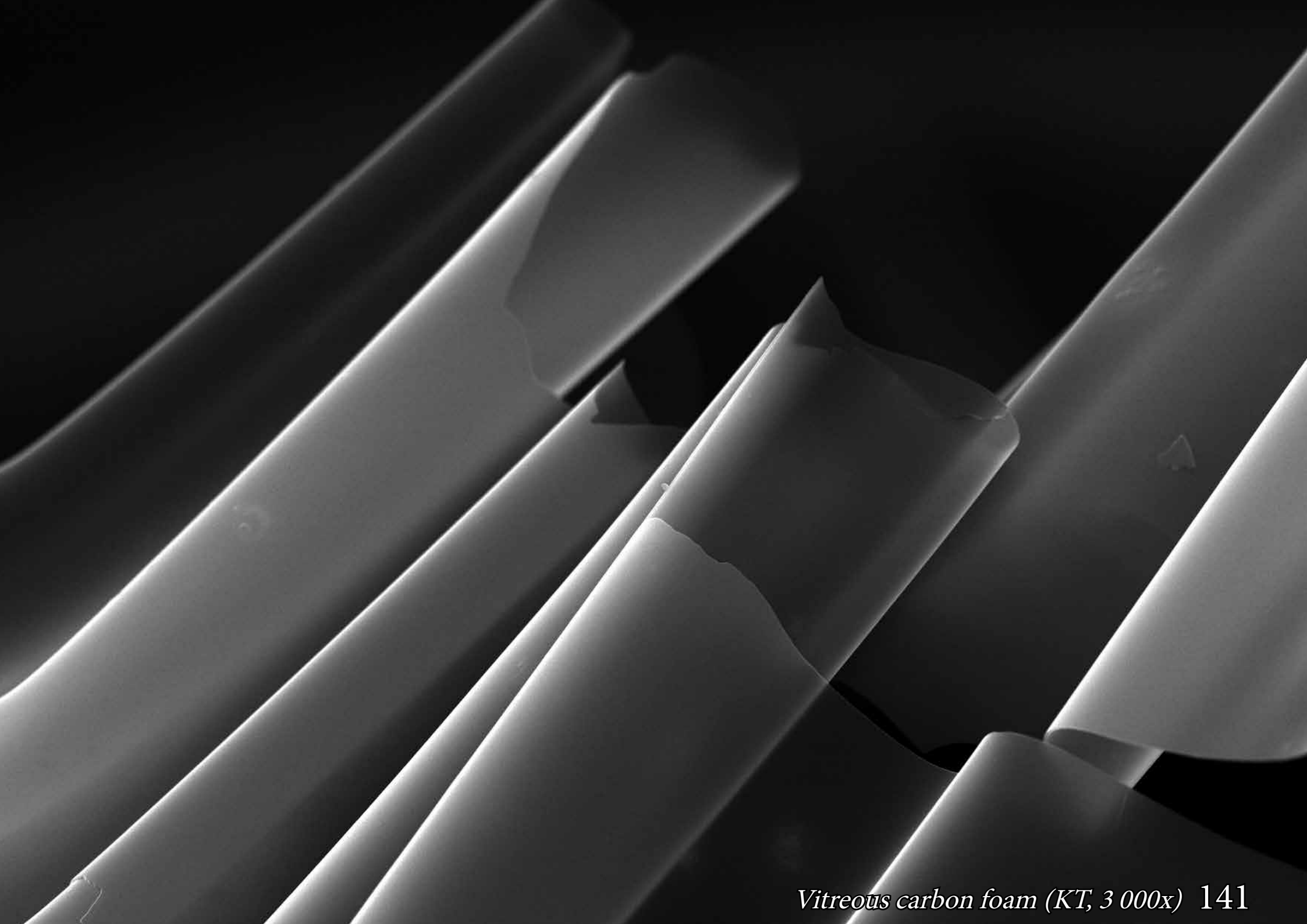

Vitreous carbon foam (KT, 3 000x) 141

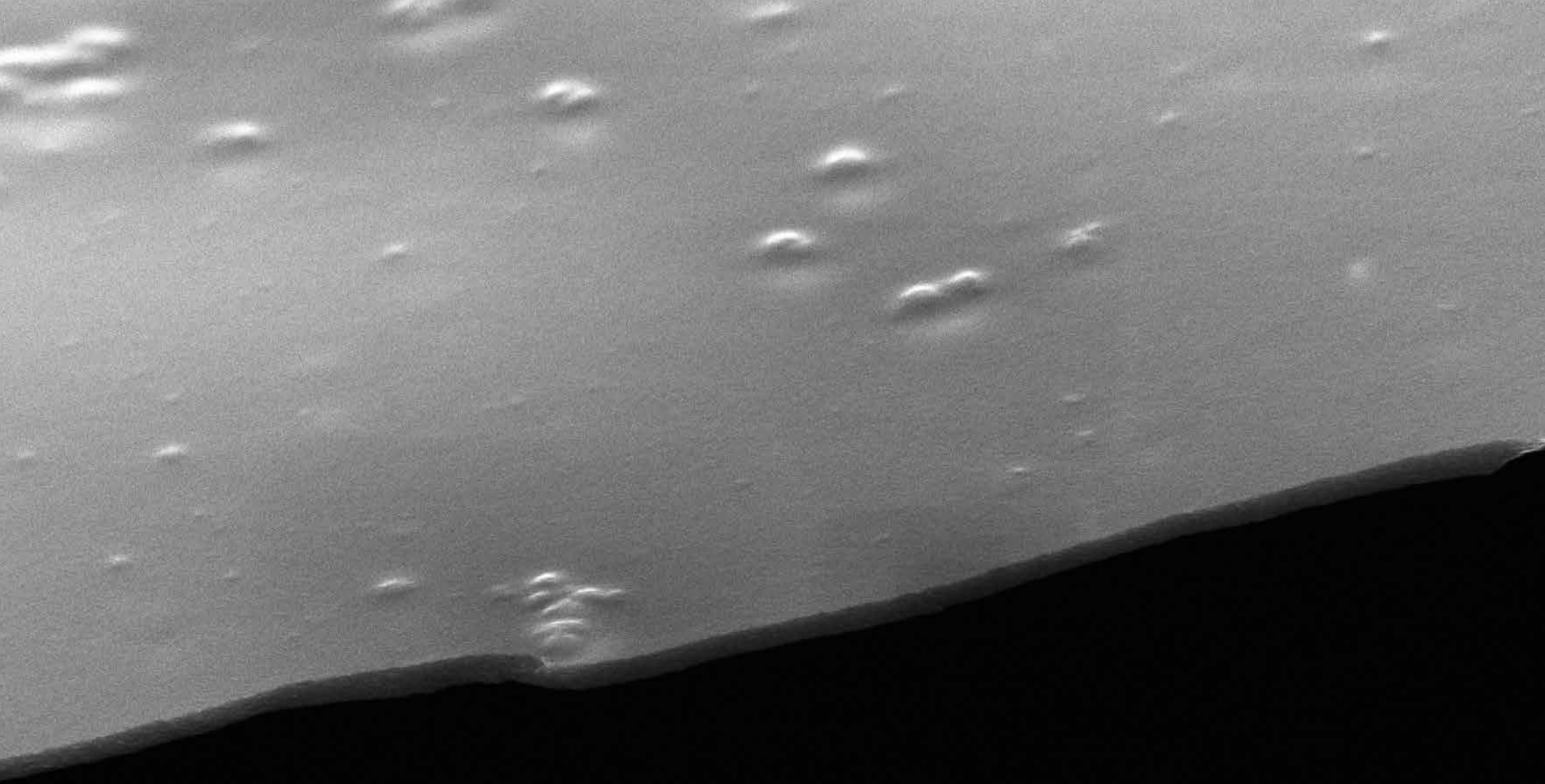

142 *Vitreous carbon foam 120 nm thick membrane (KT, 14 000x)*

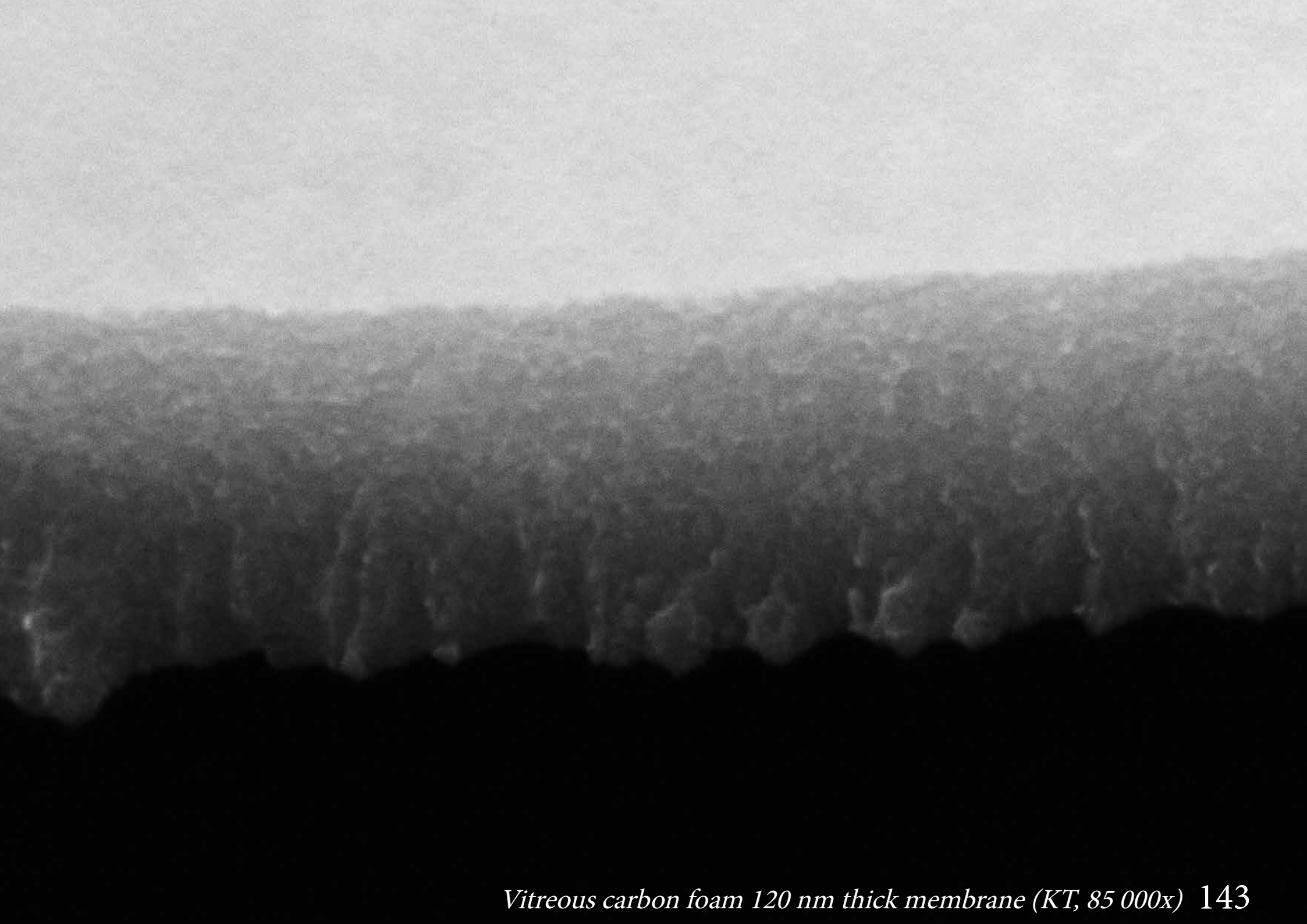

Vitreous carbon foam 120 nm thick membrane (KT, 85 000x)

Human cells on vitreous carbon foams

Non-malignant human embryonic kidney (HEK-293) and malignant neuroblastoma cells (SH-SY5Y) attached to porous carbon foam prepared from carbonized in 1100 °C sucrose.

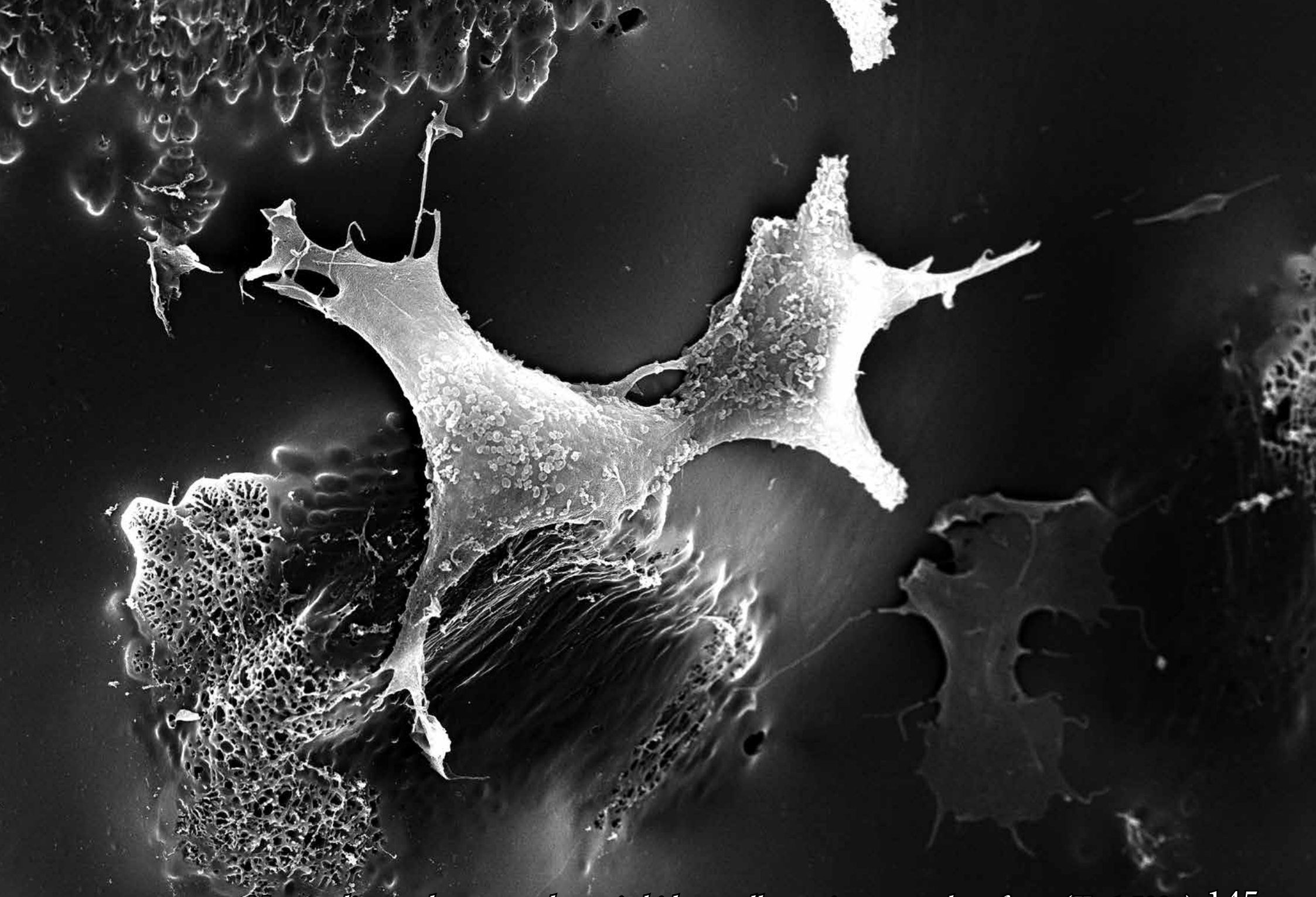

Non-malignant human embryonic kidney cells on vitreous carbon foam (JL, 1 500x)

146 *Non-malignant human embryonic kidney cells on vitreous carbon foam (JL, 1 600x)*

Non-malignant human embryonic kidney cells on vitreous carbon foam (JL, 2 500x)

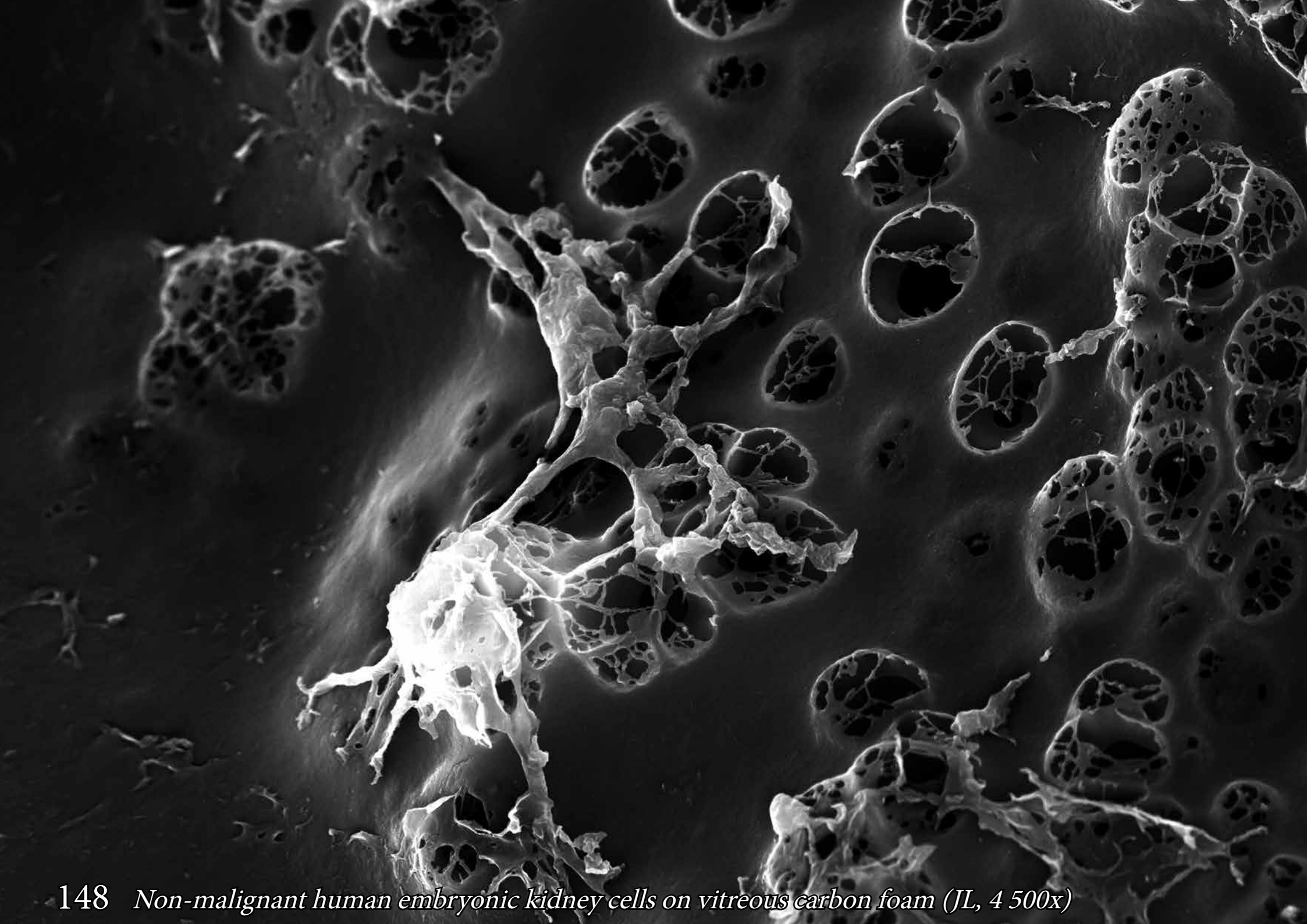

148 *Non-malignant human embryonic kidney cells on vitreous carbon foam (JL, 4 500x)*

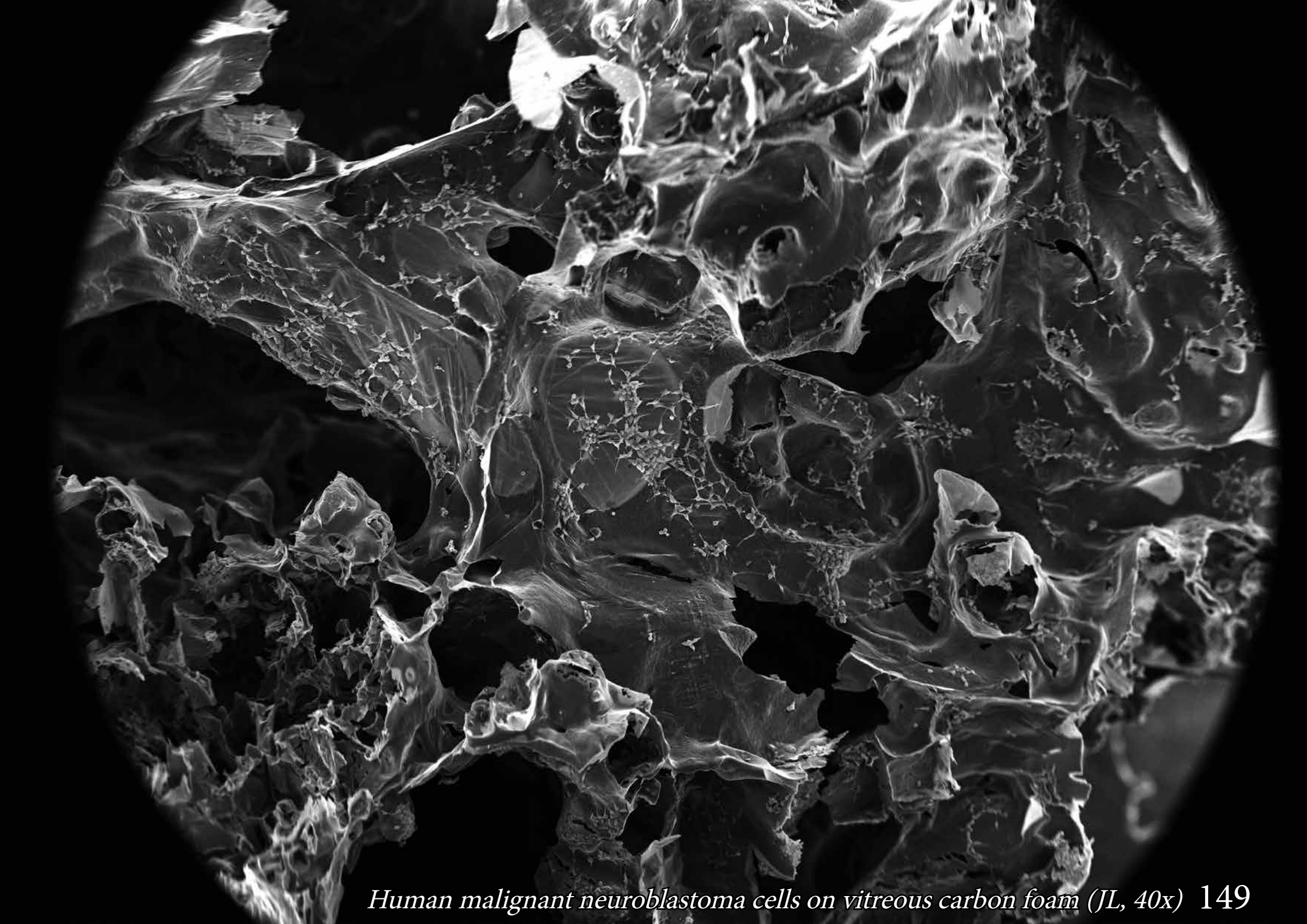

Human malignant neuroblastoma cells on vitreous carbon foam (JL, 40x)

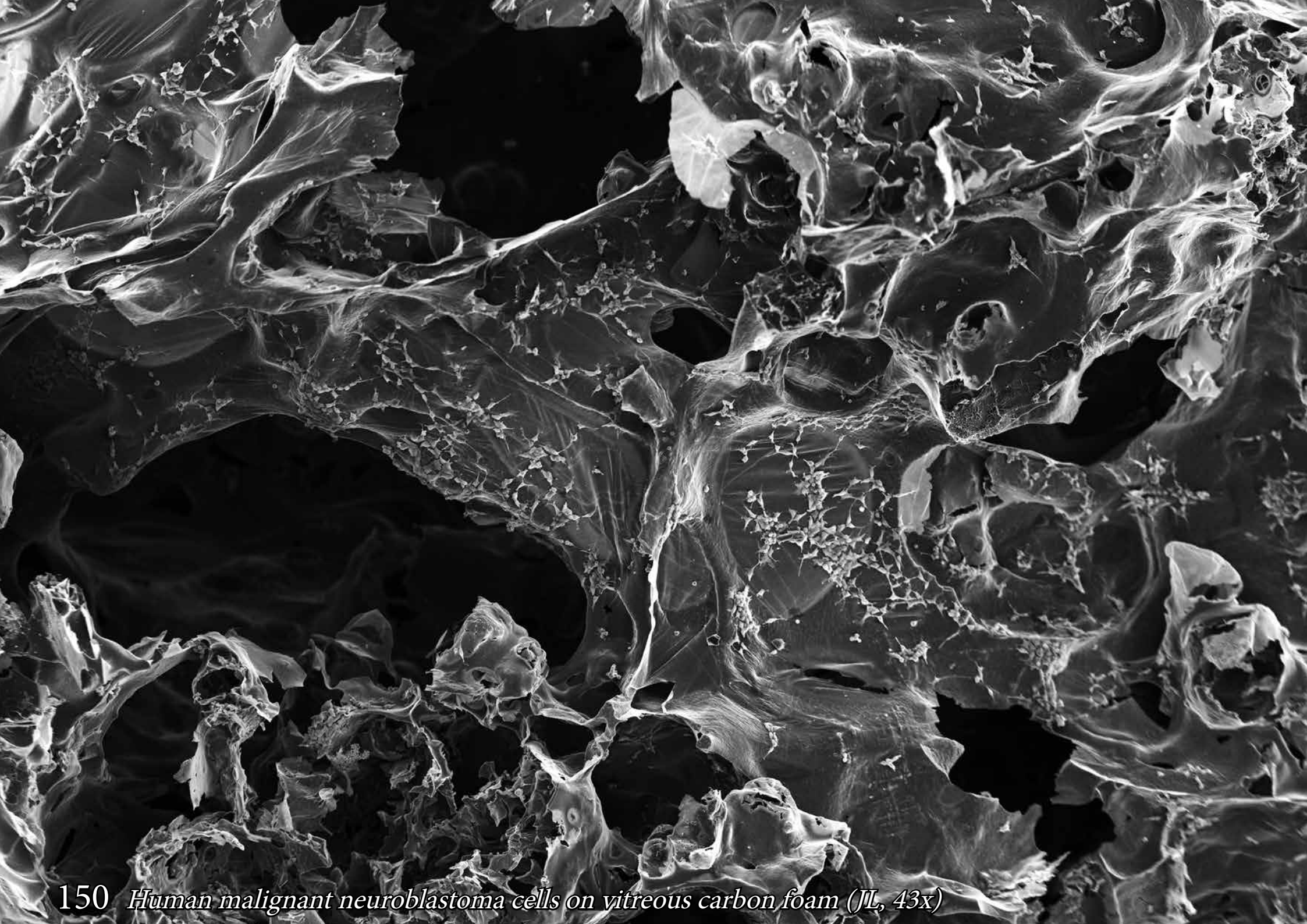

150 *Human malignant neuroblastoma cells on vitreous carbon foam (JL, 43x)*

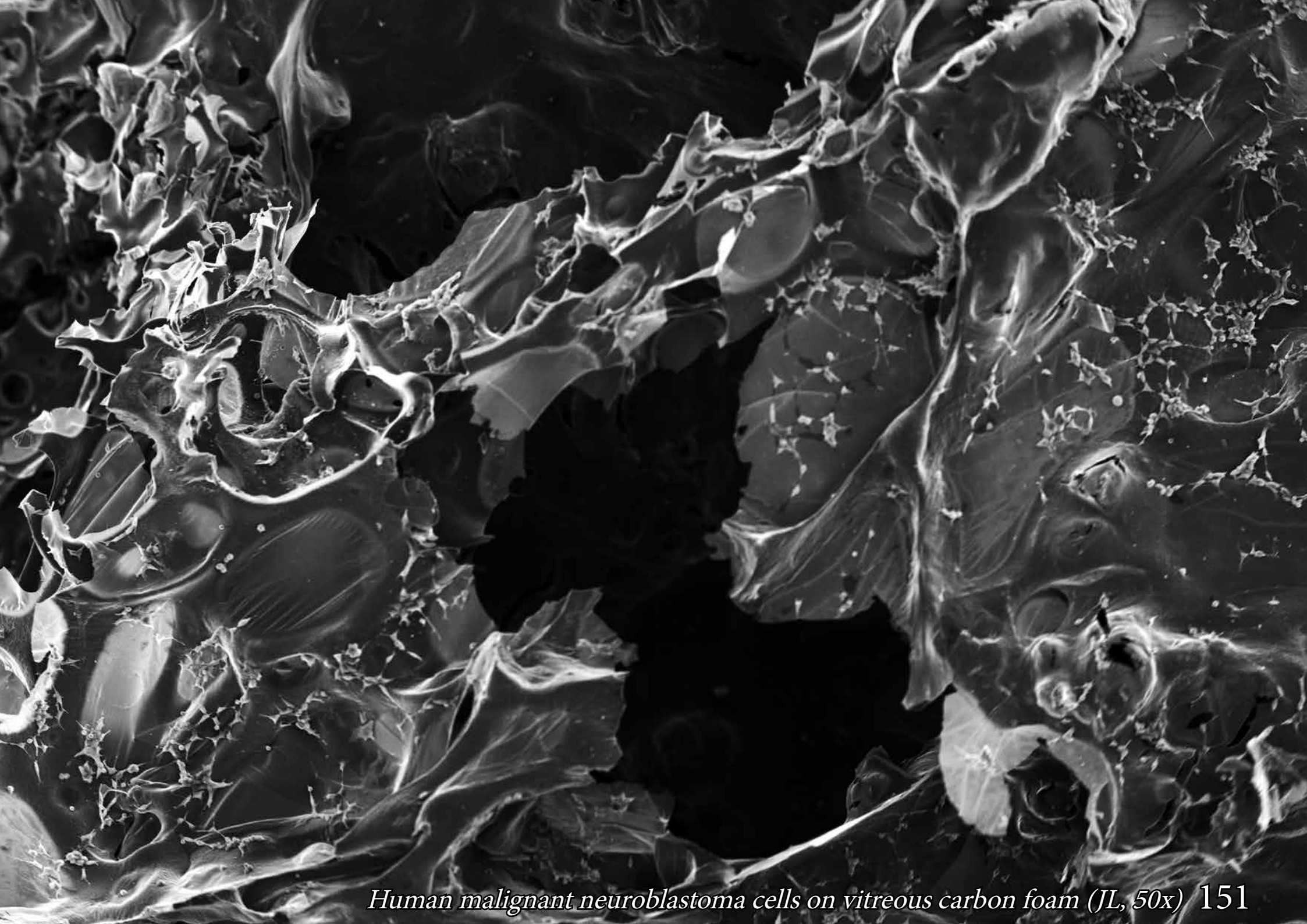

Human malignant neuroblastoma cells on vitreous carbon foam (JL, 50x)

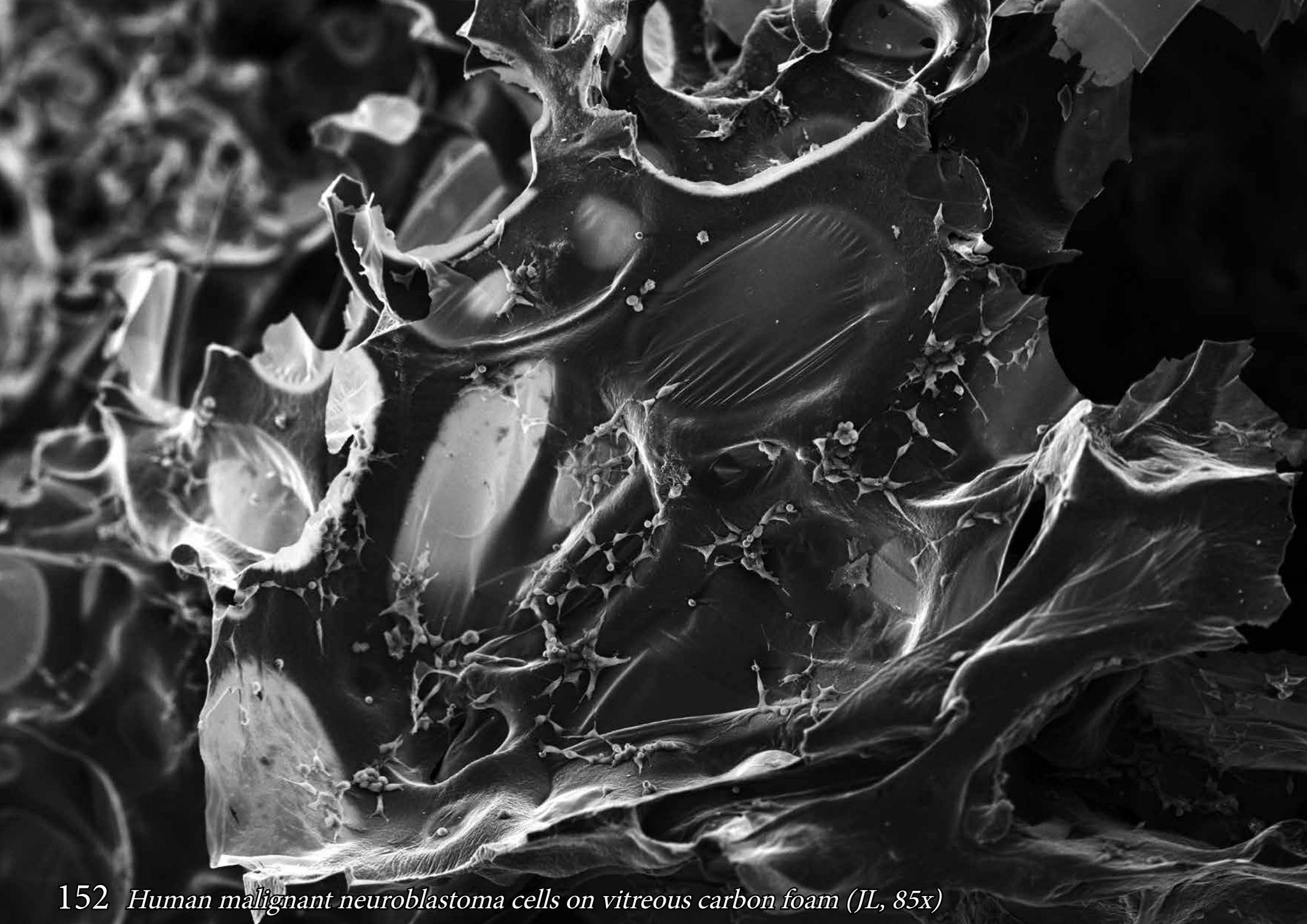

152 *Human malignant neuroblastoma cells on vitreous carbon foam (JL, 85x)*

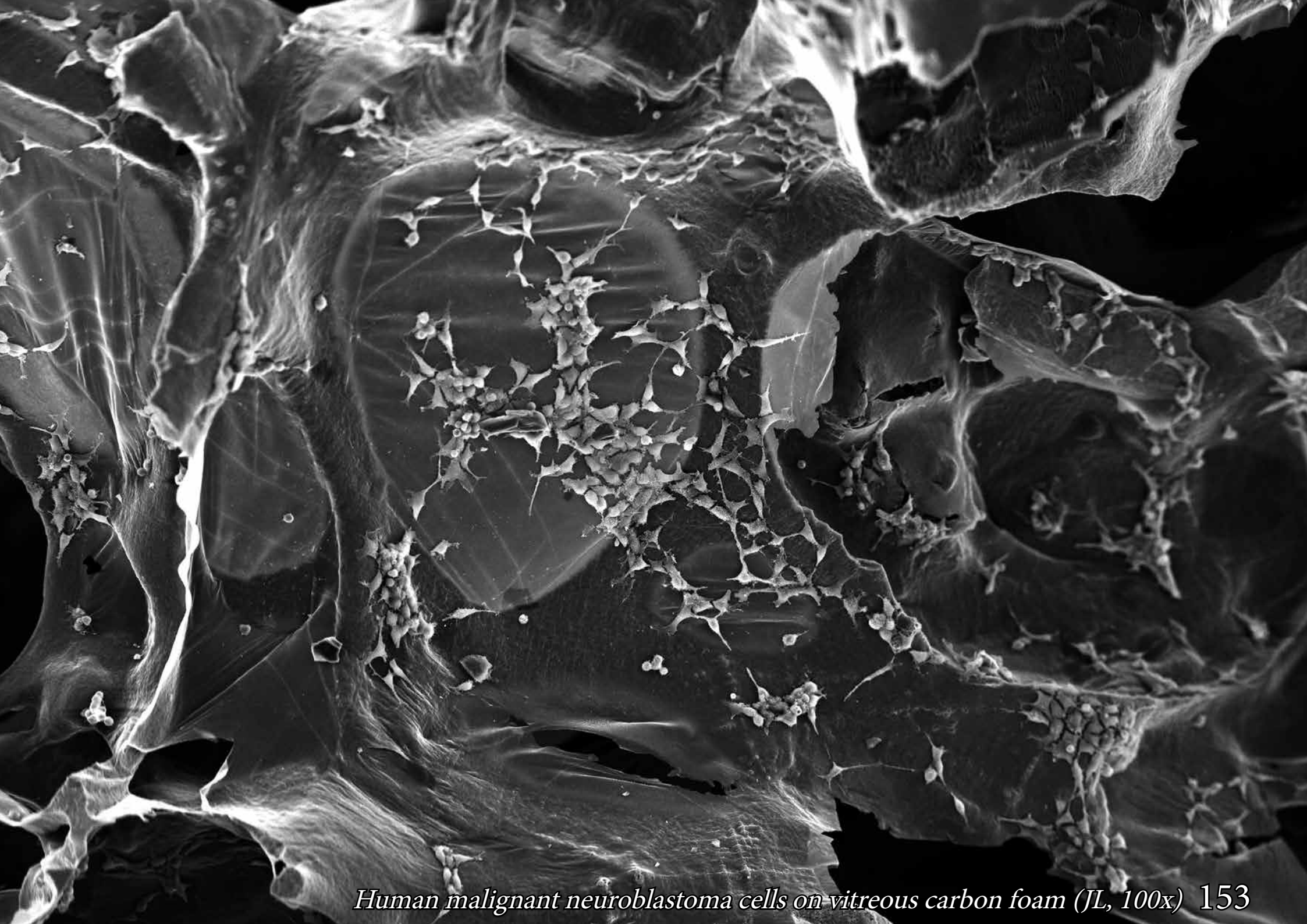

Human malignant neuroblastoma cells on vitreous carbon foam (JL, 100x)

154 *Human malignant neuroblastoma cells on vitreous carbon foam (JL, 850x)*

Human malignant neuroblastoma cells on vitreous carbon foam (JL, 900x)

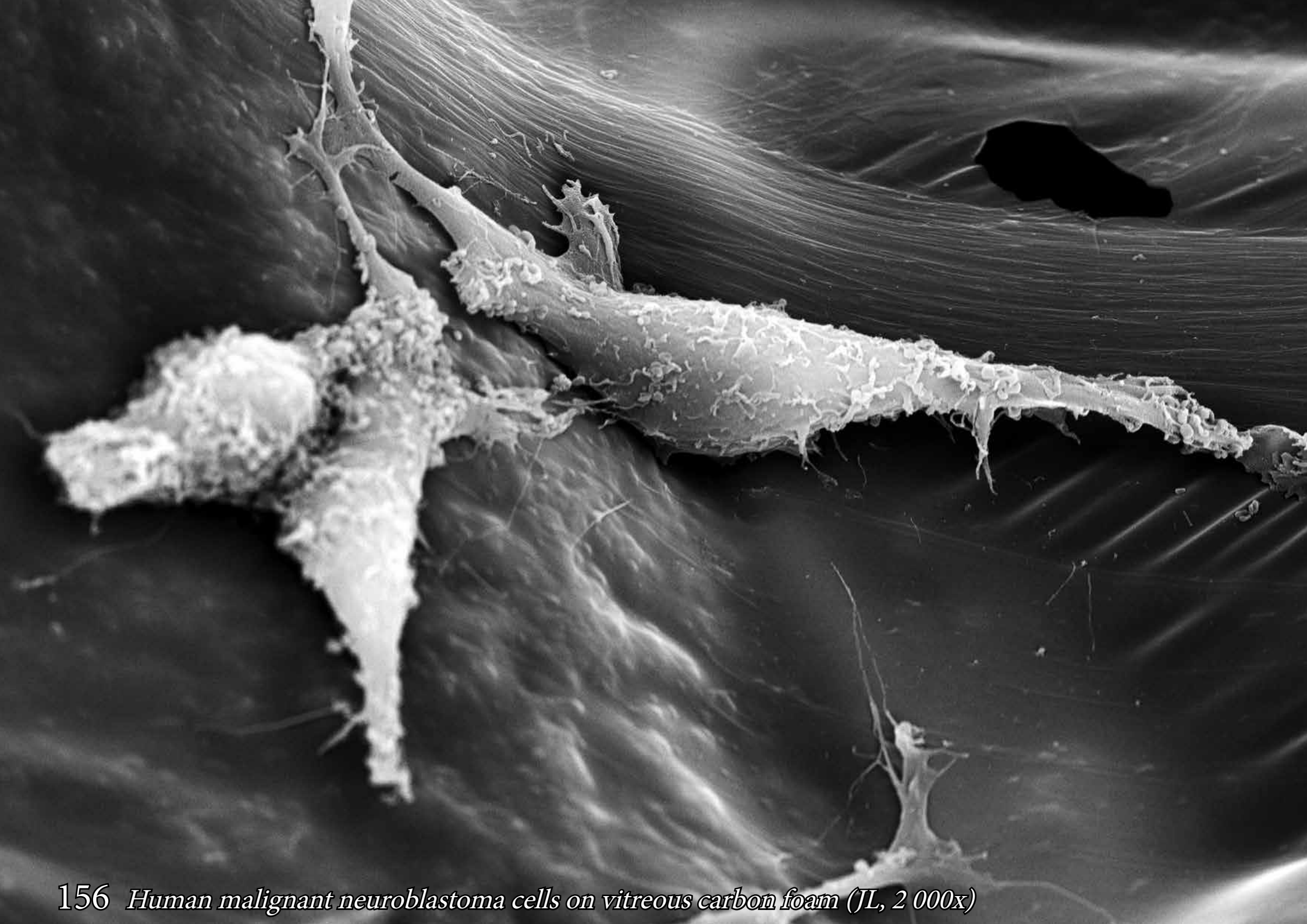

156 *Human malignant neuroblastoma cells on vitreous carbon foam (JL, 2 000x)*

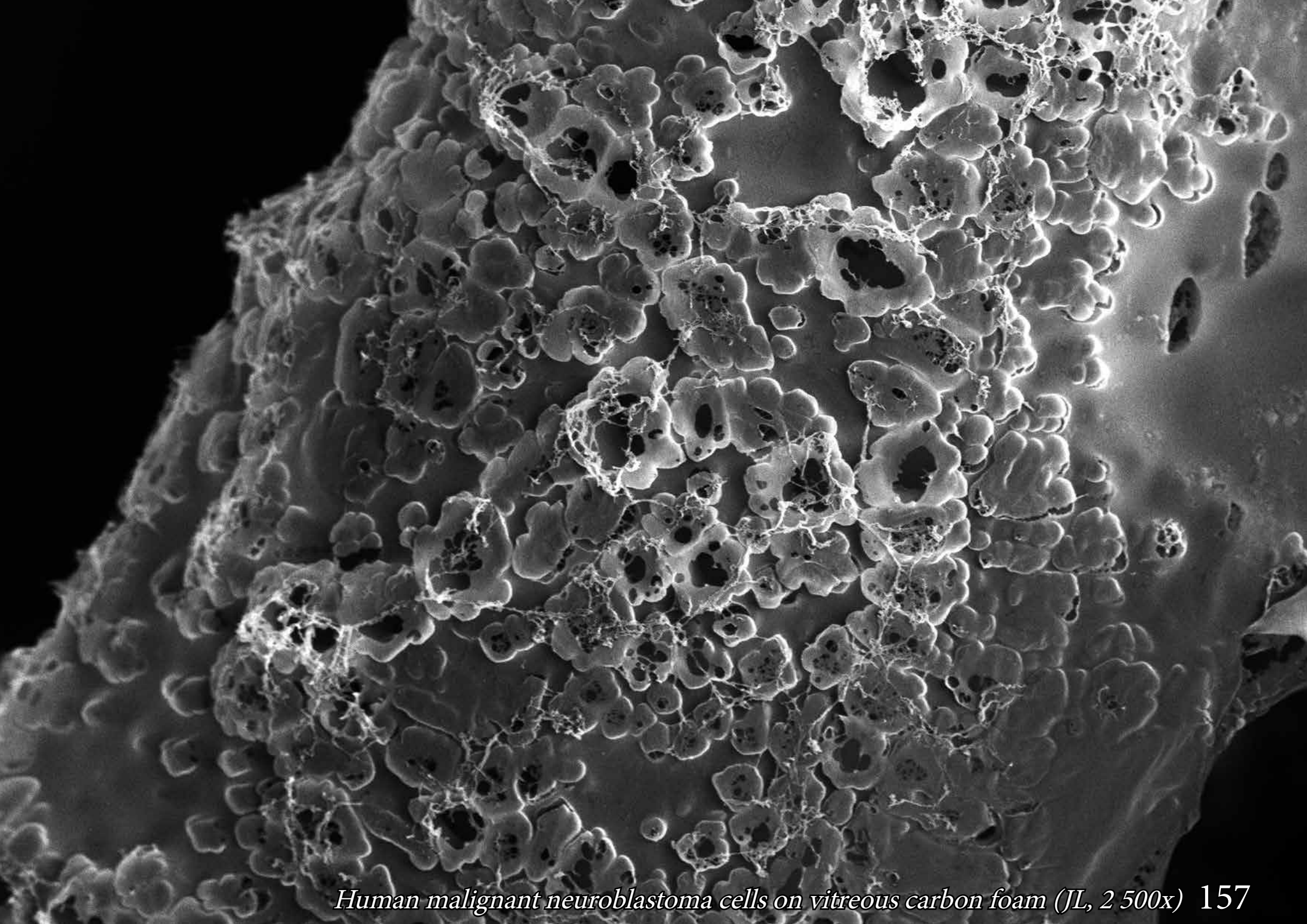

Human malignant neuroblastoma cells on vitreous carbon foam (JL, 2 500x)

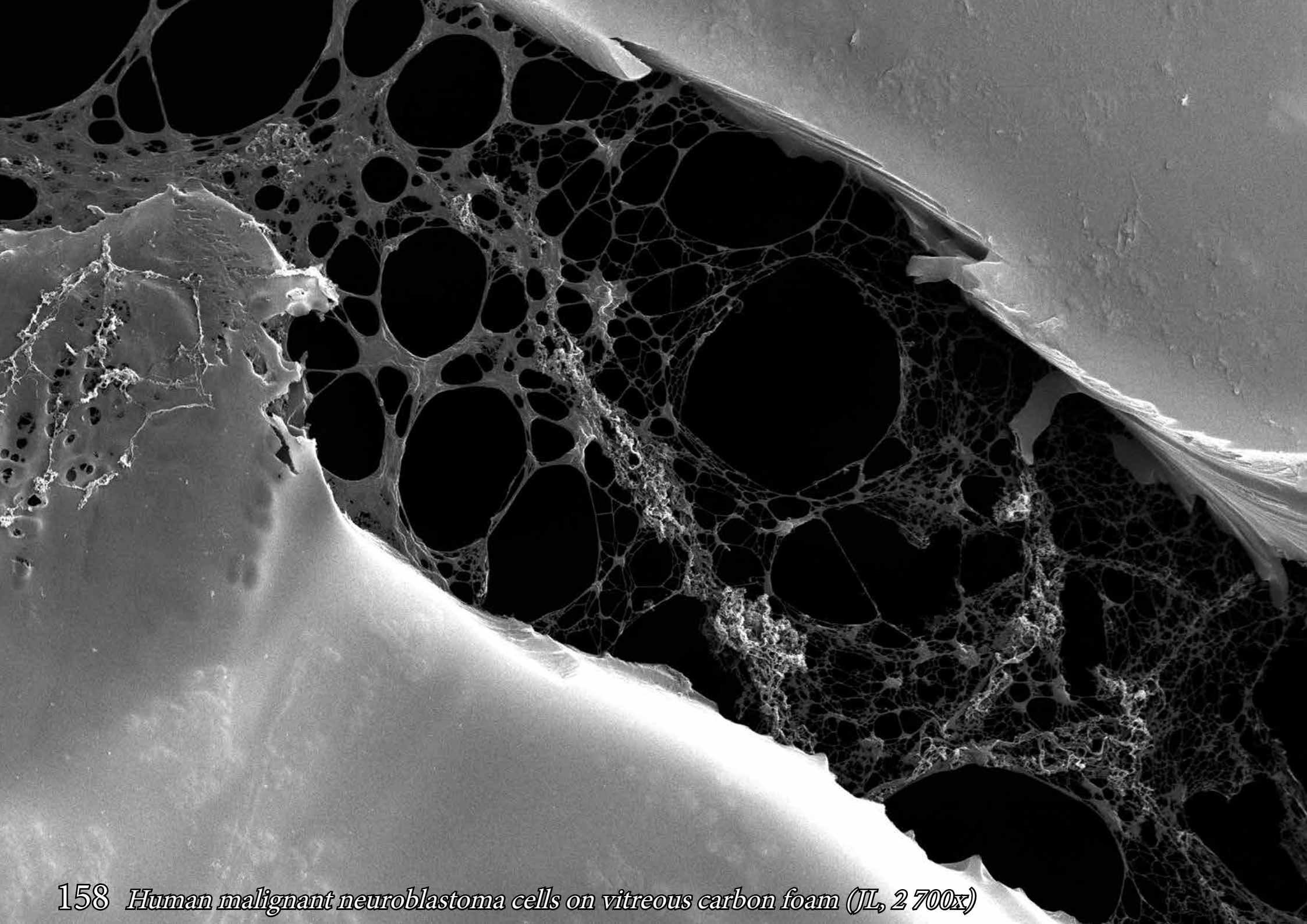

158 *Human malignant neuroblastoma cells on vitreous carbon foam (JL, 2 700x)*

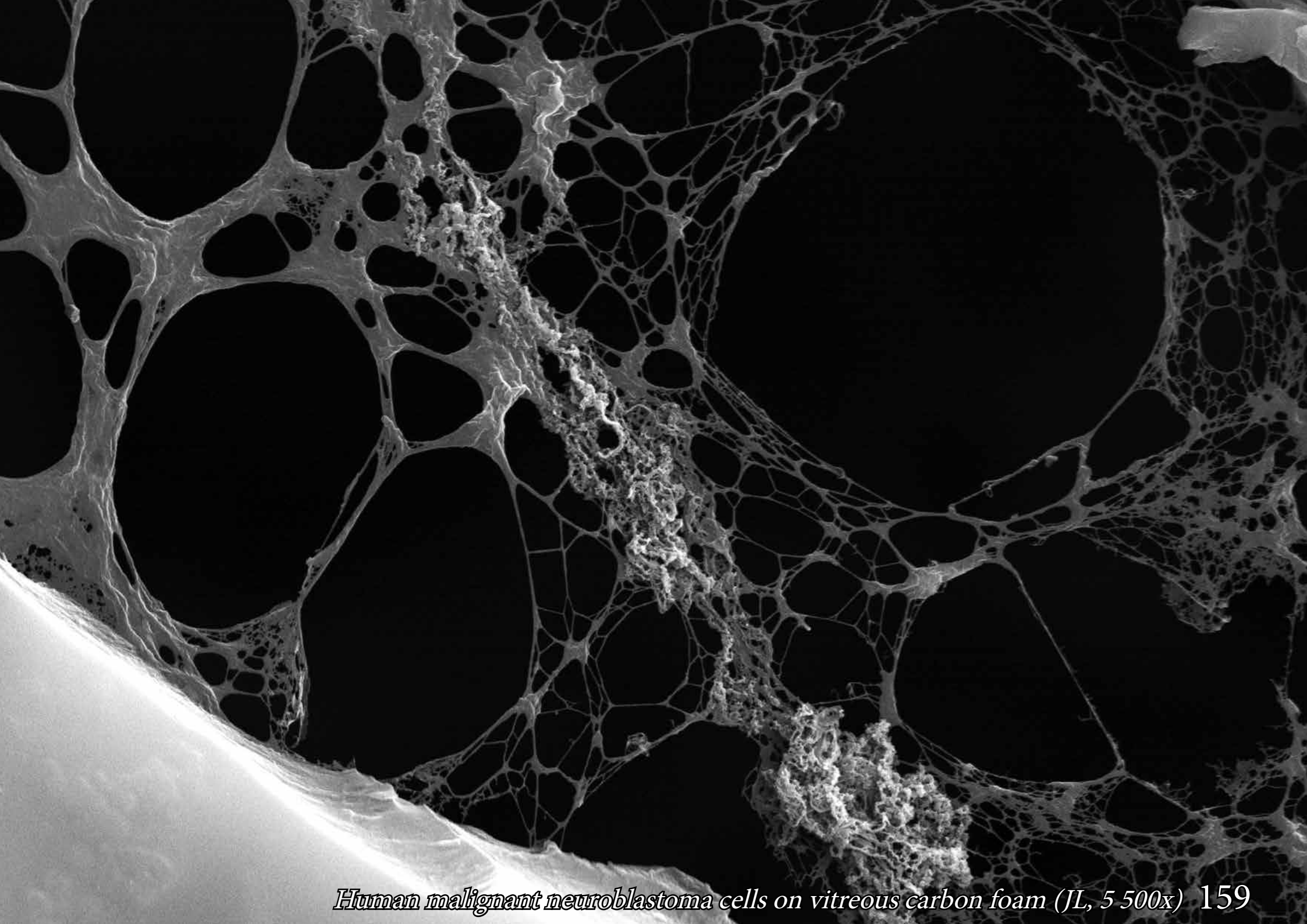

Human malignant neuroblastoma cells on vitreous carbon foam (JL, 5 500x)

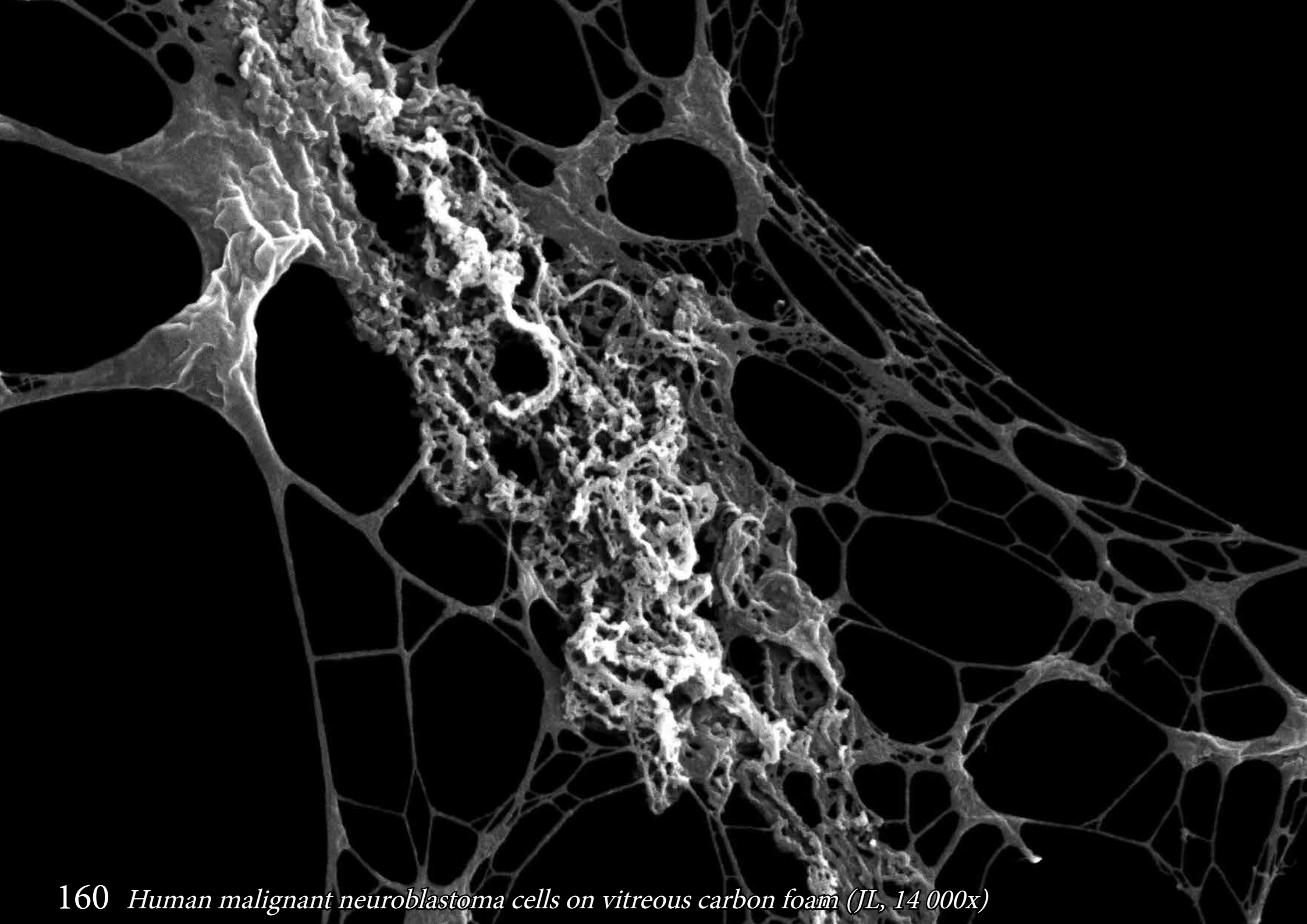

160 *Human malignant neuroblastoma cells on vitreous carbon foam (JL, 14 000x)*

Neural cells on golden strips

Neuroblastoma cells on silicon/gold grooves micro-patterns. Substrate was obtained by a photolithography process. Cells directionally grow along the grooves and show elongated morphology guided by the topography cues.

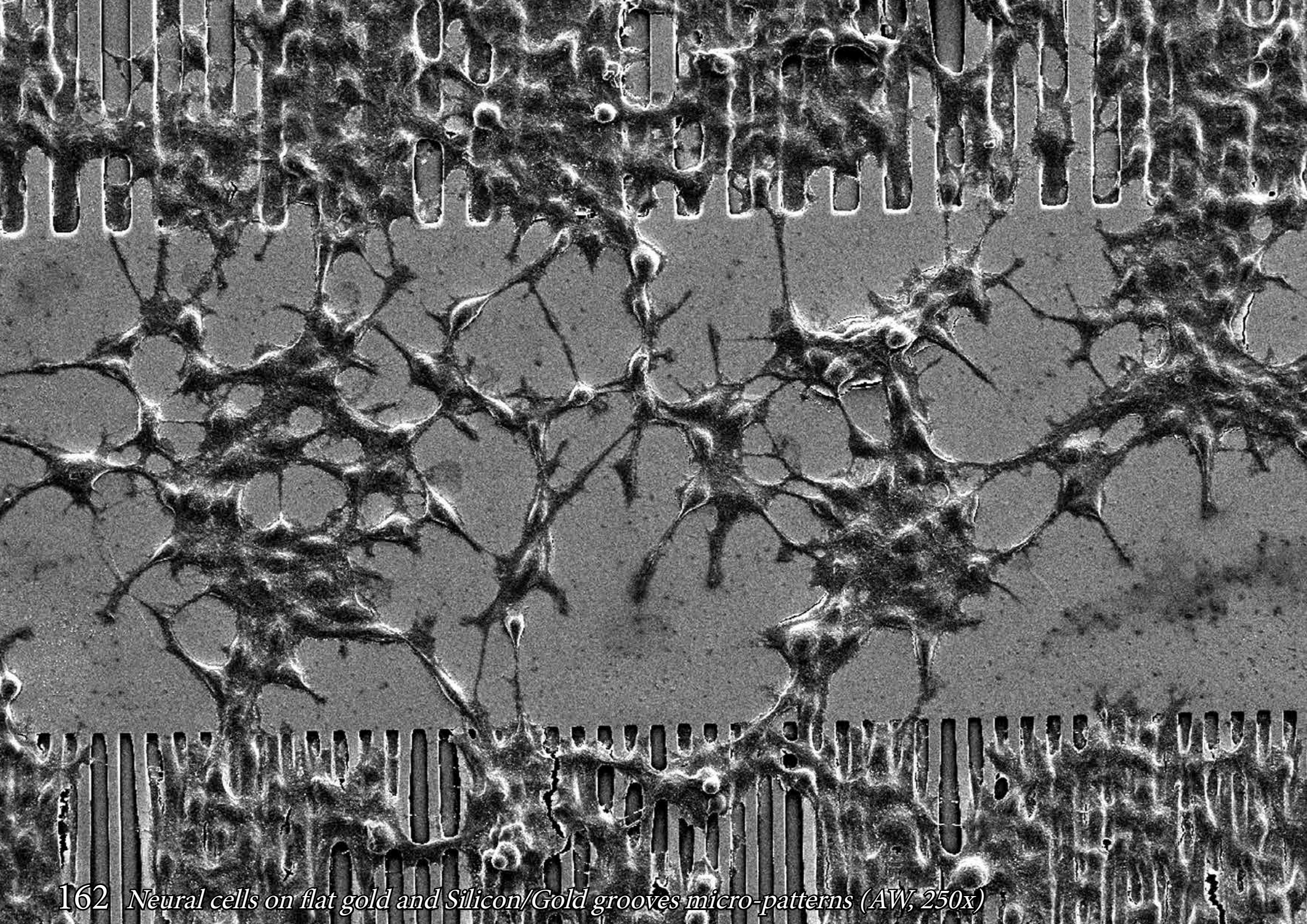

162 *Neural cells on flat gold and Silicon/Gold grooves micro-patterns (AW, 250x)*

Neural cells on flat gold and Silicon/Gold grooves micro-patterns (AW, 600x) 163

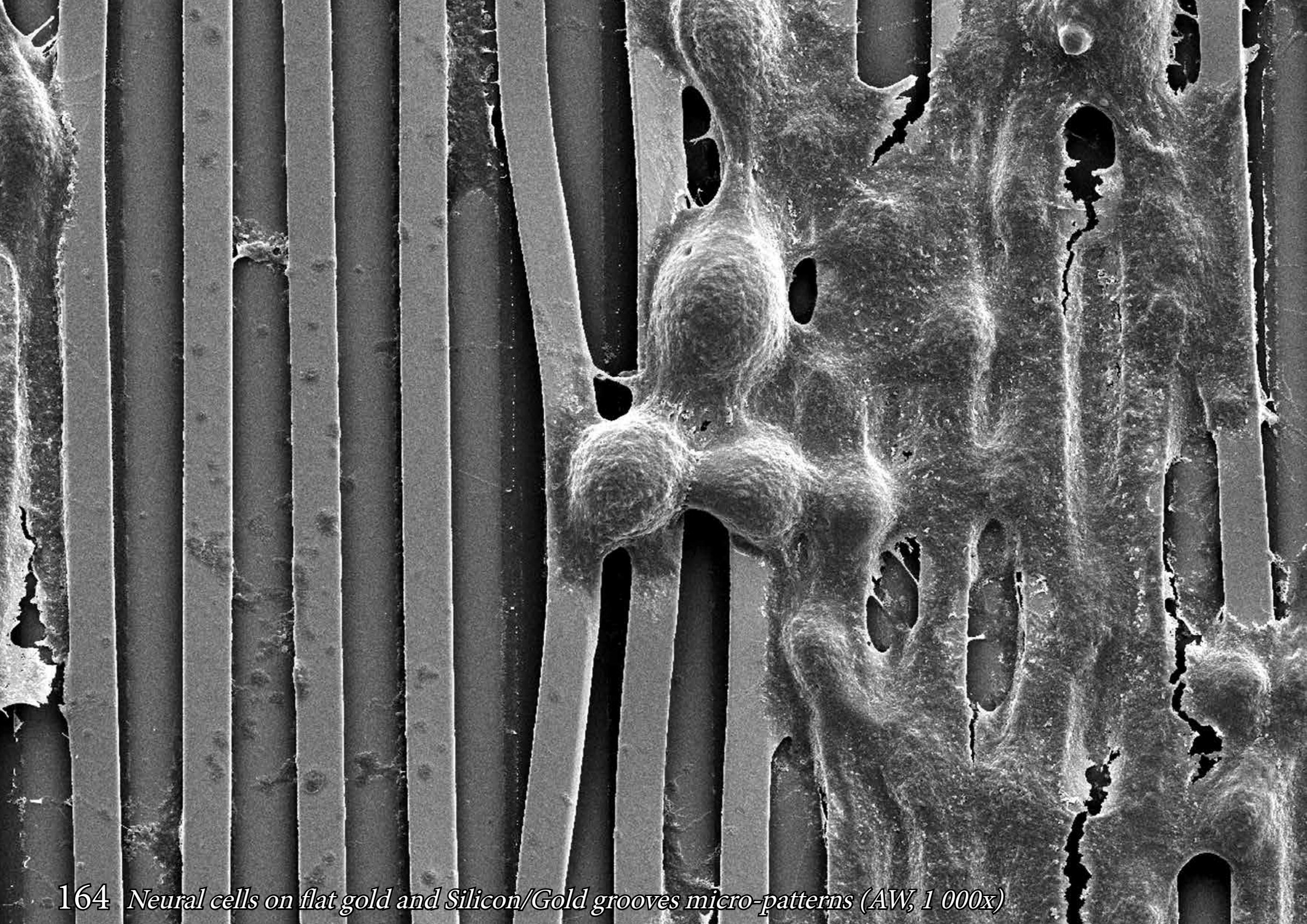

164 *Neural cells on flat gold and Silicon/Gold grooves micro-patterns (AW, 1 000x)*

Neural cells on flat gold and Silicon/Gold grooves micro-patterns (AW, 1 200x)

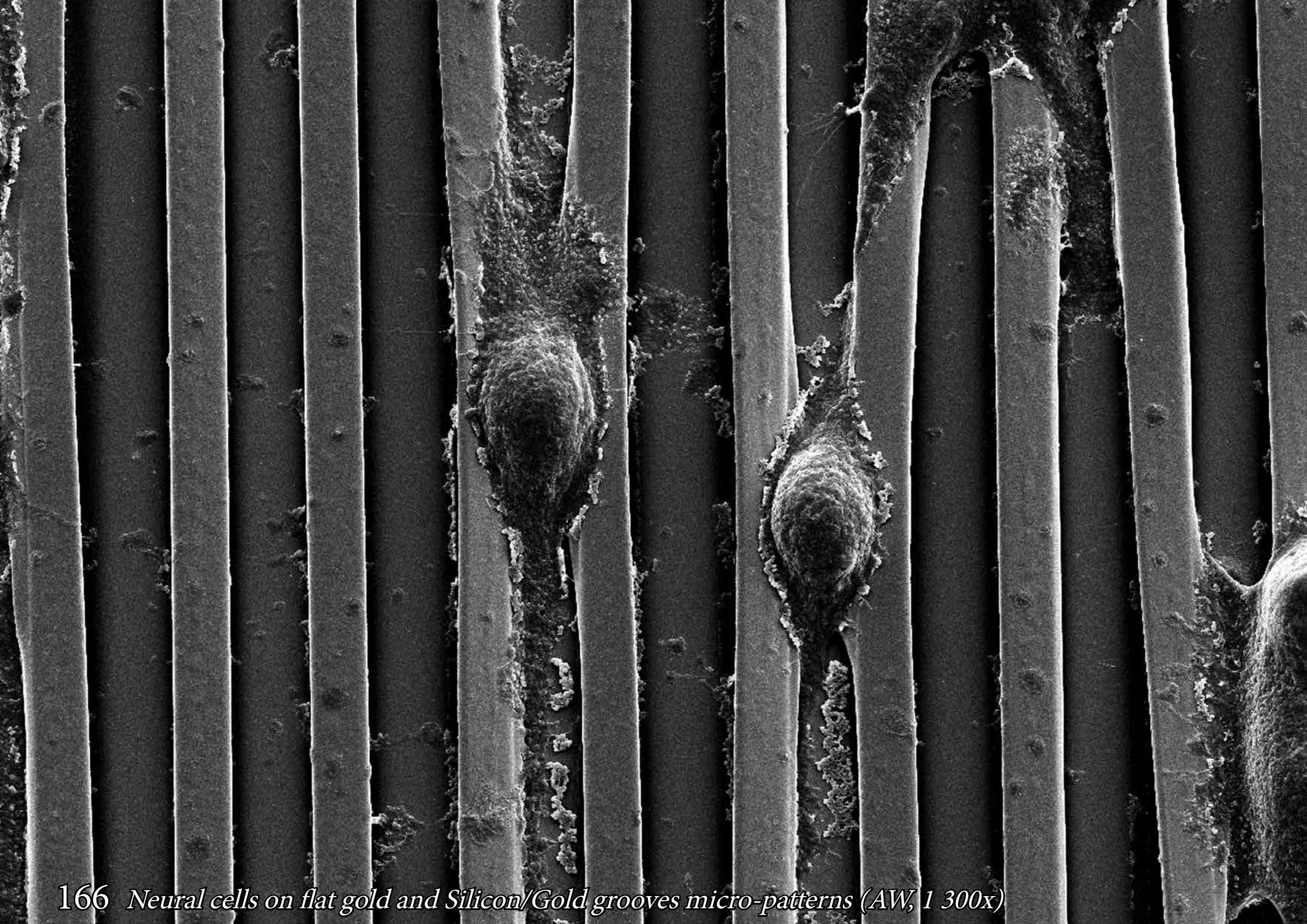

166 *Neural cells on flat gold and Silicon/Gold grooves micro-patterns (AW, 1 300x)*

Neural cells on flat gold and Silicon/Gold grooves micro-patterns (AW, 1 900x)

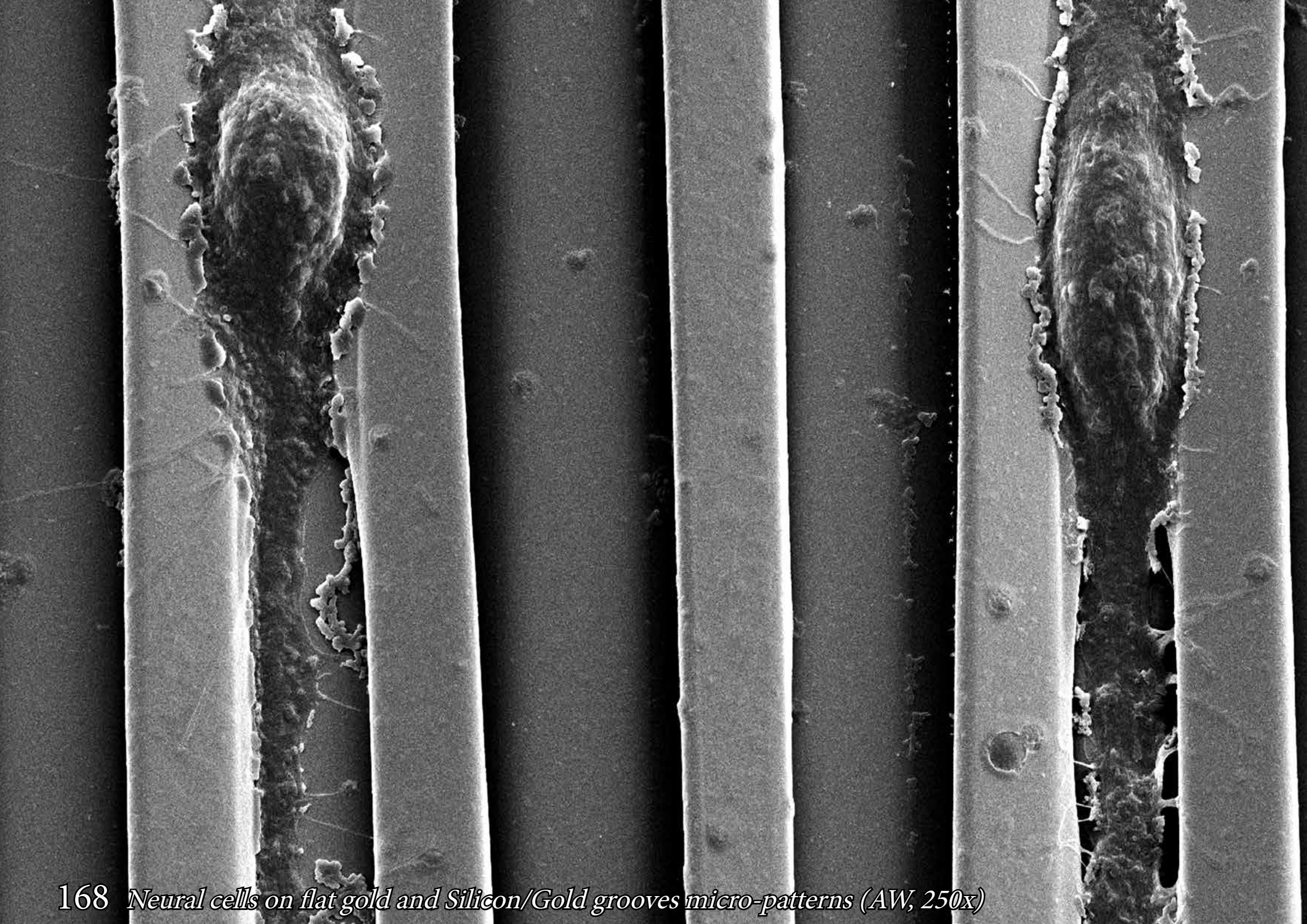

168 *Neural cells on flat gold and Silicon/Gold grooves micro-patterns (AW, 250x)*

Microstructure of nanoparticles embedded in hydrocolloids

Cryo-SEM images of hydrocolloids of silver and ultrasmall iron oxide nanoparticles (NPs) produced with *Amanita muscaria* and *Ginger rhizome* extracts for biomedical applications.

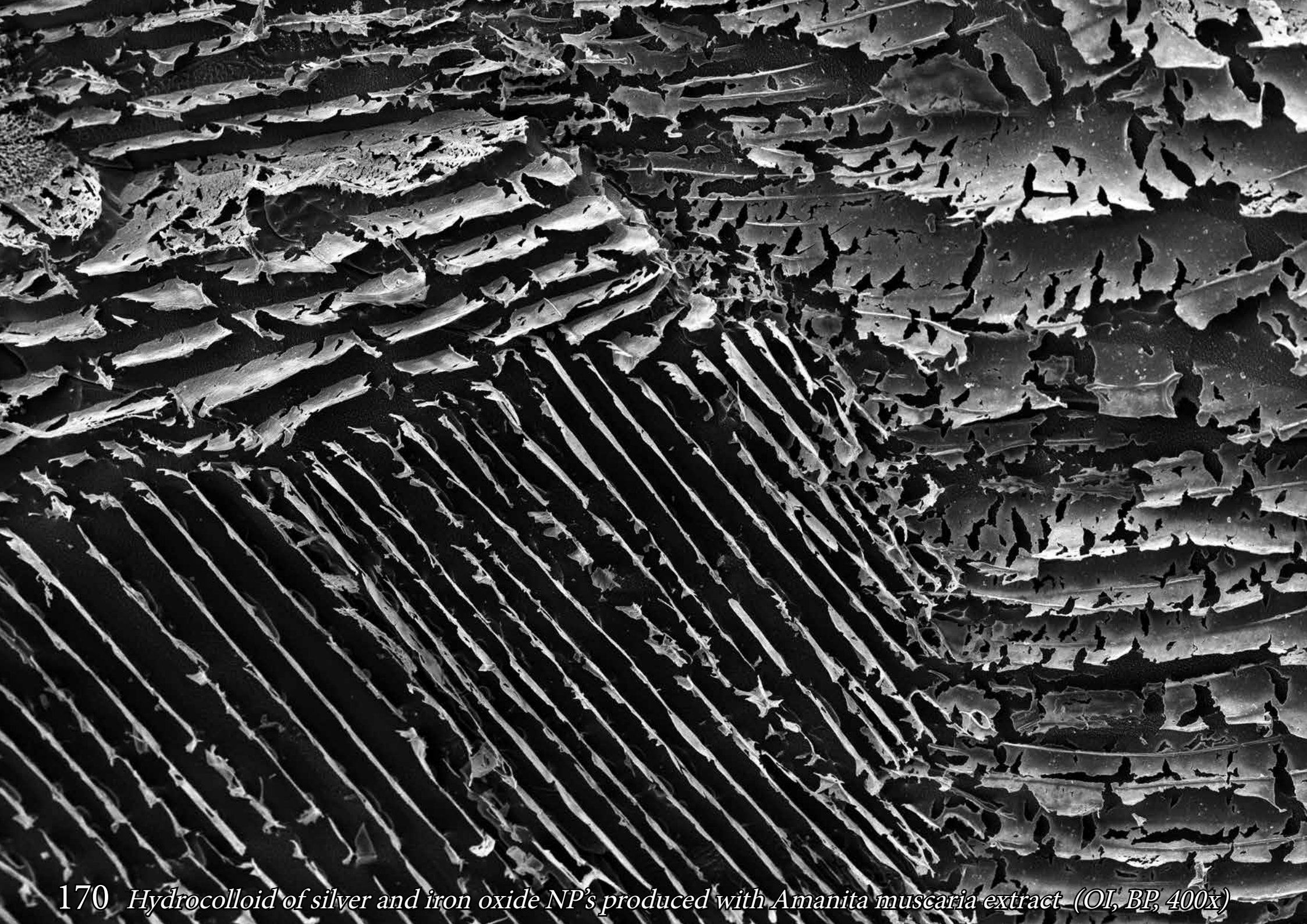

170 *Hydrocolloid of silver and iron oxide NP's produced with Amanita muscaria extract (OI, BP, 400x)*

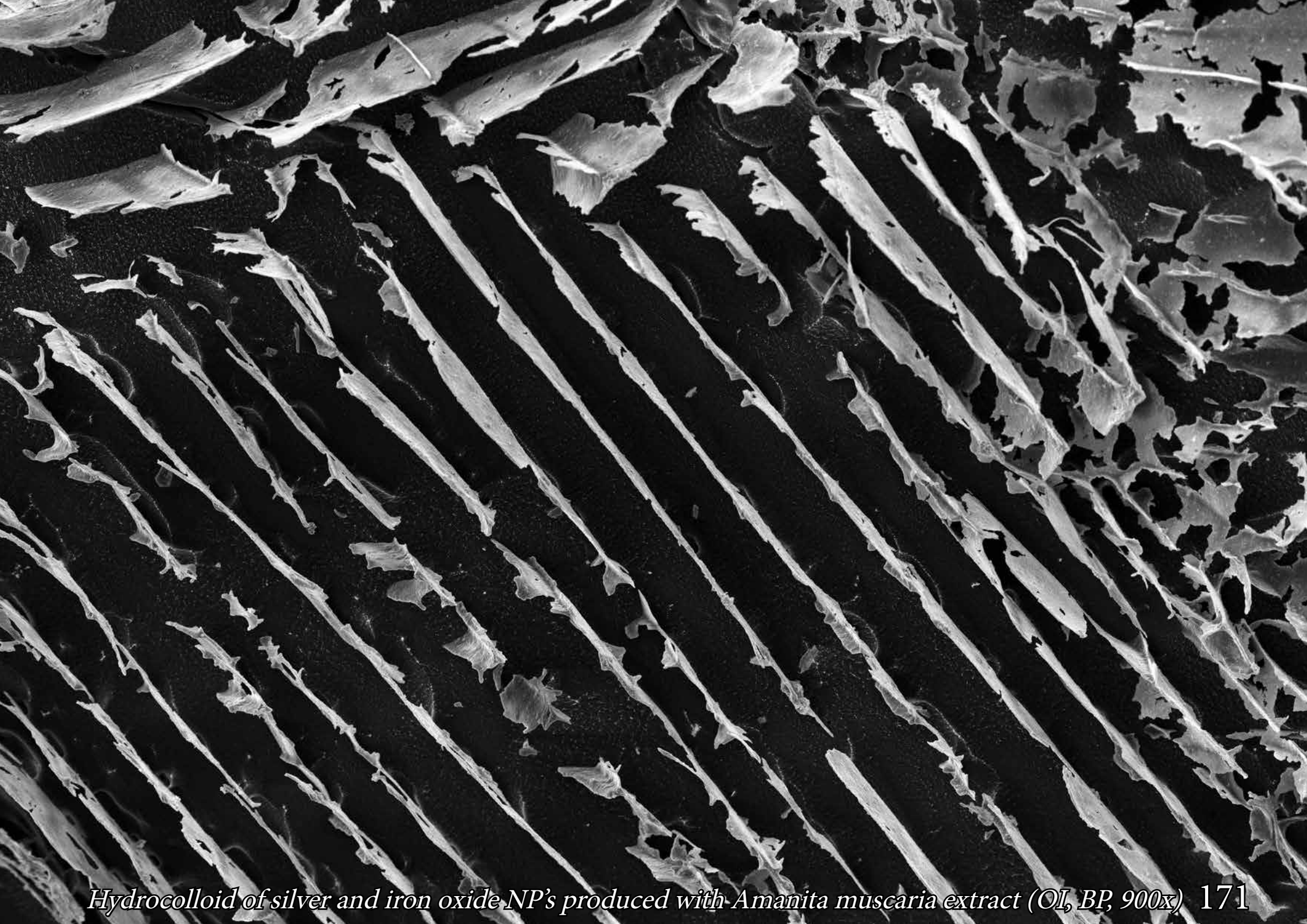

Hydrocolloid of silver and iron oxide NP's produced with Amanita muscaria extract (OI, BP, 900x)

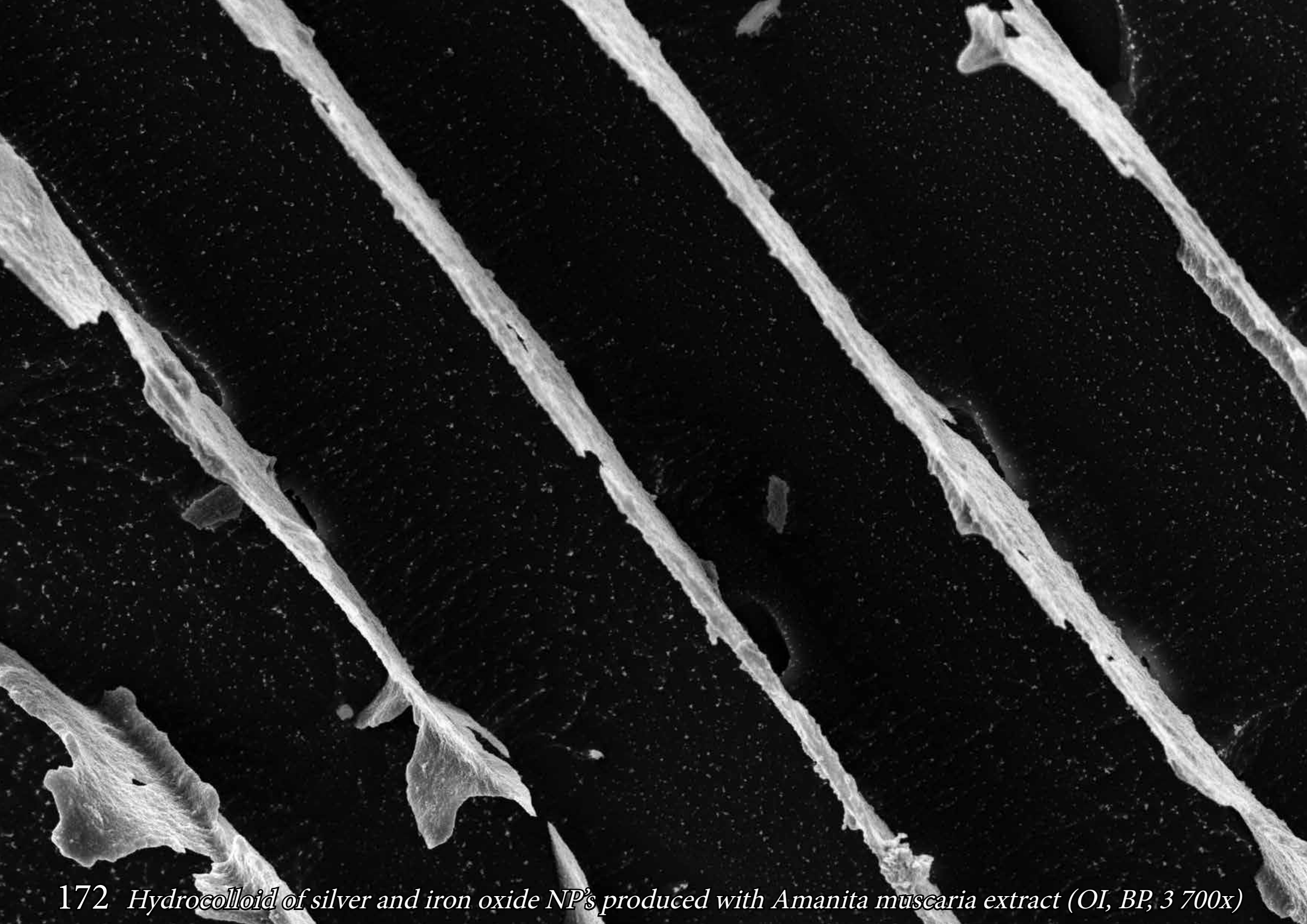

172 *Hydrocolloid of silver and iron oxide NP's produced with Amanita muscaria extract (OI, BP, 3 700x)*

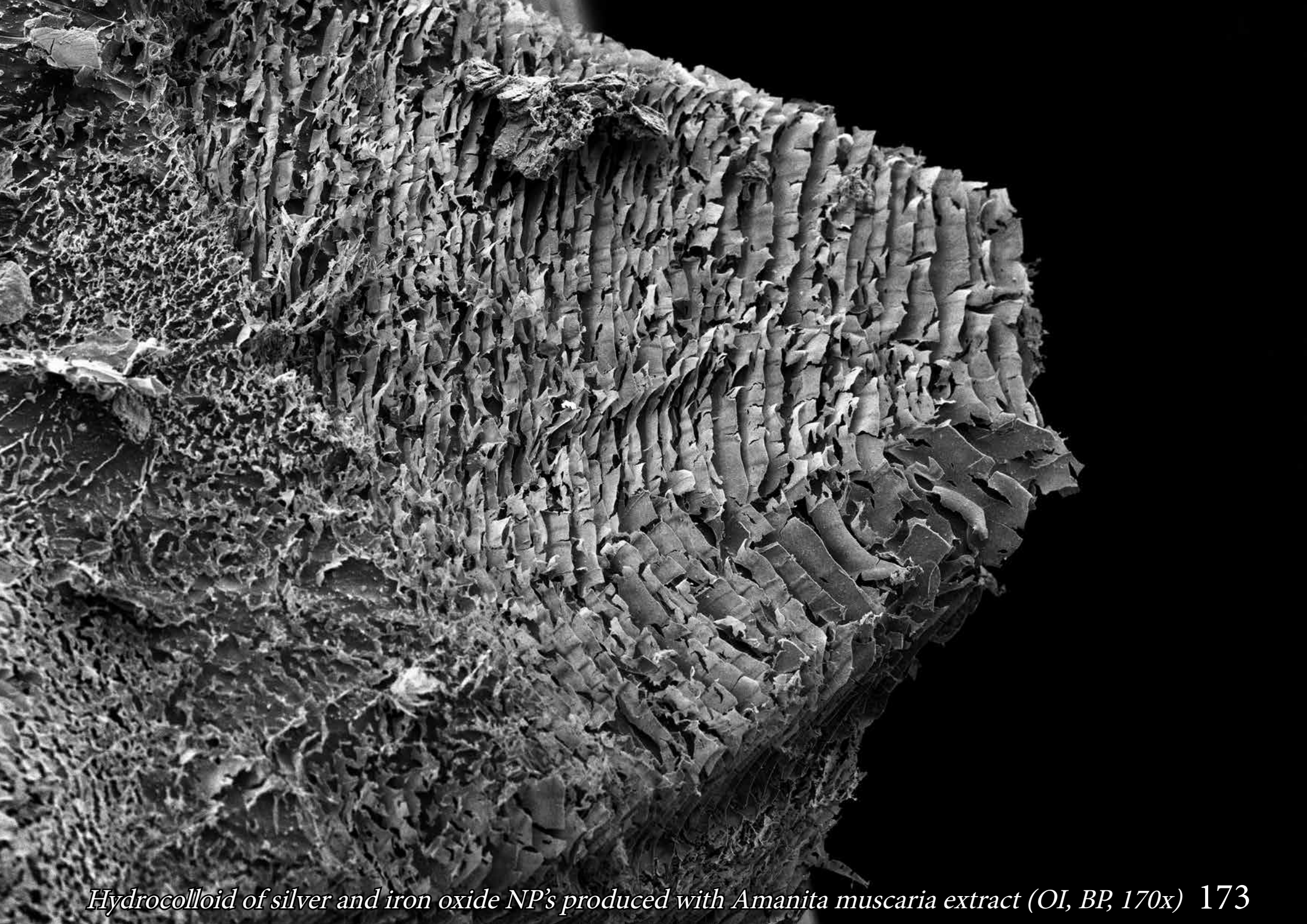

Hydrocolloid of silver and iron oxide NP's produced with Amanita muscaria extract (OI, BP, 170x)

174 *Hydrocolloid of silver and iron oxide NP's produced with Amanita muscaria extract (OI, BP, 600x)*

Hydrocolloid of silver and iron oxide NP's produced with Amanita muscaria extract (OI, BP, 1 700x)

176 *Hydrocolloid of silver and iron oxide NP's produced with Amanita muscaria extract (OI, BP, 230x)*

Hydrocolloid of silver and iron oxide NP's produced with Amanita muscaria extract (OI, BP, 750x)

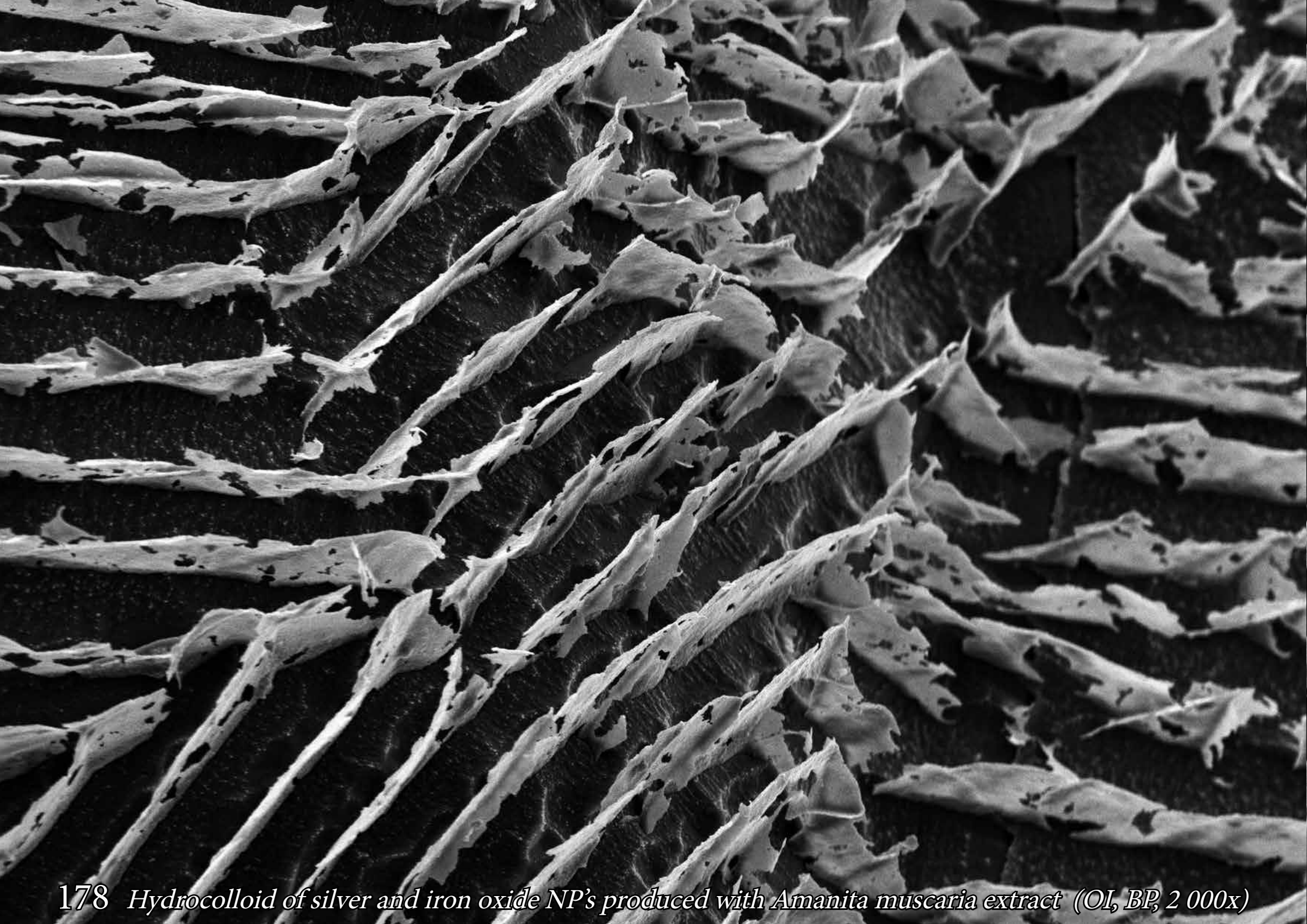

178 *Hydrocolloid of silver and iron oxide NP's produced with Amanita muscaria extract (OI, BP, 2 000x)*

Hydrocolloid of silver and iron oxide NP's produced with Amanita muscaria extract (OI, BP, 3 300x)

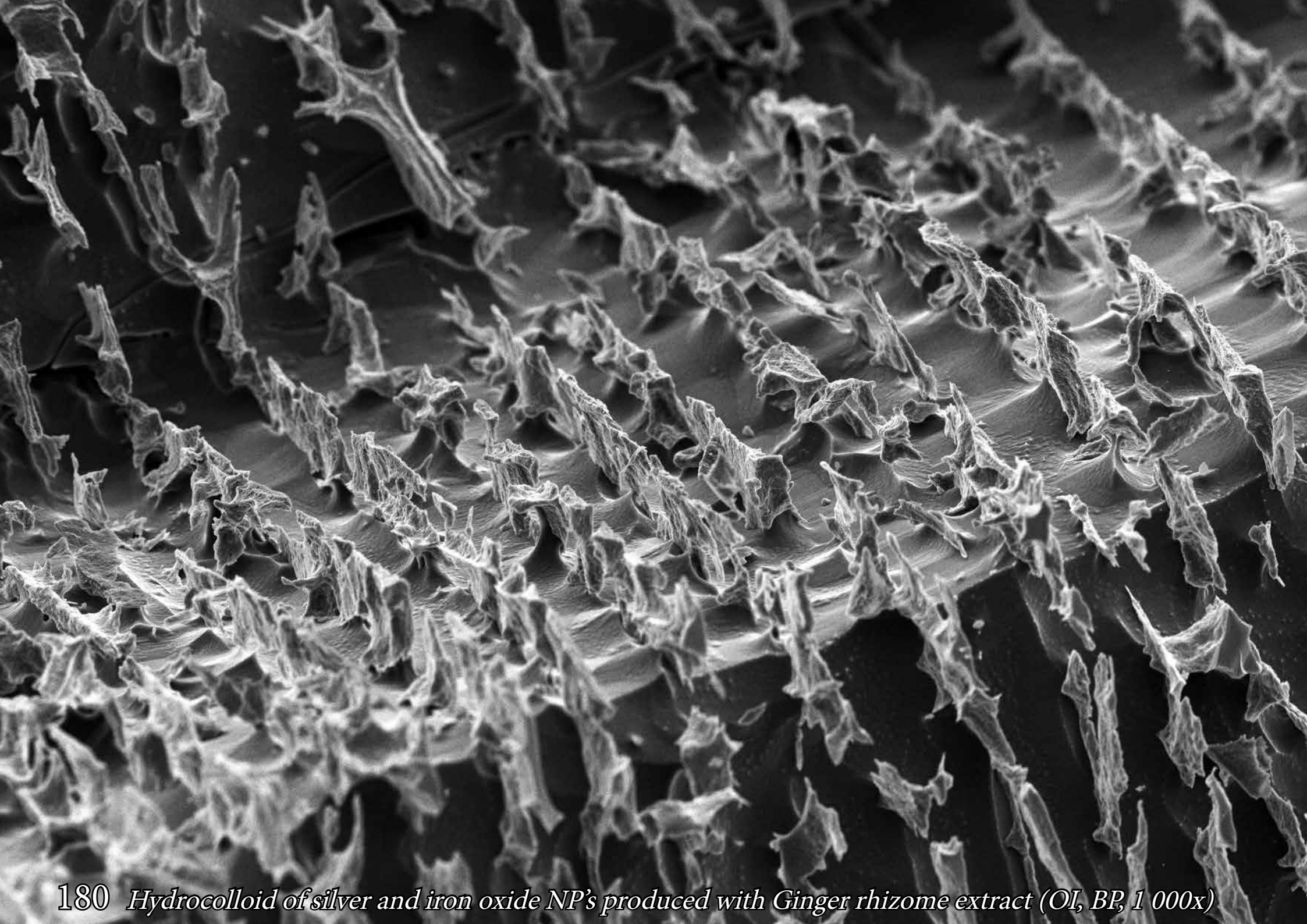

180 *Hydrocolloid of silver and iron oxide NP's produced with Ginger rhizome extract (OI, BP, 1 000x)*

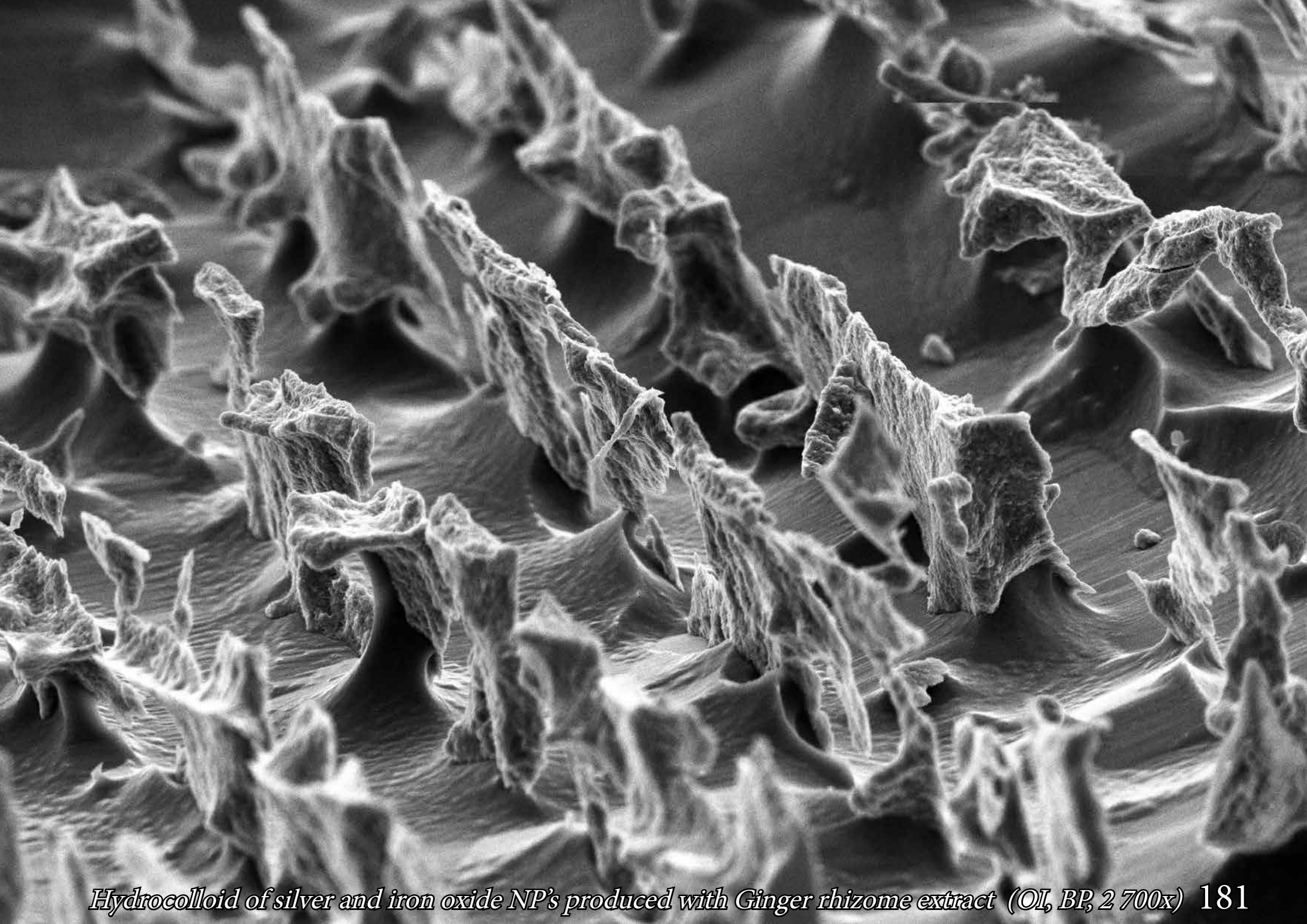

Hydrocolloid of silver and iron oxide NP's produced with Ginger rhizome extract (OI, BP, 2 700x) 181

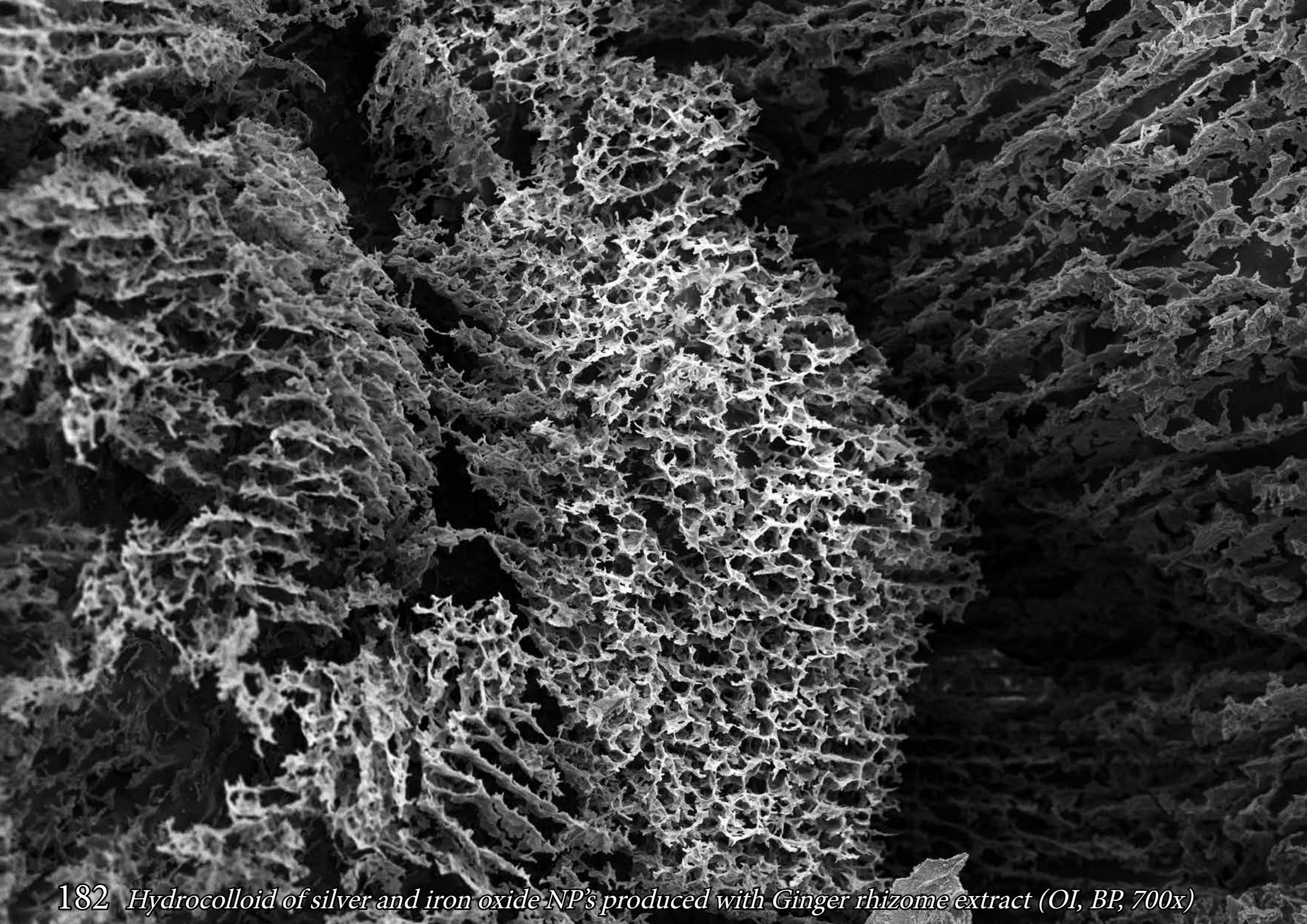

182 *Hydrocolloid of silver and iron oxide NP's produced with Ginger rhizome extract (OI, BP, 700x)*

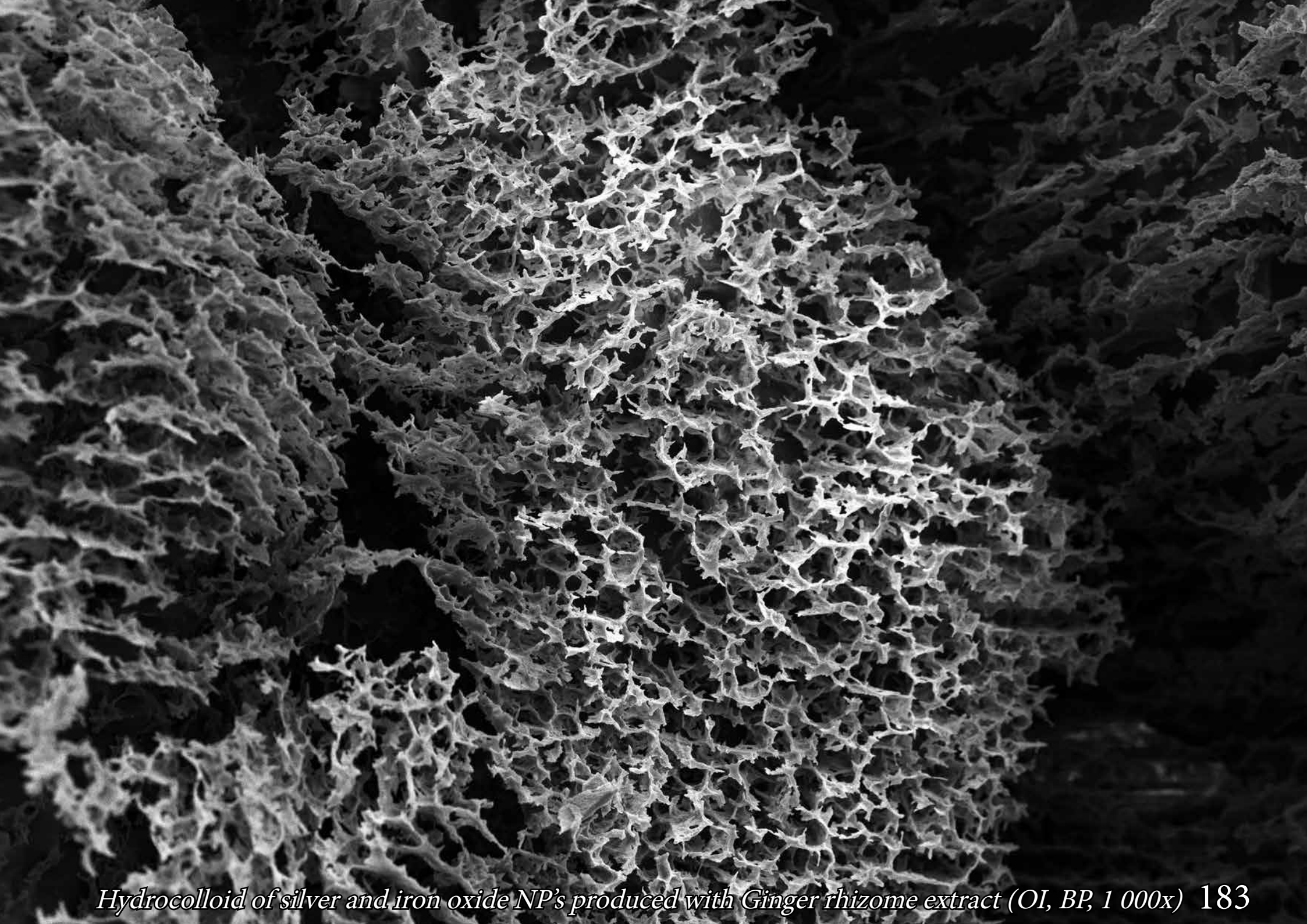

Hydrocolloid of silver and iron oxide NP's produced with Ginger rhizome extract (OI, BP, 1 000x)

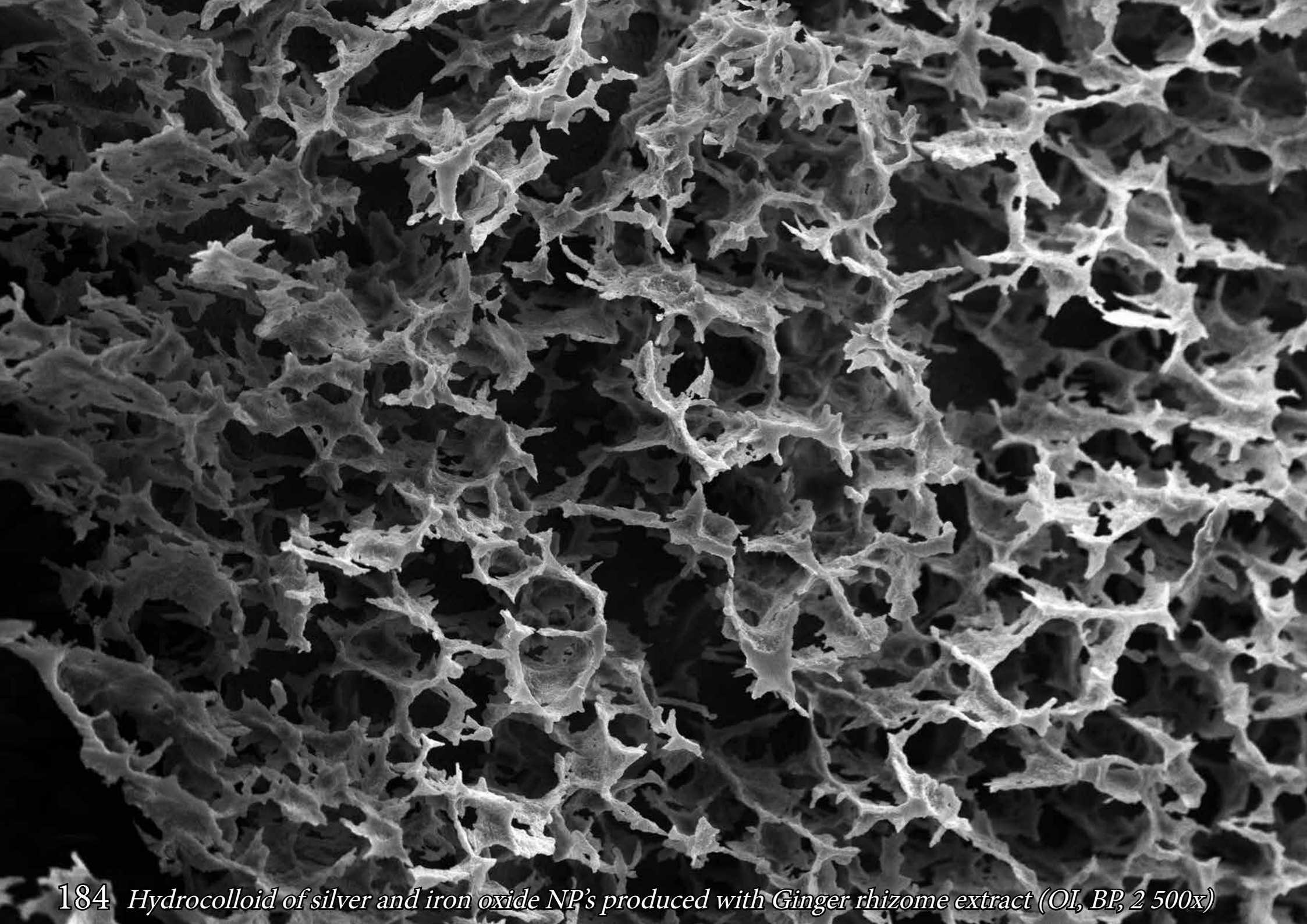

184 *Hydrocolloid of silver and iron oxide NP's produced with Ginger rhizome extract (OI, BP, 2 500x)*

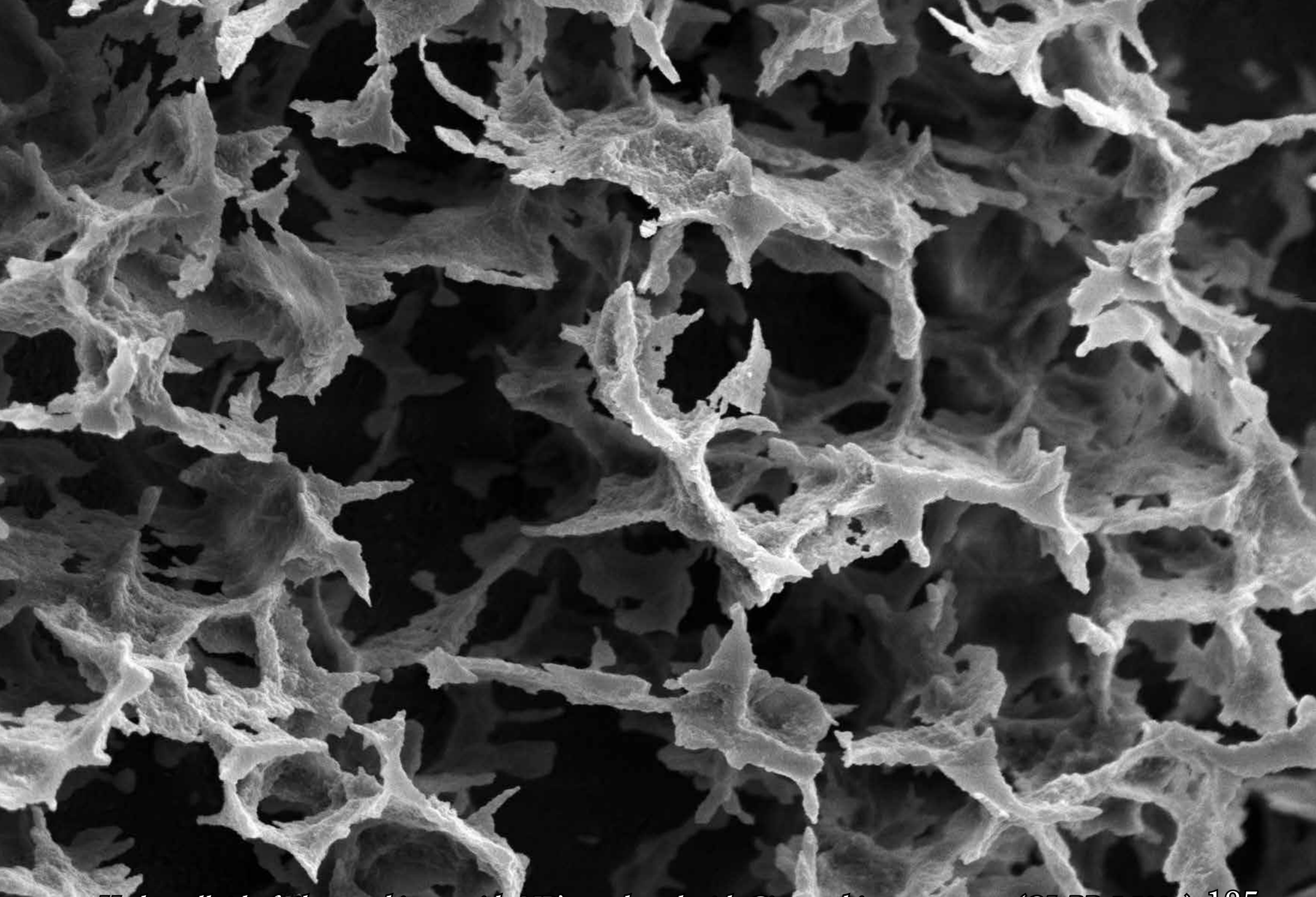

Hydrocolloid of silver and iron oxide NP's produced with Ginger rhizome extract (OI, BP, 5 500x) 185

Pig skeletal muscular tissue

Cryo-SEM images of domestic pig *Sus scrofa domesticus* musculoskeletal tissue. Fresh pig tissue was bought in a local supermarket (Poznań, Poland). Samples underwent critical point drying procedure for 45 min. Images were taken at -196 °C.

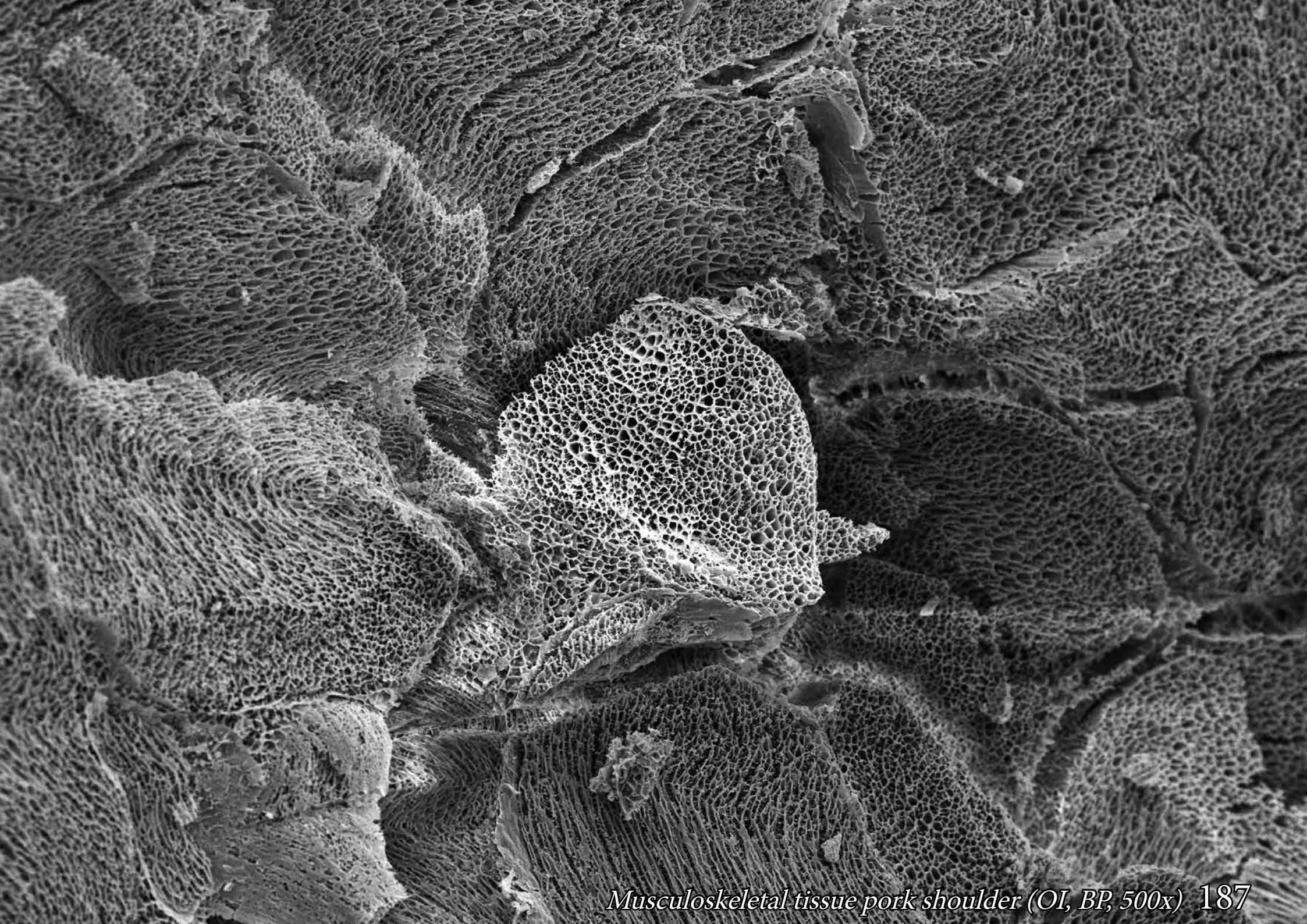

Musculoskeletal tissue pork shoulder (OI, BP, 500x) 187

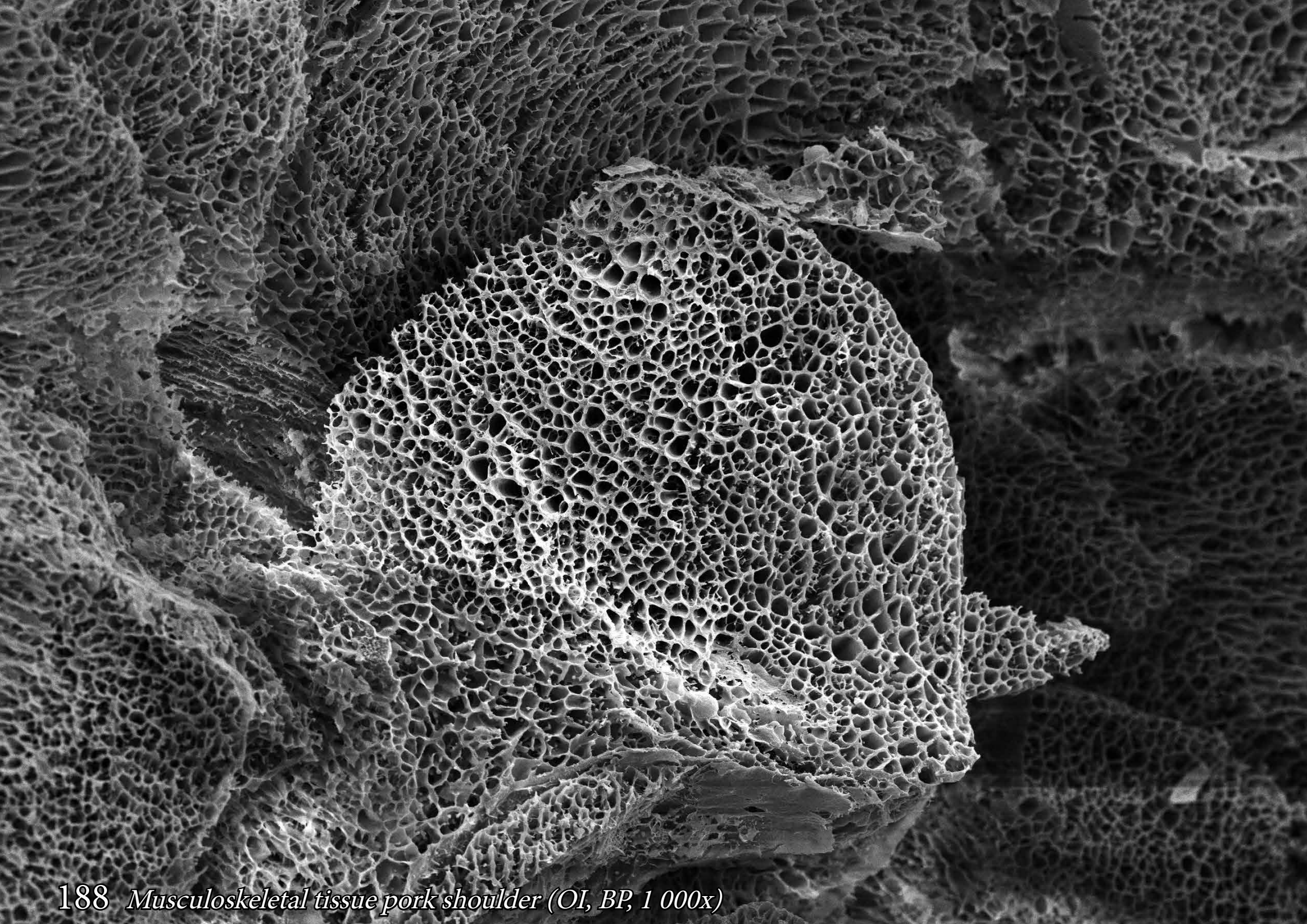

188 *Musculoskeletal tissue pork shoulder (OI, BP, 1 000x)*

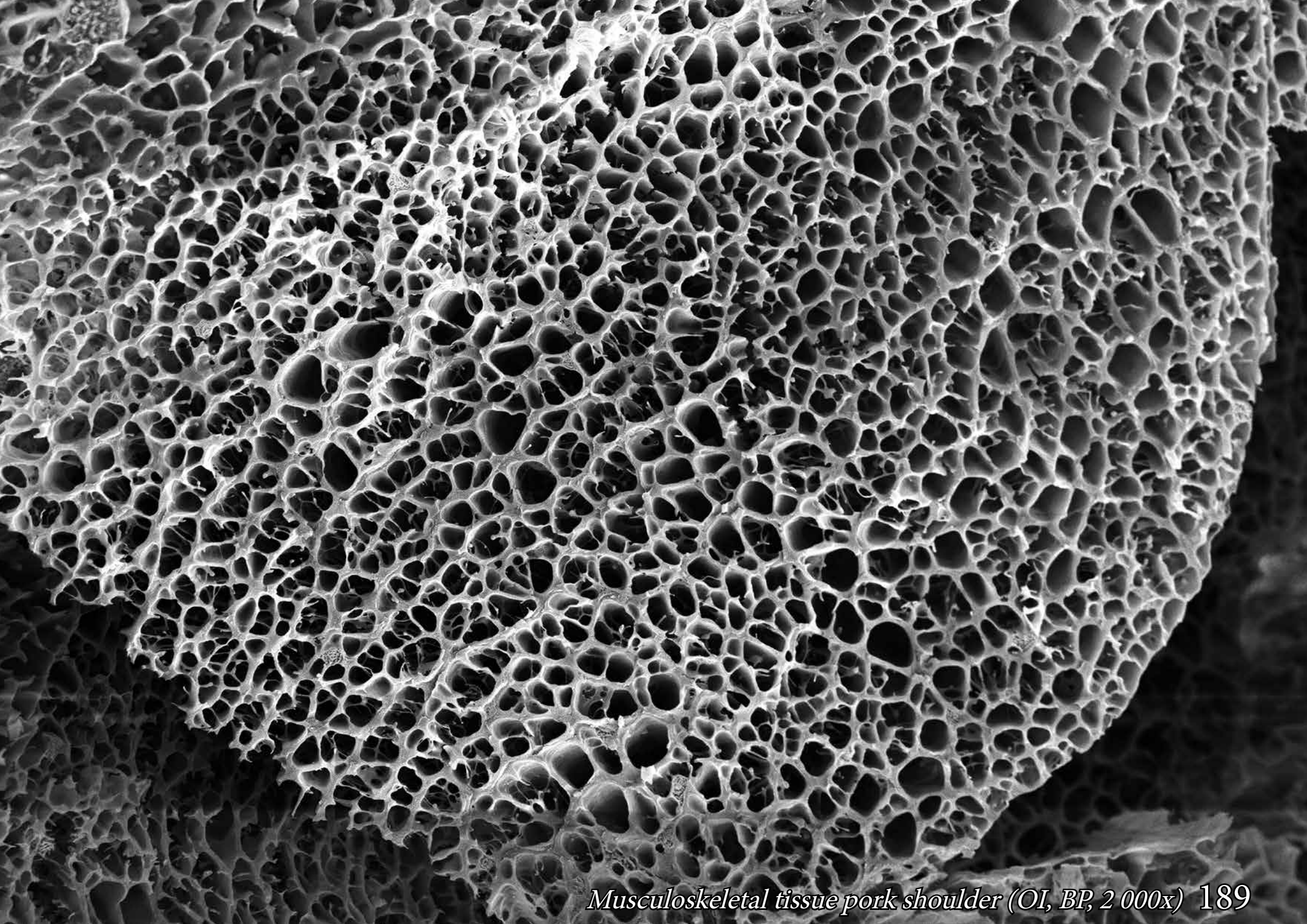

Musculoskeletal tissue pork shoulder (OI, BP, 2 000x) 189

190 *Musculoskeletal tissue pork shoulder (OI, BP, 2 000x)*

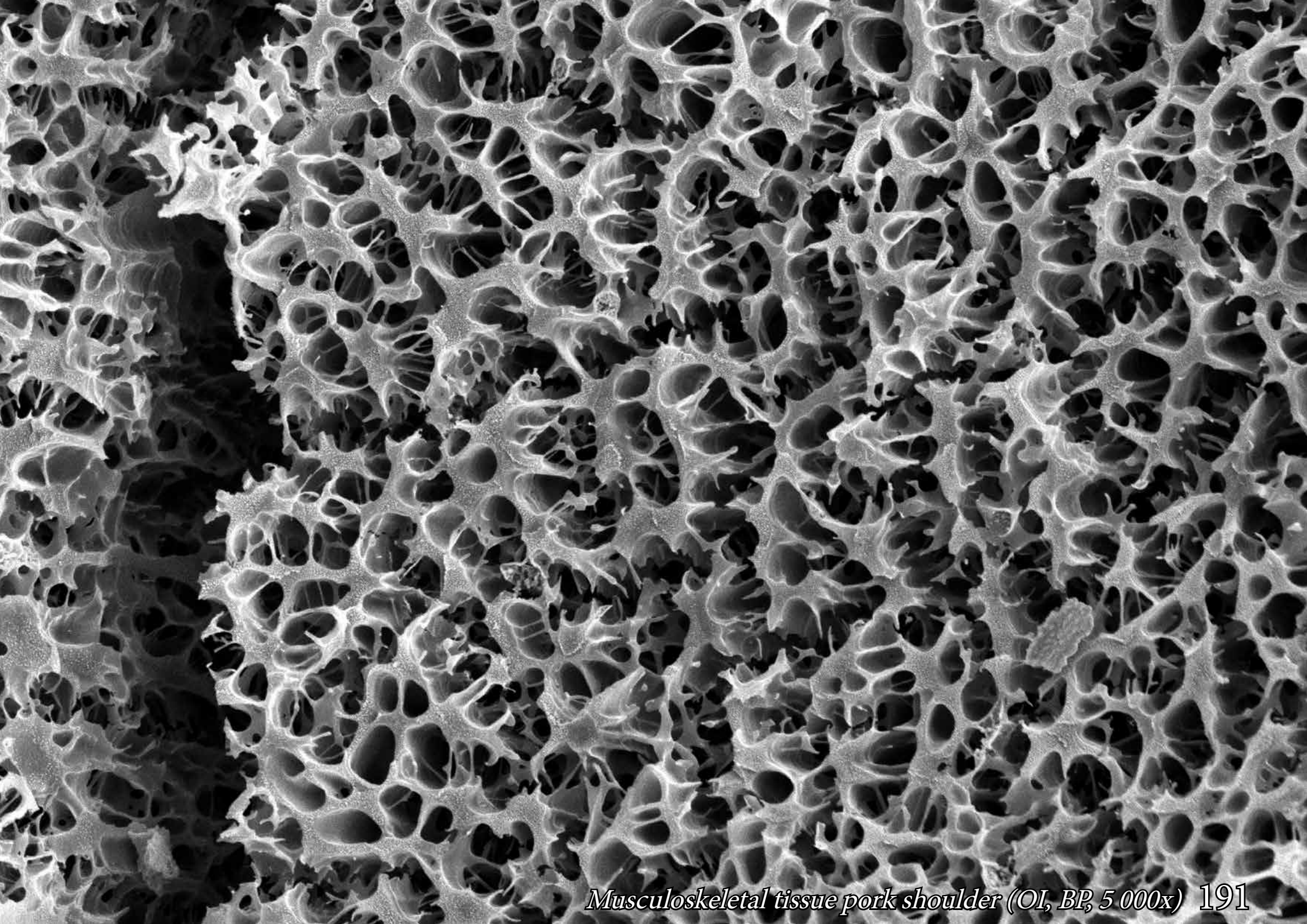

Musculoskeletal tissue pork shoulder (OI, BP, 5 000x) 191

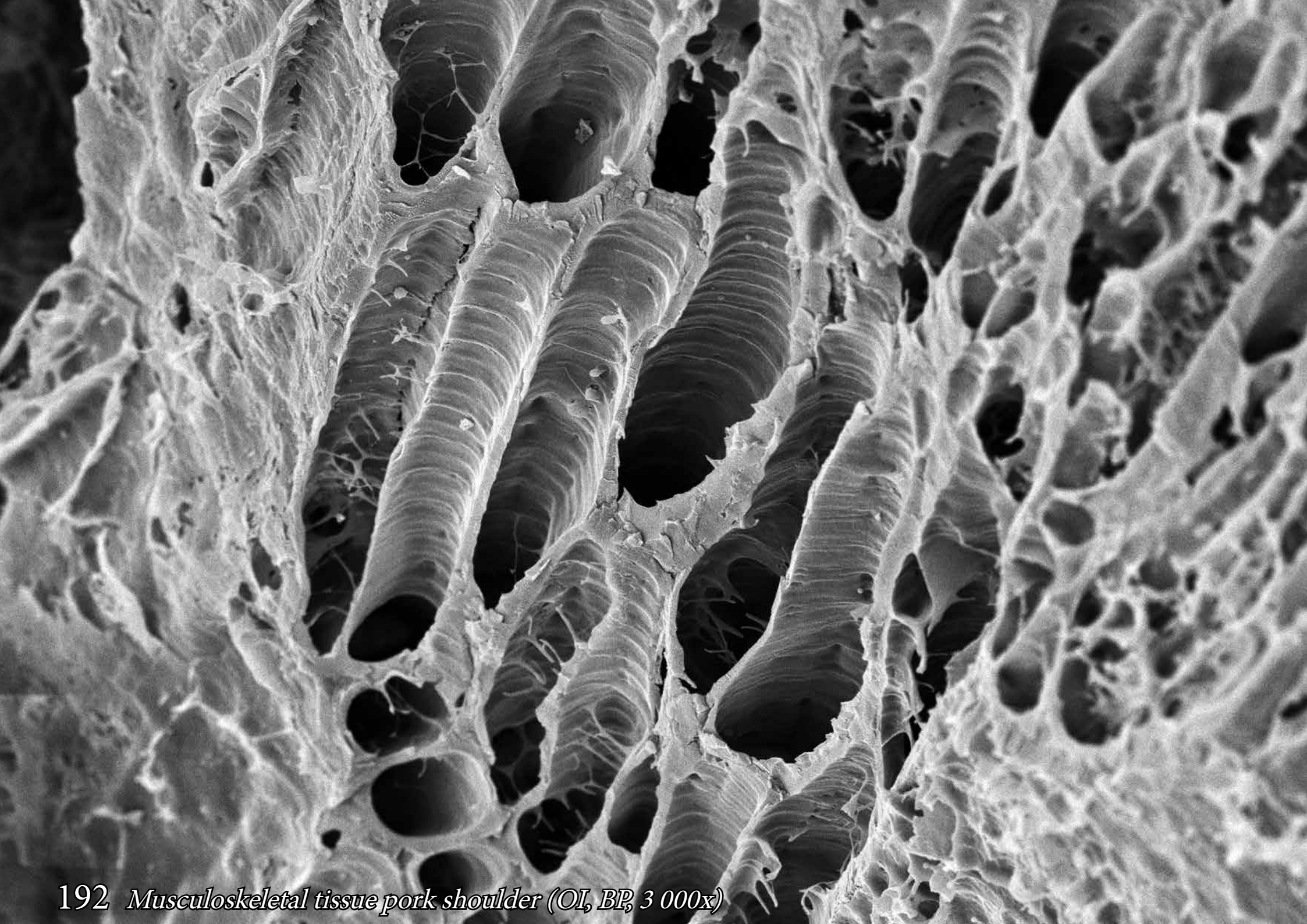

192 *Musculoskeletal tissue pork shoulder (OI, BP, 3 000x)*

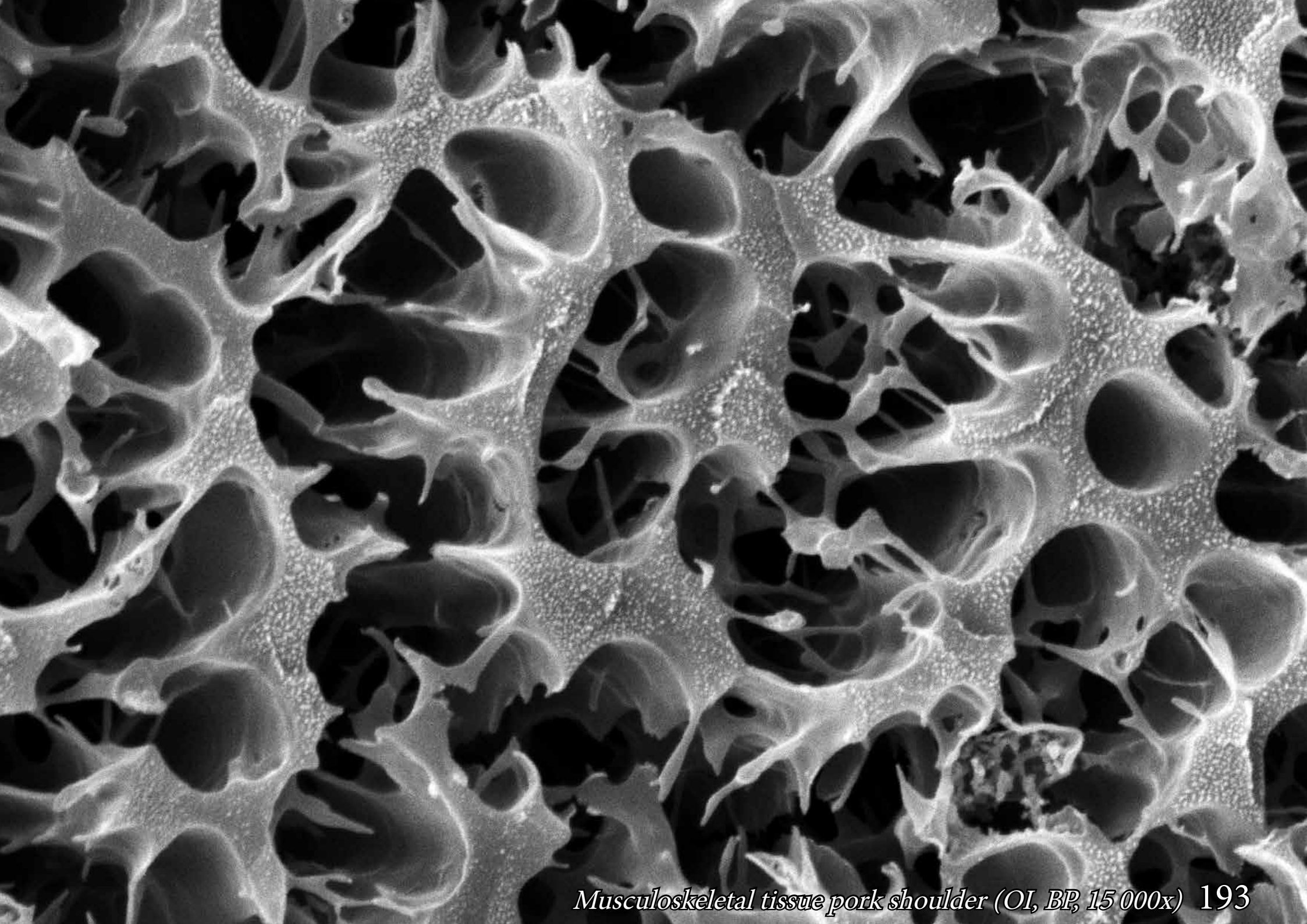

Musculoskeletal tissue pork shoulder (OI, BP, 15 000x) 193

194 *Musculoskeletal tissue pork shoulder (OI, BP, 10 000x)*

Polymer/ZnO composite

Different type of polymers were covered by a nanolayer of ZnO using Atomic Layer Deposition (ALD) to form nanocomposites that could be applied as effective gas filters or sensors.

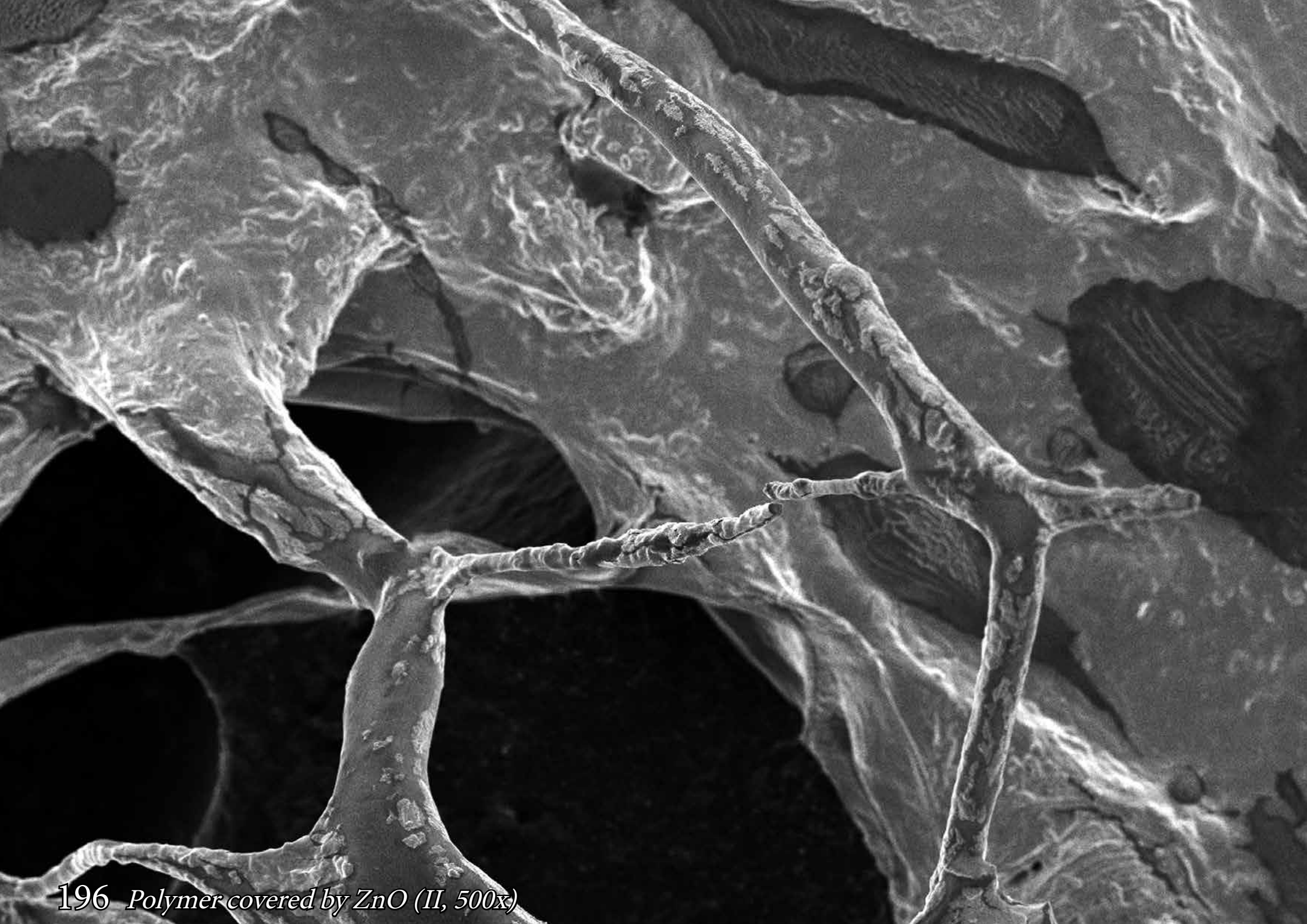

196 *Polymer covered by ZnO (II, 500x)*

Polymer covered by ZnO (II, 4 300x) 197

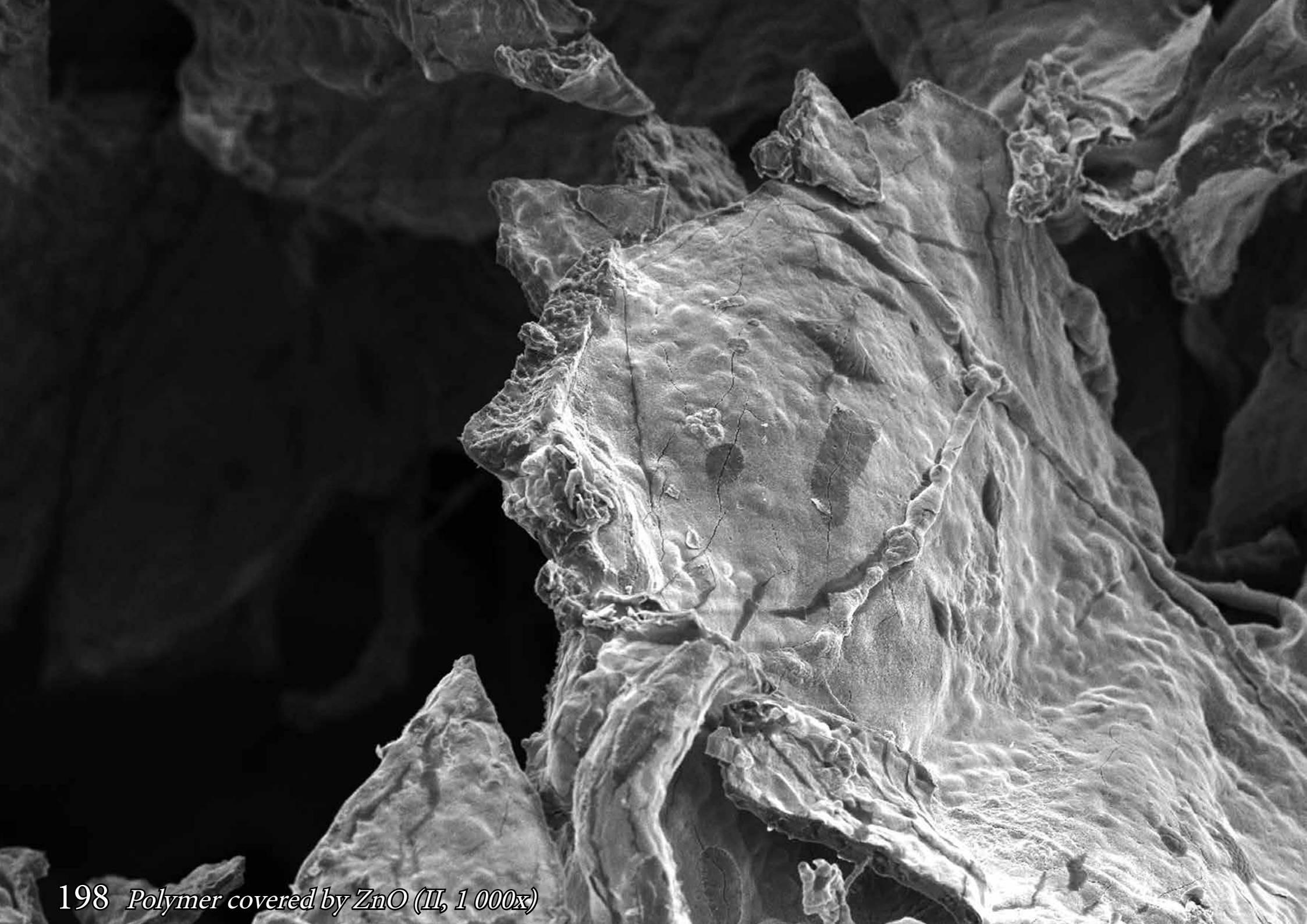

198 *Polymer covered by ZnO (II, 1 000x)*

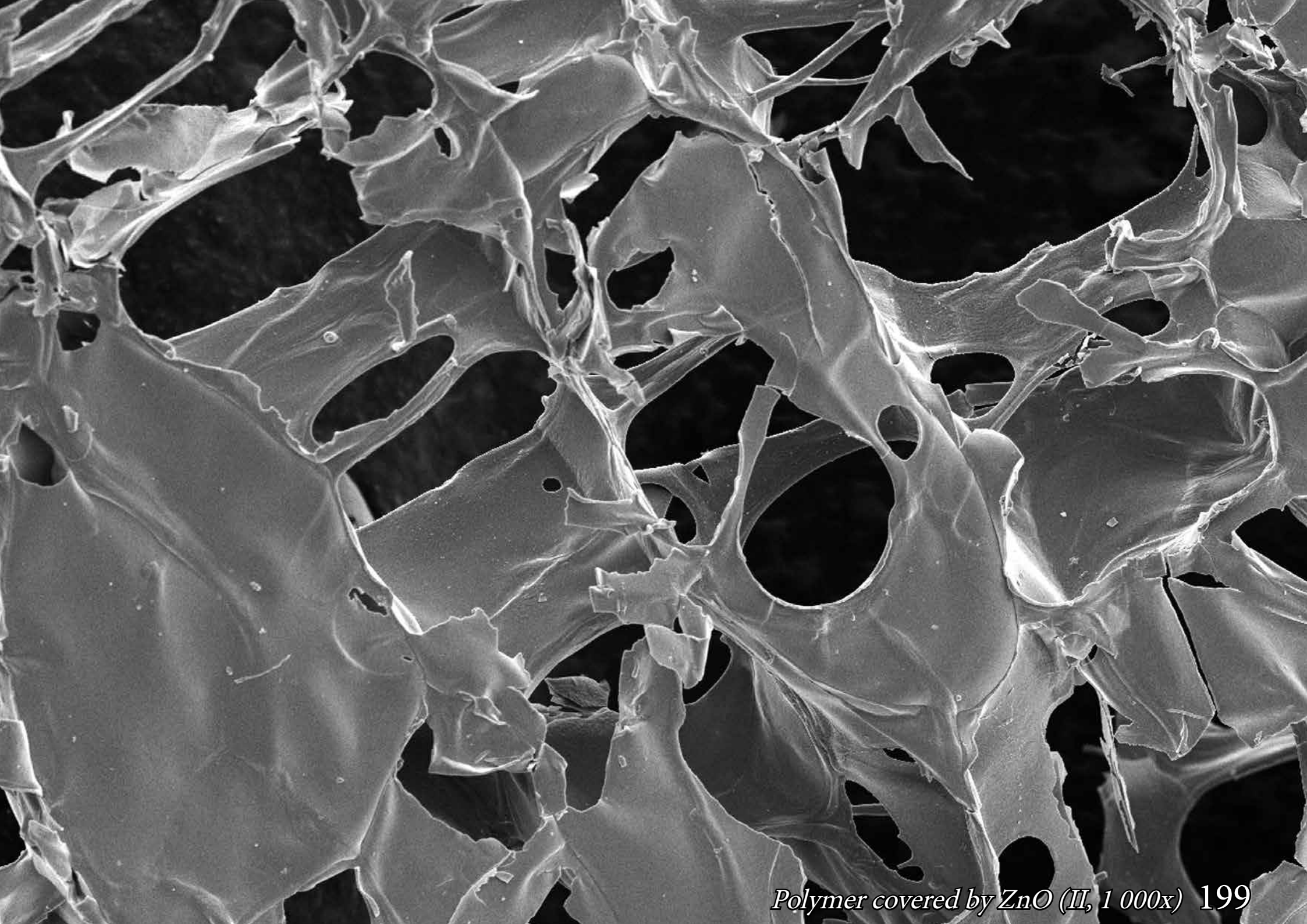

Polymer covered by ZnO (II, 1 000x) 199

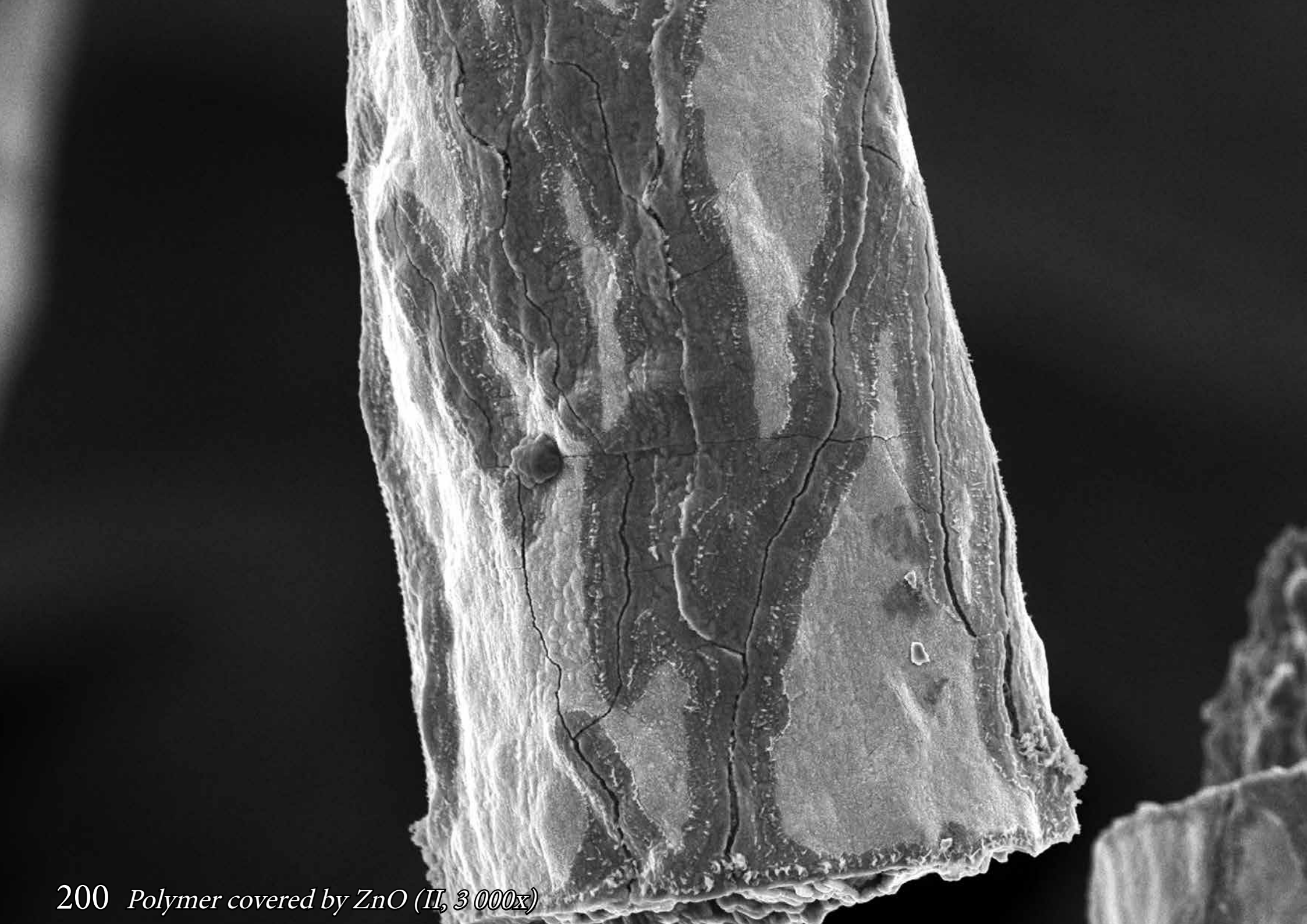

200 *Polymer covered by ZnO (II, 3 000x)*

Silica nanowires

Silica nanowires were produced by one-step metal-assisted chemical etching ($AgNO_3$ and HF) for optical biosensing applications.

202 *Silica nanowires (II, 2 000x)*

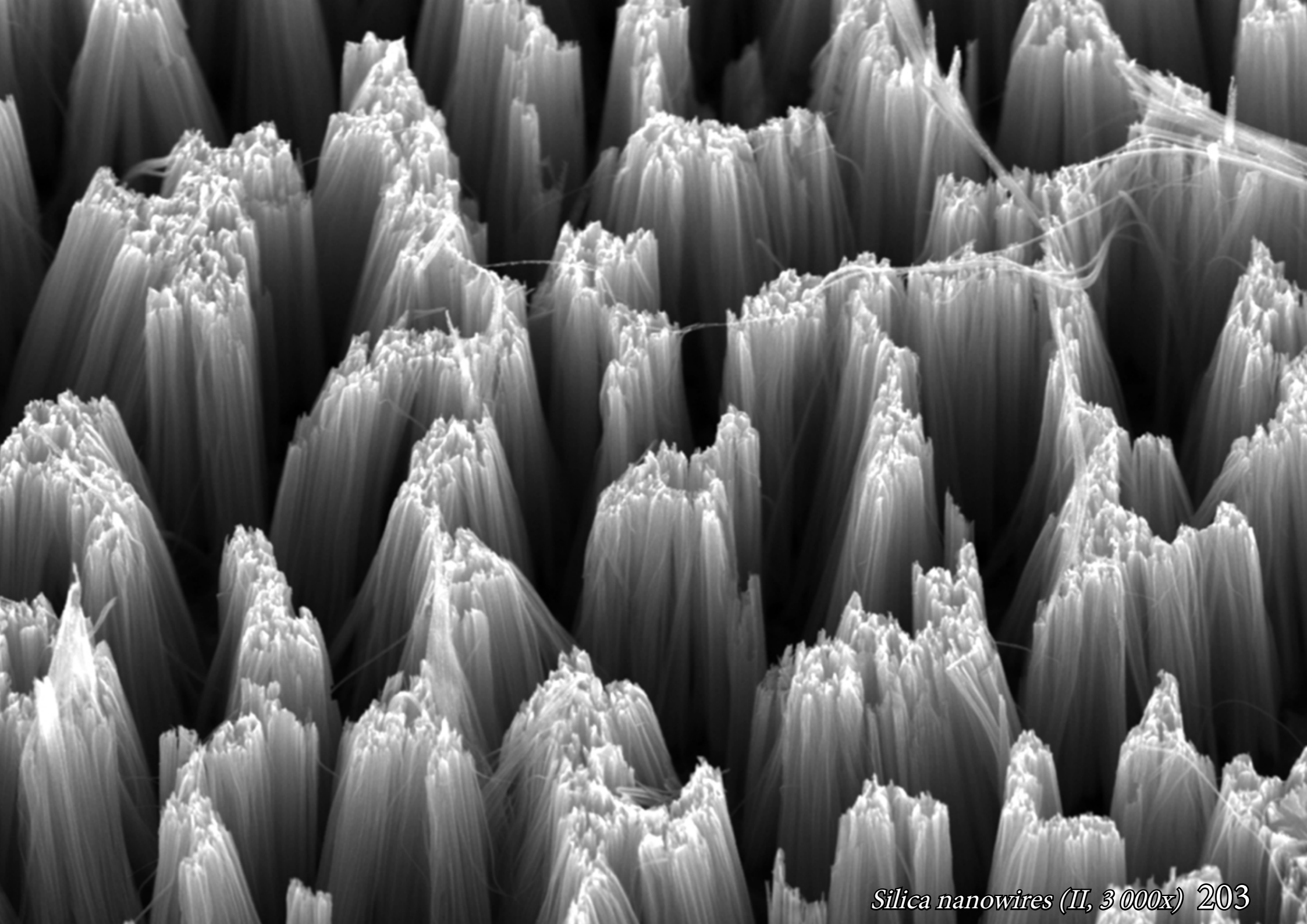

Silica nanowires (II, 3 000x) 203

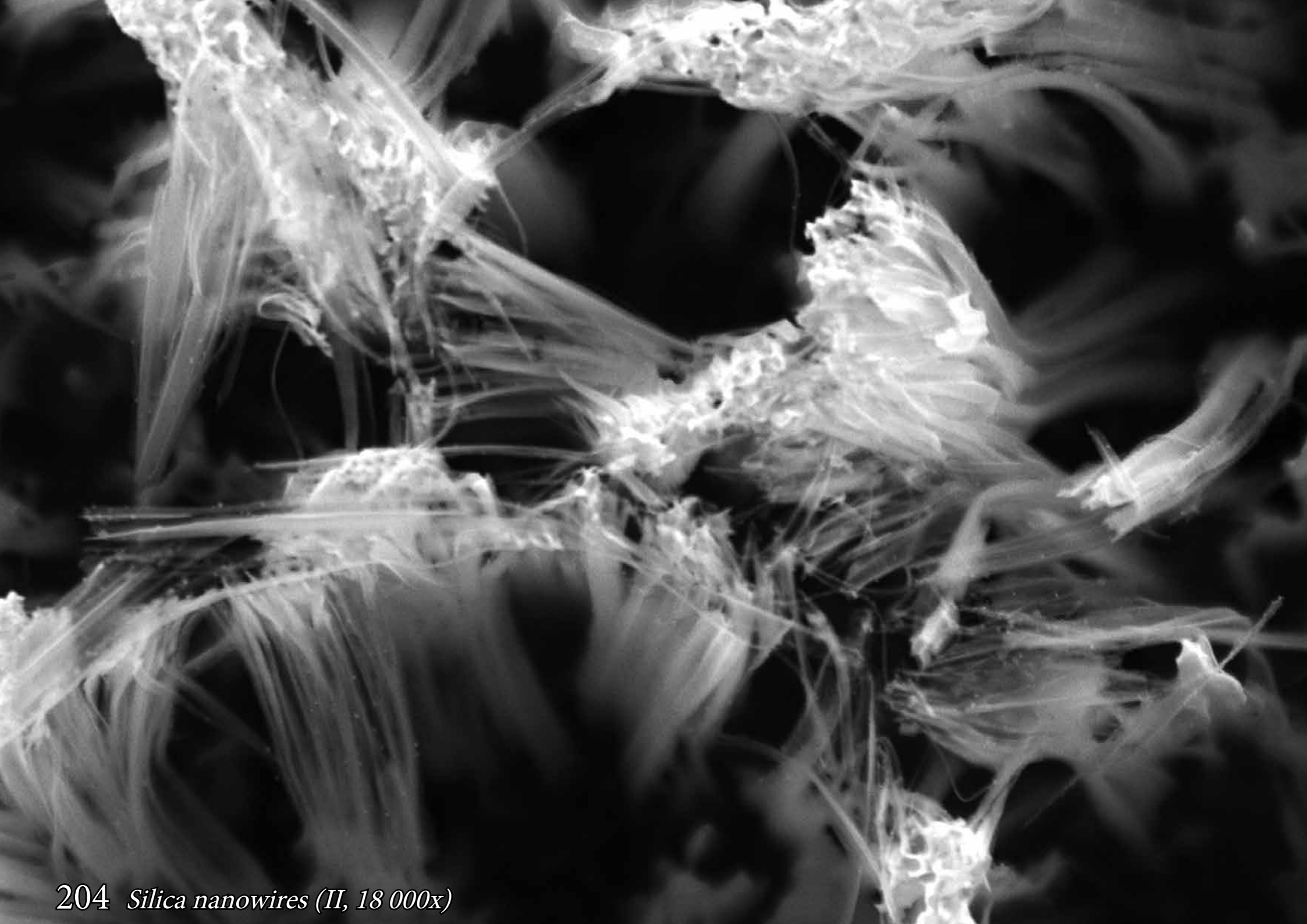

204 *Silica nanowires (II, 18 000x)*

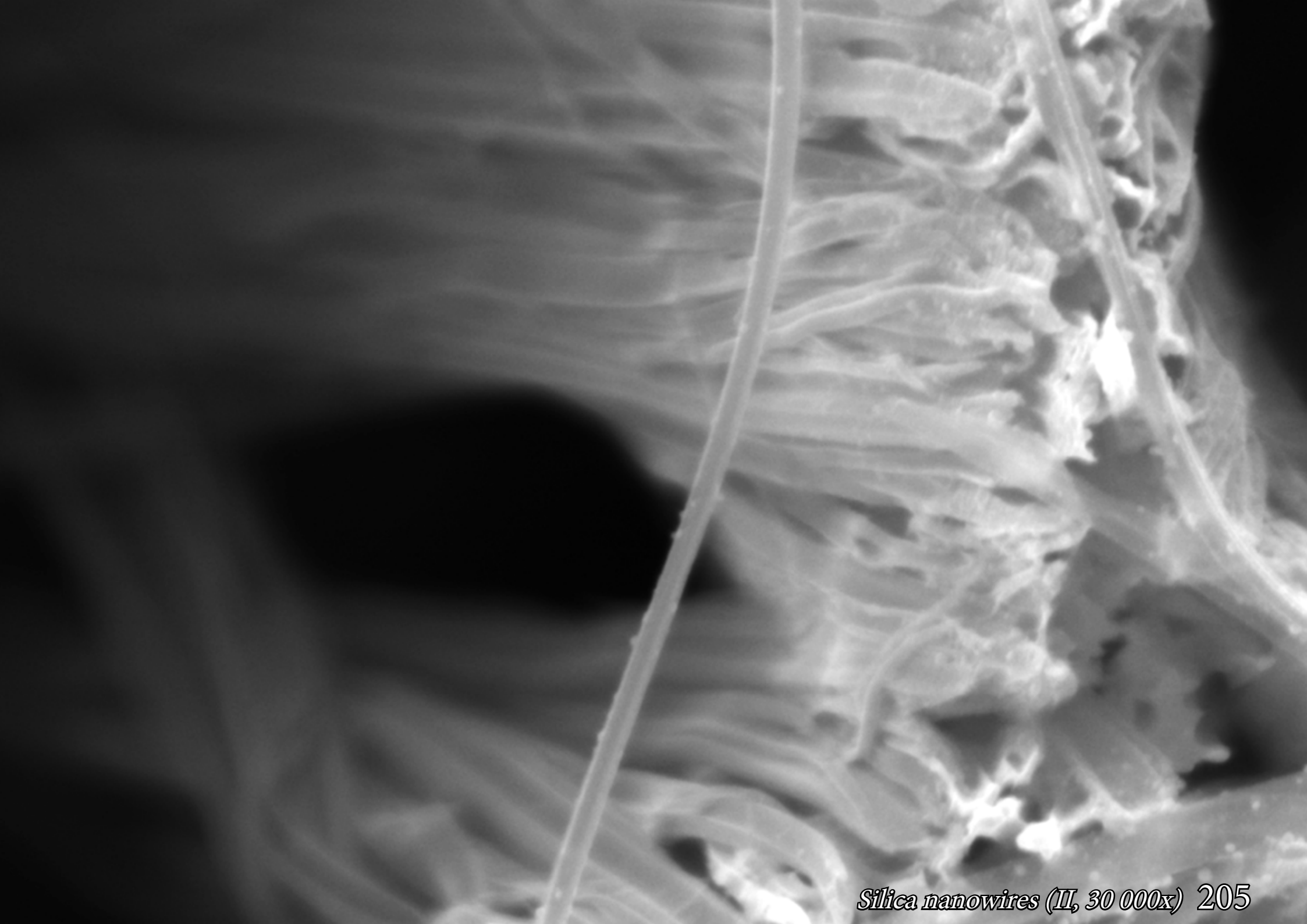

Silica nanowires (II, 30 000x) 205

ZnO hierarchical structures

ZnO flower-like hierarchical structures were obtained by hydro/solvothermal methods. ZnO structures with different morphologies can be obtained by simple tuning of the synthesis parameters. Obtained structures with high surface area have wide application in modern materials science.

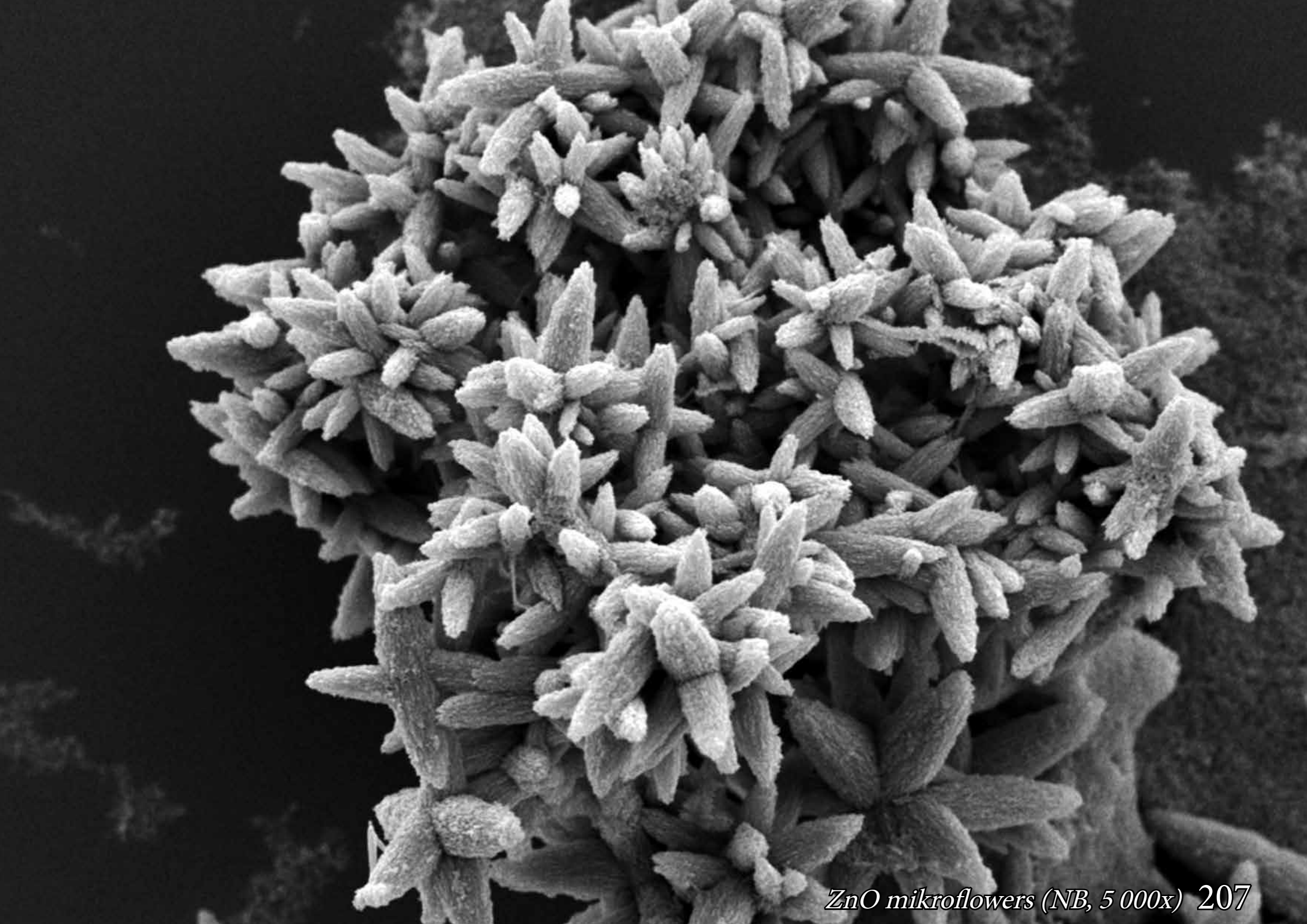

ZnO mikroflowers (NB, 5 000x) 207

208 *ZnO mikroflowers (NB, 10 000x)*

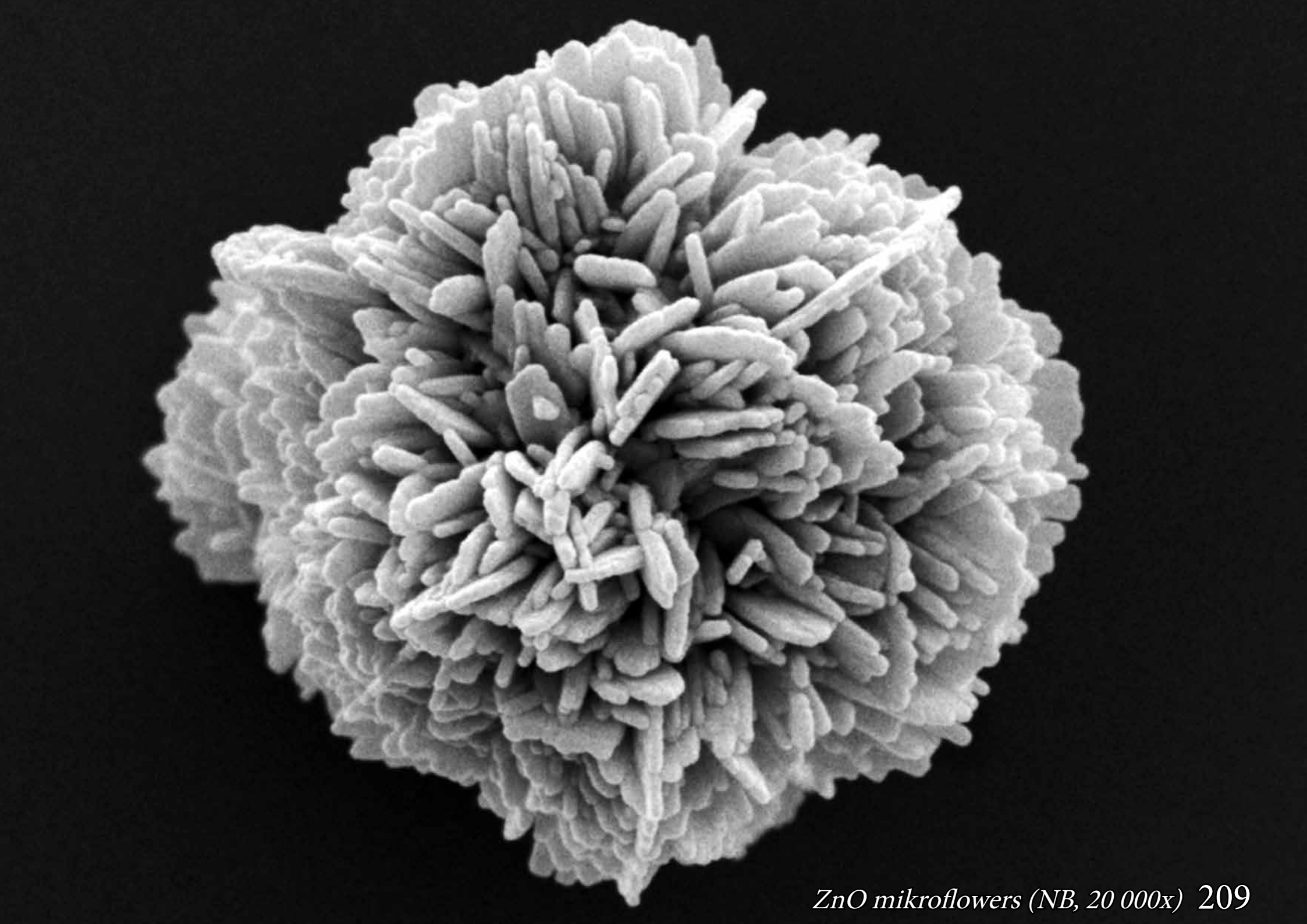

ZnO mikroflowers (NB, 20 000x) 209

Thank you very much for looking through our photo album. We hope that this short journey through variety of materials produced at the NanoBioMedical Centre will serve you, our dear reader, as a basis for further exploration in these subjects and creatively stimulate and encourage you to visit our site.